Coupled Ocean-Ice-Atmosphere Variability and Change in the Nordic Seas

A thesis submitted to the School of Environmental Sciences at the University of East Anglia in partial fulfilment of the requirements for the degree of Doctor of Philosophy.

Miriam Gwenda Bennett
University of East Anglia
Environmental Sciences

February 2026

Declaration

I, **Miriam Gwenda Bennett**, confirm that the work presented in this thesis is my own. Where information has been derived from other sources, I confirm that this has been indicated in the thesis.

Miriam Gwenda Bennett
February 2026

Abstract

The Nordic Seas form a critical interface between the Arctic and North Atlantic, mediating exchanges of heat, freshwater and dense water that influence the Atlantic Meridional Overturning Circulation. Rapid climate change is modifying sea-ice cover, boundary current pathways and upper-ocean stratification, with implications for high-latitude ocean-atmosphere coupling and water mass transformation. This thesis examines how these processes vary in the present climate and how they respond to strong anthropogenic forcing.

Observations and reanalysis data are used to investigate historic spatiotemporal variability in sea-ice conditions and upper-ocean structure along the north-east Greenland margin. Variability in the Northeast Water Polynya is shown to be primarily controlled by atmospheric circulation, while concurrent ocean changes reveal widespread warming, surface freshening and subsurface salinification, consistent with enhanced ice melt and evolving stratification.

The physical oceanography of the wider Nordic Seas is explored using the HadGEM3 global coupled climate model at low, medium and high-resolution, and the simulated diagnostics are evaluated against observation-based products. The low-resolution model does not accurately resolve the complex ocean system, while the medium-resolution has muted variability and dynamics. However, despite biases in boundary current strength, the high-resolution simulation reproduces the large-scale circulation, seasonal cycle and key hydrographic contrasts well, providing confidence in its projected response. Under a high-emissions scenario, increased inflow of Atlantic-origin water intensifies warming and salinification along boundary currents, strengthening horizontal density gradients and altering mixed layer depths.

The high-resolution future projections show a decline in dense water formation driven by rising ocean temperatures, reduced brine rejection and a poleward shift in surface-forced transformation. Meanwhile, overturning circulation within the Nordic Seas strengthens and shifts poleward, while the density of overturning decreases, implying a shoaling circulation. These results highlight competing mechanisms linking sea-ice retreat, boundary current dynamics and overturning, while reinforcing the sensitivity of the Nordic Seas to climate change.

Acknowledgements

I would like to thank my supervisory team for all their advice, ideas and support, without which this thesis would not have been possible. I am very grateful to my primary supervisor, Ian Renfrew, and my secondary supervisor, David Stevens, for their steady guidance throughout this project. Your constructive feedback, positive encouragement and the many opportunities you provided over the past few years were immensely valuable. I would also like to thank my external supervisor, Kent Moore, for his expert advice and insightful input, which greatly improved this work.

To all the friends I made along the way, thank you for your good company. I will always remember our cycle trips around East Anglia and the laughs we shared during our time in Norwich.

Finally, thank you to my family for their support and encouragement throughout.

Access Condition and Agreement

Each deposit in UEA Digital Repository is protected by copyright and other intellectual property rights, and duplication or sale of all or part of any of the Data Collections is not permitted, except that material may be duplicated by you for your research use or for educational purposes in electronic or print form. You must obtain permission from the copyright holder, usually the author, for any other use. Exceptions only apply where a deposit may be explicitly provided under a stated licence, such as a Creative Commons licence or Open Government licence.

Electronic or print copies may not be offered, whether for sale or otherwise to anyone, unless explicitly stated under a Creative Commons or Open Government license. Unauthorised reproduction, editing or reformatting for resale purposes is explicitly prohibited (except where approved by the copyright holder themselves) and UEA reserves the right to take immediate 'take down' action on behalf of the copyright and/or rights holder if this Access condition of the UEA Digital Repository is breached. Any material in this database has been supplied on the understanding that it is copyright material and that no quotation from the material may be published without proper acknowledgement.

Contents

List of Figures

List of Tables

Introduction

1.1 The Nordic Seas

1.1.1 Geographical Context

The Nordic Seas is a high-latitude sub-Arctic geographical domain situated between Norway, Iceland, Greenland and the Svalbard archipelago, encompassing the Norwegian Sea, the Iceland Sea and the Greenland Sea (Figure 1.1). The region forms a key transition zone between the North Atlantic and the Arctic Ocean and plays a pivotal role in regulating the exchange of heat, freshwater and salt between lower and higher latitudes (Mayer et al., 2020; Mauritzen, 1996; Serreze and Meier, 2019). The Fram Strait acts as the major gateway to the north, controlling the primary oceanic connection with the Arctic Ocean (Schauer and Beszczynska-Möller, 2008), although some additional exchange takes place through the shallow Barents Sea Opening to the east (Smedsrud et al., 2013); while the Greenland-Scotland Ridge marks the southern boundary where dense overflow waters flow southward to ventilate the deep Atlantic (Hansen and Østerhus, 2004; Dickson et al., 2002; Rahmstorf et al., 2015).

Owing to its location and geomorphology, the Nordic Seas are central to the structure and variability of the global climate system. Intense air-sea heat fluxes in the region contribute substantially to the transformation of warm Atlantic inflow waters into colder and denser water masses (Huang et al., 2023; Isachsen et al., 2007; Marshall and Schott, 1999; Renfrew et al., 2021), which subsequently feed the lower limb of the Atlantic Meridional Overturning Circulation (Lozier, 2019; Hansen and Østerhus, 2004; Østerhus and Turrell, 2001). In addition, strong coupling between the ocean, atmosphere and sea-ice gives rise to tightly linked feedback mechanisms that amplify climate variability (Luo et al., 2021; Screen et al., 2018). Observations over recent decades demonstrate that the Nordic Seas region is responding substantially and rapidly to anthropogenic climate forcing (e.g. Moore et al., 2022, 2015; Broomé et al., 2020; Sadatzki et al., 2020), highlighting its role as an early indicator of broader changes in the Arctic-Atlantic climate system (Polyakov et al., 2017; Rahmstorf et al., 2015). As demonstrated by Figure 1.2, the largest increases in surface temperature since 1980 are seen in the Arctic region, with the Northern Hemisphere high-latitudes showing a cumulative warming of more than 4.5 °C over this period, much larger than anywhere else on Earth (global mean temperature increase over this period is $\sim$0.94 °C).

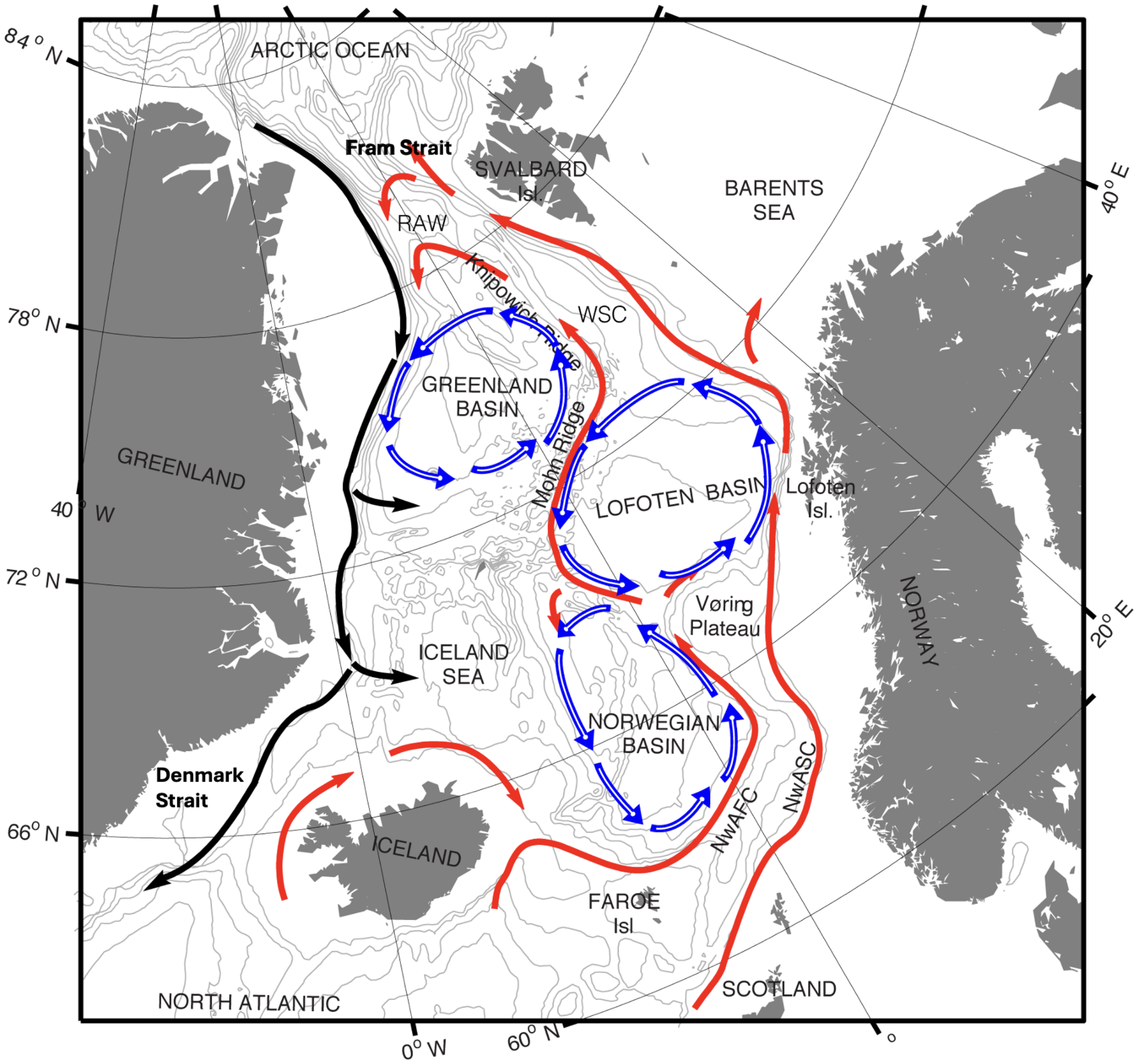

Figure 1.1: A map of the Nordic Seas region taken from Raj et al. (2019), with schematic water pathways showing the northward flowing Atlantic Water at the surface in red, and southward flowing East Greenland Current in black. The two branches of the Norwegian Atlantic Current, the Norwegian Atlantic slope current (NwASC) and Norwegian Atlantic front current (NwAFC) are also represented by red arrows. The cyclonic gyre circulations in the Norwegian Basin, Lofoten Basin and Greenland Basin are indicated in blue. See Chatterjee et al. (2018) and Raj et al. (2015) for further details. Grey isobaths are drawn for every 600 m, illustrating the bathymetry.

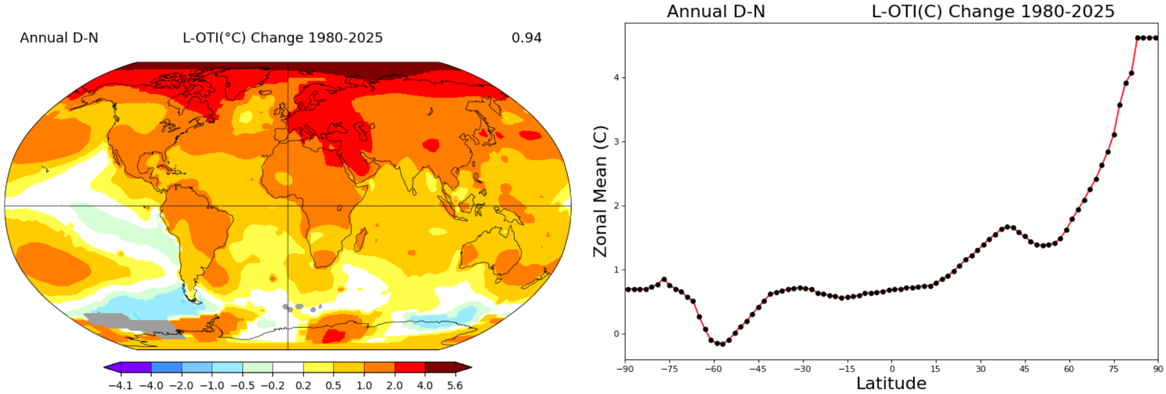

Figure 1.2: Figures from National Aeronautics and Space Administration Goddard Institute for Space Sciences (NASA GISS) show (a) the spatial distribution of the linear annual trend in global surface temperature between 1980 and 2025 and (b) a graph of the zonal mean of this temperature change. These figures are compiled using Land Surface Air Temperature data (GHCNv4) and Sea Surface Temperature data (ERSSTv5) and are available from `https://data.giss.nasa.gov/gistemp/maps/`. The number at the top right-hand corner of the map plot is an estimate for the global mean of the calculated field over the given time period. Note that a smoothing radius of 1200 km has been used.

1.1.2 Physical Oceanography

The bathymetry of the Nordic Seas is highly complex, ranging from shallow continental shelves at depths of around 250 m, to deep basins and narrow passages exceeding 5000 m (Blindheim and Østerhus, 2005; Schaffer et al., 2019; Thornes and Longva, 2007; Thiede et al., 1990). This rugged topography exerts a strong control on the regional ocean circulation, which is predominantly cyclonic and characterised by basin-scale gyres, topographically steered boundary currents and vigorous mesoscale activity (Nilsen et al., 2008; Hansen and Østerhus, 2004; Drange et al., 2006).

Prominent circulation features include the Greenland Sea Gyre (Pawlowicz, 1995; Gascard et al., 2002), a basin-wide cyclonic system associated with deep convection and long-term carbon storage in the Greenland Sea (Rhein et al., 2011), and the Norwegian Sea Gyre, which regulates the distribution and transformation of Atlantic and Arctic-derived water masses throughout the water column in the Norwegian Sea (Hátún et al., 2021). Additionally, situated in the path of Atlantic Water flow from the North Atlantic to the Arctic, the Lofoten Basin Gyre acts as the largest heat reservoir in the Nordic Seas (Raj et al., 2020) and modulates rates of boundary-interior heat transport and heat loss to the atmosphere.

The cyclonic gyre circulations dome the isopycnals in each basin, resulting in a less stratified water column which forms favourable pre-conditions for deep convection while high surface fluxes force persistent upper-ocean buoyancy loss which triggers convective mixing (Marshall and Schott, 1999). Deep convection has been observed at depths of more than 800 m in the Greenland Sea basin (Lherminier et al., 1999; Bashmachnikov et al., 2021; Brakstad, 2023). This is thought to be some of the densest deep-water renewal to occur in the Northern Hemisphere. The cyclonic gyre circulations of the Nordic Seas are illustrated with blue arrows on the map shown in Figure 1.1.

There also exist several important boundary current features in the Nordic Seas which transport water masses around the region. Along the western boundaries, the equatorward-flowing East Greenland Current (EGC) transports cold, fresh Polar Water from the Arctic Ocean along the continental shelf break of East Greenland towards the North Atlantic (Dickson and Brown, 1994; Rudels et al., 2002; Foldvik et al., 1988; Woodgate et al., 1999) and dense overflow waters exit the Nordic Seas through the Denmark Strait (Swift et al., 1980; Käse et al., 2003; Våge et al., 2011). In contrast, the eastern boundary is dominated by warm and saline Atlantic Water, which flows poleward, mainly via the Norwegian Atlantic Current (Orvik, 2022; Mork and Skagseth, 2010) and the West Spitsbergen Current (Schlichtholz and Goszczko, 2006; Walczowski and Piechura, 2011), supplying heat and salt to higher latitudes and the Arctic Ocean (Hansen and Østerhus, 2000; Orvik and Niiler, 2002; Schauer and Beszczynska-Möller, 2004). These boundary currents are represented by black and red arrows respectively in Figure 1.1.

As Atlantic inflow waters progress northward through the domain, they undergo substantial modification through heat loss to the atmosphere, freshwater input, vertical mixing and interaction with sea-ice (Mauritzen, 1996; Rudels et al., 2005). These processes, together with the sharp lateral gradients imposed by contrasting water masses and steep bathymetry, give rise to strong oceanic fronts and enhanced mesoscale variability (Isachsen et al., 2012; Spall, 2011; Jian et al., 2026). The coupled transformation of Atlantic Water into intermediate and dense waters within the Nordic Seas is a key mechanism linking the regional dynamics to larger-scale climate variability, particularly through its influence on the Atlantic Meridional Overturning Circulation (AMOC; Marshall and Schott, 1999; Eldevik and Nilsen, 2013) and the global thermohaline circulation. The significant interconnectivity of this crucial mechanism is visualised by the schematic diagrams shown in Figure 1.3.

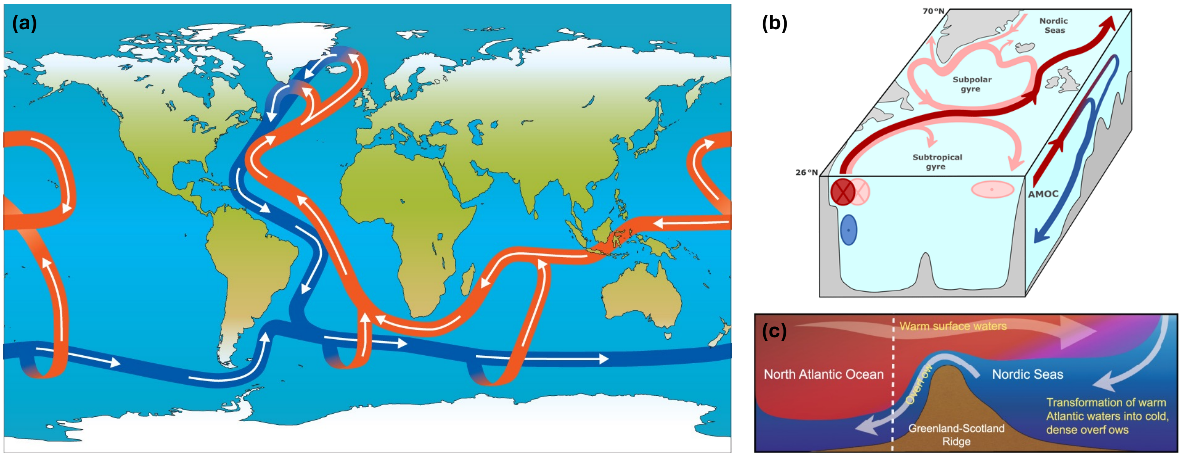

Figure 1.3: (a) A schematic illustrating global ocean circulations with blue arrows indicating cold deep water and red arrows indicating warm surface water (Chapman and Wood, 2025). (b) An idealised visual representation of the North Atlantic Current and Nordic Seas ocean circulation highlighting the interconnectivity of the Gulf Stream (red), gyre structures (pink) and Deep Western Boundary Current (blue). The zonally integrated view of the circulation shown on the side illustrates the transformation and sinking of warm upper-ocean water at high latitudes as a part of the AMOC (Asbjørnsen et al., 2024). (c) A closer look at how the dense overflow waters from the Nordic Seas contribute to the lower limb of the AMOC is illustrated with a schematic of the meridional flow across the Greenland-Scotland Ridge (Årthun et al., 2023a).

1.1.3 Sea-Ice and Atmospheric Conditions

Sea-ice in the Nordic Seas exhibits pronounced spatial, seasonal and interannual variability (Vinje et al., 2004). Perennial or near-perennial ice is typically found in the western and northern sectors, while the eastern Nordic Seas are characterised by a highly dynamic marginal ice zone (MIZ) that expands during winter and retreats during summer (Kern et al., 2010). Examples of this seasonal variability are demonstrated in Figure 1.4 with spatial maps of Arctic sea-ice concentration for mid-March and mid-September, the months of maximum and minimum sea-ice extent respectively. Over recent decades, the extent and thickness of sea-ice in the Nordic Seas has declined markedly, with the winter ice edge retreating northward in response to rising ocean and atmosphere temperatures (Serreze and Barry, 2011; Stroeve et al., 2012). This is particularly true in the area around the Svalbard archipelago, near the northern extremity of the West Spitsbergen Current pathway of Atlantic water inflow (WSC; Onarheim et al., 2014).

The annual cycle of the total sea-ice extent in the Nordic Seas resembles that for the entire Arctic region, with a peak in late winter and the lowest values in early autumn, following the summer melt season. An example from the National Snow and Ice Data Center (NSIDC) of this annual cycle in Arctic sea-ice extent is shown in Figure 1.5 (a). This graph also shows the steady evolution of the annual cycle over time, with a clear decreasing trend since the satellite record began in 1979. The linear shifting of the annual cycle visualises that the trend is largely similar for all months of the year with a mostly

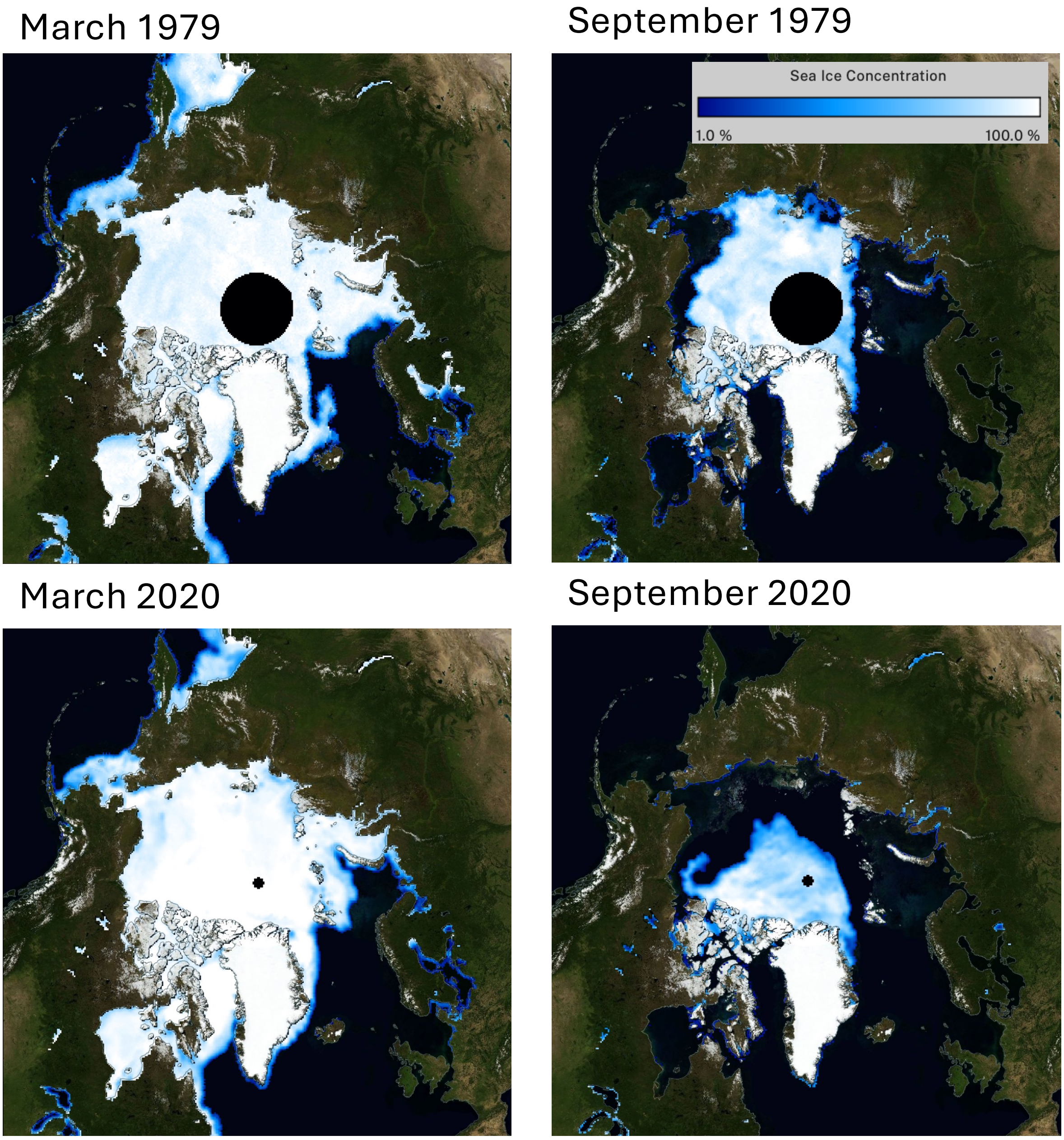

Figure 1.4: Maps showing the spatial distribution of Arctic sea-ice concentration on 15th March and 15th September 1979 (upper row) and the same dates in 2020 (lower row). The sea-ice concentration data is from NSIDC-0051 (`10.5067/8GQ8LZQVL0VL`) and NSIDC-0081 (`10.5067/U8C09DWVX9LM`) and is calculated using satellite observations from the Nimbus-7 SMMR and SSM/I-SSMIS passive microwave instruments. The figure shown here are taken from the NASA Worldview webpage (`https://worldview.earthdata.nasa.gov`).

consistent rate of sea-ice decline spatially averaged over the Arctic polar region. In concordance, time series of the average monthly Arctic sea-ice extent between 1979 and 2021 show significant negative trends for both the month of March and September in Figures 1.5 (b) and (c) respectively. This strong signal of sea-ice decline is prominent despite the relatively large natural interannual variability and it has been shown that this trend is mostly driven by anthropogenic forcing (Zhang et al., 2010; Lee et al., 2025; Mueller et al., 2018).

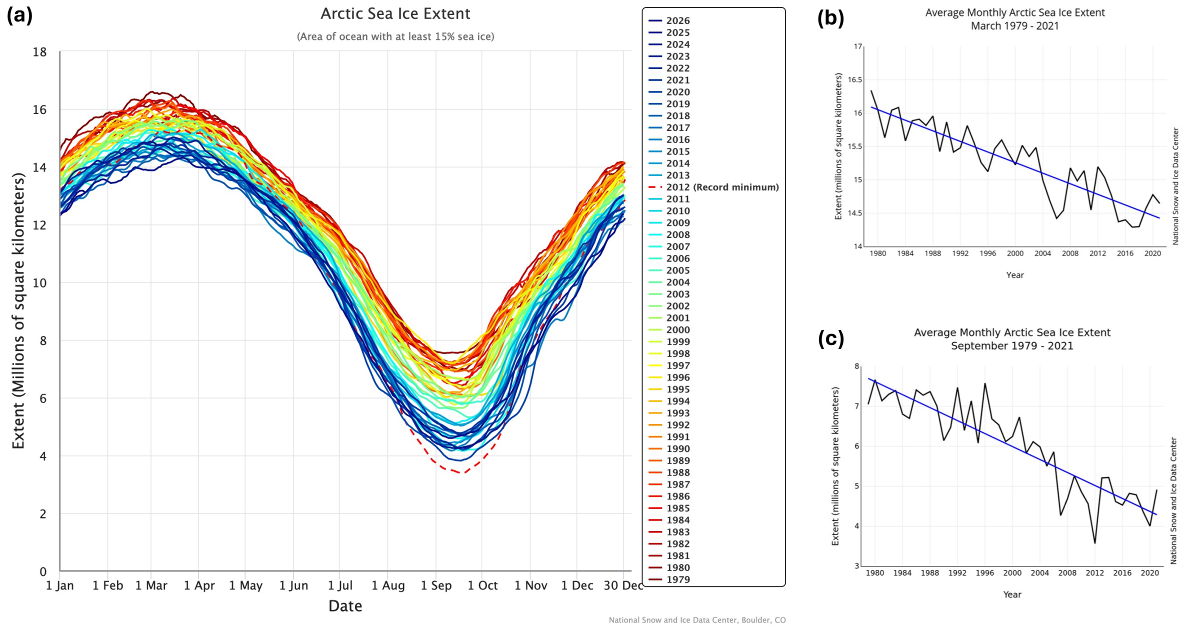

Figure 1.5: (a) The annual cycle of Arctic sea-ice extent from the National Snow and Ice Data Center (NSIDC: `https://nsidc.org/data/tools/arctic-sea-ice-chart/`) for each year since 1979, based on daily extent values with a five-day trailing mean. The results are calculated using passive microwave observations, comprising several datasets (the Sea Ice Index, AMSR2 Daily Polar Gridded Sea Ice Concentrations, and the NASA-produced Sea Ice Concentrations from Nimbus-7 SMMR and DMSP SSM/I Passive Microwave Data). (b) Average monthly Arctic sea-ice extent for March and (c) September from 1979 to 2021, with a best fit linear regression trend line, also taken from NSIDC (`https://nsidc.org/data/tools/arctic-sea-ice-chart/`).

Sea-ice variability is important as it strongly modulates freshwater input (e.g. Selyuzhenok et al., 2020), upper-ocean stratification (e.g. Lundesgaard et al., 2022) and the efficiency of atmosphere-ocean exchange (e.g. Moore et al., 2022; Barrell et al., 2023; Eldevik et al., 2012; Screen et al., 2022), thereby tightly coupling local ice conditions to larger-scale oceanic (Lique et al., 2025; Mauritzen and Häkkinen, 1997) and atmospheric dynamics (Overland et al., 2011; Screen and Simmonds, 2013; Smith et al., 2017). The Nordic Seas are subject to particularly strong atmospheric forcing (Jakobson et al., 2012), including frequent cyclones and polar lows (Bracegirdle and Gray, 2008; Stoll et al., 2018; Rojo et al., 2015; Noer et al., 2011), intense surface winds (Reistad et al., 2014) and large seasonal variations in heat fluxes (Simonsen and Haugan, 1996), which together drive vigorous coupled interactions in this region.

Polynyas, and other sea-ice features such as leads, further enhance the coupling between atmosphere and ocean (e.g. Maykut and McPhee, 1982). Polynyas are recurrent regions of open water, or reduced ice cover, within an otherwise ice-covered area (Morales Maqueda et al., 2004). By exposing the ocean surface to the atmosphere, polynyas can facilitate significant ocean heat loss (Smith et al., 1990; Ren et al., 2024), brine rejection (Haarpaintner et al., 2001) and deep or intermediate water formation (Geyer et al., 2010), thereby contributing to important mechanisms of water mass transformation and ocean ventilation. Their occurrence and persistence are controlled by a combination of atmospheric forcing, ocean heat transport and sea-ice dynamics, making them highly sensitive to changes in wind patterns and ocean stratification (Morales Maqueda et al., 2004). Under ongoing climate change, increased ocean warming, freshening and reduced sea-ice thickness are expected to alter polynya frequency, extent and seasonality in the Arctic, potentially weakening their role in dense water formation and modifying feedbacks within the Nordic Seas climate system (e.g. Smith Jr and Barber, 2007; Gillie et al., 2024; Preußer et al., 2016; Wong et al., 2025; Hoppmann et al., 2015).

Mean near-surface air temperatures in the Nordic Seas typically range from approximately 5°C in summer to around -15°C in winter (National Centers for Environmental Information, 2021). These temperatures are accompanied by predominantly northerly or north-westerly winds (Semedo et al., 2015; Holland et al., 2007), although substantial regional and seasonal variability exists (Wilkinson et al., 2022; Smedsrud et al., 2013). The temporal mean 10 m wind speeds for each season between August 1999 and May 2007 is shown in the subplots in the left column of Figure 1.6, while the subplots shown in the right column show the directional constancy and average 10 m wind vectors. This figure is taken from Kolstad (2008) and has been constructed based on QuikSCAT satellite-derived data. The lightest winds are seen during the summer months, with weak wind speeds across the region of around 5 m/s and low directional constancy. The strongest near-surface winds are seen during the winter months and particularly high wind speeds are present in the south-western sector of the Nordic Seas domain. In this area a mesoscale barrier jet system often develops along the south-east coast of Greenland, near Denmark Strait, making this location one of the windiest in the world (Petersen et al., 2009; Moore and Renfrew, 2005; DuVivier et al., 2017; Moore, 2012; Moore et al., 2008). Here, the average wintertime values reach 18 m/s and are generally of a northerly flow direction (see upper row of subplots in Figure 1.6).

The large-scale atmospheric circulation over the Nordic Seas is influenced by variability in the North Atlantic storm track and by dominant modes of climate variability such as the North Atlantic Oscillation (NAO), the Arctic Dipole and changes in the strength and structure of the polar vortex (Hurrell, 1995; Overland and Wang, 2012; Vihma et al., 2014; Walter and Graf, 2005). These modes regulate surface heat, freshwater and momentum fluxes, thereby affecting ocean heat content (Broomé et al., 2020), stratification (Kenigson and Timmermans, 2021), deep water formation (Isachsen et al., 2007; Aagaard et al., 2004) and sea-ice variability (Tsukernik et al., 2010; Wu et al., 2006; Jung and Hilmer, 2001). Periods of enhanced north-westerlies and increased cyclonic activity tend to intensify wintertime heat loss and promote dense water formation, whereas atmospheric blocking over Greenland or Iceland can disrupt storm tracks and lead to pronounced interannual variability (Woollings et al., 2010). Four examples of atmospheric circulation regimes that significantly influence the climatology in the Nordic Seas are visualised by the 500 hPa geopotential height anomalies in Figure 1.7. This Figure, taken from van der Wiel et al. (2019), is based on ERA5 data for the winter months between 1979 and 2018.

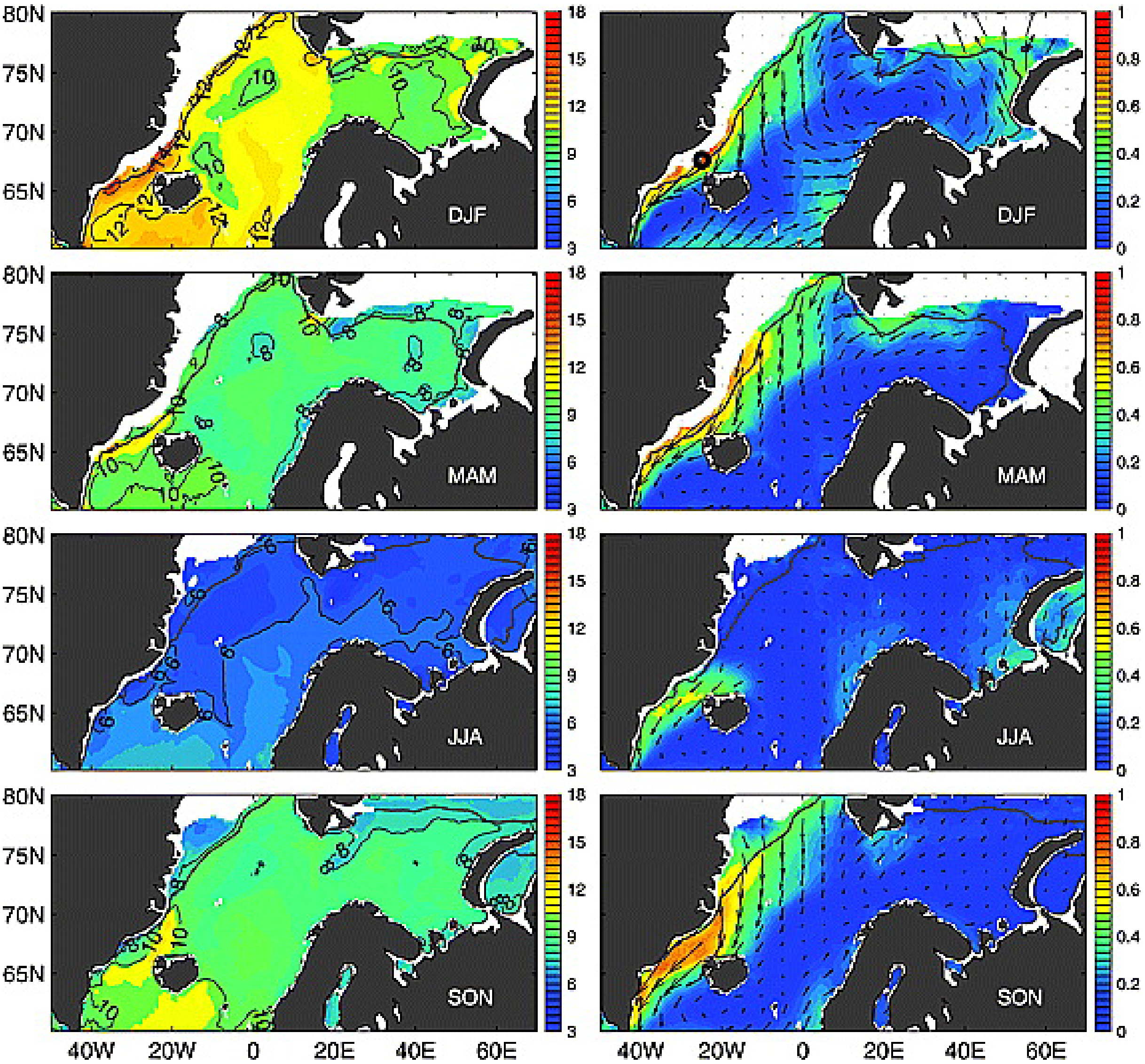

Figure 1.6: Taken from Kolstad (2008), the subplots in the left column show the temporal average QuikSCAT 10 m wind speed (m/s) for winter, spring, summer and autumn, between August 1999 and May 2007. The subplots in the right column show the associated directional constancy (shading) and average wind vectors (longest arrow is marked with a circle and translates to 11 m/s). The thick, unmarked contours indicate pixels that are covered by sea-ice 50% of the time.

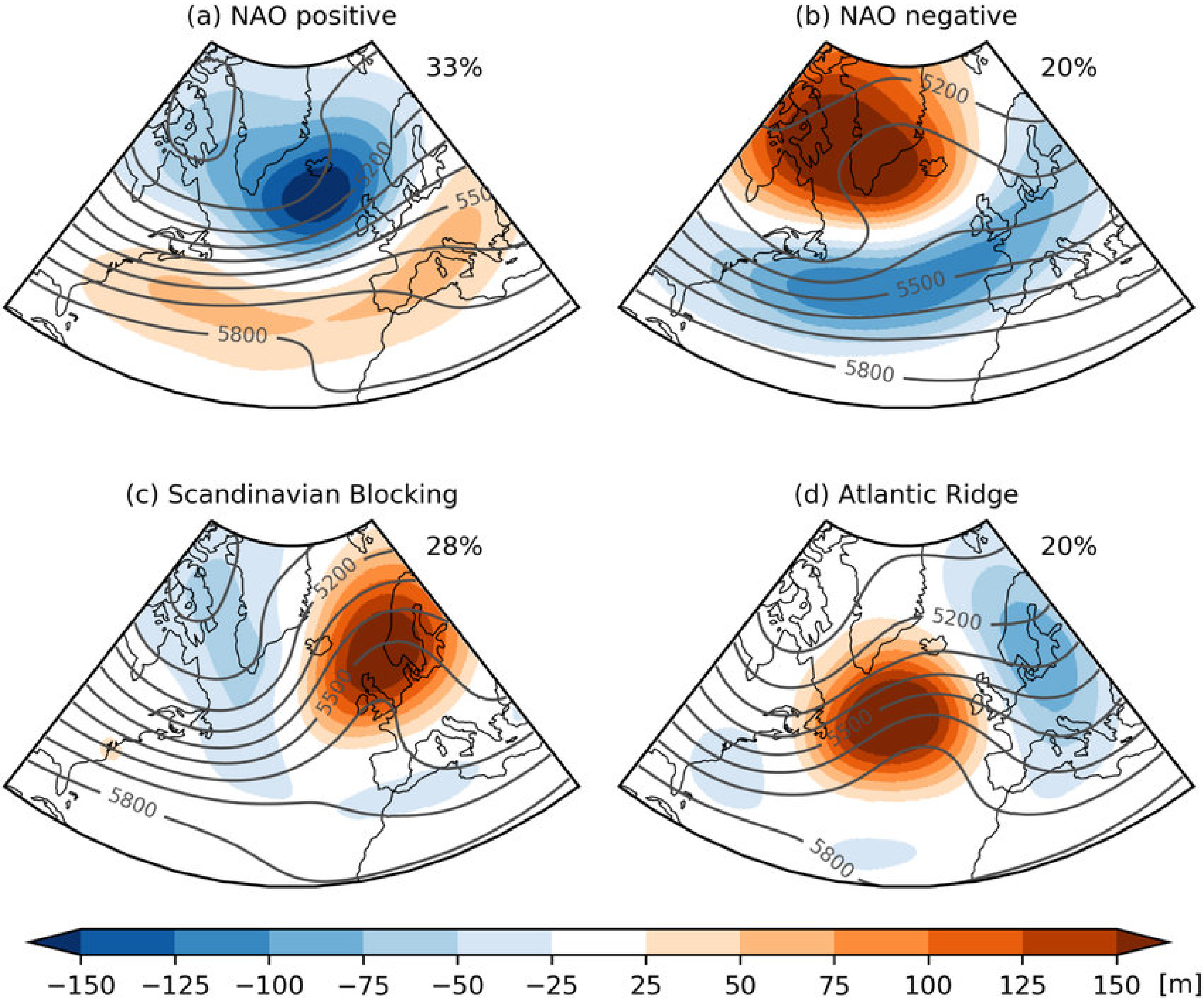

Figure 1.7: Spatial maps taken from van der Wiel et al. (2019) illustrate the four main regimes of atmospheric circulation in the North Atlantic-European domain, including (a) the NAO positive mode (b) the NAO negative mode (c) Scandinavian Blocking and (d) the Atlantic Ridge. The coloured shading shows the 500 hPa geopotential height anomaly (m) and the contour lines show the 500 hPa geopotential height (m, interval 100 m) which is indicative of the direction of flow. The percentage values denote the percentage of total days categorised in each regime, based on analysis of wintertime (DJF) ERA5 data between 1979 and 2018.

1.1.4 The Response to Climate Change

Due to the strong feedbacks between the ocean, atmosphere and sea-ice and its proximity to major freshwater sources, including the Greenland Ice Sheet, the Nordic Seas is particularly sensitive to ongoing climate change. Significant increases in near-surface air temperatures have been recorded at locations across the domain, with enhanced positive trends compared to the global average (Figure 1.2). In the Fram Strait and Barents Sea regions, trends in near-surface air temperature of up to 3°C per decade have been calculated using ERA5 and MERRA-2 data between 1992 and 2022 (Schmitt and Lüpkes, 2023).

Observations also indicate a significant ocean response, with wide-scale warming and freshening recorded over recent decades (Mohamed et al., 2022; Broomé et al., 2020; Isaksen et al., 2022; von Schuckmann et al., 2024). This is driven by a combination of increased Atlantic inflow, enhanced freshwater input from ice melt (from both sea-ice and land run-off, including melt from the Greenland Ice Sheet) and changes in atmospheric forcing (Holliday et al., 2020; Østerhus et al., 2019). These trends act to strengthen upper-ocean stratification, which inhibits vertical convection and thus could lead to reduced efficiency of deep and intermediate water formation processes (Strehl et al., 2024; Latarius and Quadfasel, 2016; Abot et al., 2023).

At the same time, declining sea-ice extent and thickness (e.g. Figures 1.4 and 1.5), particularly in the Greenland and Barents Seas, have increased wintertime air-sea heat exchange while amplifying positive feedbacks through reduced surface albedo (Screen and Simmonds, 2012). Atmospheric circulation changes, including shifts in storm tracks, wind patterns and the frequency of extreme events, further modulate surface fluxes and ocean circulation pathways (Hand et al., 2019; Zhao et al., 2019; Spall et al., 2021; Jensen et al., 2016; Du et al., 2019; Holt et al., 2018).

Collectively, these changes point toward a transition to a warmer, more stratified and increasingly seasonally ice-free Nordic Seas (Serreze et al., 2026; Isaksen et al., 2022; Barrell et al., 2023). Understanding the coupled ocean-ice-atmosphere processes governing this transition, and how these important mechanisms are responding to anthropogenically-driven environmental changes, is therefore essential for assessing the future evolution of the region and its implications for the stability of the AMOC and the global climate system.

1.2 Measuring and Modelling the Nordic Seas

1.2.1 Observational Data Collection

Observational data collection in the Nordic Seas is difficult due to the often harsh weather conditions and poor accessibility of the region. Sea-ice cover limits shipping routes while cyclone activity and regular cloud cover, along with a lack of infrastructure, inhibits extensive flight campaigns. However, historically there has always been significant interest in this remote sub-Arctic domain and since the second half of the 19th century there have been many scientific expeditions to observe, measure and record meteorological, oceanographic and cryospheric conditions in the Nordic Seas. This number is only growing with time as expanding maritime industries and offshore energy development drives increased human presence, making in-situ data collection more accessible.

In recent years, extensive analysis of observational data has demonstrated a range of responses to the changing climate in this region. Argo floats, which collect temperature and salinity profiles across the Nordic Seas, have shown trends of upper ocean warming and a freshening trend at some locations (Smedsrud et al., 2022; Almeida et al., 2023; Holliday et al., 2020; Isachsen et al., 2014). This is supported by hydrographic sections from long-term ship-based measurements (e.g. ICES) and data from moored arrays, from which heat, freshwater and volume transports can be calculated (González-Pola et al., 2019; Harden et al., 2016). Meanwhile, the OSNAP array (Overturning in the Sub-polar North Atlantic Program) provides a valuable record of overturning data in the North Atlantic which can be used to analyse AMOC strength and variability (Tollefson, 2018; Fu et al., 2025; Li et al., 2020).

In addition to in-situ measurements of the Nordic Seas, satellite altimetry data (e.g., AVISO and CryoSat-2) provide sea surface height and geostrophic currents (Müller et al., 2019; Bagnardi et al., 2021; Rose et al., 2019; Kwok and Morison, 2016; Bashmachnikov et al., 2020; Doglioni et al., 2023) while other satellite products (e.g., OSTIA, OSI SAF) can provide sea surface temperature and sea-ice concentration records (Høyer and Karagali, 2016; Høyer et al., 2012; Ivanova et al., 2014; Kern et al., 2019).

The collective observational record shows unequivocally that the Nordic Seas are experiencing ocean and atmosphere warming (Smedsrud et al., 2022; Kenigson and Timmermans, 2021; Vikhamar-Schuler et al., 2016; Eldevik et al., 2014; Moore et al., 2015), as well as increasing Atlantic Water inflow (Barton et al., 2018; Årthun et al., 2012; Lien et al., 2017; Schauer et al., 2002; Wang et al., 2022) and accelerating sea-ice decline (Onarheim et al., 2018; Årthun et al., 2012; Yamagami et al., 2022; Hwang et al., 2020; Onarheim et al., 2024; Moore et al., 2015, 2022). These changes are linked to a warming and expansion of the surface layer (Almeida et al., 2025; Mork et al., 2019), with lighter, fresher waters increasing in eastern basins (Kenigson and Timmermans, 2021; Årthun et al., 2023b) due to enhanced water mass transformation and a decrease in overflow water storage (Somavilla, 2019; Tooth et al., 2023; Shi et al., 2021; Fox et al., 2022). Moreover, as greenhouse gas emissions continue to rise the notable sea-ice retreat, especially in the south-east (Onarheim and Årthun, 2017; Moore et al., 2022), is only accelerating, despite the rate of Arctic sea-ice export steadily increasing over the last couple of decades (Spreen et al., 2020; Min et al., 2019; Babb et al., 2023).

It follows that many of these observed responses in the Nordic Seas may be attributed, at least in part, to anthropogenically driven climate forcing, because the strong trends seen in recent years exceed the normal rates of change due to natural variability.

1.2.2 Climate Modelling

Observations are extremely valuable in providing physical measurements of important processes. However, they can only inform us of the past and present, whereas climate modelling enables us to explore across longer timescales. Future projections allow for the estimation of long-term climate responses beyond the observational record, while full spatio-temporal coverage provides continuous three-dimensional fields across regions and depths where observations are sparse. With coupled models, the integration of model components also allows for research into coupled ocean, atmosphere, sea-ice and land processes for a holistic climate perspective. This allows us to improve our understanding of physical systems and is particularly vital for regions with strong ocean-ice-atmosphere coupling. Sensitivity experiments can also be run which facilitate controlled testing of responses to specific forcings (such as CO_2 emissions and freshwater input) and allow for more detailed analyses of interconnected feedback mechanisms (e.g. Sandø et al., 2010).

Given the significant benefits, climate modelling is often used to study variability and change in the Nordic Seas. For example, by using the global coupled Community Earth System Model (CESM), Årthun et al. (2019) show that continued Arctic winter sea-ice loss is tightly linked to increasing Atlantic heat transport into the Nordic Seas, highlighting the key role of Atlantification. Similarly, Onarheim and Årthun (2017) use a range of climate models (NorESM1, GFDL CM3, CESM and MPI-ESM) along with observational data to demonstrate that the Barents Sea is transitioning rapidly toward seasonal ice-free conditions, primarily due to increased Atlantic inflow and warming, while Smedsrud et al. (2022) use the Norwegian Earth System Model (NorESM) to provide a century-scale synthesis linking changes in Atlantic inflow and Nordic Seas heat loss to long-term Arctic sea-ice decline. They find that Nordic Seas heat loss dominates variability in the Arctic Ocean with Atlantic water volume and heat transport increasing over the last century with increased wind forcing and heat loss. They highlight the significance of this by showing that ocean heat transport anomalies in the Nordic Seas affect Greenland melting, sea-ice distribution and Arctic CO_2 uptake. Meanwhile, Asbjørnsen et al. (2021) use an eddy-permitting ocean model hindcast at 1/4° horizontal resolution and a Lagrangian analysis tool to demonstrate that decadal changes in Atlantic inflow to the Nordic Seas are driven by shifts in basin-scale North Atlantic circulation patterns, highlighting the importance of gyre dynamics and wind forcing in affecting the Nordic Seas inflow properties and volume transport. Together, these studies reinforce the significant value of considering the coupled system in the sub-polar latitudes, where atmosphere-ice-ocean interactions play an important role in local environmental variability. Furthermore, these results would be difficult to obtain from observational datasets alone, illustrating the value of climate model analysis in Nordic Seas research.

1.2.3 The HadGEM3 Model

In this project, to consider the changing climate in the Nordic Seas, we use the HadGEM3 global coupled model from the UK Met Office Hadley Centre, produced as part of CMIP6 (Roberts et al., 2019). This model has been shown to perform well in the sub-polar North Atlantic region, particularly at higher-resolutions, with a good representation of the AMOC (Jackson et al., 2020; Kuhlbrodt et al., 2018). Treguier et al. (2021) demonstrate that the high-resolution HadGEM3 simulations reproduce key spatial contrasts in the Nordic Seas, such as east-west differences in sea-ice cover and significant cooling of Atlantic Water as it transits the region. Barrell et al. (2023) show that the model simulates historic sea-ice and turbulent heat fluxes accurately, with improvements at higher resolution, while Andrews et al. (2020) find that historical changes in global mean surface temperature broadly follow the observed record, although there are some important quantitative differences, mostly due to strong effective radiative forcing from anthropogenic aerosols which also play a role in driving Atlantic multi-decadal variability and the AMOC (Marzocchi et al., 2021; Lozier, 2023). Overall the HadGEM3 simulations are thought to represent Arctic sea-ice change and variability well (Ridley et al., 2018; Treguier et al., 2021).

However, there are some caveats. Increasingly, studies point towards higher-resolution climate models being necessary for accurate representation, especially in the high-latitudes. For example, Treguier et al. (2021) use a high-resolution global model to show that eddy processes and recirculation strongly shape the Nordic Seas heat budget, improving agreement with observations compared to coarser models. Similarly, Wekerle et al. (2017) use a 1/12° mesh hindcast experiment to show that locally increasing grid resolution to eddy-permitting scales substantially improves the representation of Atlantic Water pathways and eddy activity in the Nordic Seas, which affects how much Atlantic heat reaches the Arctic. Studies by Treguier et al. (2021) and Bashmachnikov et al. (2023) also use 1/12° models to show that the representation of regional heat pathways and exchanges in the Nordic Seas is improved at this resolution, indicating that mesoscale eddies play an important role. In a multi-model HighResMIP study by Docquier et al. (2019), it is explicitly shown that the ocean resolution affects Arctic sea-ice and Atlantic ocean heat transport, while sea-ice biases in the medium-resolution HadGEM3 simulations are evaluated by Ridley et al. (2018) who show that the Arctic sea-ice seasonal cycle, extent and thickness/volume are broadly consistent with observational products (CryoSat-2 and PIOMAS). Menary et al. (2018) use the HadGEM3 control simulations to evaluate convection and ventilation in the North Atlantic and sub-polar regions, concluding that the high-resolution simulations show improvements in capturing multi-decadal variability in the Atlantic as well as AMOC depth and structure when compared to the medium-resolution simulations. This is seconded by Roberts et al. (2020) who demonstrate that the AMOC is better resolved in the 1/12° HadGEM3 simulations than the 1/4° simulations, along with Lai et al. (2022) who compare the Atlantic multi-decadal variability in the medium and low-resolution HadGEM3 simulations and find that ocean circulation changes are primarily driven by the North Atlantic Oscillation and salinity controlled subsurface density anomalies that persist in the sub-polar latitudes respectively.

Altogether, the literature suggests that the requirement for eddy-permitting ocean resolutions in climate models is crucial for a more realistic representation Atlantic water pathways and exchanges at Fram Strait, resulting in improved estimates of Arctic heat transport. High-resolution setups therefore give a more accurate picture of local processes (such as ocean mixing and eddy heat fluxes) which are vital for ocean dynamics in the Nordic Seas. Meanwhile the low-resolution simulations can underestimate Fram Strait transport and AMOC strength (Kuhlbrodt et al., 2018) but these are less computationally expensive and can still be useful for considering longer-run ensembles, large-scale forcing signals and statistic estimations of uncertainty. Residual biases in ocean stratification, mixed-layer depths and some seasonal heat exchanges are also known issues in the HadGEM3 simulations, even at higher-resolution, largely due to details of coupling, parameter choices and a relatively short spin-up period (Roberts et al., 2019). These problems are not uncommon. In fact Heuzé et al. (2019) synthesize observations and model results to show that many models struggle to capture the precise volume, pathways and variability of Atlantic inflow, with major implications for downstream Arctic conditions. However, as long as these issues are considered and adjusted for when analysing climate model output, valuable results can be obtained that vastly help to improve our understanding.

1.3 Scientific Motivation, Research Aims and Thesis Outline

The core aim of the research presented in this thesis is improved understanding of the Nordic Seas coupled climate system. The variability of interacting ocean-ice-atmosphere processes in this region plays a crucial role in the variability of the wider global environment, thus motivating detailed study of this high-latitude sub-polar domain. With anthropogenic forcing, there are dramatic changes being seen in the Nordic Seas and the need for mitigation is only increasing. Therefore, more accurate knowledge regarding the responses of the ocean, sea-ice and atmosphere to the changing climate is required.

By using a combination of observational datasets, reanalysis products and global coupled climate model output, we consider the past, present and future of the Nordic Seas. We focus on sea-ice variability (including a climatological study of a polynya feature near Fram Strait), changes in atmospheric forcing and the response of the ocean in terms of its structure, dynamics and interconnected feedback mechanisms. Natural variability is separated from changes driven by external forcing in both historical records and future projections in order to attribute the impact of anthropogenic climate change in detail.

The science presented in this thesis investigates coupled ocean-ice-atmosphere variability and change in the Nordic Seas in hopes of answering the following important questions:

- How is sea-ice in the Nordic Seas changing and what are the primary driving mechanisms? What are the local, regional and global-scale implications?
- What trends in ocean properties and dynamics are presently observed in the Nordic Seas? What do modelled future projections predict? Which of these responses are driven by anthropogenic forcing rather than natural variability?
- What are the wider-reaching implications of changes in the Nordic Seas climate system? How are ocean processes of dense water formation and overturning circulation predicted to respond in the future? What influence could this have on waters feeding into the Arctic Ocean and the AMOC?
- How accurate are the reanalysis products and climate simulations used in our analysis? How do model outputs of differing horizontal resolution compare? Are these datasets suitable for scientific analysis of the Nordic Seas coupled climate system in this context?

We begin by presenting an in-depth study of sea-ice in the Fram Strait region in Chapter 2, with a focus on the Northeast Water Polynya. In this chapter we analyse more than 40 years of reanalysis data to characterise the climatology of the polynya and ascertain its forcing mechanisms, considering both atmospheric and oceanic processes. We also assess the long-term changes to consider the impact of anthropogenic forcing on the Northeast Water Polynya. Some validation of the reanalysis products against other observational-based products is also provided.

In Chapter 3 we introduce the UK MetOffice's global coupled climate model HadGEM3, evaluating its output against satellite-based sea-ice products and ocean mooring data in the Nordic Seas. We consider the low, medium and high-resolution simulations and show that, although there are some minor limitations, the model is of high quality and accuracy, and thus suitable for our research (this is especially the case for the higher-resolution simulations).

We go on to present the results of the model analysis in Chapter 4, where we describe the historical record and future projections from a range of HadGEM3 simulations. The model demonstrates significant responses in sea-ice concentration, near-surface atmosphere diagnostics and upper-ocean dynamics, particularly along the East Greenland Current. Many of these changes are driven by anthropogenic forcing.

The ocean response to the changing climate is further investigated in Chapter 5. In this chapter we focus on the high-resolution HadGEM3 model to consider changes in dense water formation and overturning circulation in the Nordic Seas in significant detail. We consider the responses in gyre dynamics, volume transports and freshwater fluxes with an aim to ascertain the future impact of changes in the Nordic Seas on the AMOC and thus the wider climate system.

Finally, a thesis overview and discussion of the conclusions are given in Chapter 6, along with some ideas for future work.

In summary, the body of work presented here aims to describe the climatology and variability of the Nordic Seas coupled system and assess the response to anthropogenically-forced environmental shifts. We consider the wider-scale impacts of ocean-ice-atmosphere transformation in this important region in the hopes of highlighting its significance and informing future mitigation of extreme climate change.

The Northeast Water Polynya, Greenland: Climatology, Atmospheric Forcing and Ocean Response

2.1 Synopsis

This study was published in May 2024 in the Journal of Geophysical Research: Oceans. The publication has the same title as this chapter and the authors are Miriam G. Bennett, Ian A. Renfrew, David P. Stevens and G. W. K. Moore. The text in this chapter is unchanged compared with the article (Bennett et al., 2024). Miriam G. Bennett was responsible for the work, under supervision by Ian A. Renfrew and David P. Stevens at the University of East Anglia and G. W. K. Moore at the University of Toronto, all of whom provided valuable scientific input and helped revise the text for publication. The comments of three anonymous reviewers also helped to improve the manuscript. The abstract and appendix of the study are included in this chapter.

2.2 Abstract

The Northeast Water Polynya is a significant annually recurring summertime Arctic polynya, located off the coast of Northeast Greenland. It is important for marine wildlife and affects local atmospheric and oceanic processes. In this study, over 40 years of observational and reanalysis products (ERA5 and ORAS5) are analysed to characterise the polynya's climatology and ascertain forcing mechanisms. The Northeast Water Polynya has high spatiotemporal variability; its location, size and structure vary interannually, and the period for which it is open is changing. We show this variability is largely driven by atmospheric forcing. The polynya extent is determined by the direction of the near-surface flow regime, and the relative locations of high and low sea-level pressure centers over the region. The surface conditions also impact the oceanic water column, which has a strong seasonal cycle in potential temperature and salinity, the amplitude of which decreases with depth. The ocean reanalyses also show a significant warming trend at all depths and a freshening near the surface consistent with greater ice melt, but salinification at lower depths ($\sim$ 200 m). As the Arctic region changes due to anthropogenic forcing, the sea-ice edge is migrating northwards and the Northeast Water Polynya is generally opening earlier and closing later in the year. This could have significant implications for both the atmosphere and ocean in this complex and rapidly changing environment.

2.3 Introduction

The Northeast Water (NEW) Polynya is an important sea ice feature of the Arctic. A region of open water, surrounded by sea ice, it is situated to the Northwest of Fram Strait, over the Ob Bank continental shelf, off the coast of the Nørdoststrundingen headland of Northeast Greenland (Figure 2.1). Its centre is often located between longitudes of 5°W and 15°W and latitudes of 77°N and 81°N (Barber and Massom, 2007), but the shape and position of the polynya varies on seasonal, interannual and decadal time scales. It has a maximum areal extent of approximately 44,000 km^2 (Barber and Massom, 2007) and plays an important role in summertime atmosphere-ocean interaction for the northern European Arctic (Deming, 1993). In previous literature it has been described as a stable, annually recurring polynya that forms as a result of ice barriers both to the north and south that limit heavy ice intrusion, coupled with strong and persistent northerly winds advecting sea-ice away from the coast (e.g. Barber and Massom (2007); Tamura and Ohshima (2011); Speer et al. (2017)). However, there has been little observational evidence to confirm these descriptions, particularly in more recent years, and with the climate of the Arctic quickly changing due to anthropogenic forcing, this study aims to provide a first comprehensive climatology of the NEW Polynya, and examine its drivers and its evolution over the last few decades.

The NEW Polynya develops during most summer seasons, to various extents, and is considered one of the largest and most consistently recurring polynyas of the Arctic summer, thus having a significant impact on local atmospheric, oceanographic and biological processes (Deming, 1993). It is known to be a site of elevated biological activity and to support many Arctic species, including the critically endangered Spitsbergen stock of bowhead whale (Speer et al., 2017). The polynya is also the most important calving area for the northeast Greenland stock of walrus, and supports the largest known breeding colony of ivory gulls in Greenland (Speer et al., 2017). Given its importance for marine wildlife, many of the published studies on this polynya focus on its ecological characteristics rather than the environmental physics of the region. However, polynyas of this size and frequency can have significant impacts on local atmospheric dynamics, oceanic processes and the climate system more broadly (Barber and Massom, 2007). For example, polynyas can drive dense-water formation (e.g. Martin and Cavalieri (1989); Ohshima et al. (2016)), act as carbon sinks (e.g. Yager et al. (1995)) and increase rates of cloud formation (e.g. Dare and Atkinson (2000); Morales Maqueda et al. (2004); Monroe et al. (2021)). Polynyas can have a significant effect on atmospheric mesoscale motion, by releasing heat from the ocean to the atmosphere at a rate of one to two orders of magnitude greater than occurs with thick ice cover, leading to convective cells or circulation features (Maykut, 1982; Kottmeier and Engelbart, 1992). Additionally, polynyas are crucial to the production of new sea-ice, often being referred to as “sea-ice factories". The NEW Polynya is considered a relatively productive polynya for its size and has been

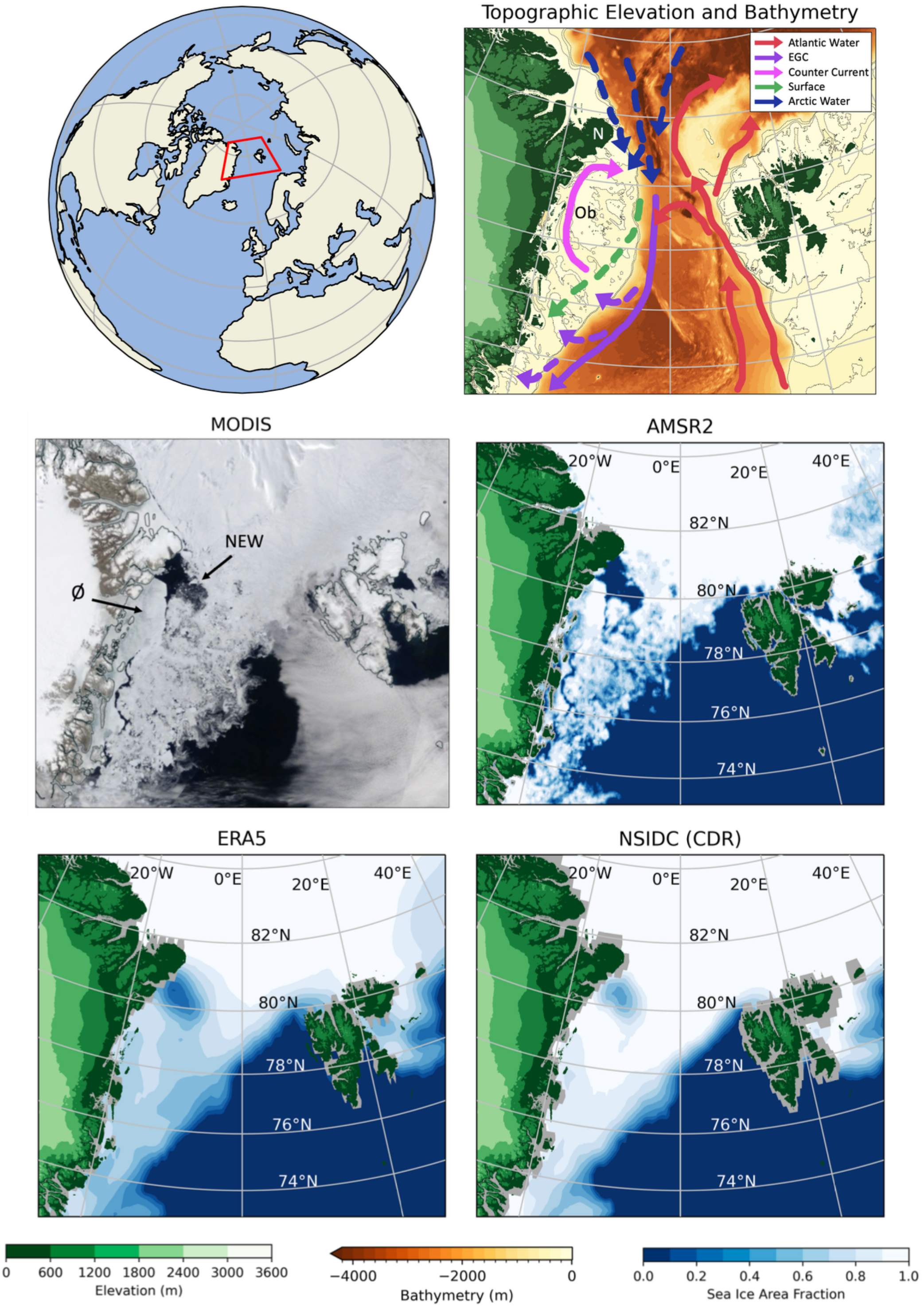

Figure 2.1: The region of interest has complex bathymetry and ocean circulation as illustrated in the upper right panel which shows the GEBCO product for bathymetry and the STRM30 product for topographic elevation. The major known and hypothesized currents are represented schematically by the solid and dashed arrows respectively. The Ob Bank (Ob) and Nørdoststrundingen headland (N) are labelled. Additionally, we show the NEW Polynya on June 21st 2020 as visualised by NASAs MODIS (Moderate Resolution Imaging Spectroradiometer) instrument (center left panel), and the equivalent daily sea-ice product from AMSR2, ERA5 and NSIDC (center right, lower left and lower right panels). The STRM30 topography is also shown here. The polynya (NEW) and Norske Øer Ice Barrier (Ø) are indicated in the MODIS Satellite image. The region of interest is highlighted in red in the upper left panel.

estimated to produce approximately 136 km^3 of sea-ice each year (Tamura and Ohshima, 2011; Iwamoto et al., 2014). As sea-ice declines throughout the Arctic, indigenous communities are facing challenges to their traditional ways of life, while new opportunities open for shipping, fishing, tourism and natural resource extraction (Meier et al., 2014). With the rising presence of human activity in this region, the requirement for improved understanding and accurate monitoring of the atmosphere, ocean and sea-ice continues to grow.

Polynyas are usually classified as being driven by either latent or sensible heat processes. Latent heat polynyas form due to divergent ice motion as a result of the prevailing winds and/or ocean currents, whereas, sensible heat polynyas develop due to high surface ocean heat fluxes (e.g. Morales Maqueda et al. (2004); Hirano et al. (2014)). The NEW Polynya demonstrates elements of both latent and sensible heat polynya processes (Barber and Massom, 2007), and thus is not easily classified according to the traditional characteristics of polynya categorisation. In previous studies (e.g. Budéus and Schneider (1995); Barber and Massom (2007); Smith Jr and Barber (2007)) the exact driving mechanisms for the formation of the NEW Polynya are ambiguous and explanations are largely speculative, mostly due to a lack of in-situ observational data. The intricate oceanography in this region adds to the uncertainty. The bathymetry of the Greenland Sea and Fram Strait varies dramatically, with depths of over 5000 m recorded in the deepest area to the west of Svalbard, known as the Molloy Deep, and in contrast, depths of just 200 m seen on the East Greenland continental shelf, known as the Ob Bank (Klenke and Schenke, 2002) (Figure 2.1). There is also a complex pattern of ocean currents, with various structures and properties, such as the West Spitsbergen Current (e.g. Moore et al. (2022)), East Greenland Current (e.g. Holliday et al. (2007); Sutherland and Pickart (2008); Jeansson et al. (2008)) and Return Atlantic Current (e.g. Rudels and Friedrich (2000); Schauer et al. (2004)). Additionally, there are more recently identified features on the continental shelf, such as the North East Greenland Coastal Counter Current (Figure 2.1) which is thought to show a seasonal cycle of variability, with northward flow in summer and southward flow in winter (Karpouzoglou et al., 2023). Many of these oceanic flow features are important in forming the high latitude branches of the global thermohaline circulation system (e.g. Weer et al. (2022); Moore et al. (2022)). Furthermore, the large annual variability of freshwater influx from the Greenland Ice Sheet plays a role in the oceanic structure here (Sejr et al., 2017) and further complicates the coupling between the atmosphere and the ocean.

Although having been identified as early as 1935 (Koch, 1935), given its remote nature, the NEW Polynya was not easily observed for some time. Following a research cruise in 1993, there were several publications. For example, Budéus and Schneider (1995) focus on the hydrography of the polynya, using observational data from buoys, and conclude that its formation is not driven by processes typical of either a latent heat nor a sensible heat polynya. The high interannual variability of the NEW polynya has been referred to in several studies (Deming, 1993; Böhm et al., 1997; Barber and Massom, 2007), although further details, and a more recent update, would be beneficial. While the interaction of the northward coastal current with the Norske Øer Ice Barrier to the west is thought to be a major factor in creating the NEW Polynya, it cannot be termed a pure latent heat polynya, as a balance between freezing rate and ice export is not present (Budéus and Schneider, 1995); while it cannot be a pure sensible heat polynya as melt alone is not the driver (Barber and Massom, 2007). Additionally, the grounding of deep-draft icebergs can prevent ice advection into the polynya from the north, leading to its expansion (Barber and Massom, 2007). At present, the dominant driving mechanisms of the NEW Polynya remain unclear.

Despite its importance for the wider Arctic and proximity to the fast changing ice edge, little is known of the physical processes leading to the development, maintenance and variability of the NEW Polynya. The spatial and temporal variability of its annual formation and closure are also undocumented. With significant improvements in both satellite measurements and reanalysis products in recent years, there is now the opportunity to comprehensively characterise this polynya. This study aims to:

- Develop a climatology of the NEW Polynya; documenting where and when it develops and characterising its variability.
- Determine what drives the formation, maintenance and variability of the NEW Polynya; for example, is it largely a result of atmospheric or oceanic forcing?
- Determine how the NEW Polynya has changed over the last few decades.
- Discuss how the NEW Polynya might continue to evolve under the changing climate and what implications this might have for other aspects of the Arctic environment.

2.4 Data

We use the ECMWF reanalysis products ERA5 and ORAS5 to examine near surface atmospheric and oceanic variables in the vicinity of the NEW Polynya.

ERA5 is the fifth generation ECMWF meteorological reanalysis (Hersbach et al., 2020). It has global coverage on a horizontal grid of approximately 31 km and has 137 vertical levels. It uses the Integrated Forecasting System (IFS Cycle 41r2). We use daily and monthly-mean output from 1980 to 2022, so starting when satellite observations of sea-ice area became routine. The evolution of sea-ice cover in ERA5 is based on a number of products over different periods of time (Hersbach et al., 2020). The UK MetOffices Operational Sea-surface Temperature and sea-ice Analysis (OSTIA) dataset is used from September 2007 to present, and this uses the EUMETSAT Ocean and sea-ice Satellite Applications Facility (OSI-SAF) 401 dataset for sea-ice concentration (Donlon et al., 2012). OSTIA provides daily updated SST and sea-ice fields, primarily sourced from infra-red and microwave satellite observations, with a horizontal resolution of approximately 0.05° (Hersbach et al., 2020; Eastwood et al., 2014; Good et al., 2020). Prior to this, between January 1979 and August 2007, the Met Office Hadley Centre HadISST2 sea-ice product was used, which had a horizontal grid of 1/4° (Titchner and Rayner, 2014) and was primarily derived from the Global Sea Ice Concentration daily data record (OSI-409a) produced by EUMETSATs OSI-SAF. ERA5 generally compares well to surface-layer meteorological observations in the Nordic Seas and in the vicinity of the sea-ice edge (e.g. Renfrew et al. (2021)), and has previously been used to study polynyas (e.g. Ding et al. (2020)).

ORAS5 is ECMWF's OCEAN5 global eddy-permitting ocean-sea-ice ensemble reanalysis system. It estimates the state of the global ocean and comprises a Behind-Real-Time component, which provides an estimate of the historical ocean state from 1979 to near present-day, and a Real-Time component, that provides the latest ocean conditions (Zuo et al., 2019). ORAS5 has global coverage with a horizontal resolution of 1/4° and 75 depth levels. We use 43 years of monthly averages of potential temperature, ocean salinity and velocity components. OCEAN5 is based on the NEMO ocean model (version 3.4.1) coupled to the LIM2 sea-ice model (the Louvain-la-Neuve sea-ice model version 2), in global configuration ORCA025.L75 (Zuo et al., 2019). Observations are assimilated through the NEMOVAR data assimilation system. This ocean reanalysis product was partly chosen to ensure consistency at the ocean surface, i.e. for sea-surface temperature, sea-ice distribution and near-surface atmospheric variables.

Where possible, results from reanalyses are compared to observational datasets, such as oceanographic profiles (see Figures 2.16 and 2.17 in Appendix A). The ERA5 sea-ice is also compared to the University of Bremen AMSR (Advanced Scanning Microwave Radiometer) and the National Snow and Ice Data Center (NSIDC) Climate Data Record (CDR) products which are available from mid-2002 (Spreen et al., 2008) and late-1978 respectively (see Figure 2.14 in Appendix A).

The Bremen product uses AMSRE data between May 2002 and December 2011, and AMSR2 from May 2012 onwards (Ludwig et al., 2020). The NSIDC product is from Scanning Multichannel Microwave Radiometer (SMMR) instruments and Special Sensor Microwave/Imager and Special Sensor Microwave Imager/Sounder (SSM/I-SSMIS) passive microwave data. The CDR algorithm output is a rule-based combination of ice concentration estimates from two well-established algorithms: the NASA Team algorithm (Cavalieri et al., 1984) and NASA Bootstrap algorithm (Comiso, 1986).

In general, there is good agreement across the sea-ice products, but the ERA5 and NSIDC products exhibit significantly more smoothing than the AMSR products, often overestimating sea-ice area fraction in the polynya region and the area of the marginal ice zone, which in reality has a more concise transition at the ice edge (e.g. Renfrew et al. (2021)). This can be seen in Figure 2.1, for example. Although relying solely on reanalyses has its limitations, given the lack of available observational datasets for this region and the aims of this study, we argue that its use is appropriate, particularly for considering long-term trends, variability and forcing mechanisms.

2.5 Results

2.5.1 Climatological Overview of the Northeast Water Polynya

The NEW Polynya generally develops in mid-June and remains open until the beginning of late-September, with its maximum extent peaking in August. Figure 2.2 shows a seasonal mean climatology from 1980 to 2022 from ERA5 reanalysis products, with the sea-ice area fraction, mean-sea-level pressure (MSLP) and 10 m winds. It is clear that there is little variation in the MSLP and near-surface wind fields over the autumn, winter and spring seasons, with a consistent pressure gradient across Fram Strait; high MSLP to the northwest over Northeast Greenland and lower pressure to the southeast, driving a relatively strong northerly atmospheric flow across the open ocean waters of the Greenland Sea (e.g. Van Angelen et al. (2011)). Although the position and shape of the sea-ice edge across Fram Strait is similar in these three seasons, there is some variation in the sea-ice cover, with a marginally lower area fraction in the vicinity of the NEW Polynya in spring and autumn, compared to winter. There is also lower sea-ice area fraction to the north and west of Svalbard in autumn than in winter and spring.

In summer the situation is quite different. The polynya is evident as an area of reduced sea-ice fraction near the coast of Northeast Greenland, with the Norske Øer land fast ice barrier to the west and the sea-ice edge to the southeast. There is almost no gradient in MSLP and consequently there is a collapse of the northerly flow regime seen in the other three seasons. Across the Greenland Sea the 10 m winds are weak and in some areas they are completely reversed in direction, with a southerly flow regime and increased directional divergence over the site of the NEW Polynya. Throughout the year there remains strong orographic winds in Northeast Greenland with the steep and complex terrain forcing numerous katabatic and barrier flows (Moore and Renfrew, 2005; Mattingly et al., 2023). These orographic flows show little seasonal variability (Figure 2.2). There appears to be an element of offshore flow near the NEW Polynya and the Norske Øer ice barrier which is more prominent in the summer months, when the northerly flow regime is weaker.

Figure 2.3 shows that the mean August ERA5 sea-ice area fraction differs significantly each year, with the location, structure and extent of the NEW Polynya changing dramatically. In the majority of years the NEW Polynya is coastal and seems to be located either to the south or east of the Nørdoststrundingen headland of Northeast Greenland. However, in some years it develops further offshore (for example, in 1982, 2003, 2005, 2014, 2019 and 2022); while in other years, particularly where there has been a large northward retreat of the sea-ice edge, the polynya merges with the open ocean (for example, in 2004, 2010, 2016, 2017, 2018 and 2021). The fact that this occurs more in recent years, suggests it is a feature of Arctic summertime sea-ice retreat. The significant interannual variability

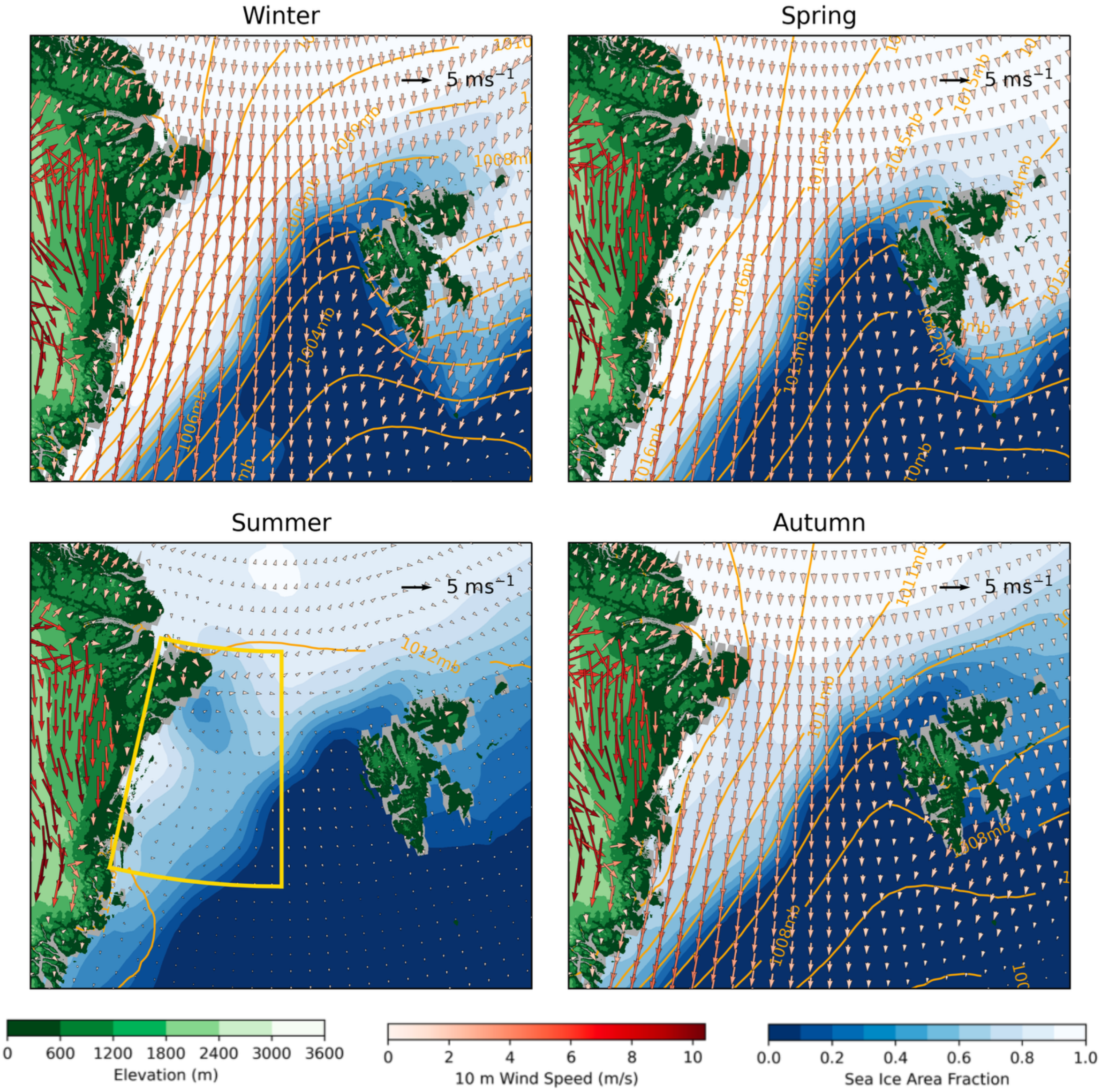

Figure 2.2: Mean Winter (DJF), Spring (MAM), Summer (JJA) and Autumn (SON) climatology from 43 years of ERA5 products from 1980 to 2022 inclusively, showing sea-ice area fraction, 10 m winds and mean sea-level pressure contours (every millibar). The STRM30 topography is shown in green. The yellow box shows the area used for spatial averages over the NEW Polynya.

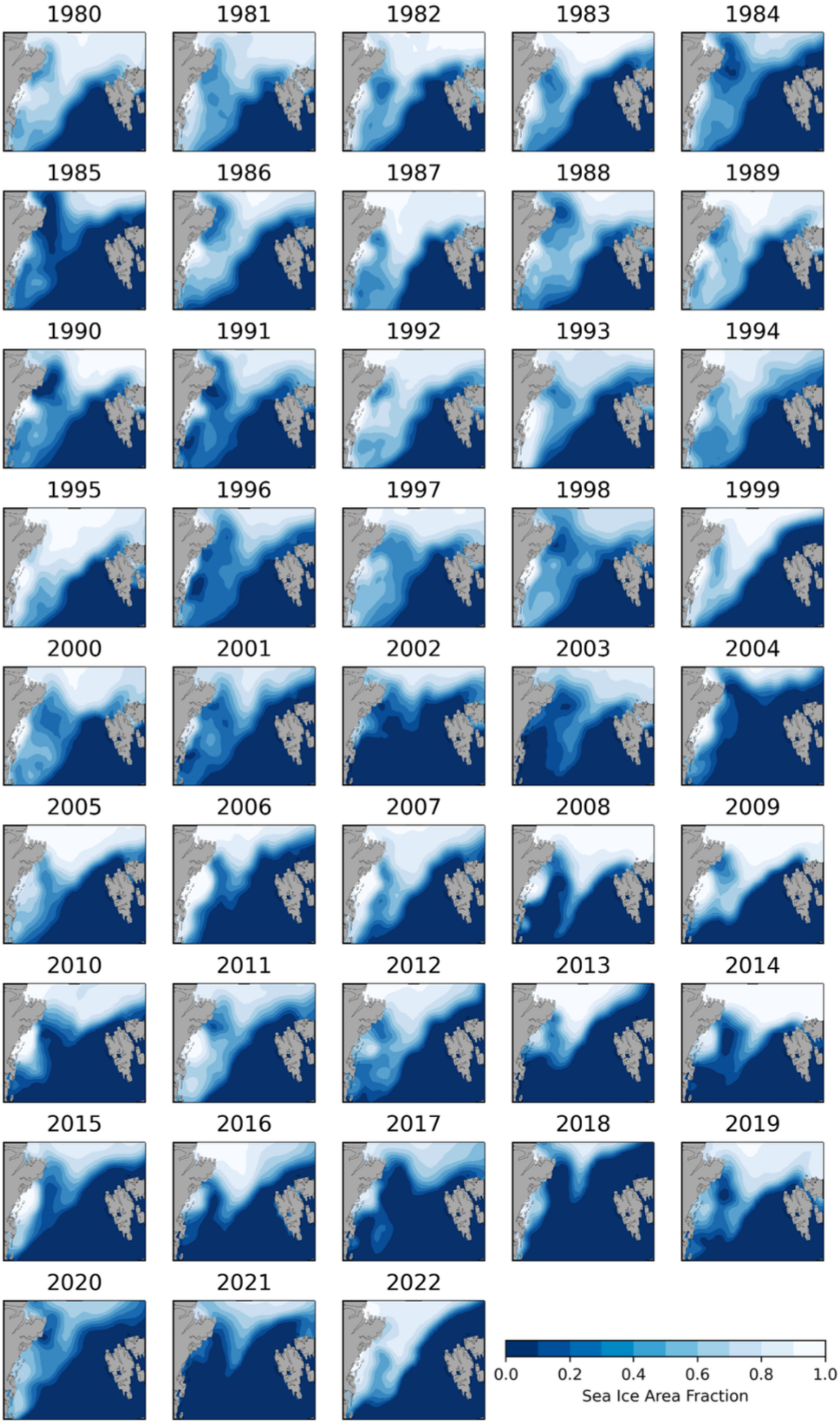

Figure 2.3: Interannual variability of the NEW Polynya, illustrated with mean August sea-ice area fraction between 1980 and 2022 from ERA5.

indicates that the driving mechanisms of the NEW Polynya are complex and changeable on an annual timescale.

Figure 2.4 (upper left panel) shows the annual frequency of 10 m winds in excess of 10 ms^{-1} for the same domain using monthly averages. The frequency is expressed as a percentage, calculated by taking the number of months where the monthly mean wind speed in the box exceeds 10 ms^{-1}, divided by the total number of months considered (516 for the annual period and 129 for the summer period), then multiplied by 100. As illustrated by the red shading there are strong winds relatively regularly in the location of the NEW Polynya, with an area of darker red (between 20% and 25%) to the east of Northeast Greenland. This correlation between a region of frequent high speed winds and the site of the NEW Polynya suggests a connection between the sea-ice distribution at the surface and the low-level wind speed. In summer, a similar area of relatively higher frequency of strong winds (6% to 8%) is shown to the north of the location of the NEW Polynya, while much of the Fram Strait and East Greenland continental shelf region shows very low frequencies ($< 2\%$), see Figure 2.4 (lower left panel). This highlights the significantly reduced 10 m wind speeds during the summer months, compared to the rest of the year, particularly along the marginal ice zone.

Figure 2.4 also shows the directional constancy (DC). This is calculated using Equation (2.5.1) and monthly-averaged 10 m zonal (u) and meridional (v) wind field components.

$$DC = \frac{\overline{u}^2 + \overline{v}^2}{\overline{u^2 + v^2}} \tag{2.5.1}$$

The directional constancy is a useful diagnostic measure of persistence in the wind field with values of more than 0.85 only occurring in regions subject to strong katabatic flows or persistent jets (Moore and Renfrew, 2005; Harden et al., 2011). It is clear that there is relatively strong directional constancy over much of Fram Strait compared to the open ocean further south. Above the NEW Polynya region there are values of approximately 0.5 to 0.6 in the same area as the higher frequency high wind speeds. Again, the co-location of these features implies persistent wind forcing of the sea-ice in the location of the NEW Polynya. The same plot for only the summer months of the year shows a reduction in this directional constancy over much of the region, including the location of the NEW Polynya. Much of the Greenland Sea has a directional constancy of less than 0.1, with only a small area of between 0.4 and 0.5 seen off the coast of the Nørdoststrundingen headland just north of the polynya site. This highlights that there are much more variable near-surface winds in summer.

The annual cycle of the NEW Polynya region is summarised in Figures 2.5 and 2.6, using spatially-averaged variables (averaged over the yellow box in Figure 2.2). Figure 2.5 illustrates the annual reduction in sea-ice from approximately mid-June to mid-October, with minima in August or September. This is mirrored by a noticeable increase in the 2

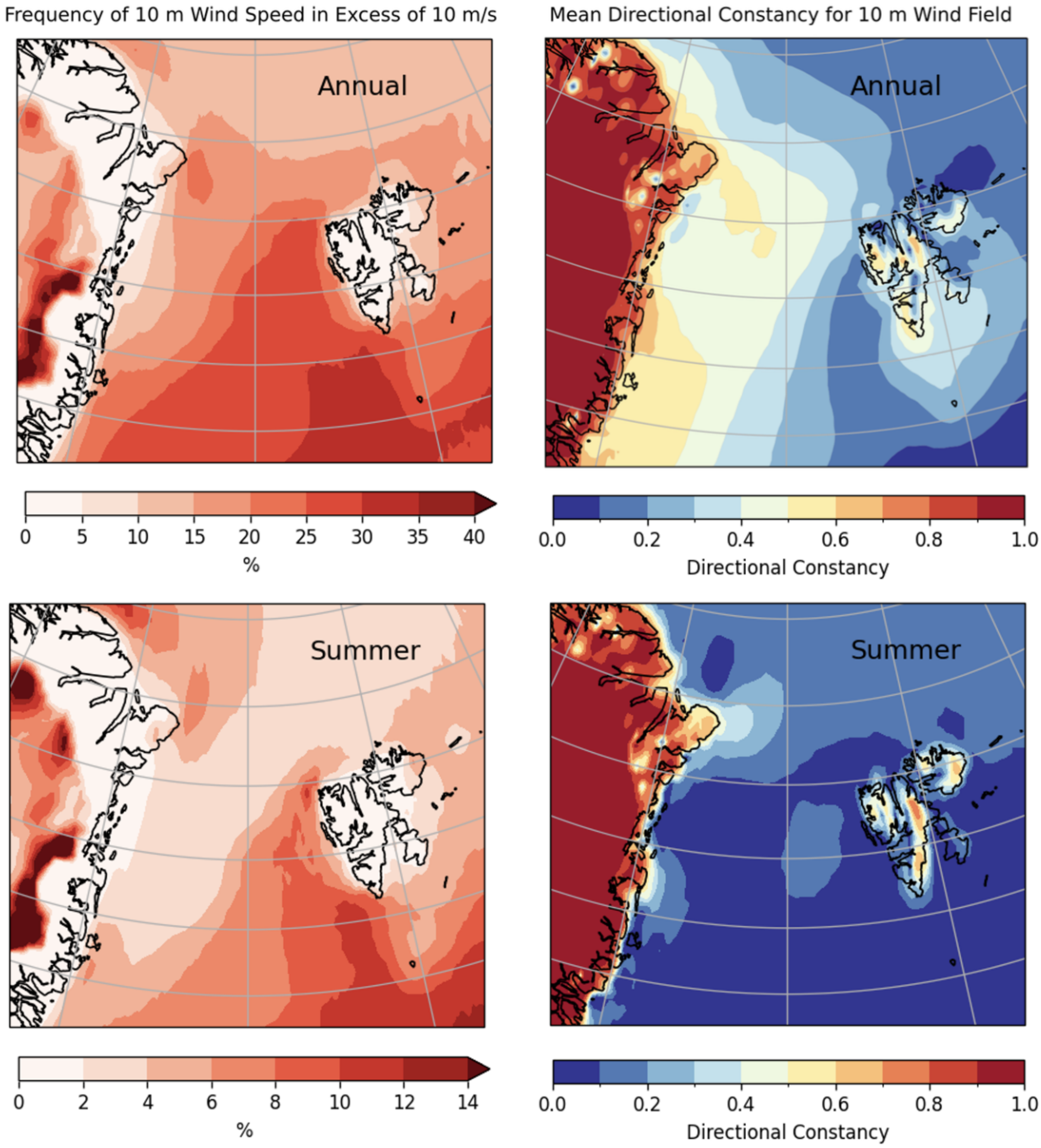

Figure 2.4: Frequency of 10 m winds in excess of 10 ms^{-1} (left column) and mean directional constancy (right column). The upper panels show results for all year and the lower panels show results for the summer months only (JJA).

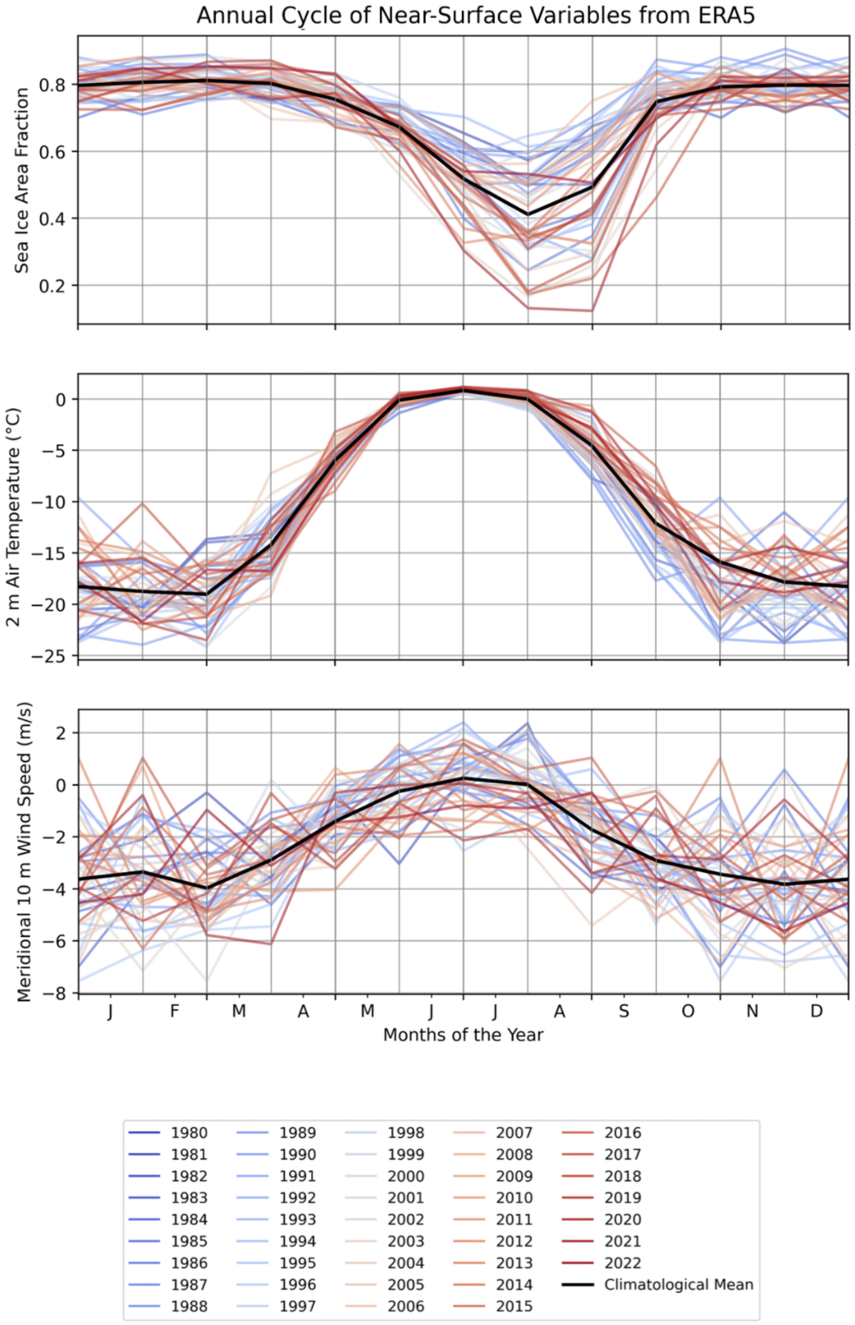

Figure 2.5: Annual cycle of monthly averaged sea-ice area fraction, 2 m temperature and 10 m meridional wind speed from ERA5 for each year between 1980 and 2022 (spatially averaged over the yellow box shown in Figure 2.2). The blue-to-red shading indicates the long-term trend. The black line represents the mean from all 43 years.

m air temperature between April and October, with a wide peak over June and July. The lag between the annual 2 m air temperature increase and the sea-ice reduction implies that the atmosphere is warming before the summertime reduction in sea-ice, rather than the sea-ice reducing and then near-surface temperatures increasing. The 10 m meridional winds (positive values indicate a southerly flow, negative values indicate a northerly flow) show a cycle of annual variability, with stronger northerly flow in the winter months and a weaker, occasionally southerly, flow in the summer months.

The evolution in time (indicated by the blue to red lines in Figures 2.5 and 2.6) illustrates a general long-term trend of sea-ice decline and increasing temperatures in this region. There appears to be no significant long-term trend in the meridional wind speeds since 1980, although there is considerable variability throughout the year and between years.

To consider the variability of the ocean beneath the polynya, monthly averages of potential temperature and salinity from ORAS5 are shown at depths of approximately 0.5 m, 20 m and 200 m (Figure 2.6). There is a clear annual cycle in the upper ocean with a near-surface potential temperature maximum and an ocean salinity minimum seen in approximately August and mid-July at 0.5 m and in August and October at 20 m, showing the influence of the surface variability on the ocean properties. The amplitude of the seasonal cycle decreases with increasing depth. At a depth of 200 m the annual cycle is less pronounced but still evident (more so with potential temperature than salinity). The fact that there is a lag in the cycle with depth implies that surface forcing of the ocean dominates over oceanic forcing of the surface. In spring, ice melts at the surface, freshening the uppermost layer of the water column and exposing it to solar radiation and warmer air temperatures. As mixing occurs the relatively warm, fresh water is mixed down so the potential temperature increases and the salinity decreases. The lags in ocean warming and freshening with depth therefore imply surface forcing.

Over these four decades, a significant ocean warming is evident at all depths. In addition, there is a decrease in salinity in the upper two depth levels of 0.5 m and 20 m, but an increase in salinity at 200 m depth. These changes are a result of anthropogenically forced warming and increased ice melt at the surface, combined with an increased flux of warmer and more saline Atlantic Water to this area via the West Spitsbergen Current (which is thought to be located at a depth of approximately 250 m in this region; Asbjørnsen et al., 2020; Tesi et al., 2021); they illustrate the “Atlantification of the Arctic" (Polyakov et al., 2017)). The NEW Polynya sees both of these climatic drivers.

2.5.2 Composite Analysis Indicates Atmospheric Forcing and Oceanic Response

In order to further assess the mechanisms that lead to the annual formation and maintenance of the NEW Polynya, a composite analysis has been applied, based on the upper and lower quartile of minimum August sea-ice area fraction. From 43 years of daily ERA5

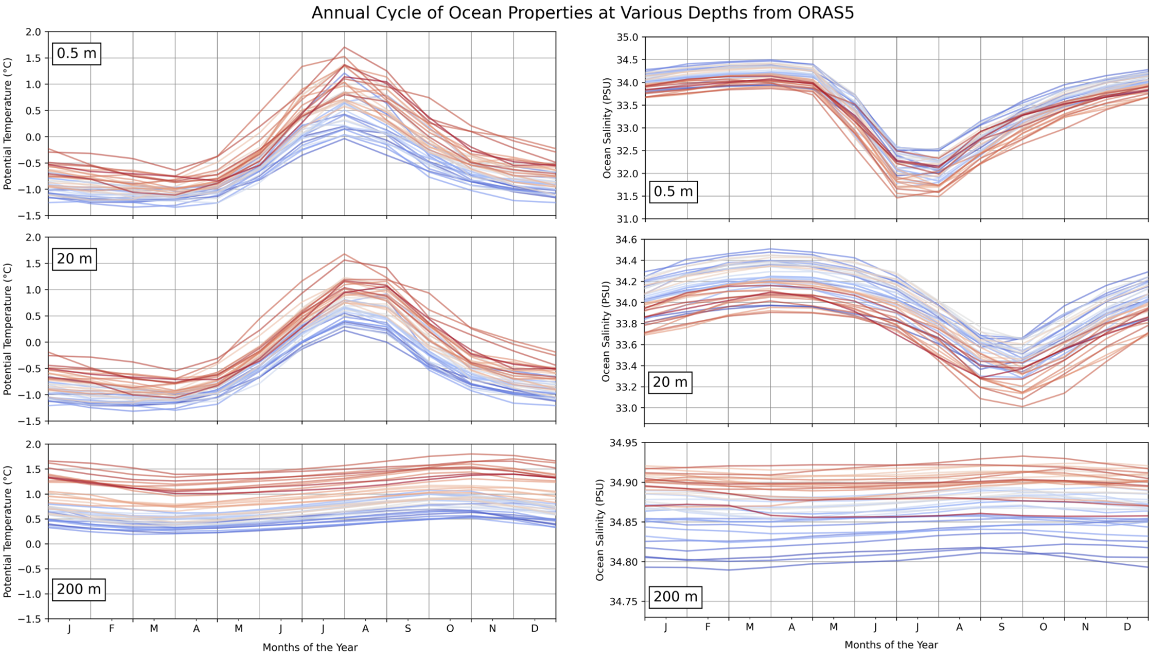

Figure 2.6: Annual cycle of potential temperature and ocean salinity at various depths from ORAS5 for each year between 1980 and 2022 (spatially averaged over the yellow box shown in Figure 2.2). The depths shown have been rounded for clarity. The true depth values are 0.5058 m, 19.43 m and 199.80 m. The blue-to-red shading indicates the long-term trend, see legend in Figure 2.5.

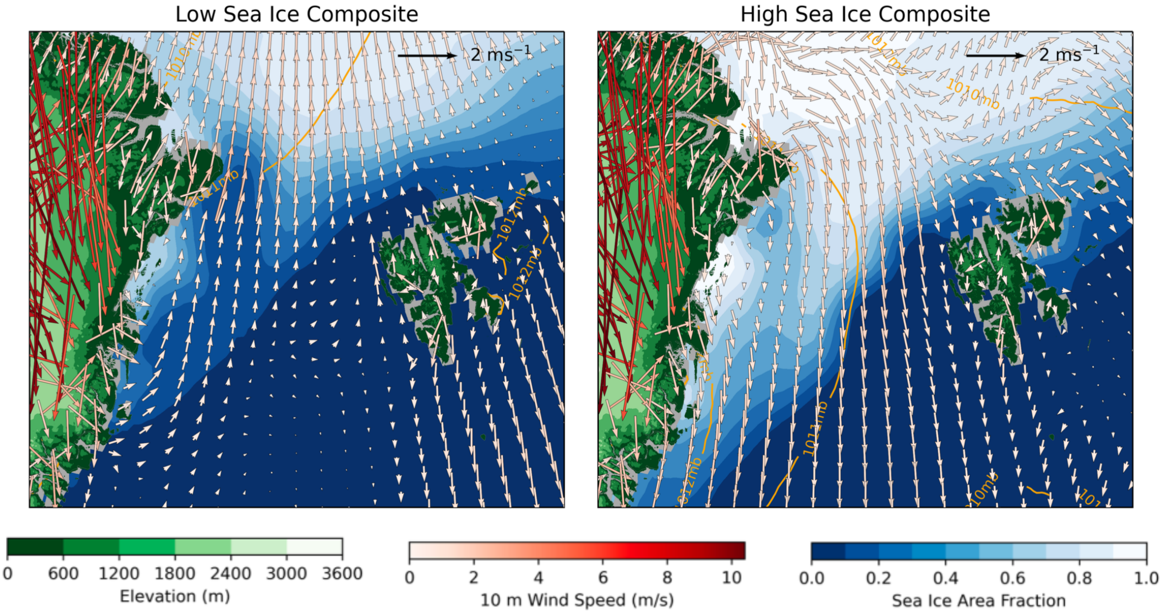

Figure 2.7: Composite mean August climatology from ERA5 using the 10 years with the highest and lowest sea-ice concentrations, respectively. The ERA5 sea-ice area fraction, 10 m winds and mean sea-level pressure fields are shown, and the STRM30 topography, as in Figure 2.2.

reanalysis products (see Figure 2.14 in Appendix A), the ten Augusts with the highest and lowest mean sea-ice area fraction in the NEW Polynya region (yellow box shown in Figure 2.2) were used to compile composite means (Figure 2.7). The ten high sea-ice years are 1980, 1982, 1987, 1989, 1992, 1994, 1995, 1999, 2007 and 2009, and the ten low sea-ice years are 1984, 1985, 1990, 1996, 2002, 2003, 2004, 2017, 2018 and 2020.

The size, shape and location of the polynya is different in each of the composite plots (Figure 2.7). The 10 m winds also show contrasting characteristics. In the high sea-ice composite, the wind field has uniform northerly flow of approximately 1 ms^{-1} over the Fram Strait region, while, in the low sea-ice composite the wind over the ocean is from the south at approximately 0.5 ms^{-1} and is more variable in direction. This stark contrast in the near-surface flow regime suggests a strong coupling between the 10 m wind field and the extent of the NEW Polynya at its maximum in August. It suggests the atmospheric flows are dictating the polynya's development. The MSLP field is weak in both composite climatologies.

To consider dynamical ocean forcing of the polynya we also look at ocean velocities in ORAS5 for the low and high sea-ice composites. Figure 2.8 shows the ERA5 sea-ice area fraction and the ORAS5 ocean velocities at depths of 0.5 m and 200 m for each composite. The East Greenland Current and West Spitsbergen Current can be seen in all panels. The high sea-ice composite shows stronger ocean velocities over much of the region north of Fram Strait, flowing southwards into the East Greenland Current. This is particularly evident near the surface but can also be seen at 20 m (not shown) and 200 m. At the site of the polynya, the low sea-ice composite shows stronger ocean velocities flowing eastward from the coast of Northeast Greenland, approximately along the pathway of the East Greenland Coastal Counter Current. The differences between the low and high sea-ice composites decrease with depth, indicating surface forcing, most likely by the near-surface winds in areas of reduced sea-ice cover. This is also illustrated in Figure 2.9 which shows the composite difference (low minus high sea-ice composite). There is little difference in the ocean velocities at 200 m depth and only small differences at 20 m (not shown). The clearest difference is at 0.5 m depth, where much of the region shows a stronger northward flow (or reduced southward flow) in the low sea-ice composite compared to the high sea-ice composite. This reflects results seen in Figure 2.7 which highlight a southerly wind regime for the low sea-ice composite in ERA5, and supports the hypothesis that atmospheric forcing largely controls the sea-ice distribution in the area of NEW Polynya.

In order to better understand the atmospheric forcing here, the MSLP field for the whole Arctic region for these composite months is considered. Figure 2.10 shows the difference between the mean July and August MSLP for the low and high sea-ice composites, calculated by taking the low sea-ice composite minus the high sea-ice composite, so the negative values (turquoise) indicate lower pressure and the positive values (brown) indicate higher pressure for years with lower summer sea-ice area fraction and a larger NEW Polynya extent. The pattern indicates enhanced southerly atmospheric flow over

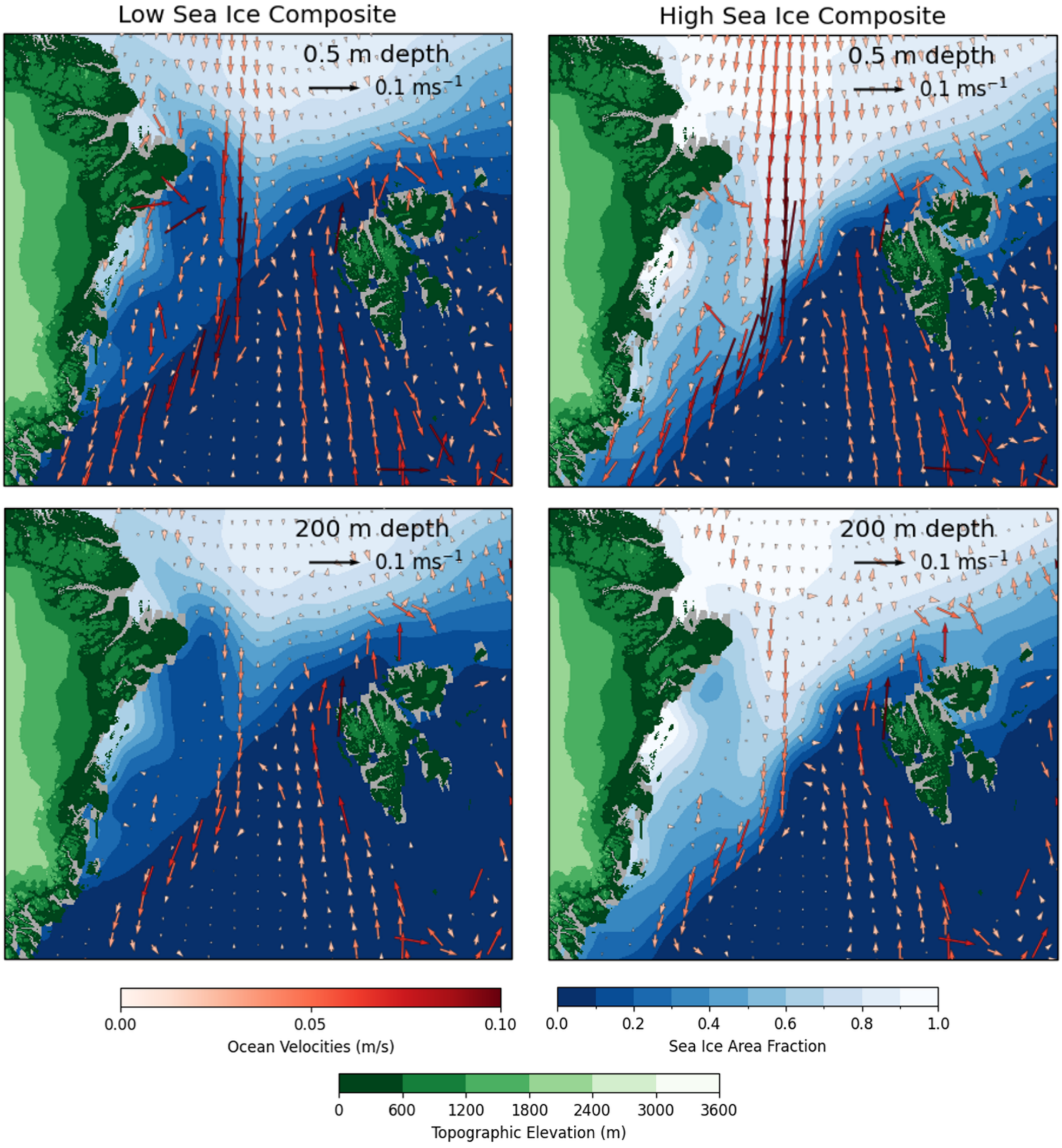

Figure 2.8: Composite mean August climatology using the 10 years with the highest and lowest sea-ice concentrations, respectively. The ERA5 sea-ice area fraction, the STRM30 topography and the ORAS5 ocean velocities at depths of approximately 0.5 m (upper row) and 200 m (lower row) are shown.

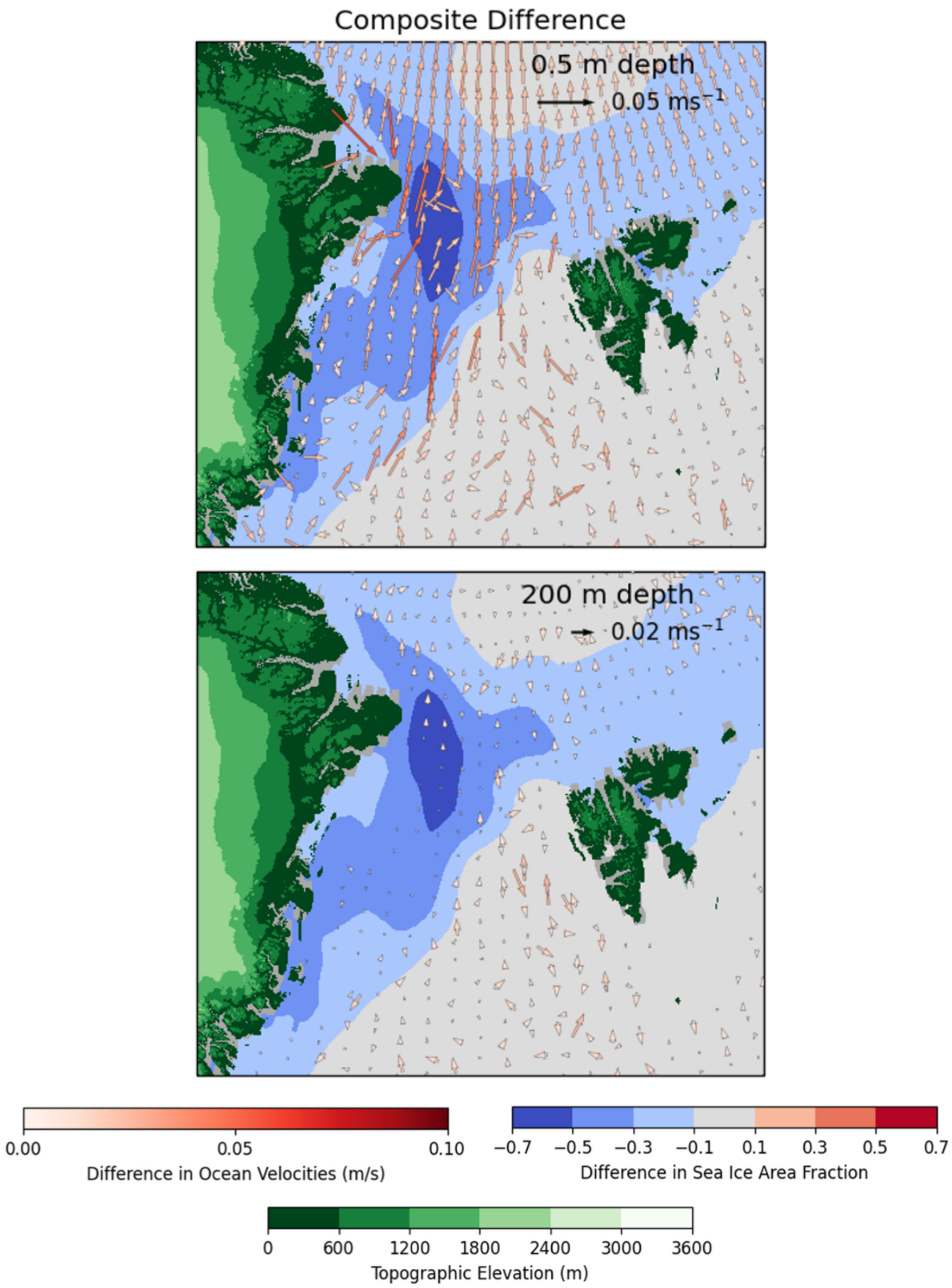

Figure 2.9: The difference between the low and high sea-ice composites shown in Figure 2.8 (low sea-ice years minus high sea-ice years), illustrating the difference in ORAS5 ocean velocities and ERA5 sea-ice area fraction.

Fram Strait associated with an anomalous high over Svalbard. This pattern consistently appears for composites of various combinations of the summer months. For example, the difference between the low and high sea-ice composites for the mean June, July and August sea-level pressure field looks very similar (not shown), suggesting a robustness to this result.

The emergence of this pattern suggests a relationship between the orientation of high and low sea-level pressure centers in the Arctic and the near-surface wind regime in the vicinity of the NEW Polynya. When there is higher pressure centered over Svalbard, and lower pressure the other side of the Arctic Basin, north of the Canadian coastline, a weak pressure gradient develops across the NEW Polynya region, with higher pressure to the east and lower pressure to the west. This is the reverse of the general mean climatology here, which usually drives northerly flow through the Greenland Sea and Fram Strait region (see Figure 2.2). The scenario during low sea-ice years (Figure 2.10), represents the collapse of this northerly flow regime and the subsequent development of a weak southerly flow associated with reduced sea-ice area fraction in the vicinity of the polynya. Therefore, it would seem that the interannual variability in the extent of the NEW Polynya is linked to the relative locations of two circulation systems over the Arctic Basin in the summer months. Note the magnitude of the differences in these MSLP systems is small, as is often the case for the summer months here.

2.5.3 The NEW Polynya Over the Last Four Decades

We now examine changes in the polynya over time. Figure 2.11 shows the period for which the NEW Polynya is classified as “open" for each year. This is determined from daily means of ERA5 sea-ice area fraction, the spatial average of which, for the box region shown in yellow in Figure 2.2, is used as a proxy for the polynya. A threshold value of 0.5 was chosen and whenever the daily mean sea-ice area fraction was less than this threshold value for ten consecutive days or more, the NEW Polynya was categorised as being open. There is some sensitivity to this threshold value and different values should be used for different sea-ice products, however, sensitivity tests suggest that the climatological trends are qualitatively similar. Equivalent results from the AMSR and NSIDC sea-ice products are shown in Appendix A (see Figure 2.15).

Generally, the polynya opens at the beginning of July and closes in mid-September, remaining open for typically 10 weeks each summer. However, this appears to have changed over the last 43 years. There is a clear trend in the timings of the annual opening and closing of the polynya, with it generally opening earlier and closing later each year. The opening trend line marks a shift in the annual formation from approximately late-June in the early 1980s to approximately mid-June in more recent years. This is mirrored by the closing trend line, with the approximate date of closure shifting from mid-September in the 1980s to early-October in more recent years. The closure trend line (0.59 days per year) is statistically significant with a p-value of less than 0.001. A similar

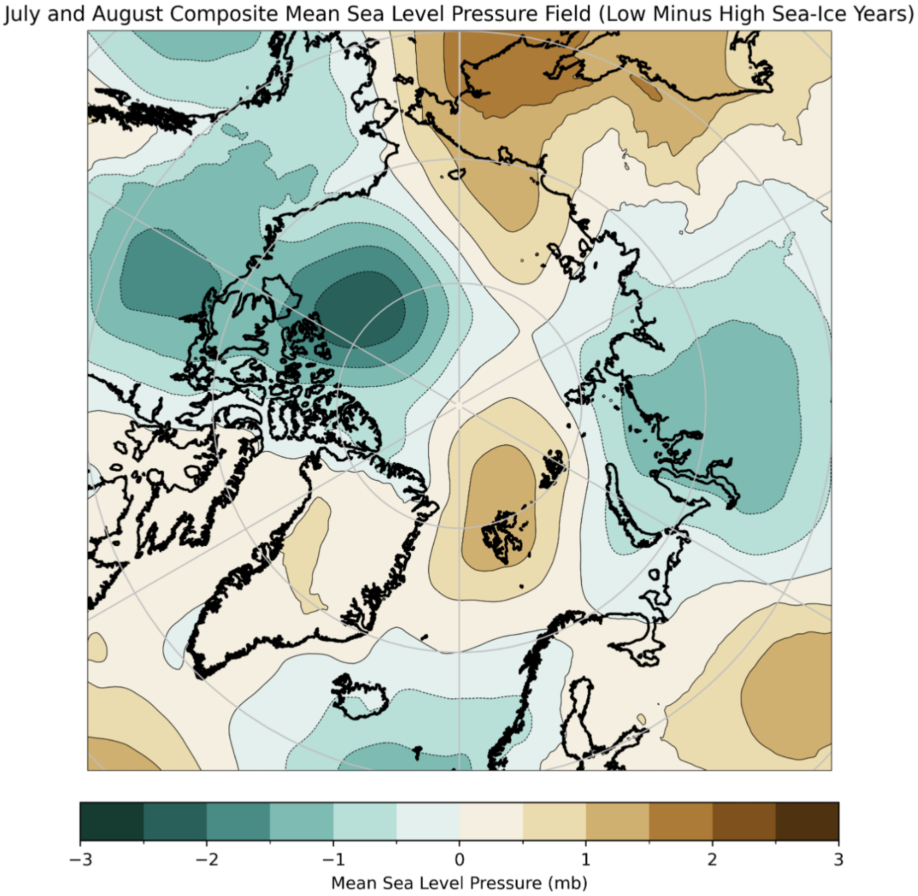

Figure 2.10: The difference between the low and high sea-ice composite pan-Arctic MSLP field for the months of July and August (low minus high sea-ice composite years).

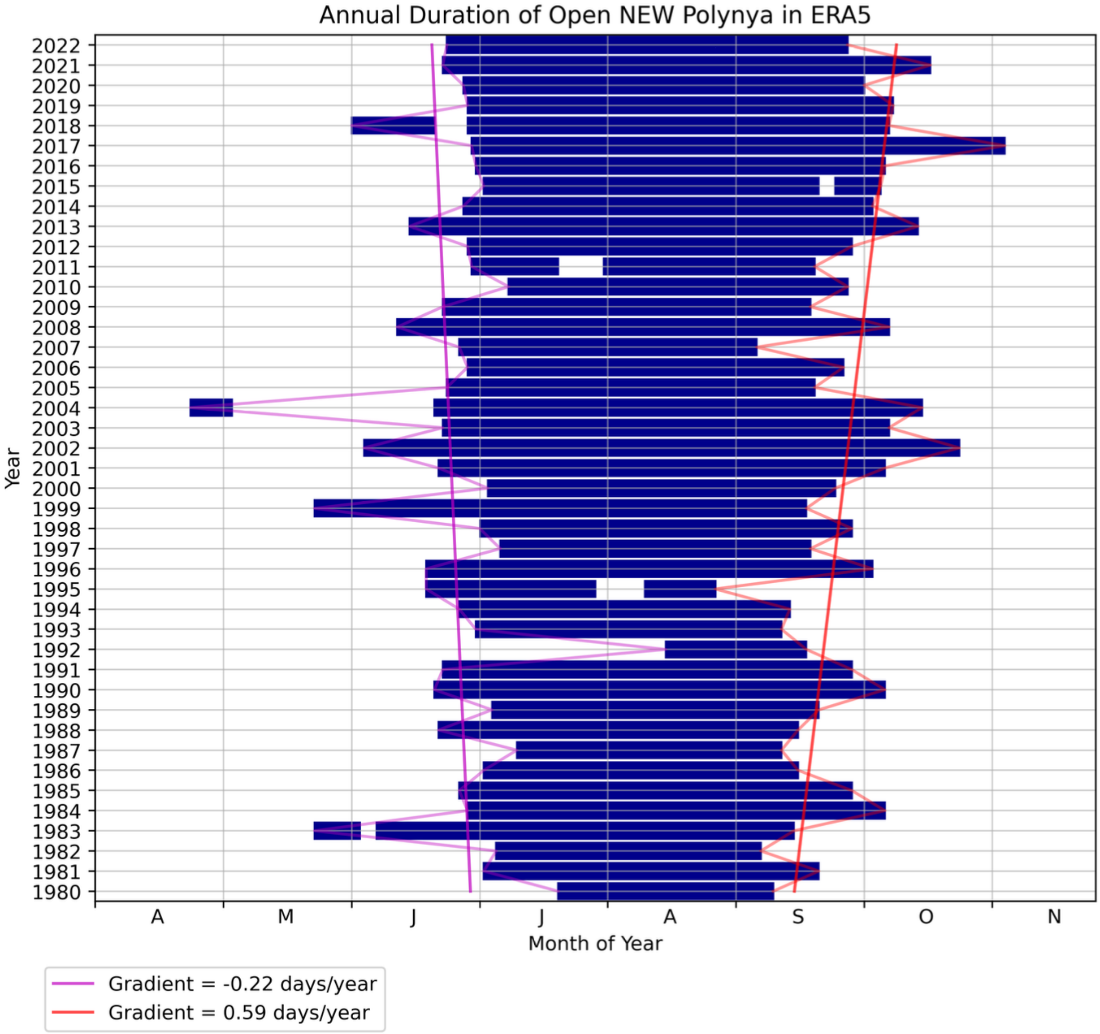

Figure 2.11: Annual timing of opening and closing of the NEW Polynya from ERA5 sea-ice area fraction. Here, a threshold value of 0.5 sea-ice area fraction (for the yellow box in Figure 2.2) and a threshold value of ten consecutive days or more was used to designate the polynya as open. The long-term trends in the opening and closing of the polynya are shown in magenta and red, respectively. The closing trend is statistically significant at the 99% confidence level.

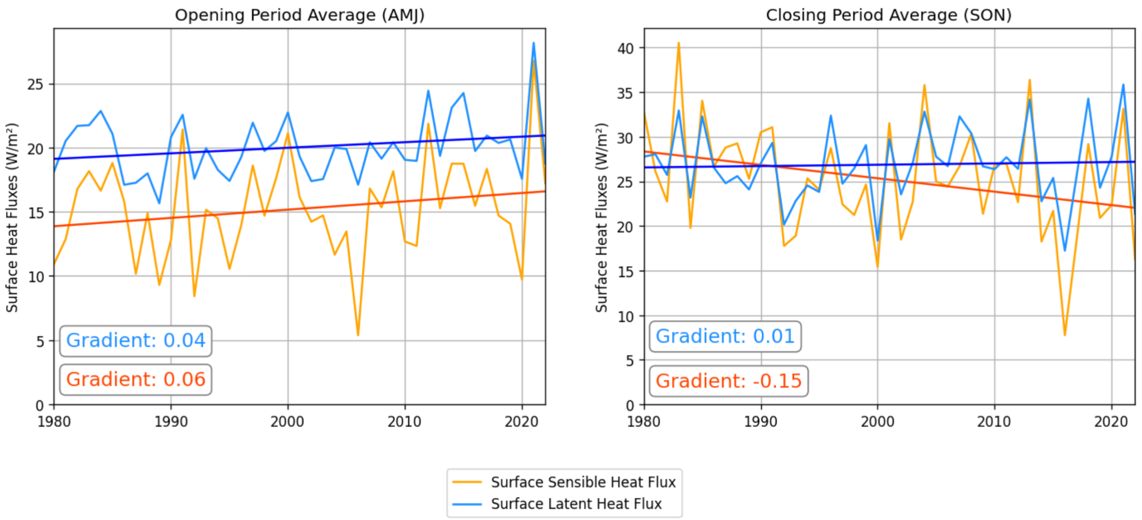

Figure 2.12: Trend in mean surface sensible and latent heat fluxes, between 1980 and 2022, spatially averaged over the yellow box shown in Figure 2.2, for the approximate polynya opening period (April, May and June) and approximate closing period (September, October and November). Data from ERA5. Note the vertical axis scale is different for each subplot. Positive values indicate an upwards flux (from ocean to atmosphere).

result is found in other sea-ice products (Figure 2.15) indicating a robustness to this result. Consequently, the annual duration of the polynya is typically now approximately 14 weeks.

This result provides some of the first tangible evidence to support predictions from earlier studies that ice-edge polynyas in the Arctic are likely to transition into large marginal ice zones as the climate continues to change (Barber and Massom, 2007)), before disappearing, possibly forever. For the first 20 years of the study period, the trend in ERA5 sea-ice area fraction for the NEW Polynya region is -0.02$\times10^{-4}$ per month, whereas the trend for the last 20 years is -1.8$\times10^{-4}$ per month, highlighting a shift at the turn of the millennium, which has also been highlighted in previous studies (e.g. Döscher et al. (2014)). It is clear that the annually recurring and stable nature of the NEW Polynya seen in the last two decades of the previous century is now in the past and that due to increased Arctic warming, as a result of anthropogenic forcing, this important polynya could soon vanish. This could have significant impacts for local wildlife and people, and the interactions between the atmosphere and the ocean.

As the variability of the annual cycle at the surface decreases, and the polynya is open longer each year, the turbulent surface heat fluxes will also be affected. Figure 2.12 shows the ERA5 mean surface sensible and latent heat fluxes in the NEW Polynya region between 1980 and 2022, for the approximate opening and closing periods, which here are taken as the months April, May, June, and September, October, November respectively. Note that for all fluxes we use positive values to indicate an upwards flux, from ocean to atmosphere, and negative values to indicate a downwards flux, from atmosphere to ocean.

There is a trend of increasing surface fluxes in the opening period. The mean surface sensible heat flux increases from approximately 14 Wm^{-2} to 17 Wm^{-2}, and the mean surface latent heat flux increases from approximately 19 Wm^{-2} to 21 Wm^{-2}. This trend could be linked to sea-ice decline over this period, which results in a larger area of the ocean surface being exposed to the atmosphere and thus can lead to enhanced upwards surface fluxes (Moore et al., 2022)). The trends indicate that the difference between the oceanic and near-surface atmospheric temperatures during the opening period is increasing, with the rate of warming of the ocean being larger than the rate of warming of the atmosphere. This is also illustrated in Figures 2.5 and 2.6 which show little variation in the spring and summer 2 m air temperature since 1980, but a significant warming of the ocean potential temperature at 0.5 m depth of approximately 1°C in spring and 1.5°C in summer. During this time of year, the ocean water is exposed to more solar radiation and warms more than the atmosphere, so as sea-ice declines in this region, the surface albedo decreases and the rate of warming increases and thus, so too does the surface sensible heat flux. The opening period trends for the surface sensible and latent heat fluxes have p-values of 0.18 and 0.14 respectively and thus are only of near-marginal statistical significance.

For the closing period, there is a negligible change in the latent heat flux since 1980 (less than 1 Wm^{-2}) and the sensible heat flux shows a decrease from approximately 28 Wm^{-2} to 22 Wm^{-2}. This indicates that the difference between the near-surface oceanic temperature and the near-surface atmospheric temperature is decreasing in the closing period with the rate of warming of the ocean being smaller than the rate of warming of the atmosphere. In Figures 2.5 and 2.6, there is an increase in the autumn 2 m air temperature of approximately 10°C since 1980 and a less pronounced increase of approximately 1°C in the ocean potential temperature at 0.5 m depth. The fact that there is an increase in the near-surface air temperature in autumn is linked to the decline in sea-ice in this region and the fact that the polynya is closing later during this period. The negative trend in surface sensible heat flux for the closing period suggests a link to the trend of the annual closure of the NEW Polynya; the formation of new ice increases the surface latent heat flux and with this now occurring later in the year, there is a negative trend for this transition period. The closing trend for the surface sensible heat flux is statistically significant with a p-value of 0.05.

Our results indicate a strong coupling between the sea-ice variability in the NEW Polynya region and the near-surface atmospheric flow regime. To investigate further, composite datasets for the periods around the opening and closing have been constructed using ERA5 daily variables (Figure 2.13). In the upper panel, prior to the opening of the polynya (which is marked at 50% sea-ice area fraction), there is steady sea-ice decline. This is associated with a small increase in 2 m air temperature of approximately 2 degrees over the 30 day period. With temperatures hovering just above 0°C here, it appears that the atmosphere near the surface has already warmed before this composite 30-day period (in winter, 2 m air temperatures are approximately -20°C , see Figure 2.5). The 10 m meridional winds show a transition from a northerly to a southerly flow regime, and the

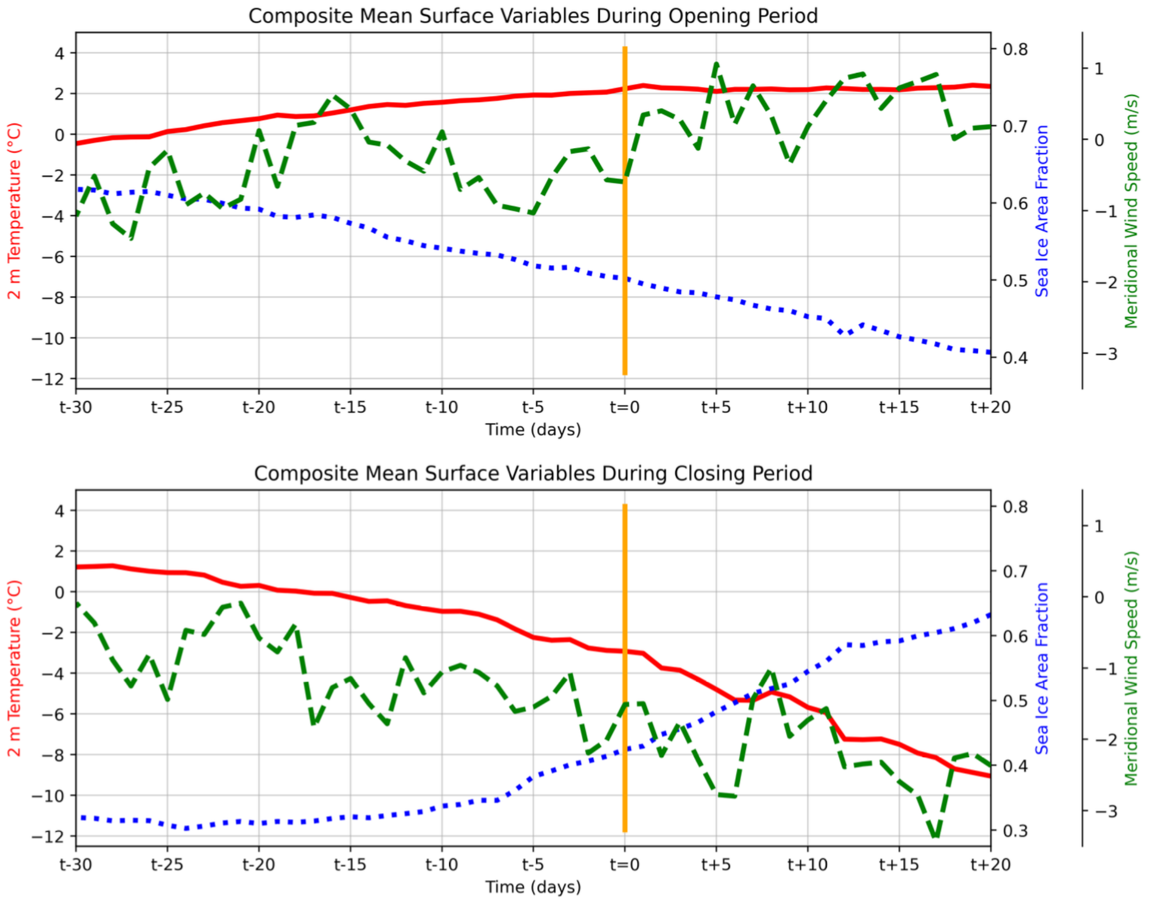

Figure 2.13: Time series showing the composite mean sea-ice area fraction (dotted blue), 2 m air temperature (solid red) and 10 m meridional wind speed (dashed green) from ERA5 for the yellow box shown in Figure 2.2 for the days in the month prior to the opening and closing of the polynya. Each daily mean is constructed from 43 years of data based on the timings of opening and closing identified previously and shown in Figure 2.11. In the upper panel, the time t = 0 represents the composite day of the polynya opening. In the lower panel, the time t = 0 represents the composite day of the polynya closing.

southerly flow tends to strengthen in the days before the day of opening, although all wind speeds are relatively low.

In the lower panel, prior to the closing of the polynya, the composite air temperature is clearly decreasing dramatically, while the sea-ice area fraction is increasing. The simultaneity of these changes suggests a more synchronous transition in the autumn months, compared to that of springtime. The 10 m meridional winds are also showing a clear trend, changing from very weak speeds close to 0 ms^{-1} to northerly speeds of approximately 3 ms^{-1}. In summary, this time series composite indicates that dynamical forcing may play a larger factor in the formation of the NEW Polynya each spring, whereas thermodynamic processes are clearly more influential in its closure each autumn.

2.6 Conclusions

The NEW Polynya and local environment show significant annual variability in atmospheric and oceanic reanalysis products. During the summer, there are higher near-surface air and ocean temperatures and a weakening (and often complete reversal) of the low-level wind regime in the vicinity of the NEW Polynya, when the polynya is at its largest. There is also very little variation in the MSLP field across the domain during summer, in contrast to the rest of the year when there is generally a large east-to-west pressure gradient across Fram Strait and a strong northerly flow regime. The summertime sea-ice minimum coincides with a maximum in near-surface air temperature and a minimum in meridional wind speed. The ocean also shows a significant annual cycle with surface intensified higher temperatures and lower salinity in the summer months. There is a lag in the ocean cycle with depth. All-together, this points to the ocean responding to surface forcing as the NEW Polynya develops.

The NEW Polynya also shows significant spatial variability throughout the 43-year period considered. The structure of the sea-ice field in this region varies on seasonal, interannual and decadal timescales.

As for much of the Arctic, there has been a decline in sea-ice in the NEW Polynya region since the 1980s, and increasing atmospheric and oceanic temperatures (at all depths). There has also been a general freshening of the upper ocean layers with a trend of salinification at 200 m. These results indicate a significant environmental response to anthropogenic forcing and demonstrate there are already dramatic climatological changes in this region.

Composite analysis indicates that the peak summertime extent of the NEW Polynya is closely correlated to the near-surface atmospheric flow regime, with weak southerly flow associated with a lower sea-ice area fraction/larger polynya, and vice versa. This is attributed to the collapse of the pressure gradient across Fram Strait, which is related to the relative locations of high and low sea-level pressure centers over the Arctic, among other factors.

Ocean velocities reflect this variation in near-surface winds, with weaker southwards ocean velocities at 0.5 m depth over much of the region during summers with a larger polynya extent, compared to those with more sea-ice cover. The composite difference in ocean velocities is surface intensified, implying atmospheric forcing, particularly when the sea-ice area is reduced.

We conclude that the annual opening and closing of the NEW Polynya is closely coupled to the near-surface atmospheric flow regime, and although it is difficult to deduce the exact physical mechanisms driving the polynyas formation, it appears that both dynamic and thermodynamic processes play important roles. Wind forcing dominates the opening, while thermodynamic forcing dominates the closure. Both latent and sensible heat processes are at play here and thus, as concluded in previous studies, the NEW Polynya is not easily classified as simply a latent or sensible heat polynya.

In the real world there is no perfect way to separate atmospheric and oceanic drivers using only reanalyses products and observations, and it is difficult to quantify individual forcing mechanisms. Our composite analyses point to a primary role of atmospheric forcing, but numerous mechanisms are at play, on various timescales. Further exploration of these, using idealised modelling work, would be an interesting topic for a future study.

The NEW Polynya is clearly opening earlier and closing later in the year. Its duration is now typically 3 weeks longer than in the 1980s. This suggests a reduction in annual variability over time and a possible complete loss of the NEW Polynya as we know it today. In the future it is likely that, for many months of the year, this region will more closely resemble a broad marginal ice zone. This will impact the local environment and wildlife in many ways. For example, reduced sea-ice cover can result in increased summertime surface turbulent heat fluxes which cause a warmer atmosphere that in turn promotes sea-ice melt: a positive feedback loop. Meanwhile, the autumn period shows a decreasing trend in surface sensible heat flux due to very fast warming of the atmosphere and a longer period of ice melt (the annual initiation of ice formation is happening later in the year). These changes will have significant implications for both the atmosphere and ocean in this complex and rapidly changing environment.

2.7 Appendix A

In order to evaluate the accuracy of the ECMWF reanalyses in this region, ERA5 and ORAS5 output was compared to other datasets where available. Sea-ice products from AMSR and NSIDC generally show a good comparison to ERA5 sea-ice, both spatially and temporally, although the magnitude of the sea-ice area fraction is often different. Figure 2.14 shows the annual cycle of variability for the daily sea-ice area fraction in ERA5, NSIDC and AMSR for the NEW Polynya region. Each year is shown with colour shading from blue in 1980 to red in 2022. Note that the AMSR sea-ice product is only available from mid-2002 onwards.

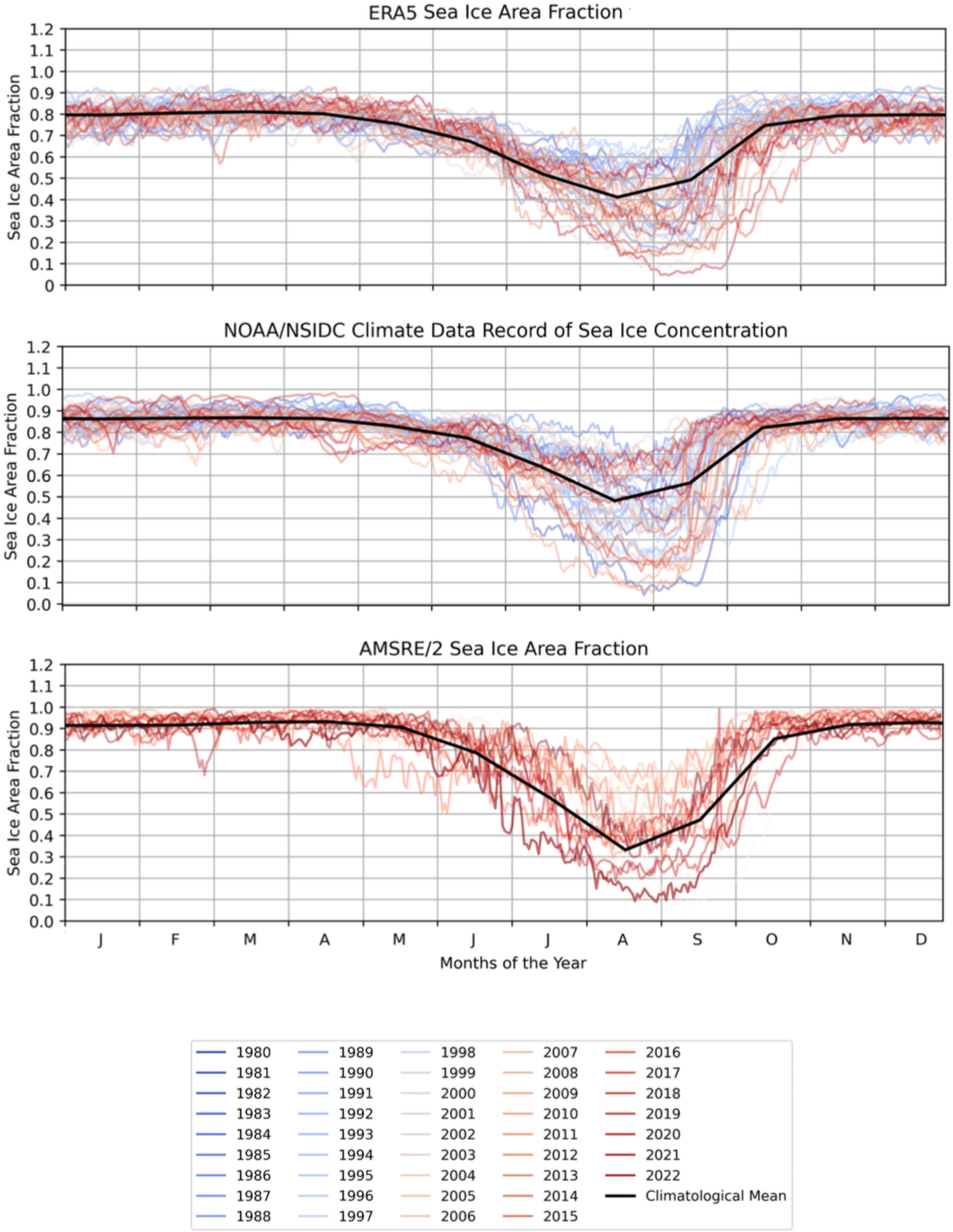

Figure 2.14: Daily sea-ice area fraction for each year for the NEW Polynya yellow box region (shown in Figure 2.2) for ERA5, NSIDC (CDR) and AMSR products as labelled.

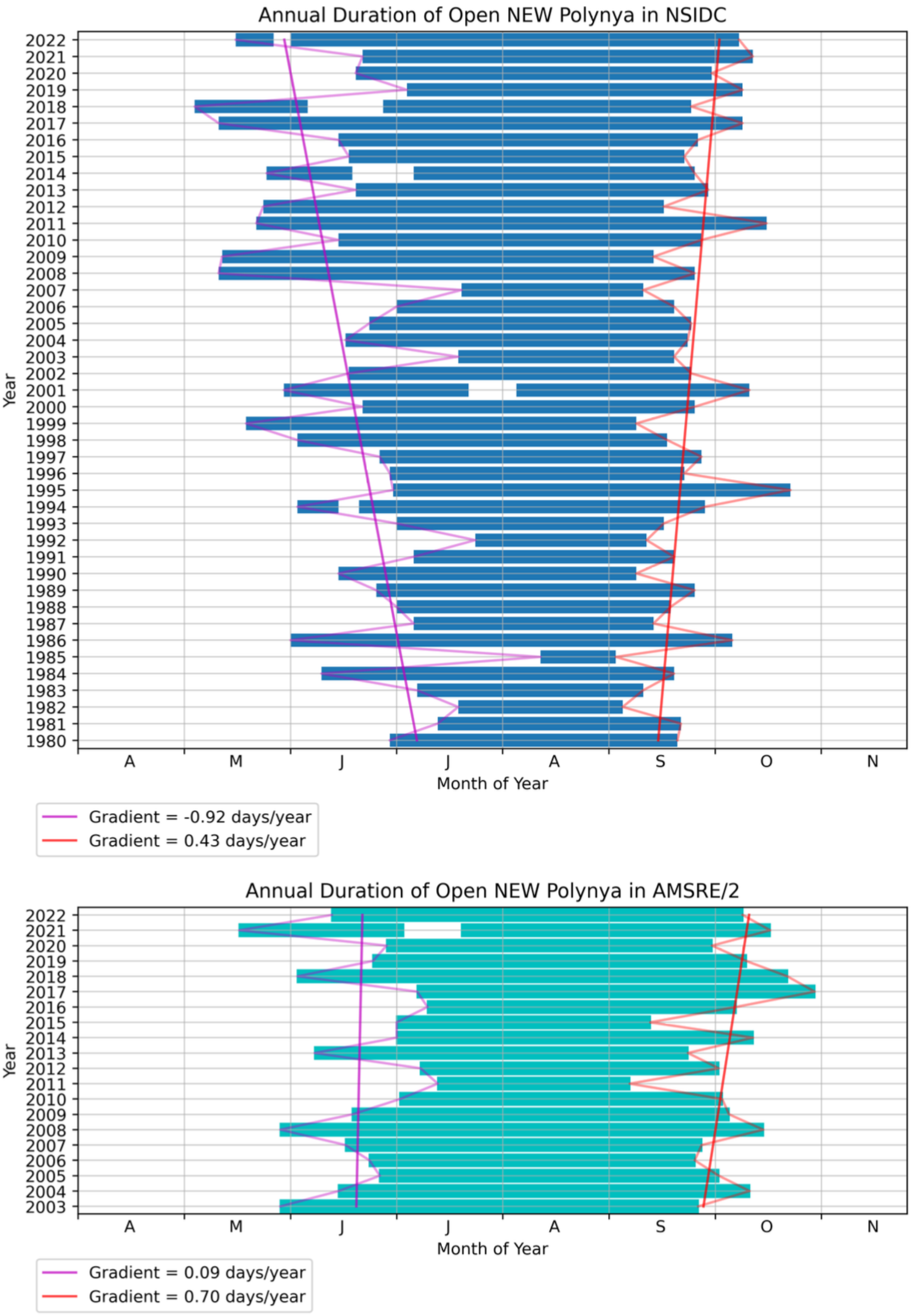

Figure 2.15: Annual timing of opening and closing of the NEW Polynya based on sea-ice area fraction (for the yellow box in Figure 2.2) from NSIDC (CDR) (upper panel) and AMSRE/2 (lower panel). Note that the AMSR products are only available between 2003 and 2022, whereas the NSIDC (CDR) product is shown from 1980 to 2022. In both cases, a threshold value of 0.75 sea-ice area fraction for ten or more consecutive days is used to represent the open polynya. The long-term trends in the opening and closing of the polynya are shown in magenta and red, respectively. For AMSR, the closing trend is statistically significant, where as for NSIDC the opening trend is statistically significant.

Figure 2.14 illustrates a good correlation across the products. When looking at spatial maps, there tends to be more smoothing in the ERA5 and NSIDC sea-ice compared to AMSR, which generally shows sharper transitions at the sea-ice edge (see Figure 2.1).

For comparison to Figure 2.11, we have also constructed a plot for the open period of the polynya using the AMSR and NSIDC sea-ice products. Here a threshold value of 0.75 was used to classify the polynya as open, a different value to ERA5, in order to account for the general shift in the magnitude of the sea-ice area fraction seen in the different products. The results are similar to that seen in Figure 2.11 with a trend in the polynya opening earlier and closing later in the year. For the AMSR product, the trend of the closing period is statistically significant with a p-value of less than 0.001, suggesting a robustness to this result. For the NSIDC product, it is only the opening trend that is statistically significant.

To assess the quality of ORAS5 data (Zuo et al., 2019)), comparisons to summertime observational CTD and XBT casts have been made where possible. Figures 2.16 and 2.17 show some examples of temperature and salinity profiles respectively, with inset maps to show the locations of the casts. The nearest ORAS5 equivalent has been plotted for each cast profile. Although there is often a fair agreement in the temperature profiles, the reanalysis tends to underestimate temperature near the surface and overestimate it beneath approximately 50 m depth. The fit appears poorer for the salinity profiles, where ORAS5 overestimates salinity throughout the water column. The ORAS5 product clearly has limitations in its representation of the ocean in this region. There is a relative paucity of observations to assimilate and point comparisons could be affected by unresolved variability. However, as used in this study, with a focus on long-term trends, variability and diagnosing forcing mechanisms, we would argue that its use is reasonable.

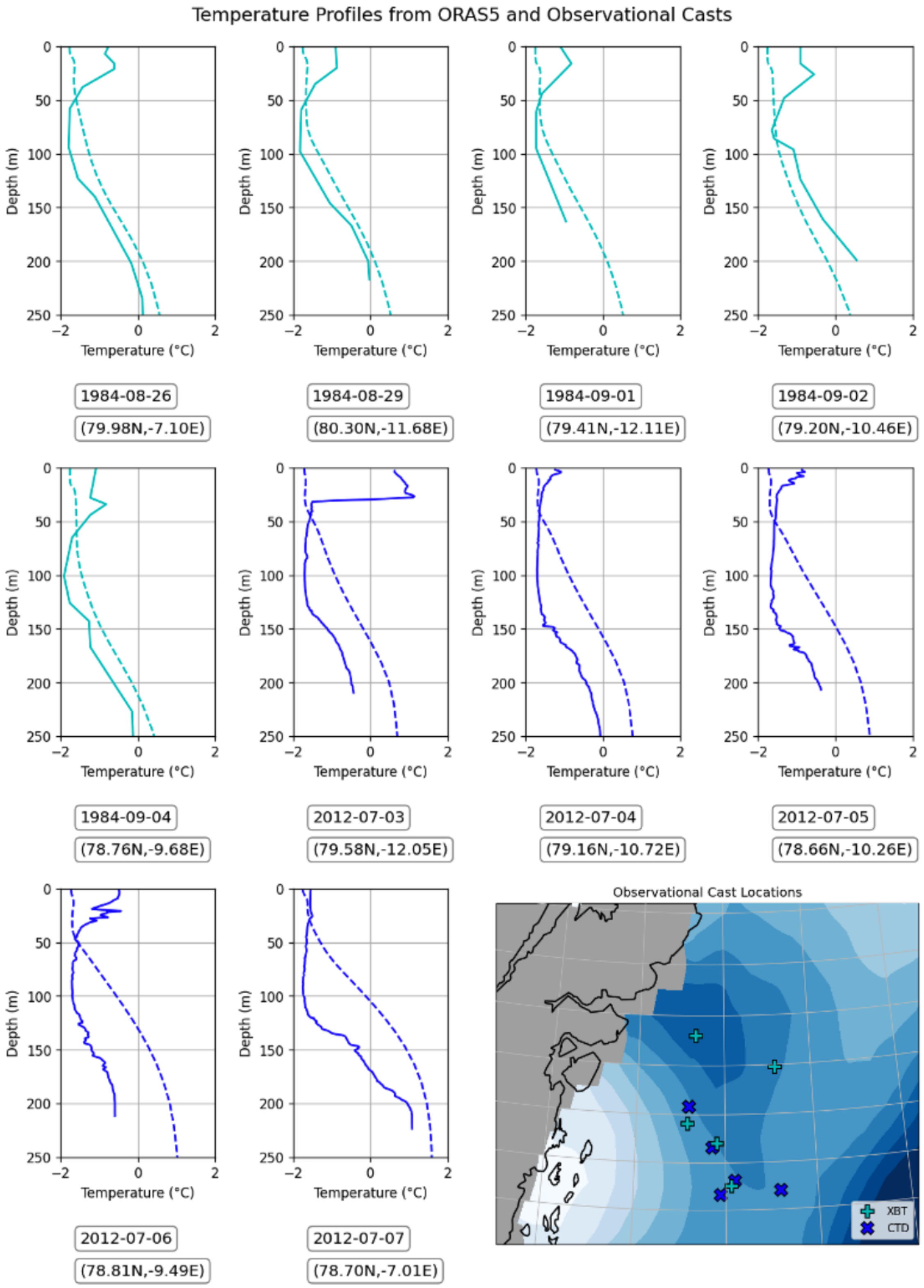

Figure 2.16: Temperature profiles from observational casts in the vicinity of the NEW Polynya (solid lines) and the nearest equivalent in ORAS5 (dashed lines). The locations of the observational casts are shown on the inset map with the mean sea-ice area fraction from ERA5, averaged over the dates shown for the casts. The XBT and CTD casts are represented by the cyan and dark blue colours respectively.

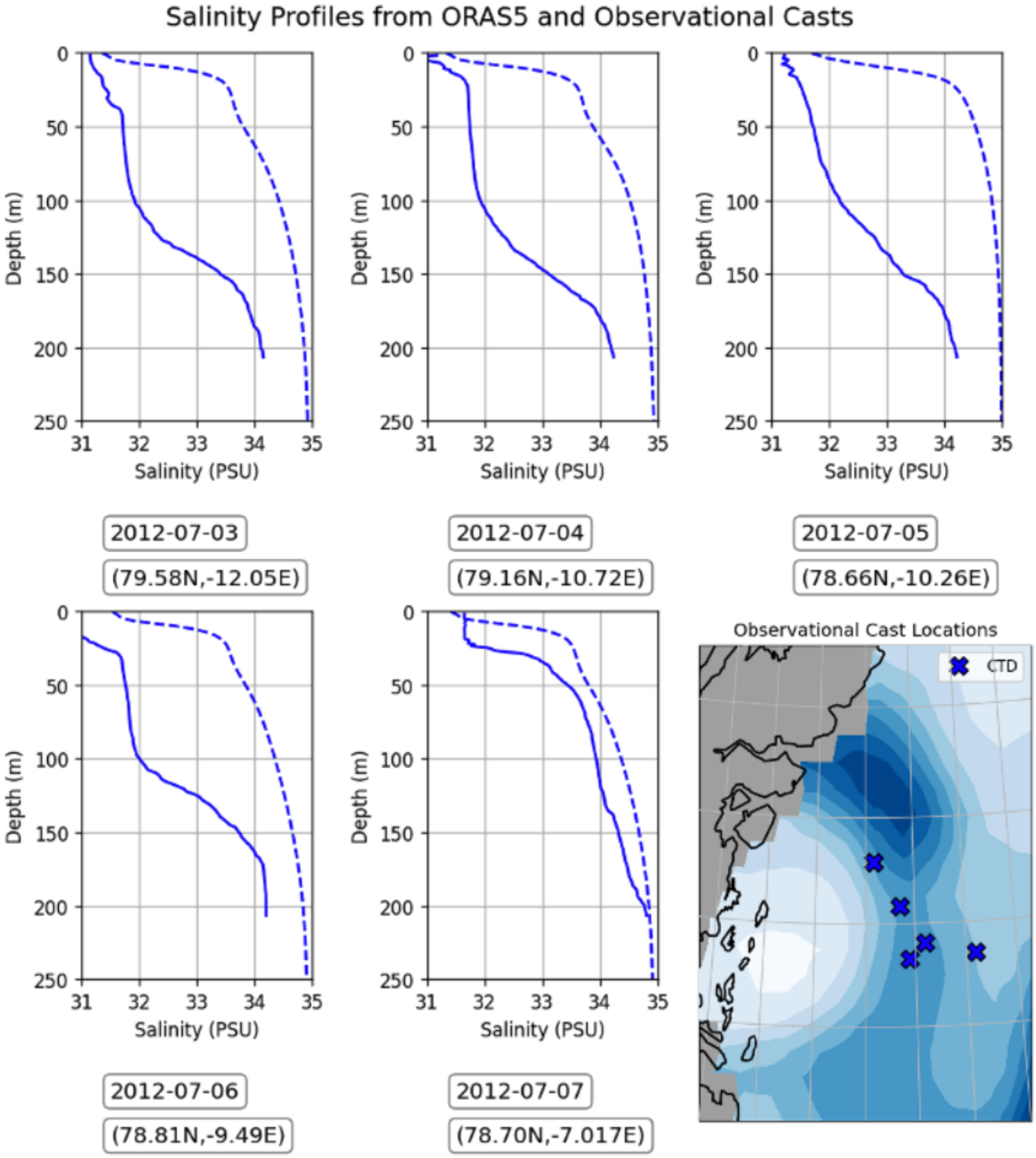

Figure 2.17: Salinity profiles from observational casts in the vicinity of the NEW Polynya (solid lines) and the nearest equivalent in ORAS5 (dashed lines). The locations of the observational casts are shown on the inset map with the mean sea-ice area fraction from ERA5, averaged over the dates shown for the casts. The XBT and CTD casts are represented by the cyan and dark blue colours respectively.

Validation of the CMIP6 Global Coupled Climate Model HadGEM3 in the Nordic Seas

3.1 Introduction

As climate change progresses, the Nordic Seas are expected to undergo significant change, with important consequences for the wider climate system. This region has already experienced anomalously strong sea surface warming (∼ 0.40°C/decade) compared to the global average (∼ 0.13°C/decade), highlighting its high climate sensitivity (Mohamed et al., 2022; Broomé et al., 2020; Isaksen et al., 2022; von Schuckmann et al., 2024).

The Nordic Seas play a central role in the high-latitude branch of the global thermohaline circulation as a major site of dense water formation feeding the Atlantic Meridional Overturning Circulation (AMOC). Changes in local heat exchange, freshwater pathways and sea-ice variability therefore have implications far beyond the region itself, influencing ocean stratification, deep ocean ventilation and climate variability across the Northern Hemisphere (Otterå et al., 2004; Tsubouchi et al., 2021; Spall et al., 2021; Smedsrud et al., 2022).

Recent observations indicate widespread warming, changes in Atlantic Water inflow, freshening in some regions and substantial sea-ice decline across the Nordic Seas (Smedsrud et al., 2022; Kenigson and Timmermans, 2021; Årthun et al., 2012; Onarheim et al., 2018). These changes are closely linked to shifts in airsea heat exchange and water mass transformation, which may alter the formation of dense waters and the structure of overturning circulation.

Although observations provide valuable measurements of these processes, they are often limited by short temporal coverage and sparse spatial sampling, particularly in the Arctic and marginal ice zone. Climate models therefore provide an essential tool for investigating longer-term variability and future change.

In this chapter, we use the HadGEM3 global coupled climate model from the UK Met Office Hadley Centre, produced as part of CMIP6 (Roberts et al., 2019), to investigate ocean and sea-ice variability in the Nordic Seas. The model performs well in the sub-polar North Atlantic, particularly at higher resolution, with a realistic large-scale circulation and AMOC structure (Jackson et al., 2020; Kuhlbrodt et al., 2018).

Before using the model to investigate climate change responses, validation against observations is necessary. Therefore we compare satellite-based sea-ice concentration products and ocean mooring observations with low, medium and high-resolution HadGEM3 simulations to assess model performance and identify important biases relevant to later analysis.

3.2 Data

3.2.1 The HadGEM3 Model

The third version of the Hadley Centre Global Environment Model (configuration 3.1), often referred to as HadGEM3-GC3.1, is a specific configuration of climate prediction models from the UK Met Office which include the NEMO (Nucleus for European Modelling of the Ocean) ocean model component on the ORCA tripolar grid (Madec and Imbard, 1996), and the CICE5.1 sea-ice model component from Los Alamos (Rae et al., 2015). These are coupled to the MetOffice Unified Model (MetUM) atmospheric model through the OASIS coupler developed at CERFACS (centre of basic and applied research) in France with the coupling period set to 1 hour (Roberts et al., 2019).

The experiments we use have a short 30-year spin-up, followed by century-long simulations. The spin-up and control experiments use mean values of the CMIP6 transient forcing datasets for aerosol, solar, ozone concentration and greenhouse gas forcings (Roberts et al., 2019). The historical simulations (1950-2014 inclusively) use the time-varying versions of these forcings. Note that the simulations used in our analysis are those representative of a high-emissions scenario (SSP5-8.5). The design of the HadGEM3 models is illustrated in Figure 3.1.

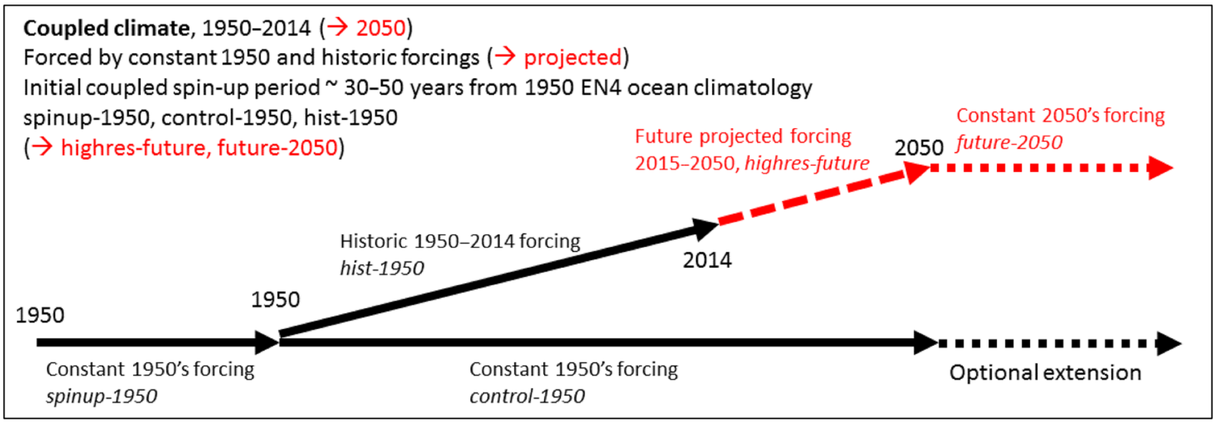

Figure 3.1: Schematic from (Roberts et al., 2019) showing the design of the HadGEM3 experiments.

For the coupled configuration, a range of resolutions is available for both the atmospheric and oceanic components. In this study we consider the high-resolution (HadGEM3-HH), medium-resolution (HadGEM3-MM) and low-resolution (HadGEM3-LL) model runs. Information on these model grid configurations is shown in Table 3.1 and illustrated in Figure 3.2, which gives a visual indication of the relative resolutions in the region of interest.

The influence of grid resolution on model output is sometimes overlooked, with many studies in fact using lower-resolution models due to computational costs and/or time constraints. However, depending on the aim of the research, this could lead to important physical processes being excluded from the analysis. For example, for HadGEM3, in the low-resolution run, ocean mesoscale features such as eddies and boundary currents are strongly tied to parametrisations and the requirements of numerical stability, whereas in the high-resolution run the eddying regime properties are increasingly explicitly resolved (Roberts et al., 2019).

Table 3.1: Model grid information for the low, medium and high-resolution HadGEM3 simulations. Note that horizontal grid resolutions are given for the mid-latitudes.

	Atmosphere		Ocean	
Model Configuration Name	Horizontal Grid Resolution	Number of Vertical Levels	Horizontal Grid Resolution	Number of Vertical Levels
HadGEM3-HH	25 km (N512)	85 up to 85 km	1/12° (ORCA12)	75 (top level 1 m thick)
HadGEM3-MM	60 km (N216)		1/4° (ORCA025)	
HadGEM3-LL	135 km (N96)		1° (ORCA1)	

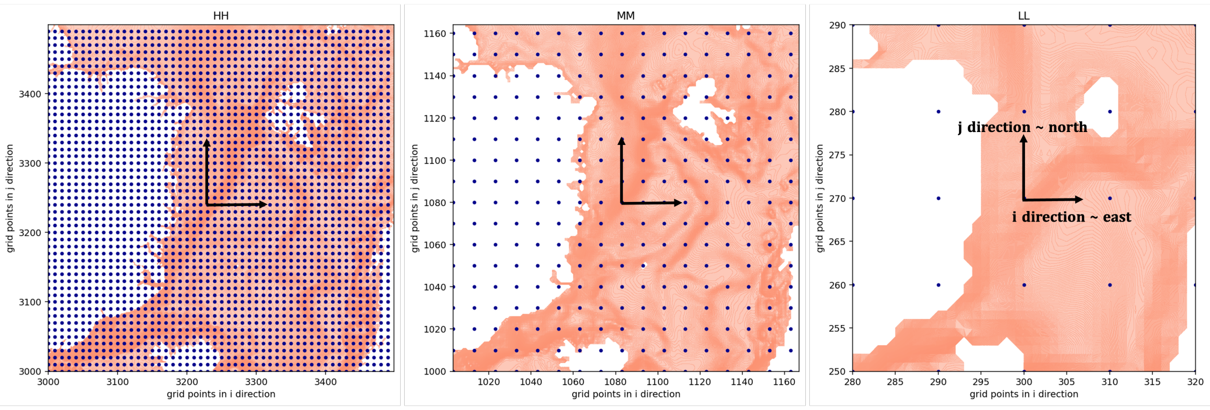

Figure 3.2: Illustration of the HadGEM3-HH, MM and LL horizontal ocean grid resolutions (every 10th grid point in both the x and y direction is shown with a black dot). Note that in this region, the model grid i and j directions approximately align with geographical north and east directions, but this is not exact and untrue for other regions. The red shading is the bathymetry.

3.2.2 The ORAS5 Reanalysis Product

ORAS5 is the most recent OCEAN5 global eddy-permitting ocean-sea-ice ensemble reanalysis system from the European Centre for Medium-Range Weather Forecasts (ECMWF). It estimates the state of the global ocean and comprises a Behind-Real-Time component, which provides an estimate of the historical ocean state from 1979 to near present-day, and a Real-Time component that provides the latest ocean conditions (Zuo et al., 2019). ORAS5 has global coverage with a horizontal resolution of 1/4° (ORCA025) and 75 depth levels. It is based on the NEMO ocean model (version 3.4.1) coupled to version 2 of the Louvain-la-Neuve (LIM2) prognostic thermodynamic-dynamic sea-ice model (Fichefet and Maqueda, 1997). Observations are assimilated through the NEMOVAR data assimilation system and the reanalysis product is forced with ERA-Interim with bulk formula plus WAVE forcing. In this work, monthly averages of potential temperature, ocean salinity and zonal and meridional velocity components are compared to ocean data from the HadGEM3 model and observational datasets.

We also use the ORAS5 sea-ice concentration for additional validation of the HadGEM3 model output. The sea-ice concentration data assimilated in this reanalysis product comes from various sources. Prior to 2007, the Met Office Hadley Center HadISST2 sea-ice product is used (Titchner and Rayner, 2014). Sea-ice data in HadISST2.1 include both reprocessed sea-ice concentration data from the EUMETSAT Ocean and Sea-Ice Satellite Application Facilities (OSI-SAF) and polar ice chart data from the National Ice Center (NIC). Sea-ice concentration in HadISST2.1 is calibrated against NIC sea-ice charts in order to ensure consistency with chart analyses prior to the satellite era (Zuo et al., 2019). The Met Office's Operational Sea-surface Temperature and Sea-Ice Analysis (OSTIA) dataset is used from 2007 to present, and this uses the OSI-SAF 401 dataset (Donlon et al., 2012).

3.2.3 Observational Sea-Ice Products and Ocean Mooring Data

Sea-Ice Products

For model validation, we use two satellite-based sea-ice concentration products: the University of Bremen AMSR product and the NOAA/NSIDC Climate Data Record (CDR), alongside the ORAS5 reanalysis introduced previously.

The AMSR product combines AMSR-E observations (2002 - 2011) and AMSR2 observations (from 2012 onwards), both derived using the ARTIST Sea Ice (ASI) algorithm with consistent calibration (Spreen et al., 2008; Su et al., 2013; Ludwig et al., 2020).

The NOAA/NSIDC CDR uses passive microwave observations from SMMR and SSM/I-SSMIS instruments and combines estimates from the NASA Team and Bootstrap algorithms (Cavalieri et al., 1984; Comiso, 1986). This product provides a longer observational record extending back to 1978.

While the products show broad agreement, ORAS5 and NOAA/NSIDC generally produce smoother ice fields than AMSR, often overestimating sea-ice concentration in polynya regions and along the marginal ice zone where the real ice edge is typically sharper (Bennett et al., 2024; Renfrew et al., 2021).

The Fram Strait Moorings

An array of ocean moorings located in Fram Strait at a latitude of approximately 78.8°N and between longitudes of approximately 10°W and 10°E, provides continuous high-frequency measurements of the ocean temperature, salinity and velocity between August 2003 and August 2019 (Beszczynska-Möller et al., 2011). The mooring array is jointly operated by the Norwegian Polar Institute which maintains moorings in the Arctic outflow in the west (East Greenland Current: EGC) and the Alfred Wegener Institute which maintains moorings in the Atlantic inflow in the east (West Spitsbergen Current: WSC).

In order to use the raw mooring data for comparison to the model output at Fram Strait, we averaged higher frequency measurements to monthly means and bi-linearly interpolated onto a two dimensional grid. We also applied some quality control to the raw mooring data and removed erroneous data points.

The Kögur Array at Denmark Strait

There is also a dataset available from a transect of moorings near Denmark Strait, called the Kögur Array (Harden et al., 2016). Each of the 12 moorings was equipped with an assortment of instruments measuring temperature, salinity, pressure, and current velocity. The data are available as a gridded dataset of vertical sections with a temporal resolution of 8 hours and spatial resolution of 8 km in the horizontal and 50 m in the vertical for the 11 month period between 29th August 2011 to 30th July 2012, allowing for model validation near Denmark Strait.

3.3 Model Validation Results

3.3.1 Sea-Ice Variability and Change

There is generally a good comparison between the model sea-ice concentration and those seen in the observations. An example of mean summer (June, July and August) sea-ice concentration for the 2010s (Figure 3.3) shows that the model generally captures the sea-ice edge but does not represent features such at the Northeast Water Polynya well.

The HadGEM3-MM model has been shown to produce ice thickness and extent that are in good agreement with reanalyses (e.g. Ridley et al., 2018; Roberts et al., 2019). The spatial distribution of the sea-ice also appears accurate from Figure 3.3, with the sea-ice edge in approximately the same location as in the observations.

Comparatively, for the HadGEM3-HH case the sea-ice edge is located farther north than in observations, whereas for the HadGEM3-LL example we see that there is the opposite problem, with the sea-ice edge located farther south. These differences point to resolution-dependent processes influencing the model sea-ice concentration.

The most significant difference in the sea-ice concentrations in this region for this summer period is the representation of the Northeast Water Polynya, which is not well resolved in any of the HadGEM3 model runs. This could lead to additional biases in the model which are not representative of the real world.

Figure 3.4 illustrates the rate of sea-ice decline over several decades for the same

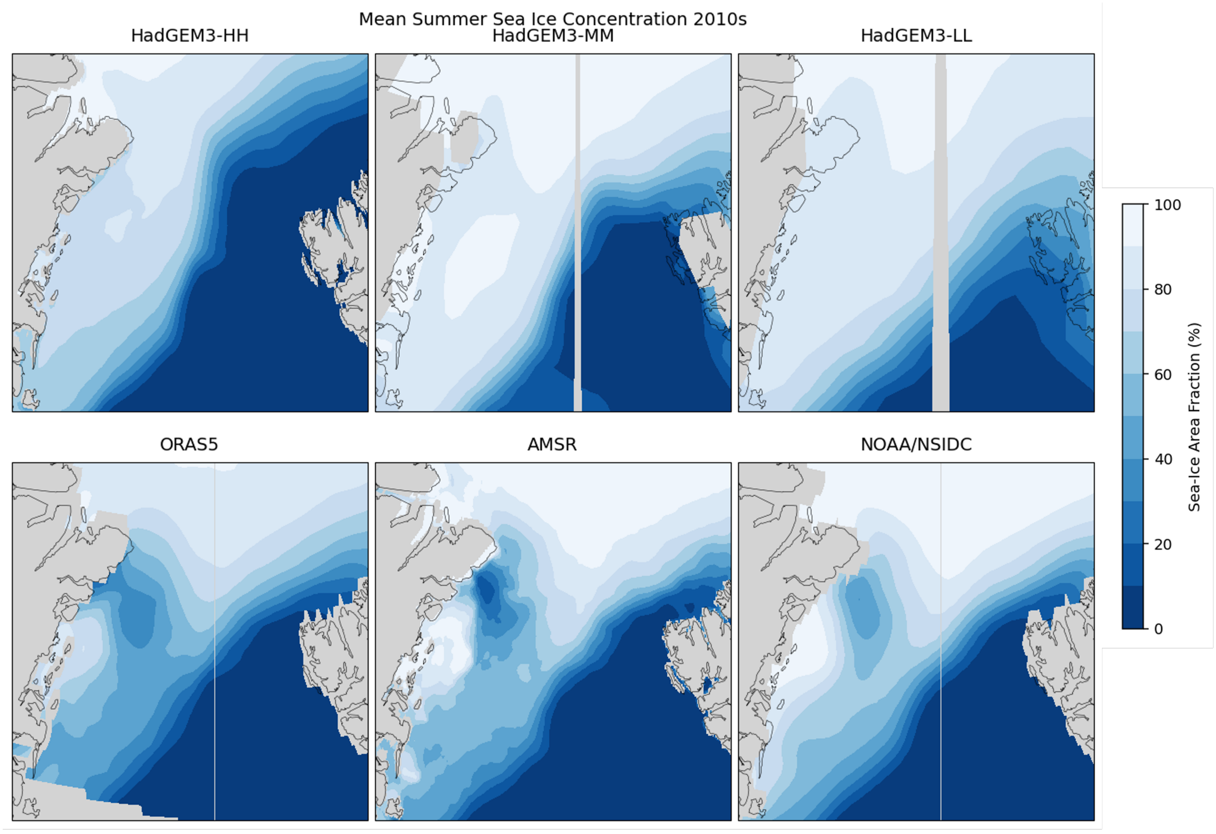

Figure 3.3: Mean summer (JJA) sea-ice concentration in the Fram Strait region for the 2010s from satellite based observations (AMSR and NOAA/NSIDC), a reanalysis product (ORAS5) and the HadGEM3 model (HH, MM and LL).

products. In all panels, we see the 50% sea-ice contour lines retreat northwards over time, as expected with increasing Arctic temperatures. Overall, the model compares well to the available observations, although the rate of sea-ice retreat appears faster in HadGEM3-HH. We see that, especially in the region North of Svalbard, there is more sea-ice decline in the high-resolution model. For example, the light blue line represents the mean 50% sea-ice contour for the 2010s. In observations, this line runs across the domain from East Greenland in the lower-left of the panel to North Svalbard in upper-right. In the model, the MM and LL simulations compare quite well for this decade. For the HH simulation, however, this contour line runs much farther north, reaching latitudes of approximately 83°N, to the north of Svalbard.

If we consider the seasonal changes, we see that a lot of this sea-ice decline in the model occurs in the summer and autumn months. Figure 3.5 shows the same decadal mean 50% sea-ice contours but for only the summer season (June, July and August). Here, it is clear that the sea-ice retreat is much faster in the high-resolution model than in the observational products. This figure also illustrates that the model does not capture smaller features in the sea-ice; details like the NEW Polynya are missing. The reason behind this remains unclear but could be linked to the representation of the smaller scale ocean circulation systems on the continental shelf or the variability of near-surface wind forcing which likely both impact the development of the polynya (as discussed in Chapter

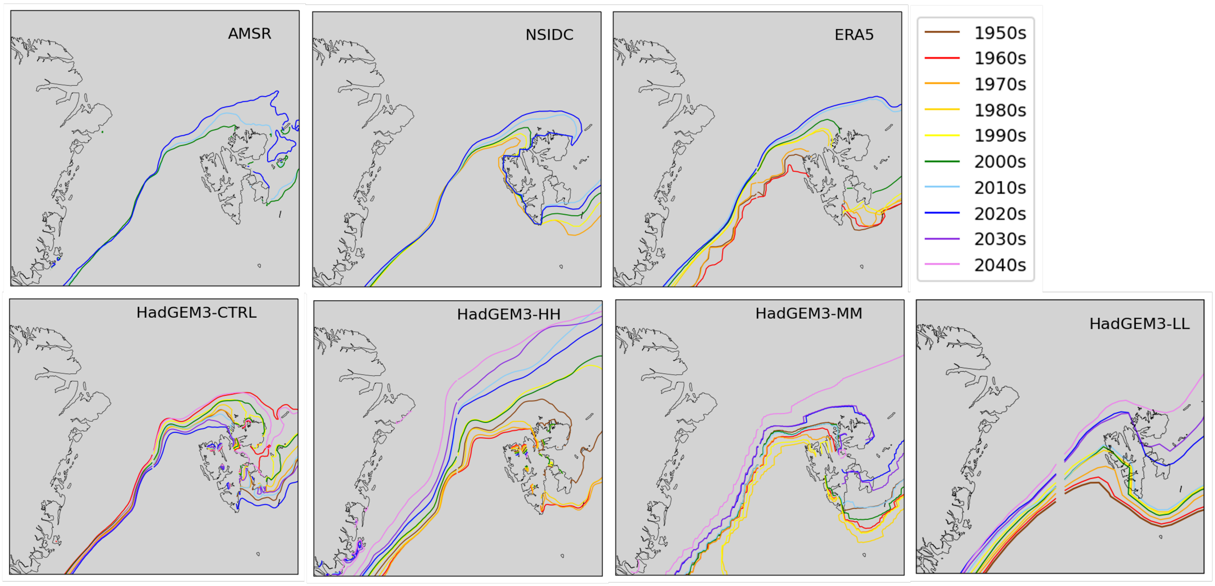

Figure 3.4: The decadal mean 50% sea-ice contours in the Fram Strait region show long-term retreat in observational datasets (AMSR, NSIDC, ERA5) and model output (at all three resolutions).

2).

Figure 3.6 shows that the story is similar for the other seasons, with autumn particularly showing dramatic sea-ice retreat in the model which is not shown in the other products. What remains consistent throughout the seasons is that the rate of decadal sea-ice decline increases with model horizontal grid resolution suggesting a dependency on smaller-scale processes that are resolved in the higher-resolution simulations but not at lower resolutions. Given that rising temperatures due to poleward heat transport are thought to be the primary driver of Arctic sea-ice decline, it follows that the higher-resolution simulations with stronger poleward heat transport are also the simulations with faster rates of sea-ice decline in the Nordic Seas (e.g. Smedsrud et al., 2022; Docquier et al., 2019; Shu and et al., 2022).

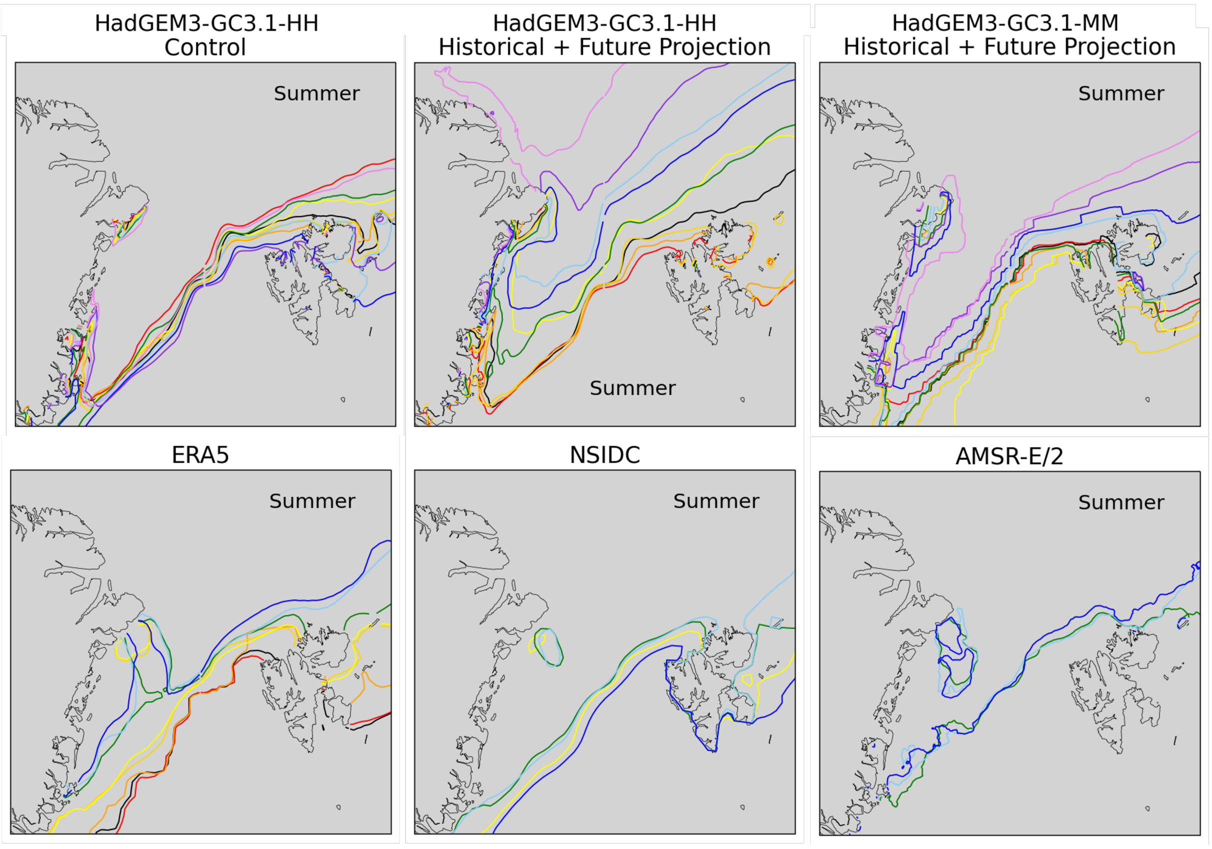

Figure 3.5: The decadal mean 50% sea-ice contours for the summer months only (June, July and August) indicate a faster rate of change in the HadGEM3-HH simulation than seen in current observational data and the HadGEM3-MM simulation.

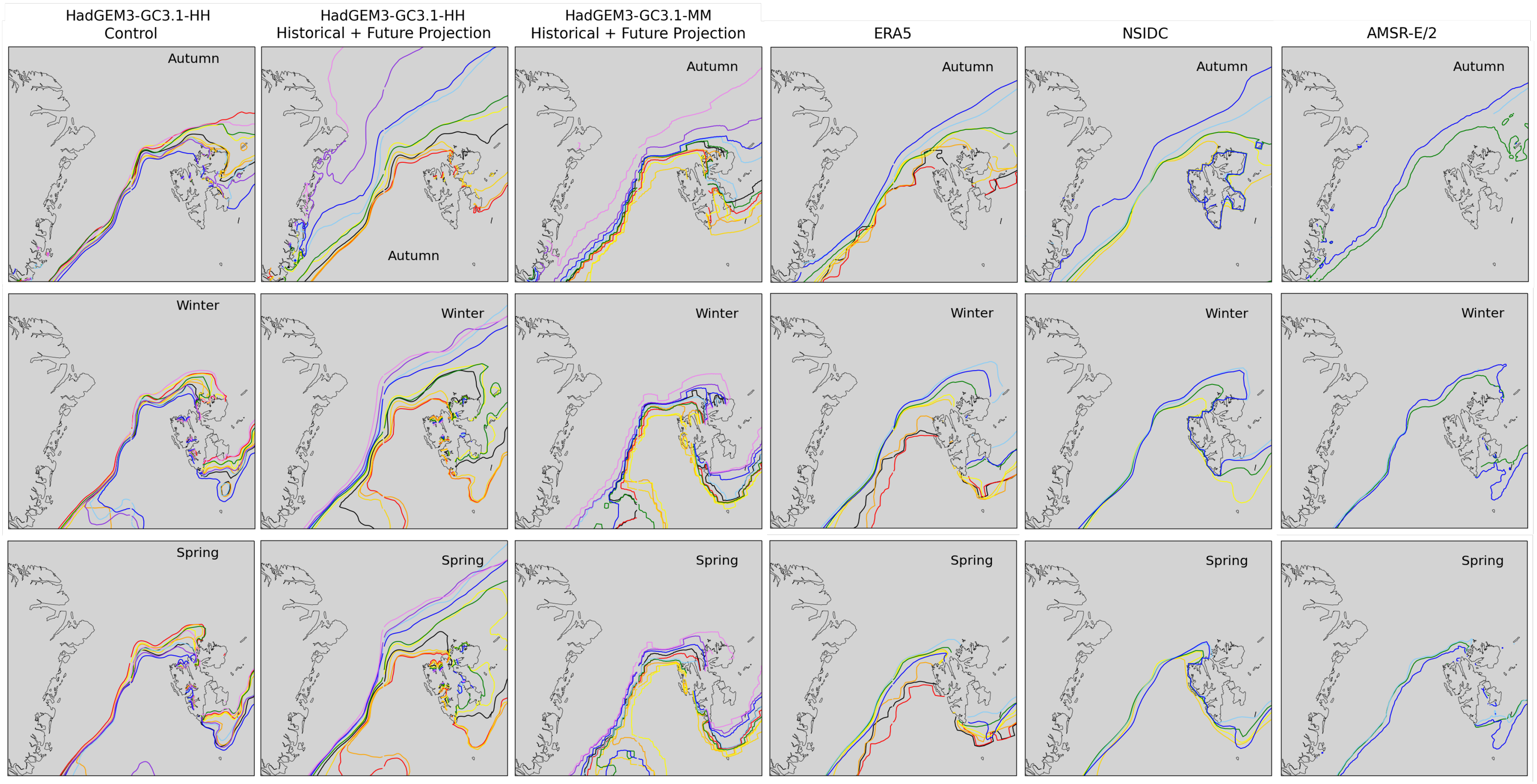

Figure 3.6: The decadal mean 50% sea-ice contours for the autumn (SON), winter (DJF) and spring (MAM) seasons, with a particularly dramatic response seen in the HadGEM3-HH simulations. Significant change is also seen in the autumn months in the observational data.

3.3.2 Mean Ocean Characteristics

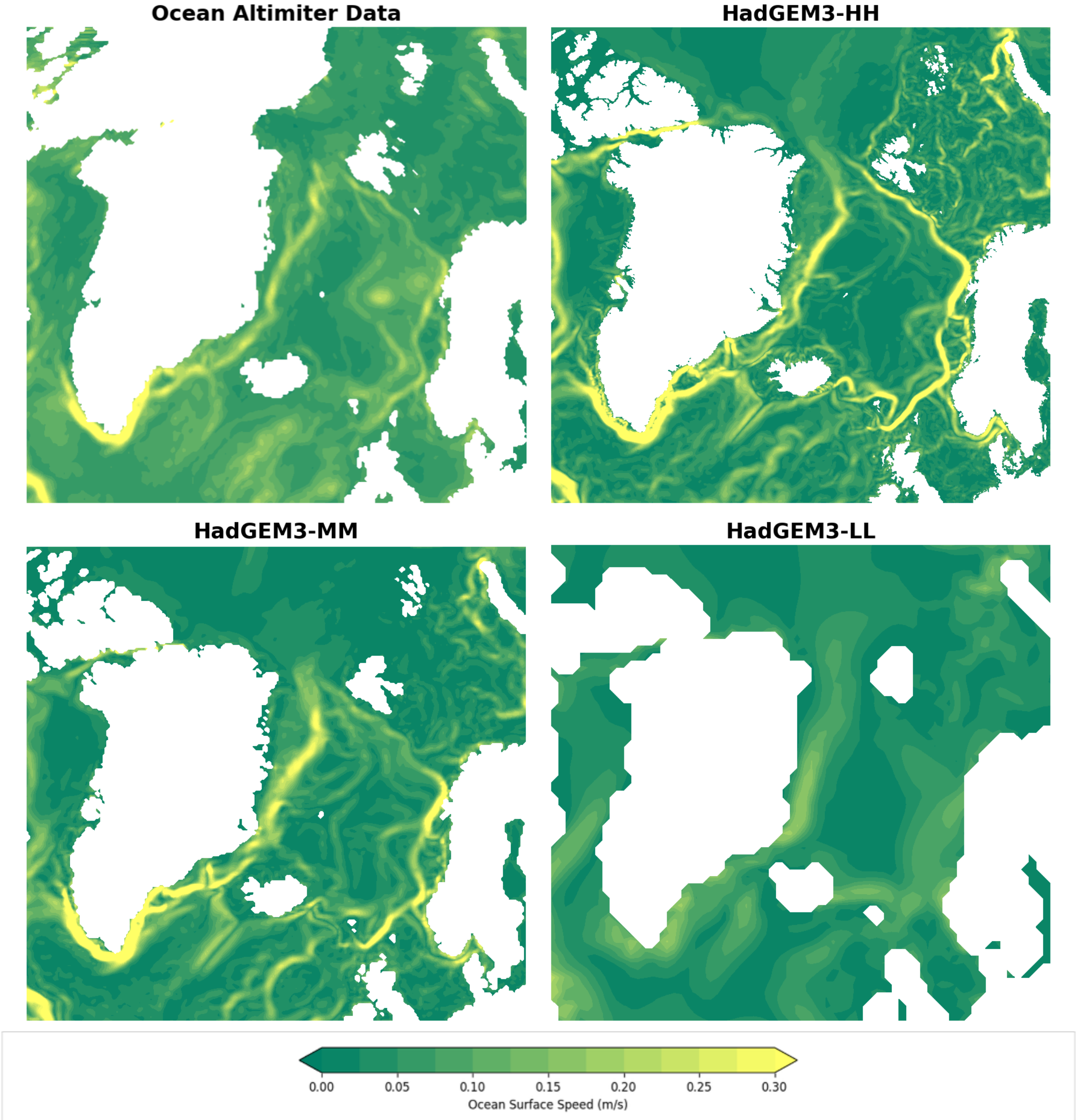

Figure 3.7: Mean ocean surface speed for the period between January 1st 2020 and January 1st 2025 from observational ocean altimeter data from Ocean Surface Current Analyses Real-time (OSCAR) with the all-time mean (1950-2050) from the HadGEM3 simulations (high, medium and low resolution). Note that the altimeter data has been reformatted so that it has the same projection as the model grid.

The Nordic Seas is a complex region for ocean dynamics, with strong near-surface boundary currents, smaller interacting circulation systems, vertical mixing, dense water formation and significant exchange with the Arctic and North Atlantic through the Fram Strait and Greenland-Scotland Ridge respectively. Many of these important features are well captured by the high and medium-resolution HadGEM3 simulations. A comparison of the mean ocean surface speed against observational altimeter data (shown in Figure 3.7) demonstrates that the model has a realistic representation of Atlantic inflow and

Arctic outflow pathways at 1/4° and 1/12° horizontal grid spacing. However, these are not well resolved in the low-resolution simulation, where the average current speeds are notably reduced and the circulation pathways are poorly defined. It should also be noted that, at these latitudes, the altimeter data does not capture smaller-scale ocean features particularly well either.

This aligns with findings from both Petit et al. (2023) and Lai et al. (2022). These studies show that the higher-resolution HadGEM3 runs develop stronger, sharper boundary currents and faster upper-ocean velocities along basin boundaries.

3.3.3 Model Evaluation at Fram Strait

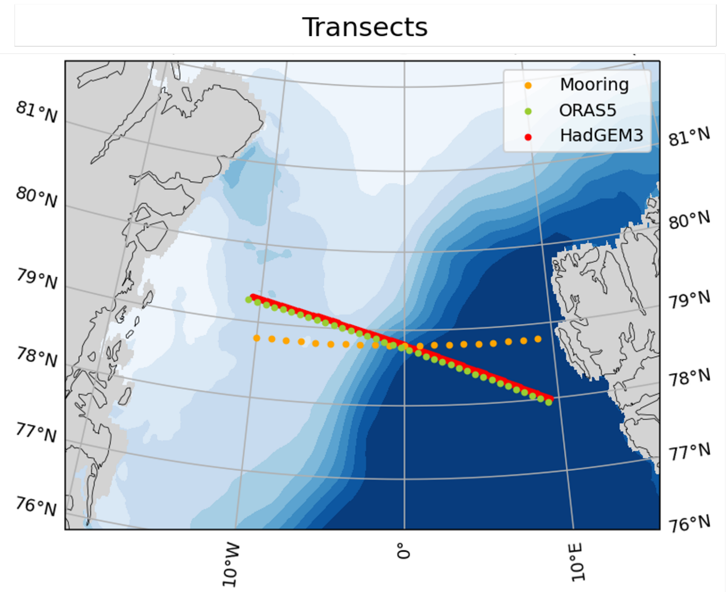

Figure 3.8: A map showing the locations of ocean moorings at Fram Strait and the nearest transects in HadGEM3 and ORAS5 along model grid lines.

At Fram Strait (Figure 3.8) mooring data are available for a period of 16 years, allowing us to validate the HadGEM3 model in this region. As illustrated by Figure 3.9, overall the ocean properties and dynamics in the model compare well with observations. The warmer and more saline Atlantic Water, which flows northwards near the surface in the West Spitsbergen Current (WSC), is well captured in the temperature, salinity and velocity fields (eastern edge of cross-section). Although, note that this current is faster and warmer in the high-resolution simulation than in observations, and slower and cooler in the medium and low-resolution simulations. Mean potential temperatures and ocean velocities reach maximum values of over 6°C and over 0.2 m/s respectively in the high-resolution model, more than 2°C and 0.05 m/s higher than the maximum values from the mooring observations.

The southward-flowing cold and fresh water in the East Greenland Current (EGC) is also well represented in the model at high-resolution (western edge of cross-section), but the current is less well captured in the low-resolution results. The ORAS5 product does not capture the ocean dynamics as well here, with the velocity in the boundary currents being too low (less than 0.1 m/s) compared to the mooring observations ($\sim$ 0.18 m/s).

T-S diagrams from the transects at Fram Strait show that the water properties here are well represented in HadGEM3 (Figure 3.10). As discussed in literature (e.g. Langehaug and Falck (2012); Rudels et al. (2005)), there are three main water masses in this region.

1. Polar Water: this is cold, fresh, near-surface and sits on continental shelf or flows southward in the EGC

2. Atlantic-Origin Water: this is warm, saline, near-surface and flows northwards in the WSC or gets recirculated

3. Deep Water: this is cold, saline, dense, overflow water

All three water masses are captured by the products, with a few small differences. The Polar Water in the model and in ORAS5 is fresher than in the observations. This may be partly due to the observations not covering the surface waters. The Atlantic Water is warmer and more saline in the high-resolution model than in the other products. The Deep Water is well constrained with similar properties across the products.

Compared to mooring observations at Fram Strait, the HadGEM3-HH model represents the mean ocean structure and water properties in the early 2000s well. On average, the dynamics of the boundary currents and larger-scale circulations, such as the Greenland Sea Gyre, are also well captured by the model (e.g. see Figure 3.17). However, it is also important to consider the temporal variability of these metrics.

3.3.4 Variability at Fram Strait

The Hovmöller plots in Figure 3.11 show (a) potential temperature in red-blue shading and (b) ocean salinity in purple-green shading. These are shown for the period between 2003 and 2019, with subplots for each of four datasets; the mooring observations, the ORAS5 reanalysis product, the HadGEM3-HH transient run and the HadGEM3-HH control run. We focus on the high-resolution simulation here as it has been shown to be broadly more realistic than the lower-resolution simulations.

As demonstrated by these Hovmöllers there is no significant trend over this period, but the datasets generally compare well. There is a reduced seasonal cycle in the control model run compared to the transient case, suggesting an increased variability in the annual cycle at Fram Strait in response to climate change forcing. We also see that temperatures are generally higher in the transient run than in the control, with fresher waters in the west. Also note that ORAS5 does not demonstrate as strong of a seasonal cycle in salinity in the west as the other products.

If we consider the 100 year period from the model (Figure 3.12) we see an enhanced salinity gradient across Fram Strait in the transient run compared to the control run, with fresher water in the west and more saline water in the east. This projection for future

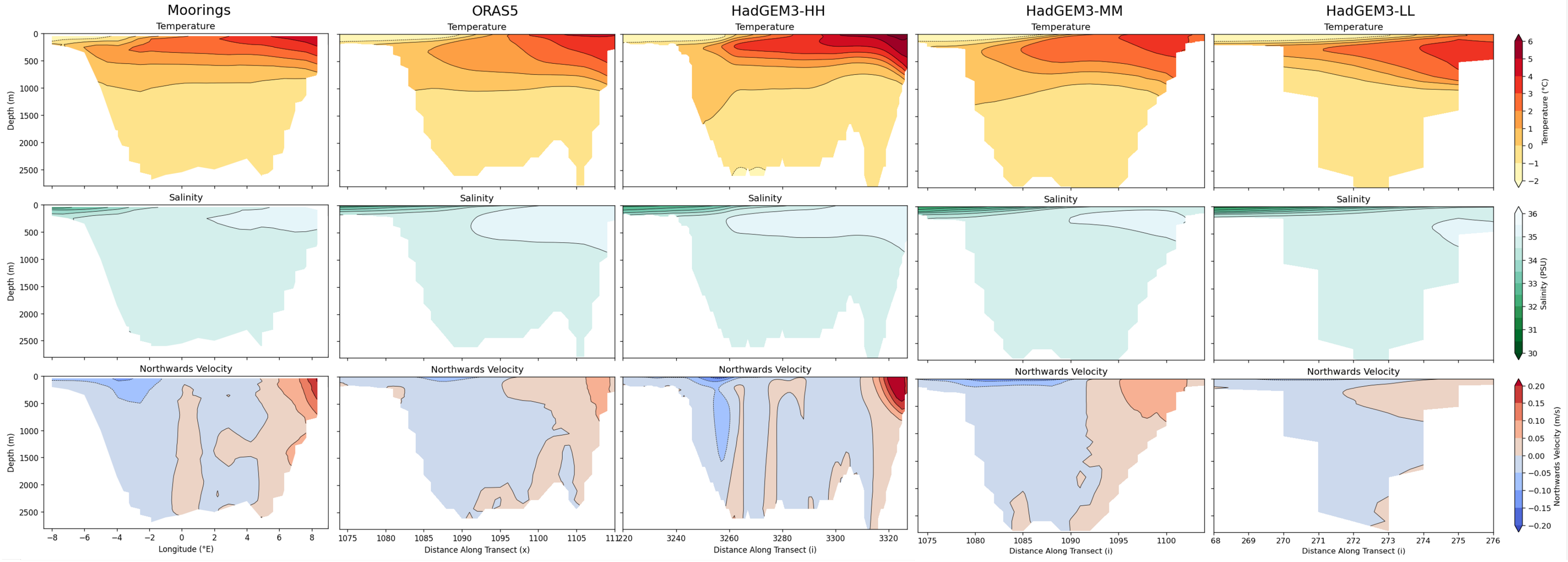

Figure 3.9: Mean potential temperature, ocean salinity and quasi-northwards ocean velocity for the transects at Fram Strait using mooring observations, the ORAS5 reanalysis product and the HadGEM3 model at high, medium and low-resolutions.

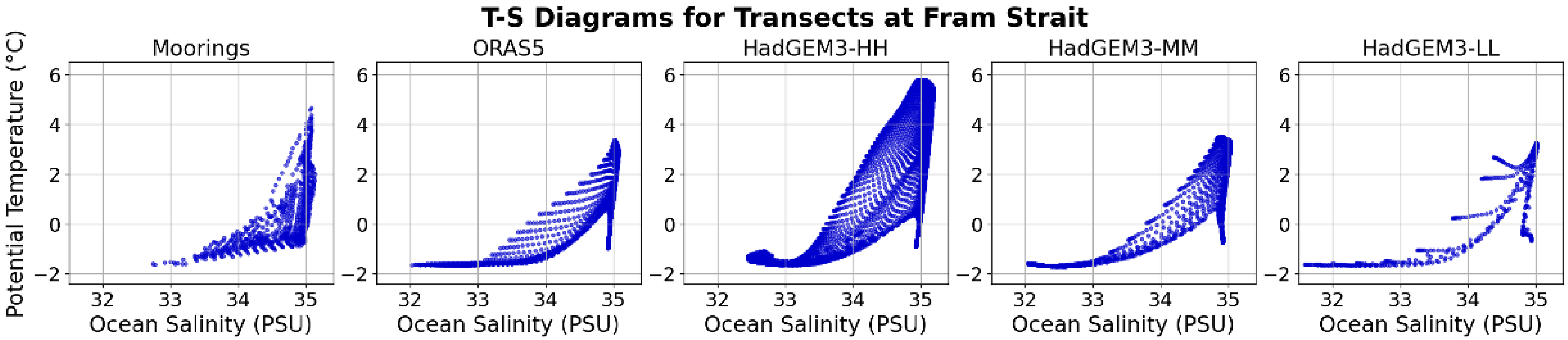

Figure 3.10: T-S diagrams from the time-mean transects at Fram Strait for all products.

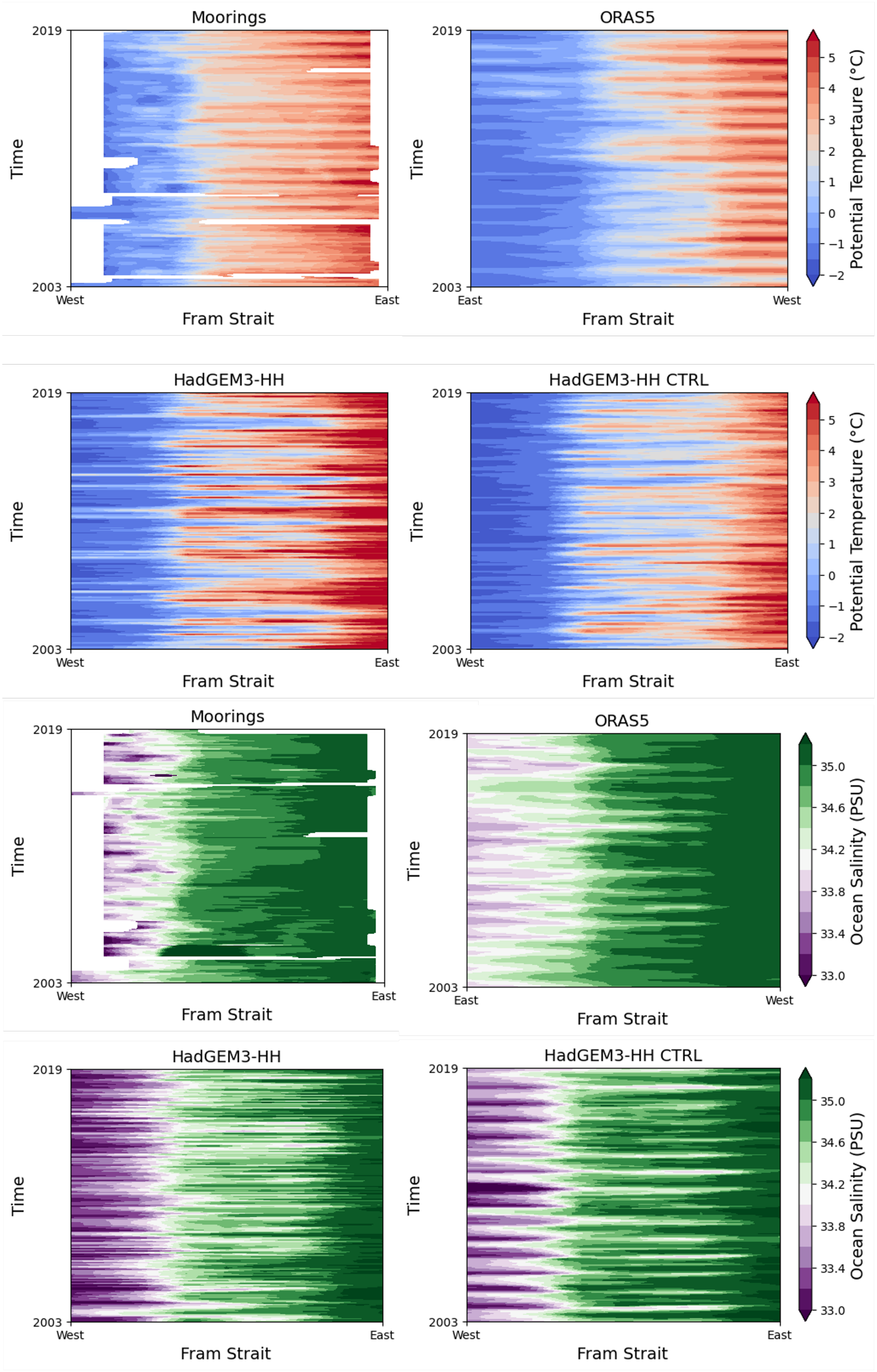

Figure 3.11: Hovmöller plots showing 16 years of (a) potential temperature and (b) ocean salinity at Fram Strait, averaged over the upper 200 m, for the moorings, ORAS5 and HadGEM3-HH transient and control runs.

changes in salinity will likely result in changes in the density gradient too, which could have important impacts on the ocean dynamics in this region.

We can also see a clear warming trend in the high-resolution transient model run that is not shown for the control case. There is visible warming across the entire transect with projections for maximum temperatures of well over 6°C in the east of Fram Strait by 2050. We can also see the advance of the warmer Atlantic-Origin Water from the east towards the west of Fram Strait over time.

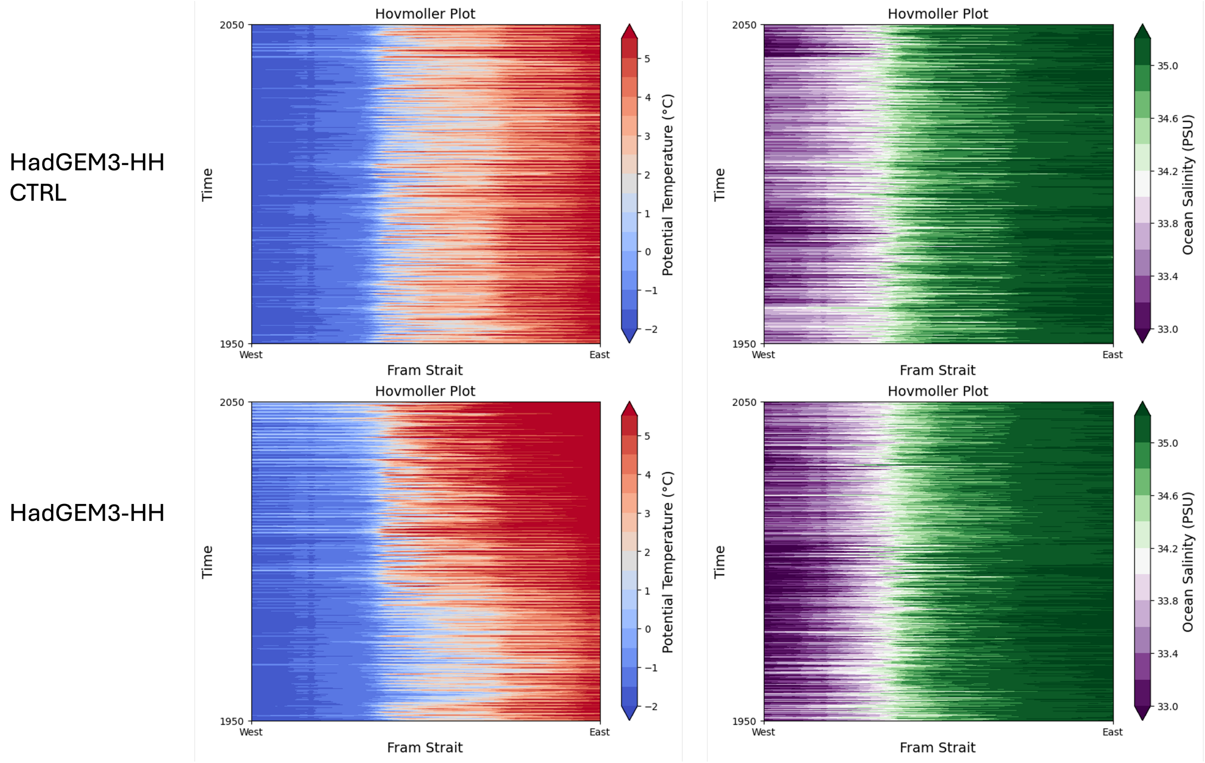

Figure 3.12: Hovmöller plots showing 100 years of (a) potential temperature and (b) ocean salinity at Fram Strait, averaged over the upper 200 m, for HadGEM3-HH transient and control runs.

3.3.5 The Westward Advance of Atlantic-Origin Water at Fram Strait: A Comparison to Findings by de Steur et al. (2023)

Using the mooring data at Fram Strait de Steur et al. (2023) conclude that the upper ocean warmed significantly between 2003 and 2019. They show that the warmer and more saline Atlantic Water is having a greater presence in central Fram Strait, particularly in winter, and that this results in reduced sea-ice thickness and extent, acting as a positive feedback loop. As highlighted in the previous section (e.g. Figure 3.12), the HadGEM3-HH model shows a similar result, with warmer temperatures extending further towards the west of Fram Strait over time in response to climate forcing.

In their study de Steur et al. (2023) use two moorings, F14 and F11, to consider variability within the EGC, both onshore and offshore respectively. The location of these two moorings at Fram Strait is shown in Figure 3.13 which is taken from the paper. Note they only consider data recorded at approximately 55 m depth in their analysis.

As shown in their study, the F14 on-shelf mooring shows a significant trend of gradually increasing potential temperature in summer, as well as a pronounced increase in seasonality as autumn temperatures rise and there are increasingly prolonged warmer periods lasting longer into the year (until November or even December in some cases).

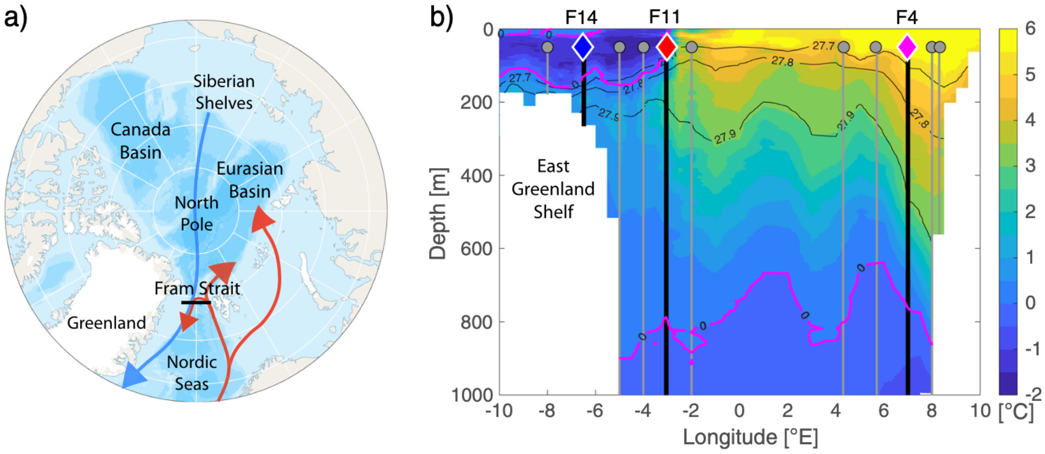

Figure 3.13: Figure taken from de Steur et al. (2023) showing (a) map of the Arctic Ocean with schematic arrows illustrating the cold outflow of Polar Water from the Arctic to the East Greenland Current (blue arrow) and the warm inflow of Atlantic Water into the Arctic Ocean and its recirculation in Fram Strait (red arrows), and (b) vertical cross section of temperature in the Fram Strait at 78°50’N in September 2018 (obtained from shipboard hydrography) marking the locations of the moorings F14, F11, and F4 with thick vertical black lines and blue, red and magenta diamonds, respectively. The background colouring is ocean temperature with 0.5°C intervals and the magenta lines mark the 0°CC isotherm.The location of the section in Fram Strait is marked in subplot (a) with the thick horizontal black bar.

The F14 mooring has a mean summer (July, August, September) temperature trend of 0.19 °C/decade, while the winter (January, February, March) trend is much smaller but also positive at 0.07 °C/decade. de Steur et al. (2023) suggest that this trend does not correlate to any significant trend in ocean salinity at this location, although there is a small increasing trend here too. The salinity observations have a less distinct seasonal cycle and large interannual variability demonstrating large variability in the halocline waters transported southwards on the shelf.

The HadGEM3-HH model has similar values for both potential temperature and ocean salinity at this location (Figure 3.14).The control run shows reduced variability, with no significant trend, suggesting these changes are driven by a response to climate change.

The ORAS5 reanalysis product shows similar results until the year 2015, at which point there appears to be a significant step change to increased temperature. From 2015 onwards, apart from in 2017, summer temperatures at this location in ORAS5 reach above freezing. Generally, there are also higher salinity values for this warmer period in ORAS5,

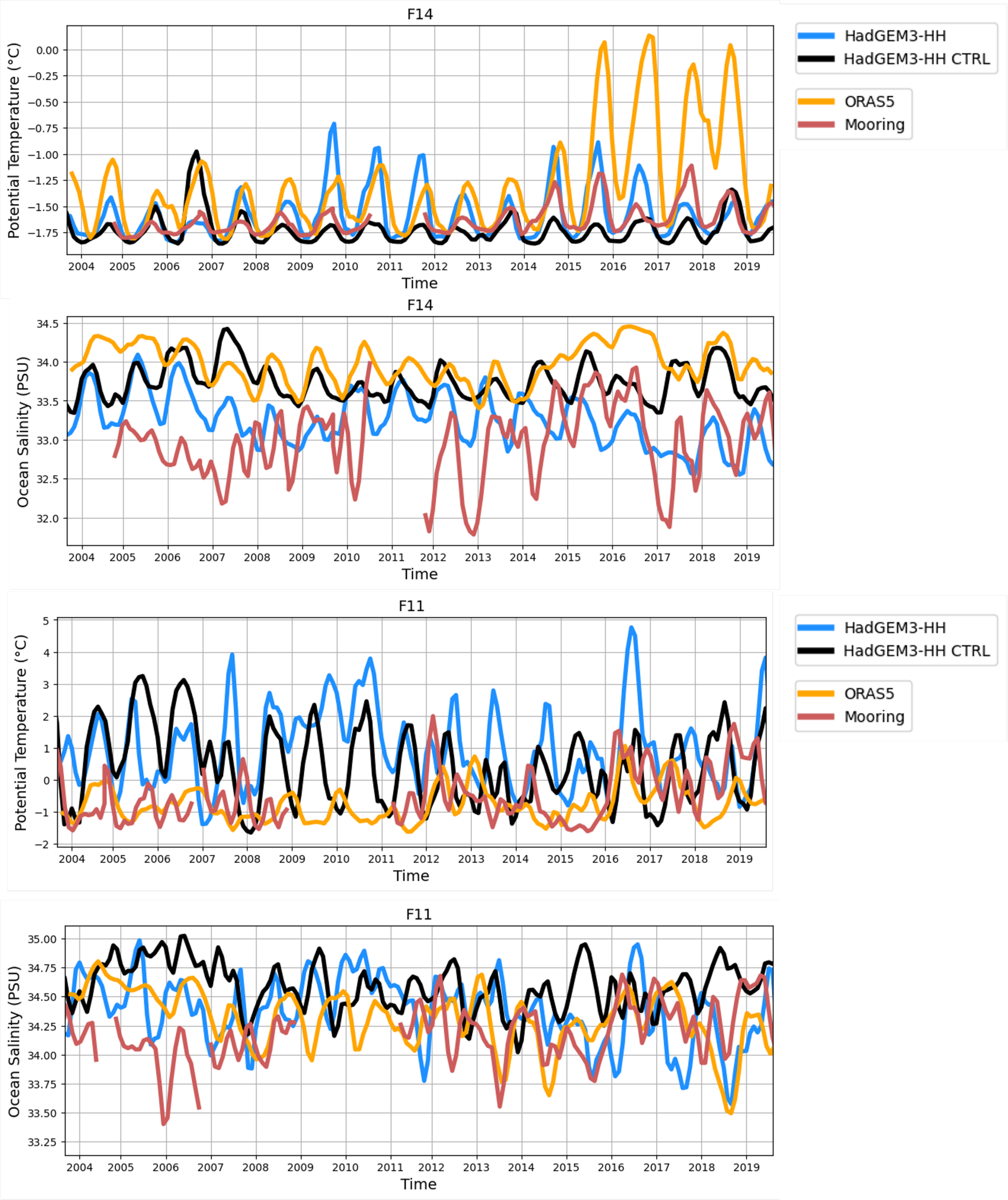

Figure 3.14: Time series of potential temperature and ocean salinity at 55 m depth for the F14 (upper subplots) and F11 (lower subplots) locations. Results from the transient and control HadGEM3-HH simulations are in blue and black respectively while the observations based data from ORAS5 and the moorings are in orange and red respectively.

suggesting an increased presence of Atlantic-Origin Water.

The salinity at F14 in the other products shows no clear trend, with a more consistent seasonal cycle in the model than in the mooring observations, which appears more variable. Together, these changes point to a warming of the on-shore component of the EGC, **not** due to an increased presence of Atlantic-Origin water but due to increased warming from the surface, as concluded by de Steur et al. (2023).

In comparison, the mooring data at F11 (off-shore component of the EGC) shows a step change increase in 2015, much like as shown for F14 in ORAS5. Here, the observations show a significant increase in temperature and salinity in the summer of 2015, with elevated values remaining from then on all year round, even in winter (Figure 3.14). This location appears more impacted by broader Nordic Seas wide increases in ocean temperature. The annual cycle is more variable at this location indicating that this location is less impacted by annual changes in, for example, sea-ice melt and formation as it is further off-shore.

If we consider the period for which the model data and reanalysis product are available, we see that there are clear differences in the trends at the F14 and F11 locations (Figure 3.15). There are increasing potential temperatures at the F14 location in ORAS5 and HadGEM3-HH (but not in HadGEM3-HH CTRL), whereas at the F11 location, there is much higher variability in the potential temperature. This is particularly noticeable for the winter period which differs significantly year-to-year, unlike at F14.

There is no significant trend in the ocean salinity in either of the two locations, with high interannual and inter-decadal variability in both cases. Note that for F11, ORAS5 generally shows higher salinity values than the model.

In de Steur et al. (2023), they show that the changes in the ocean properties over this 16 year period differ greatly between the two locations. This is particularly clear when we consider the seasonal cycles in potential temperature and salinity (Figure 3.16).

As illustrated in these figures, the response in the annual cycle of variability is well captured by the model and the reanalysis product. The gradual warming trend at F14, particularly in the autumn months, is well resolved. This trend is not seen at F11 where there is higher interannual variability across the properties.

Altogether these findings point to a westward advance of Atlantic-Origin Water at Fram Strait, which is simulated reasonable well in the high-resolution HadGEM3 model. This change is clear in the potential temperature diagnostic but more variable in the ocean salinity data, where there are also larger model biases.

3.3.6 Model Evaluation at Denmark Strait

For additional validation of the HadGEM3 model, we also use the Kögur Array at Denmark Strait. The locations of the moorings, and the equivalent data points in the model, are shown in Figure 3.17. Note that for ease of computation, we take model data from a transect on the model grid close to the geographical location of the Kögur Array, so that

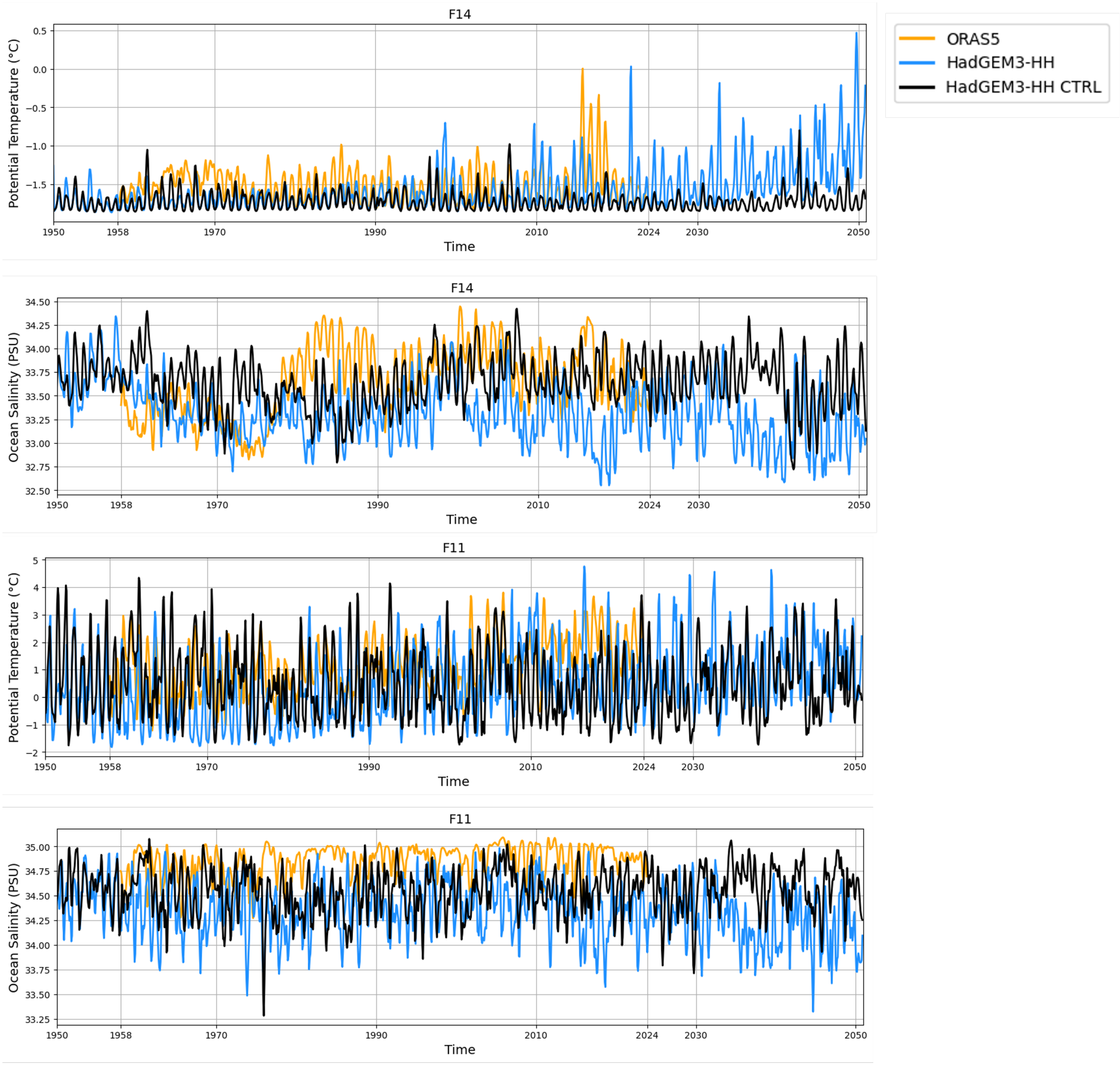

Figure 3.15: Time series over the 101 year period of the model run of potential temperature and ocean salinity at 55 m depth for the F14 (upper subplots) and F11 (lower subplots) locations. Results from the transient and control HadGEM3-HH simulations are in blue and black respectively while the observations based data from ORAS5 are in orange.

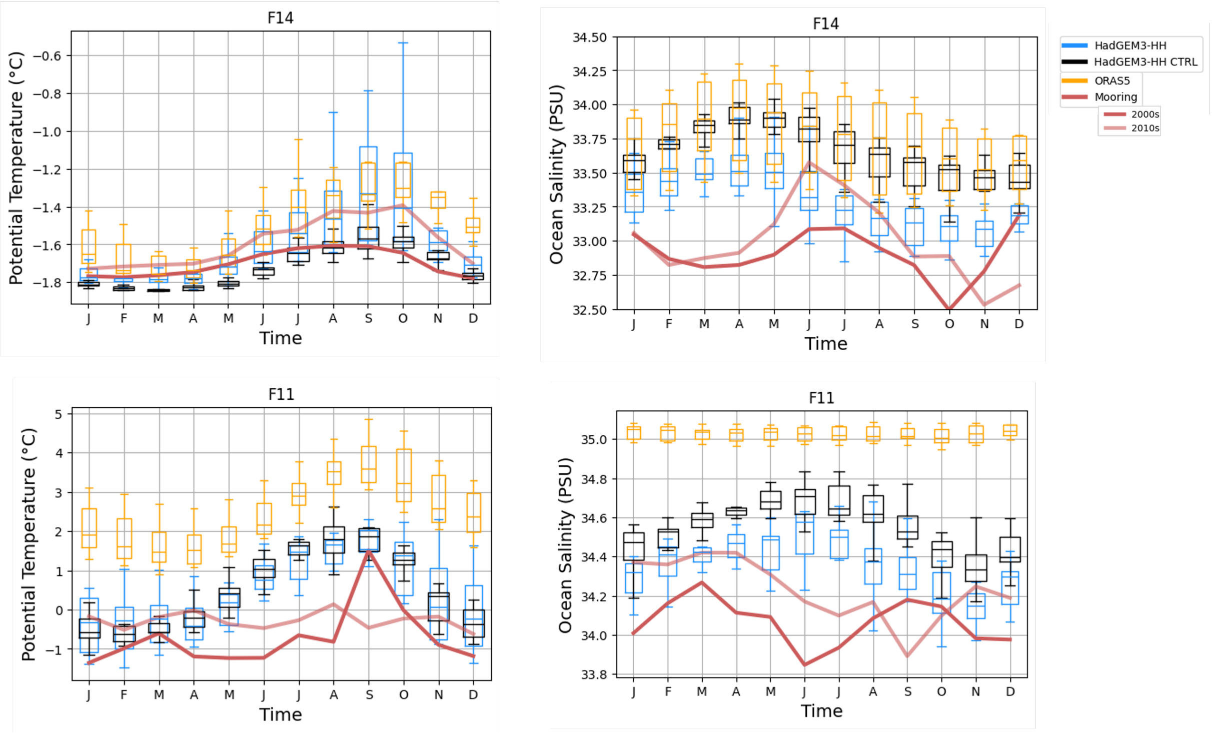

Figure 3.16: Time-mean annual cycles of potential temperature (first column) and ocean salinity (second column) at the F14 and F11 mooring locations (first and second row respectively) for the period between 2003 and 2019 for all the products. The results from the mooring data is shown for each decadal mean (2000s and 2010s).

the cross-sections show ocean velocities directed perpendicular to the transect line.

As illustrated in Figure 3.18, the mean transects for potential temperature, ocean salinity and along-current velocity for this period of time compare well. Bearing in mind that the transects do not align perfectly, the HadGEM3-HH model captures the complex ocean circulation systems at Denmark Strait (see Figure 3.17), even resolving smaller features such as the pathways of the Separated EGC and North Irminger Jet (NIJ) seen in observations (e.g. Harden et al., 2016). These dynamical details are reduced in magnitude and almost lost completely when using the medium and low-resolution model runs respectively (Figure 3.18).

With respect to the water properties at Denmark Strait, the mean temperature and salinity profiles from the HadGEM3-HH model resemble those from the mooring observations. The dynamics of the EGC are well captured in the high-resolution simulation with the location and magnitude of the surface velocities similar to those shown in the observations. Note that the model shows the warmer and more saline water of the North Icelandic Irminger Current (NIIC) which lies outside the reach of the Kögur Array measurements but has been observed in other studies using, for example, ship data (Semper et al., 2022; Casanova-Masjoan et al., 2020).

The ORAS5 and HadGEM3-MM products show weaker ocean velocities in the boundary currents, and thus have muted extremes in temperature and salinity at these locations. The low-resolution model does not represent the ocean dynamics at Denmark Strait well,

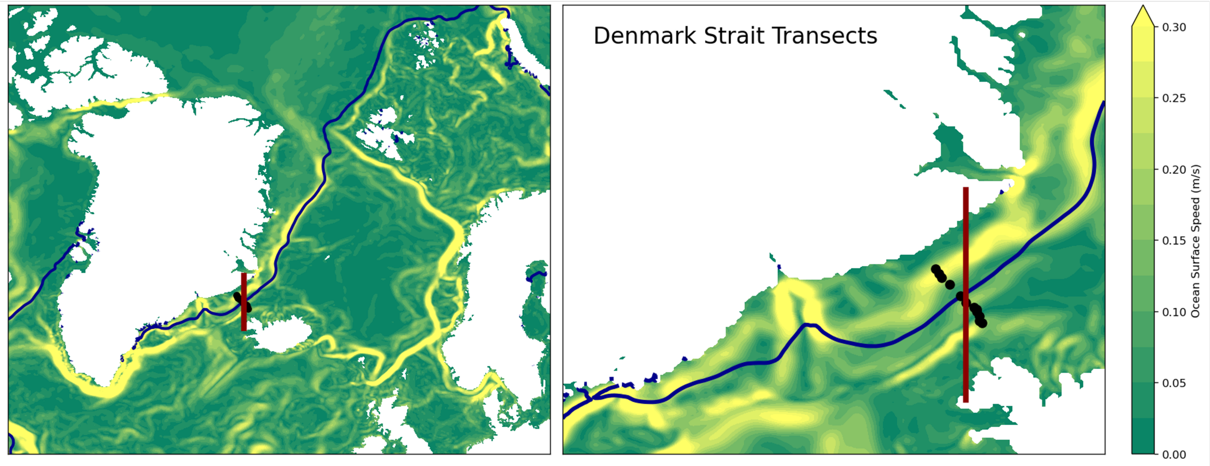

Figure 3.17: Maps showing the location of the transects used at Denmark Strait on the mean surface velocity from HadGEM3-HH for the 2010s. The Kögur Array moorings are shown by the black dots and the red line indicates the nearest transect on the model grid used in the other products. The blue line indicates the mean 15% sea-ice contour from HadGEM3-HH for the 2010s.

with significantly weaker and shallower boundary currents (EGC and NIIC). Additionally, it does not capture the temperature or salinity gradients across the transect and has a significantly less accurate representation of the bathymetry. Only the general circulation pattern is captured in the low-resolution, which should be noted when considering research using this model configuration.

The T-S diagrams from the 10-month mean for each of the product transects (Figure 3.19) illustrates the differences in the water properties here. The model and reanalysis show fresher and warmer water than is seen in the mooring observations.

Hovmöller plots for the same transects and 10 month period highlight the difference in the seasonal cycle with grid-resolution (Figure 3.20).

The moorings (higher frequency data) show a seasonal cycle in temperature and salinity, with increased fresh water in the northern half of the transect in the autumn and early winter months. This is also associated with higher temperatures across the transects. Then the more saline water advances from the south of the transect towards the north, resulting in an increase in salinity over the later winter and spring period. We also see a cooling over this period before, at the start of the summer months, there is an increase in temperature, particularly to the south. There is no clear seasonal cycle in the ocean velocity, although there appears to be a flux of eastward flowing water in the northern region associated with fresher waters during an autumn event.

These features are largely similar for the other products, although the magnitude of the seasonal cycles in temperature and salinity are reduced with coarser model grid resolution. The annual cycle is well represented by the ORAS5 reanalysis product with warming and freshening periods captured at approximately the correct time and location as in the observations. However, the boundary current velocities are underestimated, as is also true for the HadGEM3 medium and low-resolution simulations. For the high-resolution simulation the boundary current velocities are of a more comparable strength, along with the other diagnostics. For the medium and low-resolution simulations there tends to be too much cold, fresh water (particularly in the autumn period) and not enough warmer, more saline water (likely linked to the underestimation of the eastward ocean velocities).

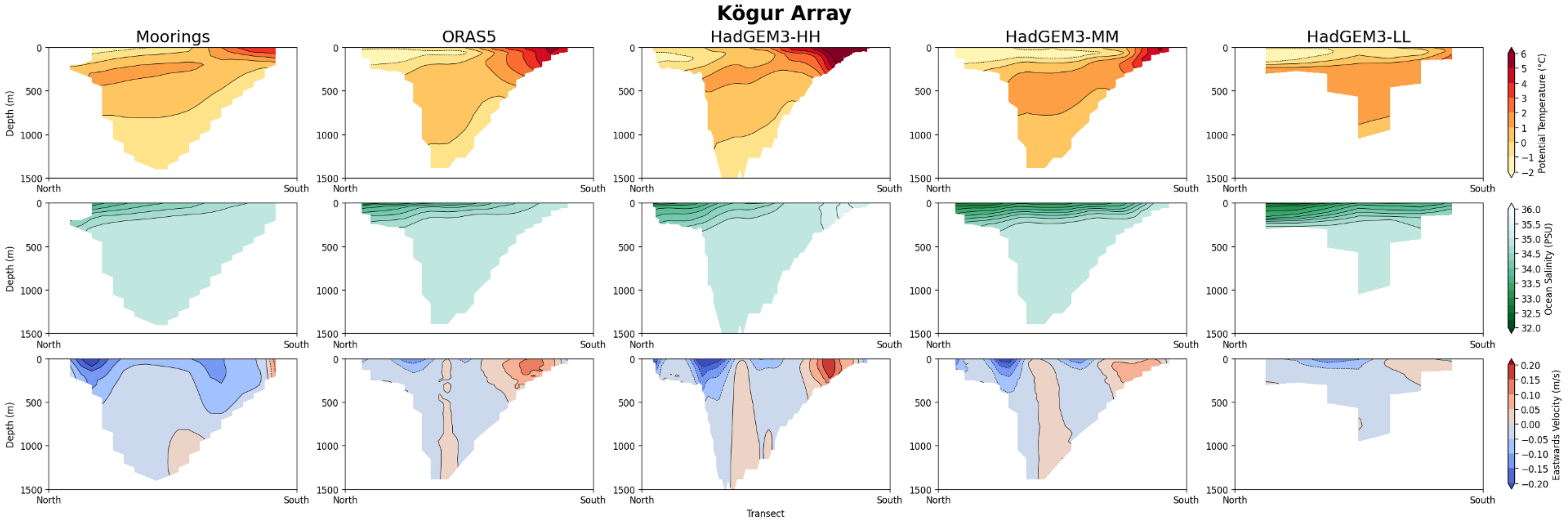

Figure 3.18: Mean potential temperature, ocean salinity and quasi-northwards ocean velocity for the transects at Denmark Strait using mooring observations, the ORAS5 reanalysis product and the HadGEM3 model at high, medium and low-resolutions.

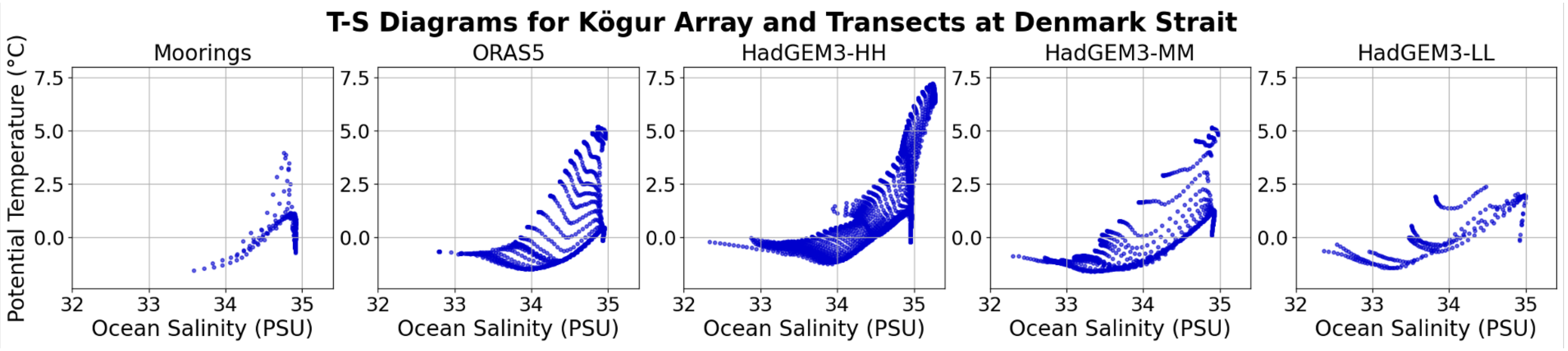

Figure 3.19: T-S diagrams from the transects at Denmark Strait for all products.

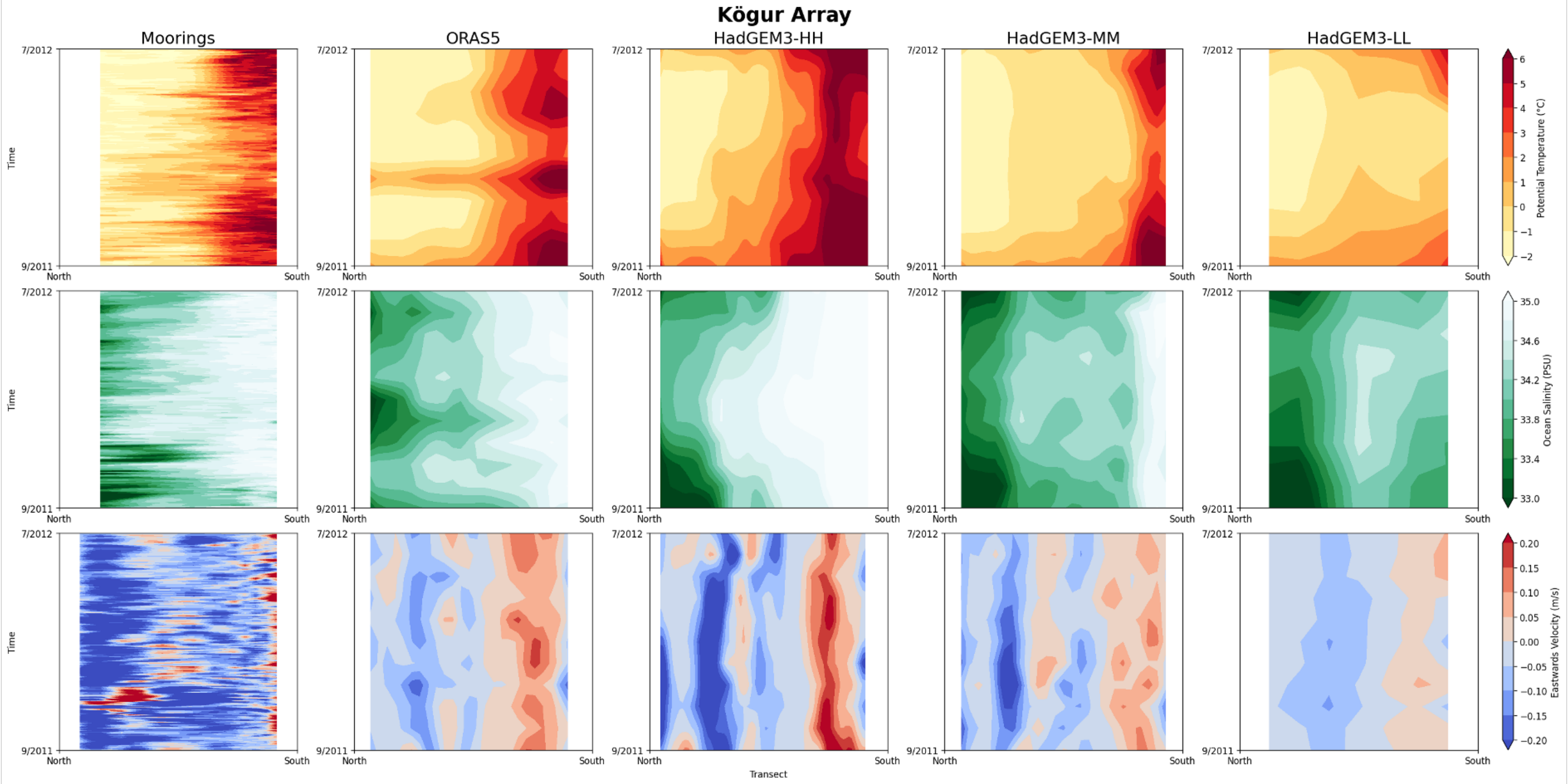

Figure 3.20: Hövmoller plots showing 10 months of (a) potential temperature, (b) ocean salinity and (c) along-flow velocity (perpendicular to the transect) at Denmark Strait, averaged over the upper 200 m, from the mooring data, the ORAS5 reanalysis product and the high, medium and low-resolution HadGEM3 transient simulations.

3.4 Conclusions

In this chapter we have validated the HadGEM3 global coupled climate model against observational sea-ice and oceanographic data in the Nordic Seas, highlighting differences between the high, medium and low-resolution simulations.

We find that the sea-ice concentration is reasonably well resolved, although some details are lost (e.g. the Northeast Water Polynya) and the rate of sea-ice decline is accelerated compared to currently available observations, particularly in the high-resolution configuration. However, the model can still be useful in providing information about long-term change and future climate scenarios.

The ocean properties and dynamics in the region also compare well to observations, although mooring data suggests that the boundary current velocities are slightly elevated, particularly in the high-resolution run. This results in enhanced inflow of warm and saline water to the Arctic (which likely plays a role in the rapid sea-ice decline here seen in the model). The model also produces higher velocities in the EGC, with a stronger flow of cold, fresh water towards the North Atlantic.

Time series illustrate the differences between on-shelf and off-shelf temperature and salinity within the EGC (comparisons to de Steur et al. (2023)) with the impacts of climate change clearly seen when comparing with the control runs (e.g. signifiant warming at the surface and the mechanism of westward advance of Atlantic Origin water are both resolved by the transient model).

The model generally captures the seasonal cycle of the upper ocean at Fram Strait with clear differences between Atlantic Water inflow and Arctic Water outflow in east and west Fram Strait respectively. The change in this cycle through time is more variable in the observations than in the reanalysis product and the model.

At Denmark Strait, the model also compares well to observations for ocean properties and dynamics, but again, the boundary currents are perhaps too strong in the high-resolution and too weak in the low and medium-resolution simulations. As at Fram Strait, we see that this leads to warmer Atlantic Water and fresher Polar Water than seen in the mooring data.

A Century of Change in the Nordic Seas: Comparing Results from High, Medium and Low Resolution HadGEM3 Simulations

4.1 Introduction

The Nordic Seas play a pivotal role in the global climate system by regulating exchanges between the Arctic and the North Atlantic. In addition, this region is a key site for dense water formation, contributing to the northernmost cell of the Atlantic Meridional Overturning Circulation (AMOC) and its stability is critical for the large-scale redistribution of heat and freshwater around the global thermohaline ocean circulation system (Mauritzen, 1996; Våge et al., 2015).

The Nordic Seas are highly sensitive to anthropogenically driven climate change, yet uncertainties remain regarding how this tightly coupled atmosphere-ice-ocean system will evolve in the future. Observational datasets and reanalysis products show robust warming trends in both the ocean and atmosphere as global mean temperatures rise under continued greenhouse gas forcing (Beszczynska-Möller et al., 2012; Polyakov et al., 2020). Meanwhile, sea-ice extent has declined markedly over recent decades, particularly in Fram Strait and around Svalbard, regions that act as key gateways for exchange between the high and mid-latitudes (Kwok et al., 2009; Onarheim and Årthun, 2017).

These changes impact regional air-sea interactions and feedback mechanisms, with consequences for both local ecosystems and the broader climate system. For instance, reduced sea-ice cover enhances ocean-atmosphere heat fluxes, modulates convection and can influence storm tracks (Screen and Simmonds, 2010; Koenigk et al., 2015). Moreover, drastic reductions in sea-ice affect local communities and wildlife that rely on its seasonal presence (Post et al., 2013).

Given that variability in the Nordic Seas can trigger ecological and environmental responses across many spatial and temporal scales, improved understanding of its future trajectory is vital. Global coupled climate models are valuable tools that allow us to investigate these processes and analyse both historical variability and plausible future scenarios.

In this chapter, we use HadGEM3 simulations to examine the response of the sea-ice, the near-surface atmosphere and the upper ocean in the Nordic Seas under a high-emissions scenario. By comparing results from high, medium and low resolution simulations, we assess how model resolution influences the simulated climate response in this climatically critical sub-polar system.

4.2 Data

HadGEM3 is a state-of-the-art climate model from the UK Met Office and is widely used within CMIP6 and IPCC AR6 studies, including high-emissions scenario projections (SSP5-8.5), which we focus on in this work. It is well suited to studying climate change in the Nordic Seas because it couples the NEMO ocean model, the CICE sea-ice model and the Met Office Unified Model atmosphere (MetUM), allowing a physically consistent representation of ArcticAtlantic exchange, sea-ice retreat, and AMOC-related processes (e.g. Sicard et al., 2022; Kageyama et al., 2021; Kuhlbrodt et al., 2018; Selivanova et al., 2024; Andrews et al., 2020).

A key strength of HadGEM3 is its ability to run at multiple ocean resolutions, allowing assessment of how model resolution influences important processes such as boundary currents, overflows and shelf-basin exchange. In the higher-resolution configurations (N216ORCA025 and N512ORCA12), the model provides improved representation of circulation pathways critical to the Nordic Seas, particularly across Fram Strait and the GreenlandScotland Ridge (Roberts et al., 2019; Petit et al., 2023). Previous studies have also shown good performance in simulating large-scale ocean transports, heat budgets, freshwater distribution, and broad patterns of sea-ice variability (de Boer et al., 2018; Treguier et al., 2021; Tsubouchi et al., 2018; Zhang et al., 2023; Yool et al., 2021).

However, important limitations remain. In lower-resolution configurations, narrow gateways such as Fram Strait and Denmark Strait are poorly resolved, which affects overflow representation and eddy processes (Roberts et al., 2019). Biases in Arctic sea-ice and subsurface hydrography can also influence Atlantic Water inflow pathways and upper-ocean stratification, while uncertainties remain in the model sensitivity of the AMOC under greenhouse gas forcing (Docquier et al., 2024; Petit et al., 2023).

In Chapter 3, medium and high-resolution HadGEM3 simulations were shown to compare reasonably well with observations, although boundary current velocities were overestimated. This leads to enhanced northward heat and salt transport in the Atlantic inflow pathways and stronger southward freshwater export in the East Greenland Current, contributing to faster simulated sea-ice decline than currently observed. These biases are important when interpreting future projections.

Overall, HadGEM3 provides a strong framework for investigating the coupled oceaniceatmosphere response of the Nordic Seas to climate change, while allowing model limitations and uncertainty to be explicitly considered.

4.3 Results

As greenhouse gas emissions from anthropogenic sources continue to increase, global mean temperatures continue to rise, with the fastest responses seen in the high-latitudes. With drastic warming in the polar regions comes a reduction in sea-ice volume (Gascard et al., 2019). The sea-ice is a crucial feature of the polar landscape, particularly in the Arctic, and its decline impacts many important aspects of the climate system, from the local to the global scale.

The Nordic Seas are particularly vulnerable to the changing climate. Anthropogenically-driven variability here is likely to have a cascading effect on both regional and global climate patterns (e.g. Holt et al., 2018; Hand et al., 2019; Zhao et al., 2019; Spall et al., 2021; Jensen et al., 2016; Du et al., 2019). For example, water mass transformation in the Greenland Sea plays a significant role in feeding dense water to the AMOC but this processes is susceptible to temperature and salinity changes (e.g. Otterå et al., 2004; Tsubouchi et al., 2021; Spall et al., 2021; Glessmer et al., 2014; Latarius and Quadfasel, 2016; Hand et al., 2019). Additionally, the region acts as a major carbon sink by absorbing large quantities of atmospheric carbon dioxide and carrying it to the deep ocean (Jeansson et al., 2011; Frigstad et al., 2021; Pedersen et al., 2025). The largely atmospheric-driven export of sea-ice from the high Arctic towards the North Atlantic is also pertinent, with Fram Strait acting as the main gateway for exchange between the sub-polar North Atlantic and the Arctic Ocean (Smedsrud et al., 2011, 2017; Wei et al., 2019).

While observations are useful for monitoring recent changes, climate models allow us to look forward in time, giving us valuable insights into possible future scenarios. Hence, to consider how the Nordic Seas might change from the past to the future, we compare results from historical simulations and future projections in the HadGEM3 global coupled climate model (Roberts et al., 2019). We consider high, medium and low resolution model runs to show that the characteristics and rate of change can differ with horizontal grid resolution. To better understand the possible impacts of climate change in the Nordic Seas we first look at near-surface changes over the period of the HadGEM3 simulations, which start in 1950 and end a hundred years later in 2050.

4.3.1 Near-Surface Changes in the Nordic Seas between the 1950s and 2040s

Spatial maps showing the mean near-surface potential temperature for the first and last decade of the 100 year simulation, and the difference between these, show the response of the region to climate forcing (Figure 4.1). As expected, between the 1950s and 2040s, there is significant warming in the Nordic Seas across all three resolutions. Increasing temperatures are seen throughout the domain but the magnitude of warming is not consistent everywhere; there is significant spatial variability.

The largest response is shown in the low resolution simulation, with increases of more than 5°C in the central Norwegian Sea, the Barents Sea and the region south of Svalbard. There is also a strong warming of more than 5°C seen in the high resolution simulation, but in a more confined region to the north of Svalbard, along a section of the West Spitsbergen Current pathway.

In areas of sea-ice cover, such as to the north of Greenland, the change in potential

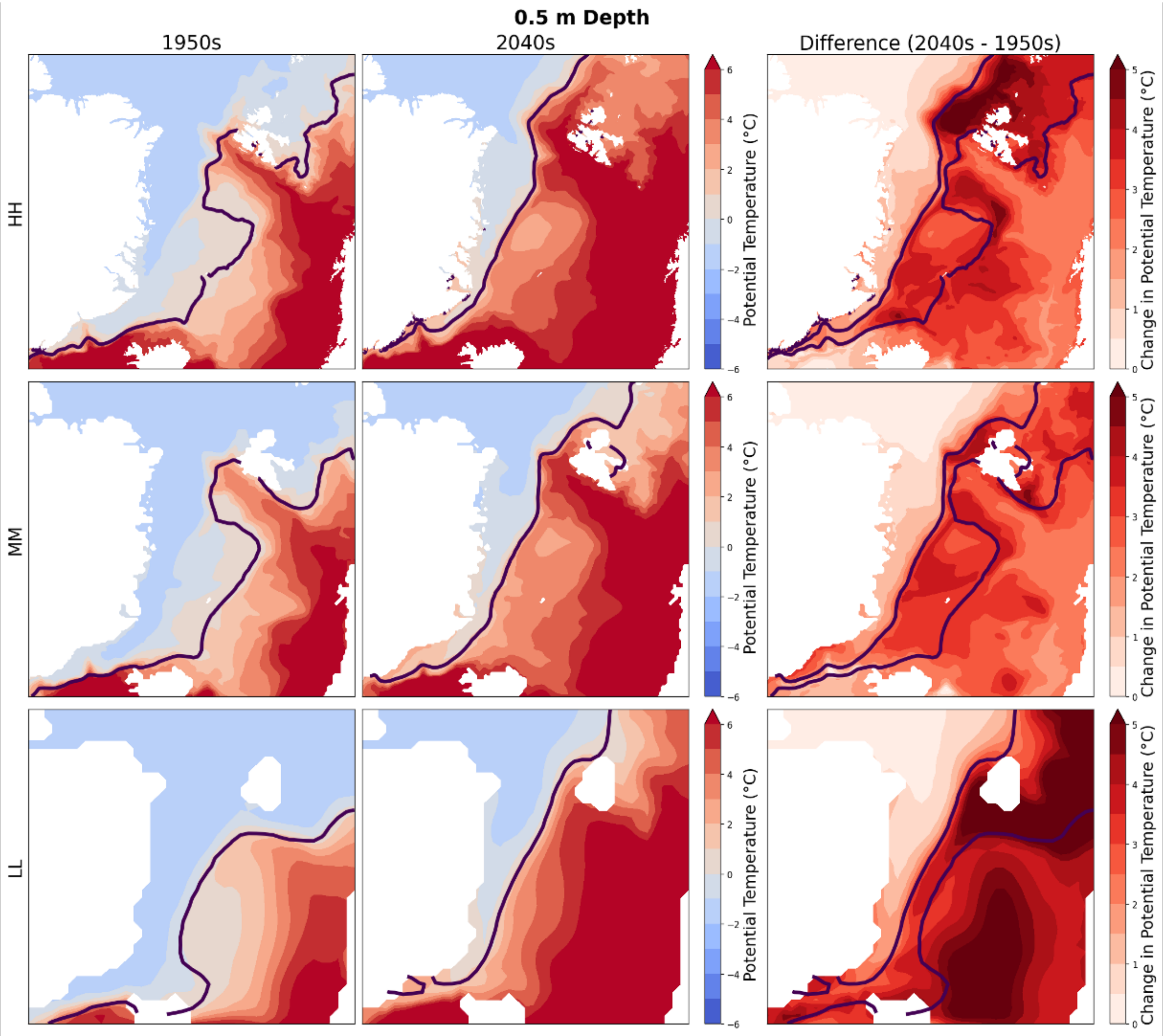

Figure 4.1: Mean potential temperature at 0.5 m depth for the 1950s, the 2040s and the difference between these two decadal means (2040s minus 1950s). The decadal mean 15% sea-ice contour is shown in each panel by the thicker dark purple line. Note that the domain is shown on the model grid. The upper row shows the results from the high resolution HadGEM3 simulation, the middle row for the medium resolution simulation and the bottom row for the low resolution simulation.

temperature is reduced and remains approximately consistent across the model resolutions at less than 1°C. This highlights the important role of sea-ice in limiting the warming at the ocean surface.

The spatial pattern of temperature change in the Nordic Seas indicates that the regions of largest change are those fed by boundary currents which transport relatively warm and saline Atlantic-Origin water towards the Arctic, for example, the West Spitsbergen Current which transports heat towards the north of Svalbard (particularly clear in the high resolution) and the Norwegian Current which feeds into the Barents Sea (particularly clear in the low resolution).

The exterior boundaries of the Greenland Sea Gyre are also particularly sensitive to climate forcing. The significant increase in potential temperature here, seen in both the medium and high resolution, could be a result of increased recirculation and mixing of Atlantic-Origin waters from the boundary currents into the Greenland Sea Gyre. Changes in atmospheric circulation patterns (such as the North Atlantic Oscillation) can also impact the ocean properties in the Greenland Sea Gyre. Whether the phase of the atmospheric oscillation intensifies or inhibits the cyclonic circulation impacts the rate of heat loss to the atmosphere, enhancing or reducing the recirculation of warmer Atlantic-Origin Water and further contributing to warming or cooling. Additionally, the reduction in sea-ice cover at the surface affects atmosphere-ocean heat fluxes which play a significant role in the properties and structure of the water column here.

As discussed in Chapter 3, the ocean warming seen in the high resolution HadGEM3 model is faster than seen in present-day observations but analysis of the model can still provide extremely valuable information and overall this simulation has the most realistic representation of the Nordic Seas climate system, especially regarding the ocean dynamics. The rate of ocean warming in the medium resolution model compares better to observations but the smaller-scale ocean dynamics (such as eddy processes) are not as well resolved. Meanwhile, evaluation of the low resolution simulations suggest that such a coarse grid spacing does not capture important processes and results are not representative of the real world. See Chapter 3 for more details on the evaluation of HadGEM3 simulations in the Nordic Seas.

If we consider the near-surface ocean salinity (Figure 4.2) we see that, for all three resolutions, the region around Svalbard, while being a region of significant warming is also a region of increased salinity. Meanwhile a freshening trend is seen in regions of sea-ice cover and on the continental shelf of East Greenland. The spatial pattern of the overall trend is very similar across the model resolutions here. The largest response is again seen in the low resolution simulation, with the magnitude of the change between the 1950s and 2040s generally decreasing with increasing resolution.

One difference is that the Iceland Sea region shows a small increase in salinity over this period in the high and medium resolution simulations but in fact shows a small decrease in the low resolution case. This is likely due to the poor representation of smaller-scale ocean circulation systems in the Iceland Sea in the low resolution simulation.

The fact that the regions of strongest warming over this period generally co-locate with the regions of largest increases in salinity suggests that the two responses are linked. Although a warming is seen throughout the domain, the rate of warming is slower where there is a freshening trend, likely due to increased freshwater flux from sea-ice melt and land run-off. Where there is a higher rate of warming, there is also generally an increase in salinity, due to increased inflow, recirculation and mixing of warmer and saltier Atlantic-Origin Water via the Norwegian Atlantic Current and West Spitsbergen Current pathways.

The responses of the temperature and salinity diagnostics are also reflected in the change in calculated potential density. Here we see a strong decrease in density where

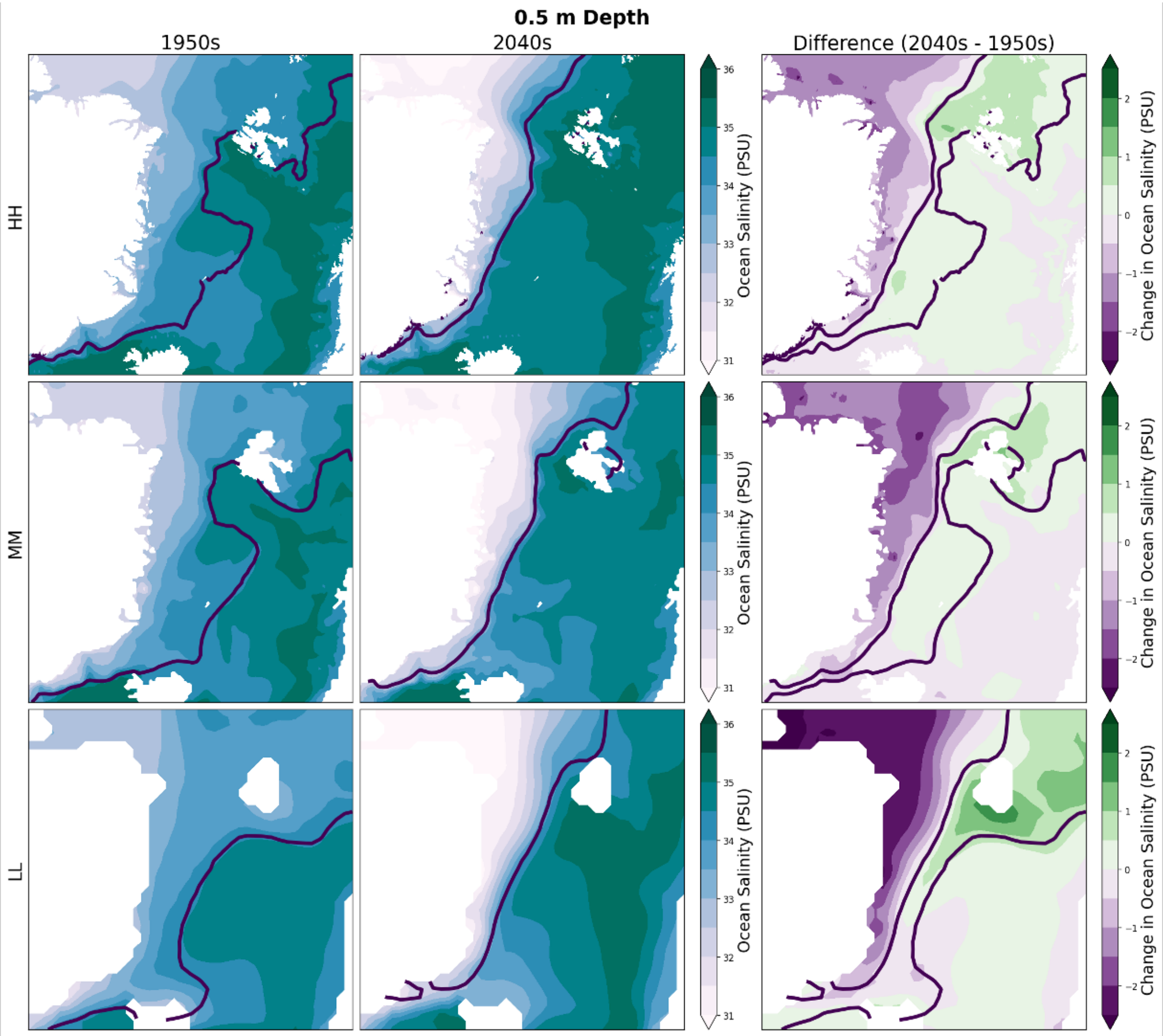

Figure 4.2: Mean ocean salinity at 0.5 m depth for the 1950s, the 2040s and the difference between these two decadal means (2040s minus 1950s). The decadal mean 15% sea-ice contour is shown in each panel by the thicker dark purple line. Note that the domain is shown on the model grid. The upper row shows the results from the high resolution HadGEM3 simulation, the middle row for the medium resolution simulation and the bottom row for the low resolution simulation.

there is a strong freshening trend and an increase in density around Svalbard, in the region of increased salinity and of highest warming (Figure 4.3). The spatial pattern of the density changes are similar in all three grid resolutions, indicating a robustness to this result. Although, there is a small increase in the potential density within the Greenland Sea Gyre in the high and medium resolution simulations which appears not to be captured in the low resolution case at all.

Density changes are important as the vertical structure of the Nordic Seas is largely determined by the buoyancy properties of the water column. The stratification of warmer, less dense surface layers atop cooler, denser, deeper waters is crucial for densification and influences the water mass transformation which feeds overflow water into the northern branch of the AMOC. The regions of reduced density in Figure 4.3 are projected to

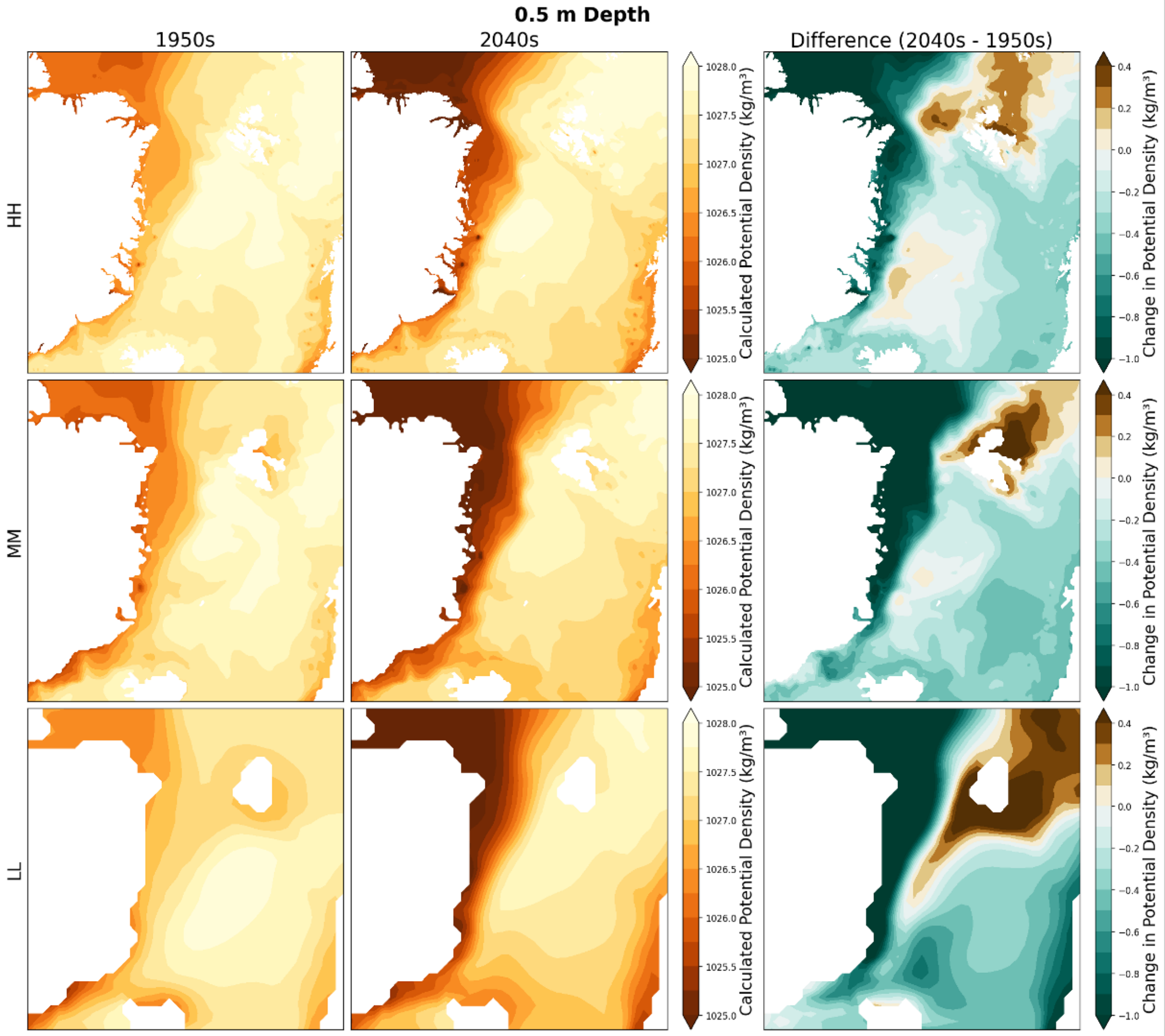

Figure 4.3: Mean calculated potential density at 0.5 m depth for the 1950s, the 2040s and the difference between these two decadal means (2040s minus 1950s). The upper, middle and lower rows show the high, medium and low resolution results respectively.

become more stratified which inhibits vertical mixing and densification.

With differing trends in the density response predicted for different regions of the Nordic Seas, the horizontal density gradient marking the boundary between these regions will increase in strength in the future. As a lightening of the upper ocean occurs on one one side of the density front and a densification on the other, there will be a tightening of the isopycnals along that density front. This can lead to enhanced circulation via geostrophy.

The response of the ocean surface velocities is shown in Figure 4.4. At the high and medium resolutions, the ocean velocity patterns are similar, although, the speeds of the boundary currents are generally higher in the high resolution simulation. This is especially evident for the West Spitsbergen Current and Norwegian Current/Norwegian Atlantic Current as it flows from the north coast of Norway around the west of Svalbard and towards the Arctic Ocean.

Moreover, there are many smaller-scale dynamical features captured in the high res-

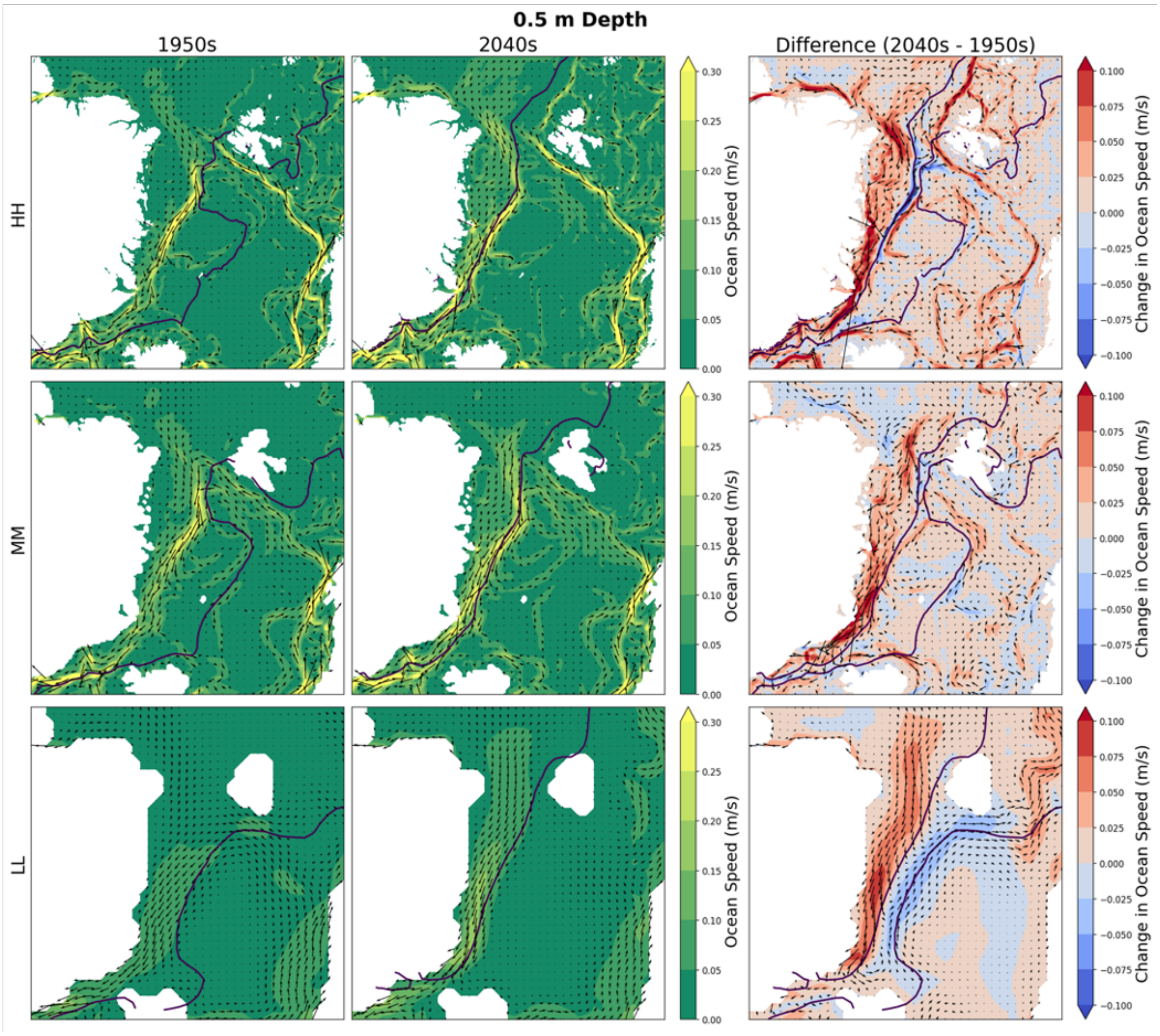

Figure 4.4: Mean ocean velocities at 0.5 m depth for the 1950s, the 2040s and the difference between these two decadal means (2040s minus 1950s). The decadal mean 15% sea-ice contour is shown in each panel and the upper, middle and lower rows show the high, medium and low resolution results respectively.

olution that are not seen in the medium resolution. For example, the current through Nares Strait in Northern Greenland (Münchow, 2006; Rabe et al., 2010), several surface currents in the Barents Sea (Loeng et al., 1997; Ozhigin et al., 2011) and the Irminger Current and East-Icelandic Current in the Iceland Sea (e.g. Semper et al., 2022; Pickart et al., 2017; Macrander et al., 2014; Perkins et al., 1998). The geographical extent of the Greenland Sea Gyre also appears larger in the high resolution simulation.

In any case, we can see significant differences when these are compared to the low resolution simulation, where most details are lost due to the much coarser grid spacing. In fact, only the general large-scale circulation is represented here and there is a significant response in this between the 1950s and 2040s.

The difference subplots in Figure 4.4 illustrate the change with climate forcing at all three resolutions. In the high resolution, an increase in the ocean surface velocities is generally seen in most areas. There is a significant increase in ocean speed along the Norwegian Atlantic Current/West Spitsbergen Current in the high resolution of approximately 0.07 m/s between the 1950s and 2040s. This current pathway also appears to extend much further north in the future projection, which would indicate increased transport of Atlantic-Origin Water towards the higher latitudes. This is not seen in the medium or low resolutions. However, in the low resolution there is an increase in transport from the North Atlantic towards the Barents Sea. Together these changes explain the different responses in temperature, salinity and density at different model resolutions already seen in these regions in the previous figures.

In the high resolution simulation, the velocity of the East Greenland Current is also projected to increase and we see a widening/offshore shift in it's core pathway with climate forcing. This is illustrated by the increase in southward flow along the eastern edge of the current and a relative decrease along the western edge, closer to the continental shelf. This is not as apparent in the other simulations, although there is a relative decrease in velocity to the east of the EGC in the low resolution representing a reduction in the circulation of the Greenland Sea Gyre.

As evidenced by reanalysis data there is strong horizontal circulation in this region (Årthun et al., 2023b) and the intensification of Nordic Seas boundary currents has been demonstrated by both observational and modelling studies in recent years. For example, using satellite altimetry Oziel et al. (2020) show a clear increase in surface velocities along the Norwegian Atlantic Current pathway and Polyakov et al. (2020) measure an increase in the near-surface current speeds and vertical shear using moorings in the eastern Eurasian Basin (from 2004 to 2018). Additionally, Wang et al. (2020) present model results from a Finite Element Sea-ice Ocean Model (FESOM) that show a strengthened Atlantic Water inflow through Fram Strait towards the Arctic Ocean due to enhanced boundary current flow and strengthened gyre circulation.

In all three of these resolutions, the HadGEM3 simulations show a significant increase in the quasi-southward flowing ocean velocities on the continental shelf of East Greenland.

This change appears to be robust across the three grid resolutions, although given the substantial lack of observational data here it is difficult to obtain any physical evidence that supports this. The source of this response also remains unclear and whether or not these changes affect the ocean properties and dynamics at the Denmark Strait Overflow is unclear at present. The change in the downwards stress acting on the ocean surface is shown in Figure 4.5. This response is similar in all three grid resolutions and indeed we see a large increase in the southward stress along the continental shelf of East Greenland, where there are increases in ocean surface velocity (red shading in difference subplots in Figure 4.5), while elsewhere, particularly in areas of significant sea-ice decline, there is a notable decrease in the surface stress (green shading in difference subplots in Figure 4.5). This results suggest that the wind stress does not contribute significantly to the response in ocean circulation, which is primarily driven by geostrophic changes.

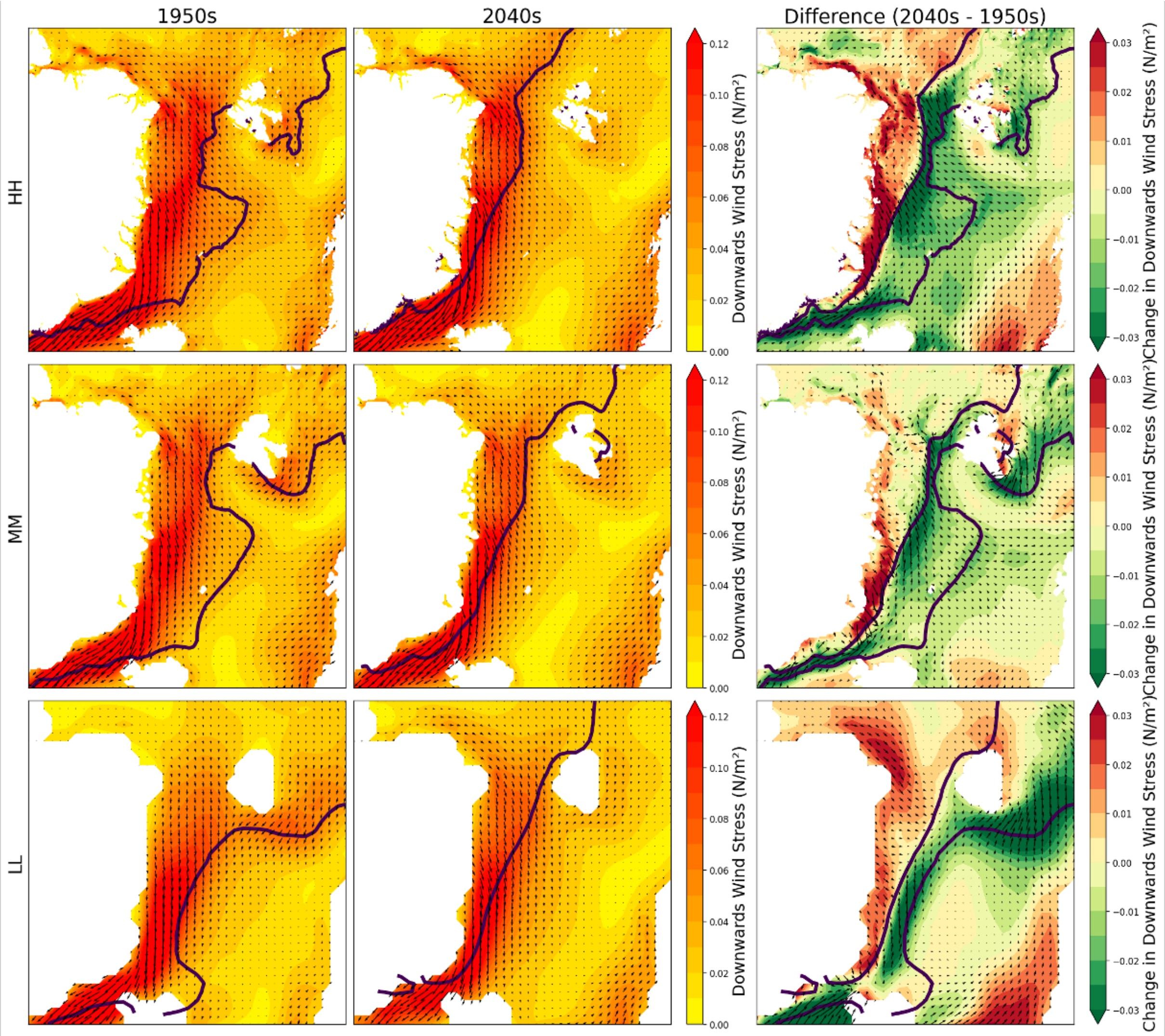

Figure 4.5: Mean downward stress acting on the ocean surface for the first and last decade and the difference between these. The decadal mean 15% sea-ice contour is shown in each panel and the upper, middle and lower rows show the high, medium and low resolution results respectively.

As illustrated in Figure 4.6, the mean spatial distribution of the downwards (atmo-

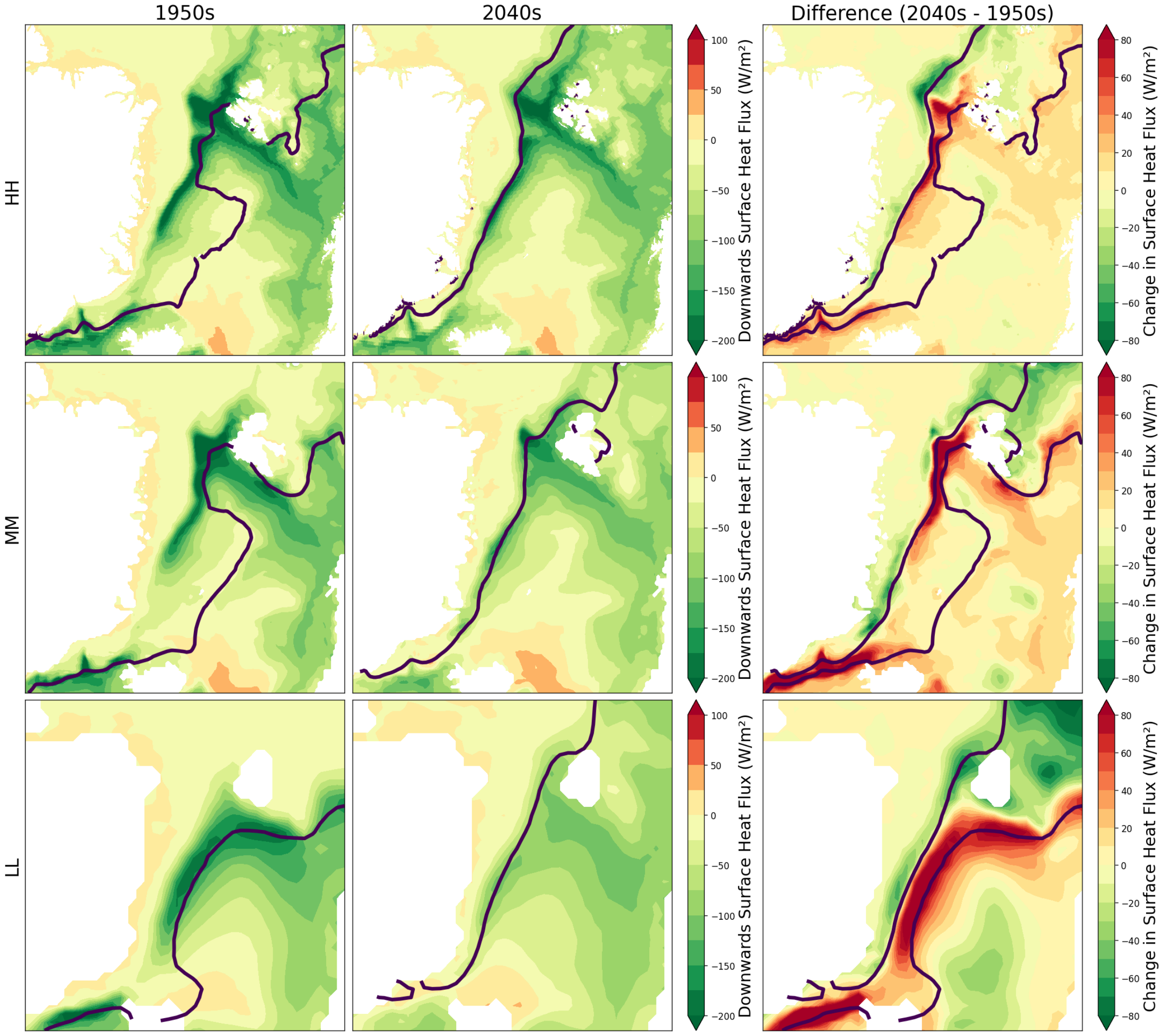

Figure 4.6: Mean downwards surface heat flux (from atmosphere to ocean) for the first and last decade and the difference between these. The decadal mean 15% sea-ice contour is shown in each panel and the upper, middle and lower rows show the high, medium and low resolution results respectively.

sphere to ocean) surface heat flux is similar in the 1950s and 2040s for all model resolutions. In this region, the strongest heat fluxes (sometimes over 100 W/m^2) act in the upwards direction, transferring heat from the ocean to the atmosphere (hence the negative values in Figure 4.6). These are seen near the sea-ice edge and within the marginal ice zone. There are also relatively strong upward fluxes along the pathway of the West Spitsbergen Current. This is where warmer ocean water is transported northwards and interacts with colder air, resulting in a large transfer of heat from the ocean to the atmosphere. An analysis of the surface heat fluxes in the HadGEM3 simulations in the Nordic Seas, and the tight coupling of their response to local sea-ice decline, is presented by Barrell et al. (2023). They demonstrate that the strongest wintertime surface sensible and latent heat fluxes typically occur just downstream of the sea-ice edge but under a climate change scenario, future projections show significant reductions in wintertime air-sea turbulent fluxes (particularly in the interior of the Nordic Seas) and a notable reduction in their decadal variability. In turn, this response impacts water mass transformation (Moore et al., 2015) and thus ocean properties and dynamics in the region (Moore et al., 2022; Buckley and Marshall, 2016; Ivanov, 2023). Smedsrud et al. (2022) provide an in-depth synthesis of Atlantic Water cooling in the Arctic over the last century, based largely on an ocean-sea-ice model forced by a reanalysis atmosphere, corroborated by hydrographic and sea-ice observations. They quantify and describe this mechanism, showing that heat loss to the atmosphere is largest in the Nordic Seas (60% of the Arctic total) with large variability linked to the frequency of Cold Air Outbreaks and cyclones. They calculate the mean annual heat flux in the Nordic Seas to be 45.08 W/m^2 (between the years 1900 and 2009) and find a significant trend in increased total heat loss to the atmosphere (since 1900). This process of ocean-to-atmosphere heat flux is important in regulating the global climate system.

In Figure 4.6, it is demonstrated that the HadGEM3 simulated response of the surface heat fluxes to climate forcing closely follows the sea-ice decline. With the strongest near-surface winds seen along the sea-ice edge, this is often where the maximum upwards surface fluxes are found. As the sea-ice edge retreats northwards, this maximum is also shifted towards higher latitudes. In all three resolutions, we see that the strongest increase in upwards flux is seen in areas of significant sea-ice loss, such as along the ice front in the Greenland Sea and in the region to the north-east of Svalbard (where there has been significant warming).

In addition, we see a marked decrease in the upwards heat flux just to the south of these areas. This is due to the relative shift of the maximum surface heat flux away from these regions. These results point to a northwards shift in the sites of ocean cooling, ventilation and water mass transformation, which are all crucial mechanisms for dense water formation and the AMOC (Moore et al., 2015, 2022; Chafik et al., 2020; Gebbie and Huybers, 2011; Mauritzen, 1996; Pemberton et al., 2015).

Note that the responses here in the high and medium resolutions are very similar and although the magnitude of the change seen in the low resolution is greater in comparison, the spatial distribution of the response of surface heat flux appears largely robust across the model resolutions. In has been shown in previous studies that higher resolution atmospheric model component is important for more realistic orography (Jung et al., 2012) and improved representation of wind-driven gyres in the Sub-Polar North Atlantic (Jung et al., 2014; Condron and Renfrew, 2013), while the higher resolution ocean model component has a more accurate representation of inflow and outflow pathways which redistribute heat around the Nordic Seas (Roberts et al., 2019; Petit et al., 2023; Treguier et al., 2021; Williams et al., 2018), both of which are important mechanisms for surface heat fluxes (Barrell et al., 2023).

As changes in ocean temperature and salinity can lead to changes in the stratification of the Nordic Seas, which is important for water mass transformation, one model diagnostic that is useful to consider is the calculated mixed layer depth (see Figure 4.7). The mixed

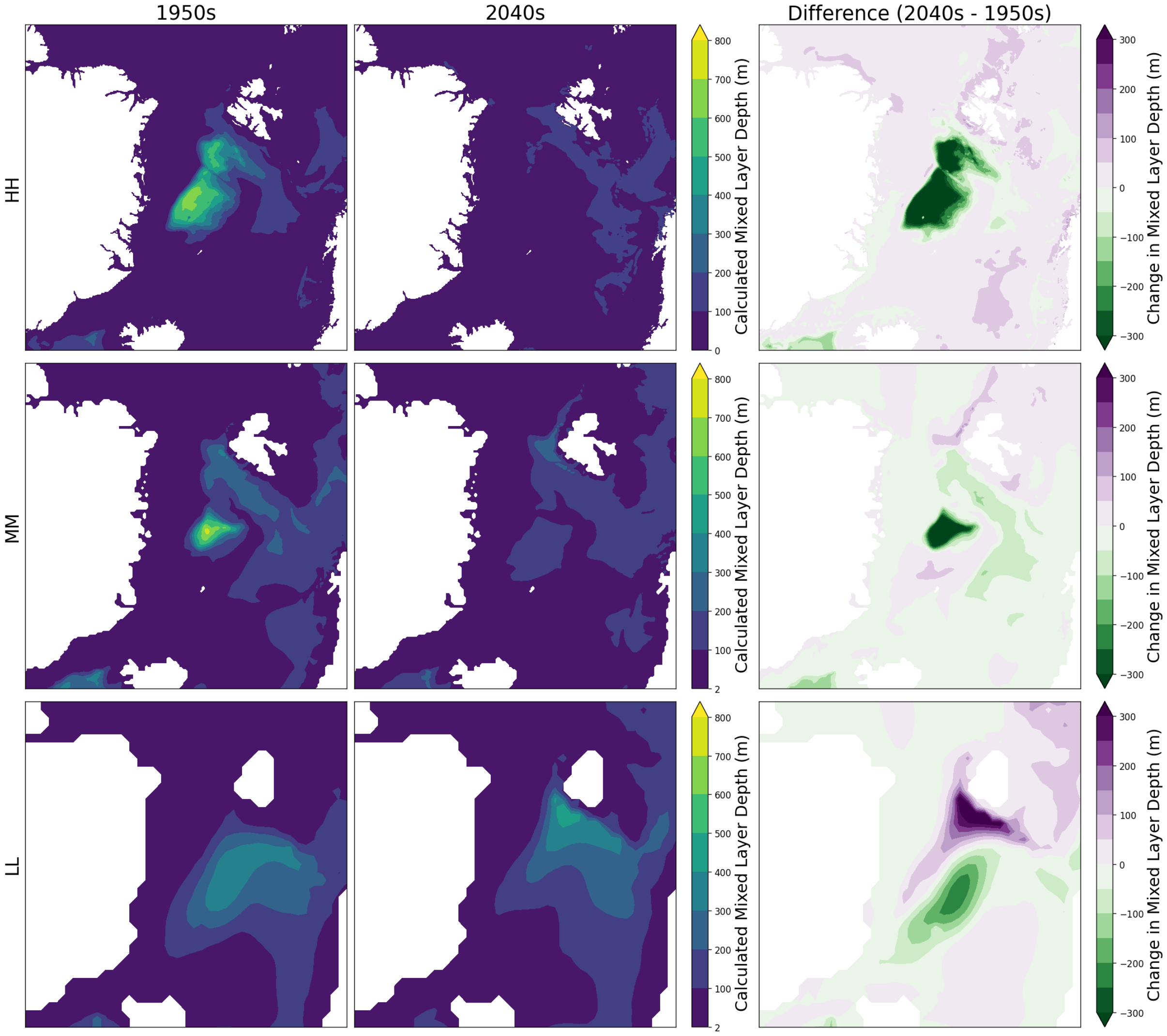

Figure 4.7: Mean calculated mixed layer depth for the first and last decade and the difference between these. The upper, middle and lower rows show the high, medium and low resolution results respectively. Note that the results have been calculated to account for the strongly stratified upper-ocean at this high-latitude location, rather than using the model output mixed layer depth which is calculated using a threshold criteria more suitable for mid-latitude oceans.

layer depth is generally small in the Nordic Seas with an average value of between 20 and 80 m. In the Greenland Sea Gyre though, values are higher (closer to 500 m) due to enhanced vertical mixing and open-ocean convection.

The high and medium resolution HadGEM3 simulations capture this spatial distribution of the mixed layer depth well. In both cases, in response to climate forcing, there is a significant reduction in the mixed layer depth within the Greenland Sea Gyre and a smaller increase in the region around Svalbard. This shallowing of the mixed layer in the Greenland Sea indicates an increase in stratification and a decrease in water mass transformation which could trigger a significant reduction in dense water formation. Meanwhile the increase around Svalbard and in the northern Barents Sea suggests enhanced vertical mixing and local convection, supporting the results shown in the previous figures.

The low resolution simulation has a region of higher mixed layer depth in the Nordic Seas but its geographical location is incorrect and it is too shallow. Like the other resolutions, it also shows a decrease in mixed layer depth in this locality but it also shows a large increase in mixed layer depth along the West Spitsbergen Current pathway, around the west coast of Svalbard. This is likely due to the overestimation in the warming and salinification in this region demonstrated in Figures 4.1 and 4.2.

Many of the near-surface changes discussed in this section are also seen throughout the water column, although the magnitude of the response tends to decrease with depth. For the sake of succinctness we have thus far focussed on near-surface atmosphere-ocean-sea-ice processes but we have also considered these diagnostics at other depth levels, although we do not show all those figure here. Some of this information is provided in the next section, where we consider changes along the EGC in three-dimensional space.

4.3.2 A Focus on Projected Changes in the East Greenland Current

The East Greenland Current (EGC) is the pathway of largest export from the Arctic Ocean to the North Atlantic. This near-surface boundary current transports cold fresh water from Fram Strait to Cape Farewell along the continental margin to the east of Greenland. It is a major freshwater sink for the Arctic Ocean and the most significant contributor to sea-ice export from the Arctic towards lower latitudes. As early as 1968, measurements estimated the average annual speed in the upper 500 m of the EGC to vary between 0.06 and 0.12 m/s (Aagaard and Coachman, 1968). More recent observations have recorded the core speed of the shelf-break EGC to be between 0.2 and 0.4 m/s with a secondary surface polar-water jet with speeds of approximately 0.2 m/s (Håvik et al., 2017a).

Although initially thought to be relatively stable as it is bathymetrically constrained to the shelf break, the EGC in fact exhibits significant variability in both strength and structure (Sutherland and Pickart, 2008; Håvik et al., 2017b; Wilkinson and Bacon, 2005). This can be driven by seasonal and interannual variability (for example in sea-ice cover), changes in eddy generation due to interaction with the topographic sea bed, and the influx of/mixing with different quantities of water masses from different sources. Observations from within the EGC are sparse and often not over a long enough period of time to conclusively evaluate its response to climate change. However, recent data has suggested that the boundary current is getting warmer and perhaps more variable (de Steur et al., 2023; Håvik et al., 2017b).

To consider how the EGC might change in the future under a climate change scenario we use the HadGEM3 simulations to study changes along the current pathway over the 100 year period. We also compare the high, medium and low resolution simulations to highlight that predictions of change in the EGC vary with horizontal grid resolution.

We use an EGC current box as defined by Moore et al. (2022). This is shown in

Figure 4.8 with the time-mean ocean surface speed in the coloured shading. As visualised in the figure, the high and medium-resolution simulations resolve the complex system of boundary currents and gyre circulations in the Nordic Seas relatively well, including the EGC, but these important ocean features are not well defined in the low-resolution simulation.

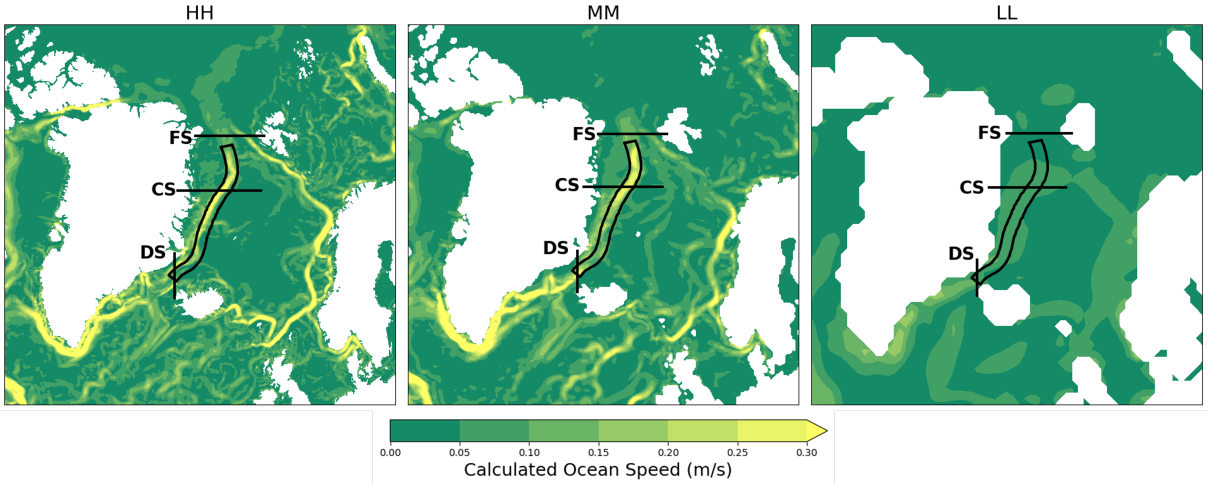

Figure 4.8: Spatial maps of the current box used to consider the East Greenland Current in the analysis and the transects used for cross-sections, with FS, CS and DS representing the Fram Strait, the Cross-Shelf and the Denmark Strait transects respectively. The background shading shows the time-mean (1950-2050) ocean surface speed for the high, medium and low resolution simulations.

Time series of annual mean diagnostics in this current box indicate that the properties and dynamics of the EGC do change between 1950 and 2050 (Figure 4.9). Note that for these spatial averages we use the upper 500 m only and the nature of the c-grid NEMO component has been taken into account.

As expected, the potential temperature along the EGC is projected to increase with climate forcing. This trend is robust across the model resolutions at approximately 0.02 °C/year in all three cases. While the high and medium resolutions show similar results, temperatures are systematically around 0.5 °C lower in the low resolution simulation. In the high resolution, the mean temperature rises from around 0.7 °C in the 1950s to around 2.4 °C in the 2040s. A similar change is seen in the medium resolution. Meanwhile, in the low resolution, temperatures go from around -0.4 °C in the 1950s to around 1.4 °C in the 2040s. There are several potential drivers of this warming; rising atmospheric (and generally ocean) temperatures, increased mixing with warmer water masses, heat transport within the ocean.

There is also an increasing trend in the mean ocean salinity along the EGC in the HadGEM3 model, although this is much more subtle at a value of approximately 0.0004 PSU/year on average. This is interesting as it shows that the rising influx of saline Atlantic-Origin Water dominates over the increasing freshwater flux from both ocean transport and external sources at the surface (e.g. land run off, precipitation and sea-ice melt). These changes in salinity could lead to changes in the density structure and

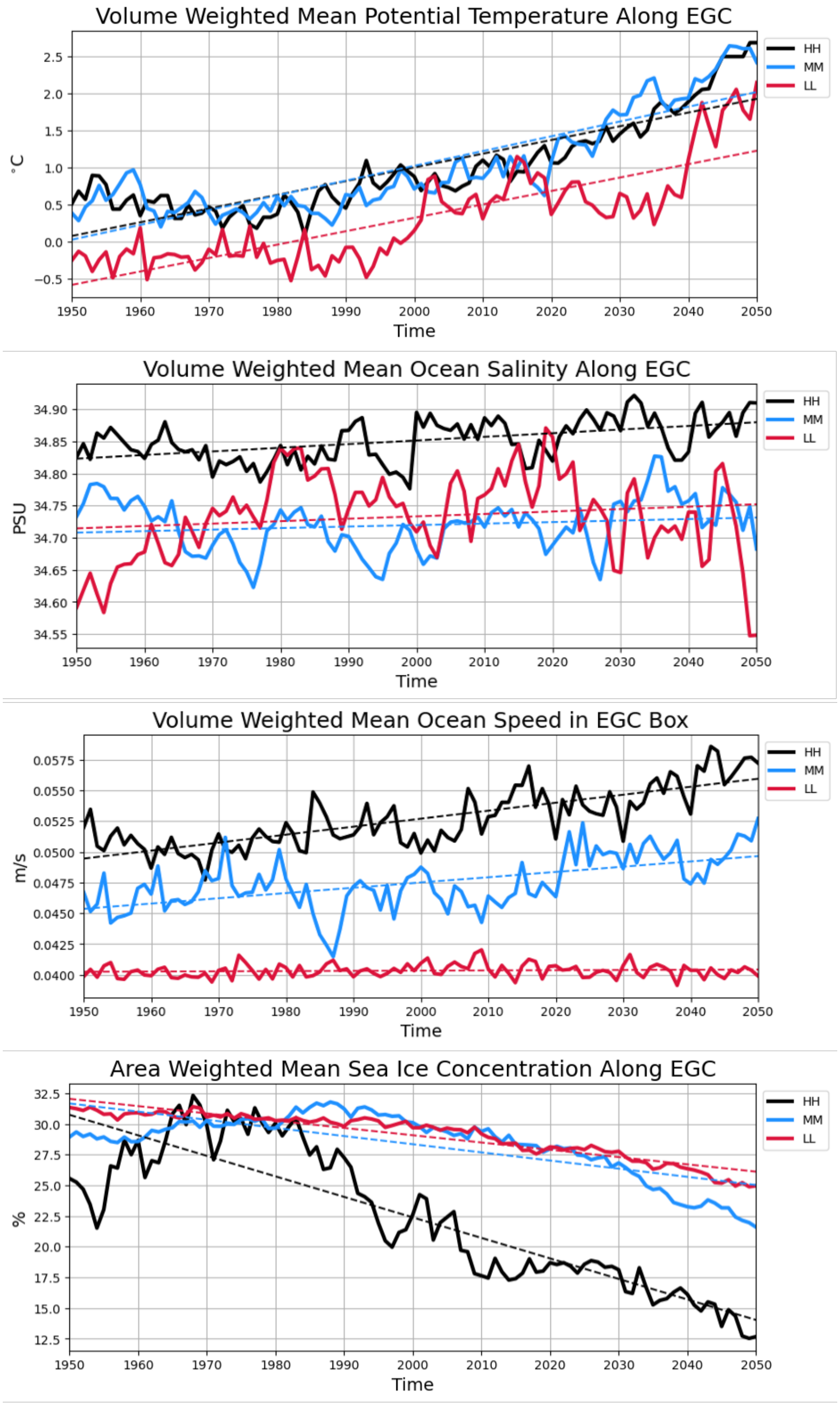

Figure 4.9: Annual mean time series for variables spatially averaged over the EGC box (upper 500 m) show the impact of horizontal grid resolution on the boundary current response to climate forcing. From top to bottom, the potential temperature, ocean salinity, ocean speed and sea-ice concentration is shown.

stratification of the EGC, thus driving a dynamical response in the boundary current.

Results for the mean ocean speed of the EGC show a clear dependency on model resolution. In fact, the two appear to be proportional here, with the mean ocean speed, and the rate of change with time, increasing with grid resolution. The all-time mean speed for the high, medium and low resolutions are approximately 0.053 m/s, 0.048 m/s and 0.041 m/s respectively. Similarly, the trends in ocean speed in the high and medium resolution are around 0.00006 m/s/year and 0.00005 m/s/year respectively, with little trend seen in the low resolution model.

Although observational measurements of ocean velocities within the EGC are sparse, a study by Håvik et al. (2017a) use synoptic shipboard sections between Fram Strait and Denmark Strait to measure the shelf-break EGC peak speed (in summertime), calculating it to be in the range of between 0.2 and 0.4 m/s. Meanwhile, Richter et al. (2018) demonstrate that the mean southward core velocities in sections in the northern Fram Strait region are between approximately 0.08 and 0.26 m/s. In another study, Sutherland and Pickart (2008) quote a typical mean EGC speed of approximately 0.1 m/s, while the coastal EGCC jet can often have much higher local maxima near the surface (0.5 - 1.0 m/s) according to hydrographic transects. Furthermore, Le Bras et al. (2018a) use data from the OSNAP mooring array (between 2014 and 2016 at ∼60°N) and find peak velocities in the order of 0.05 - 0.3 m/s, depending on the core pathway, depth and season. Some of these values are comparatively higher that we find in the HadGEM3 simulations but note that we consider a spatial mean for a box region in the approximate location of the current, which includes some areas outside the core EGC pathway and undoubtedly reduces the mean value somewhat.

To better consider the three-dimensional response of the EGC, we take cross-sections at three transects and look at changes between the 1950s and 2040s. We use three transects; one at Fram Strait, one at the shelf-break in the Greenland Sea and one at Denmark Strait. The locations of these transects has been chosen to match those used in previous observational analysis (the Fram Strait moorings and the Kögur Array at Denmark Strait). These are illustrated for the three model resolutions by the maps in Figure 4.8. Figures 4.10, 4.11 and 4.12 show the ocean velocity profiles for these cross-sections and how they are projected to change with climate forcing.

If we consider the cross-section at Fram Strait (Figure 4.10) we see that the vertical structure of the southwards flowing EGC to the west and the northward flowing West Spitsbergen Current (WSC) to the east are captured by the velocity fields in the high and medium resolution models. They also capture numerous recirculation cells which are a result of interactions between Atlantic inflow water and Polar Water in central Fram Strait.

The vertical structure of the boundary currents is poorly represented in the low resolution case and the magnitudes are significantly lower, at values of less than 0.05 m/s compared to maximum values of 0.1 m/s and 0.2 m/s for the medium and high resolutions. In fact, there is a clear positive correlation here between the speed of the boundary currents and the resolution of the simulation.

The difference plots highlight a strengthening of the southward flow in the EGC and an intensification of the northward transport in the WSC, particularly in the high and medium resolution scenarios. These changes are most pronounced in the upper 1000 m, suggesting a reorganization of the upper ocean Atlantic inflow and Arctic outflow pathways at Fram Strait (Moore et al., 2022). The low resolution simulation exhibits comparatively weaker anomalies. Overall, the results indicate that projected climate change leads to a strengthening of both the northward flow in the WSC and the southward return flow in the EGC here. The cross-sections are consistent with the surface currents shown in Figure 4.4.

At the Cross-Shelf transect (Figure 4.11) we see the EGC flowing southward along the continental shelf-break of east Greenland. Again, the high and medium resolutions are comparable, with maximum ocean velocities of over 0.2 m/s but the low resolution does not resolve the vertical structure of the boundary current and the ocean velocities remain at less than 0.05 m/s. At this location, between the 1950s and 2040s, there appears to be widening of the EGC. Also, the core of the EGC is projected to shift off-shore, away from the continental slope and towards the central Greenland Sea. This is particularly evident in the high resolution where there is a slowing to the west of the flow and a speeding up to the east. This shift in the core pathway towards the east is less apparent in the medium resolution and not shown in the low resolution. This dynamical response in the EGC aligns with changes seen in the spatial maps of ocean surface velocity in Figure 4.4 from Section 4.3.1.

We also see a projected increase in the velocity of the EGC at Denmark Strait (Figure 4.12). The ocean currents here are complex, with several smaller-scale circulation systems and two interacting branches of the EGC (Våge et al., 2013) but these are well resolved by the high and medium-resolution simulations. The low resolution does not capture these details. The increase in the velocity of the southward flow at Denmark Strait could have important wide-reaching consequences as the overflow here feeds into the AMOC.

The projected increase in speed along the EGC (as well as the other boundary currents in the Nordic Seas) could be driven by a number of forcing mechanisms. Baroclinic forcing, for example, where stronger density gradients in the upper ocean could be enhancing the geostrophic shear and accelerating the southward current flow. Cross-sections showing the calculated potential density at the Fram Strait, Cross-Shelf and Denmark Strait transects are shown in Figures 4.13, 4.14 and 4.15 respectively. These show a significant lightening trend on the continental shelf of east Greenland and in the upper ocean but a densification at greater depths. The opposing trends in these two regions results in an increasing density gradient at the boundary, which largely coincides with the location of the EGC pathway, suggesting that the baroclinic forcing is important. This is in agreement with suggestions from Årthun et al. (2023a) that increasing baroclinicity could enhance water mass transformation.

Barotropic forcing could also play a role in the increased speed of the EGC, particularly as the wind forcing increases with reduced sea-ice cover. The intensification of northerly winds along the coast of east Greenland could directly strengthen the EGC through Ekman transport and coastal upwelling.

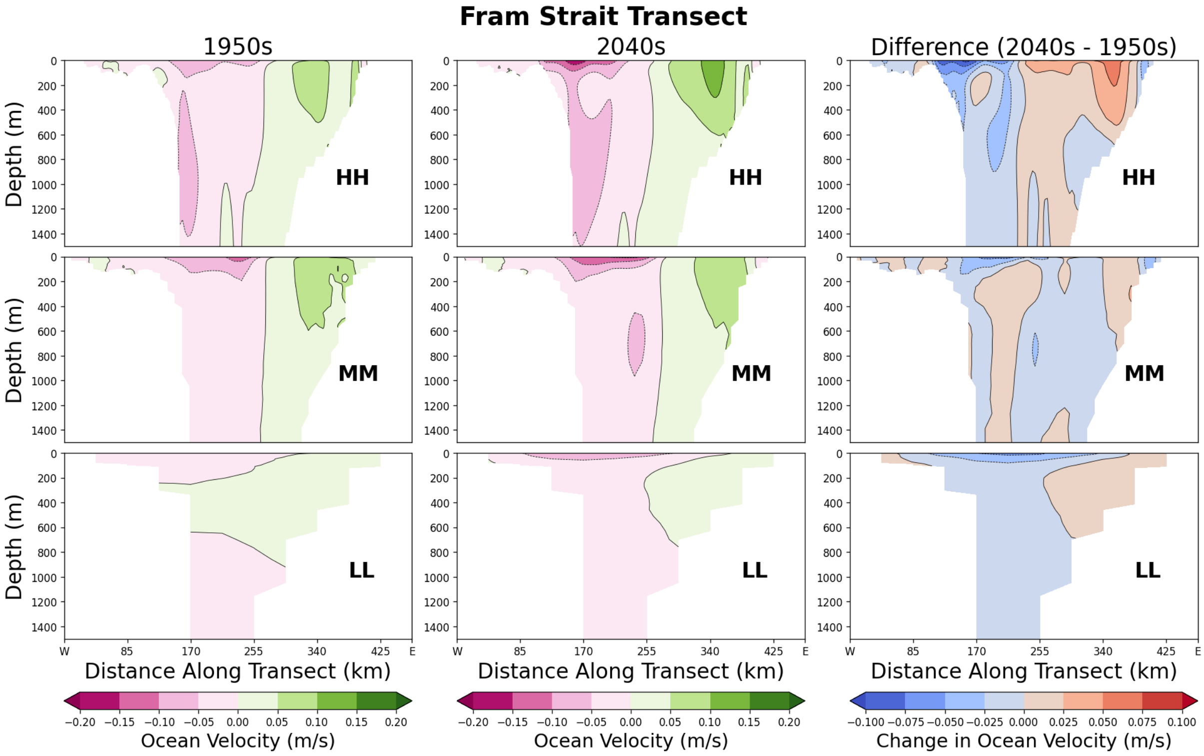

Figure 4.10: Cross-sections showing the upper 1500 m of mean quasi-northwards ocean velocity at Fram Strait for the 1950s, the 2040s and the difference between these decadal means (2040s minus 1950s), for each model grid resolution.

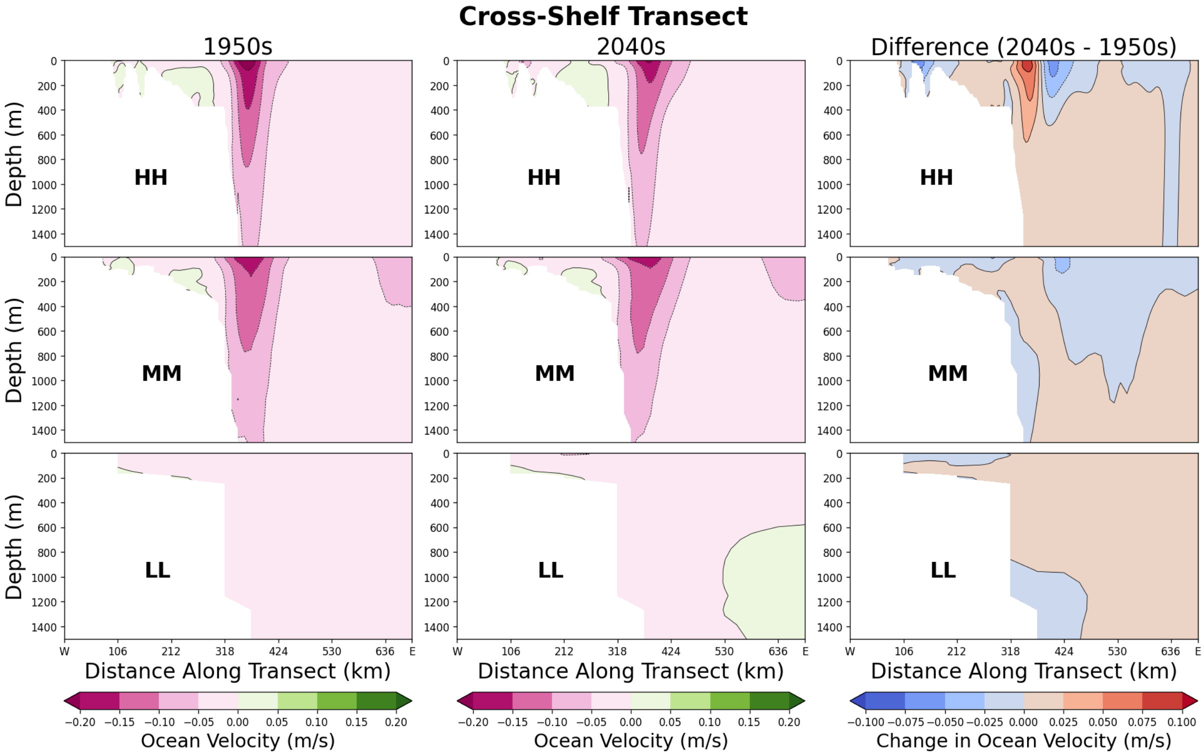

Figure 4.11: Cross-sections showing the upper 1500 m of mean quasi-northwards ocean velocity at the Cross-Shelf Transect for the 1950s, the 2040s and the difference between these decadal means (2040s minus 1950s), for each model grid resolution.

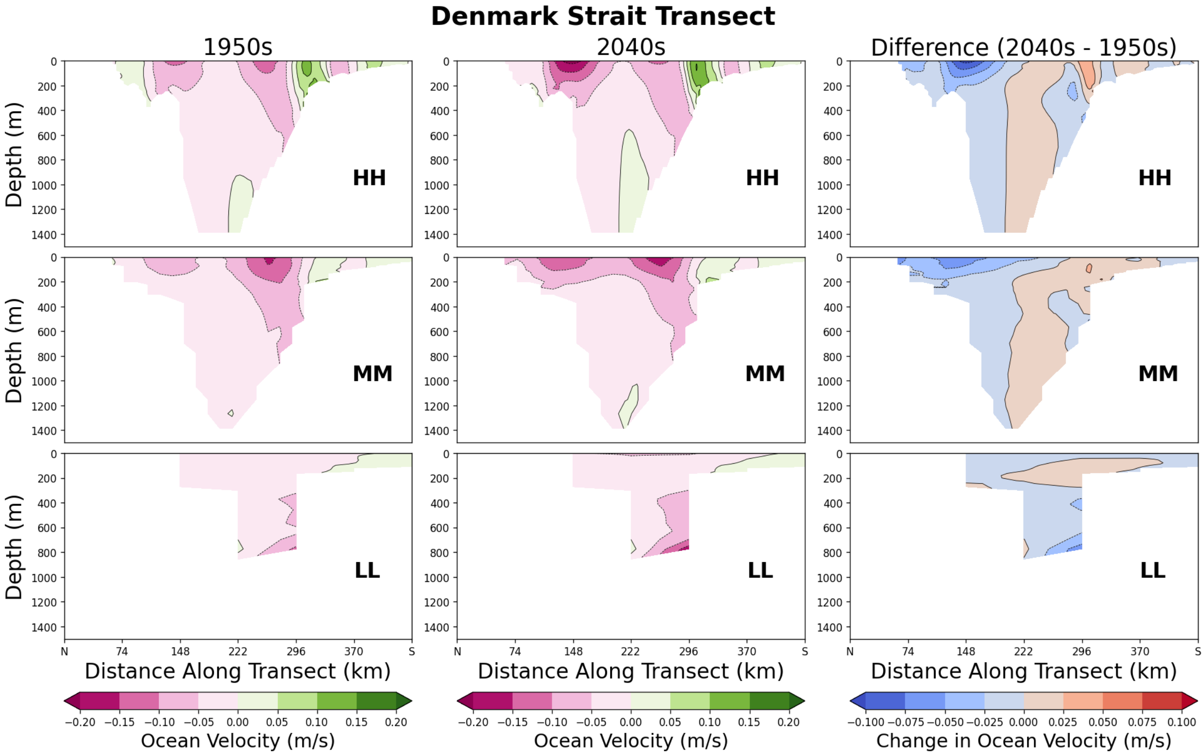

Figure 4.12: Cross-sections showing the mean quasi-northwards ocean velocity at Denmark Strait for the 1950s, the 2040s and the difference between these decadal means (2040s minus 1950s), for each model grid resolution.

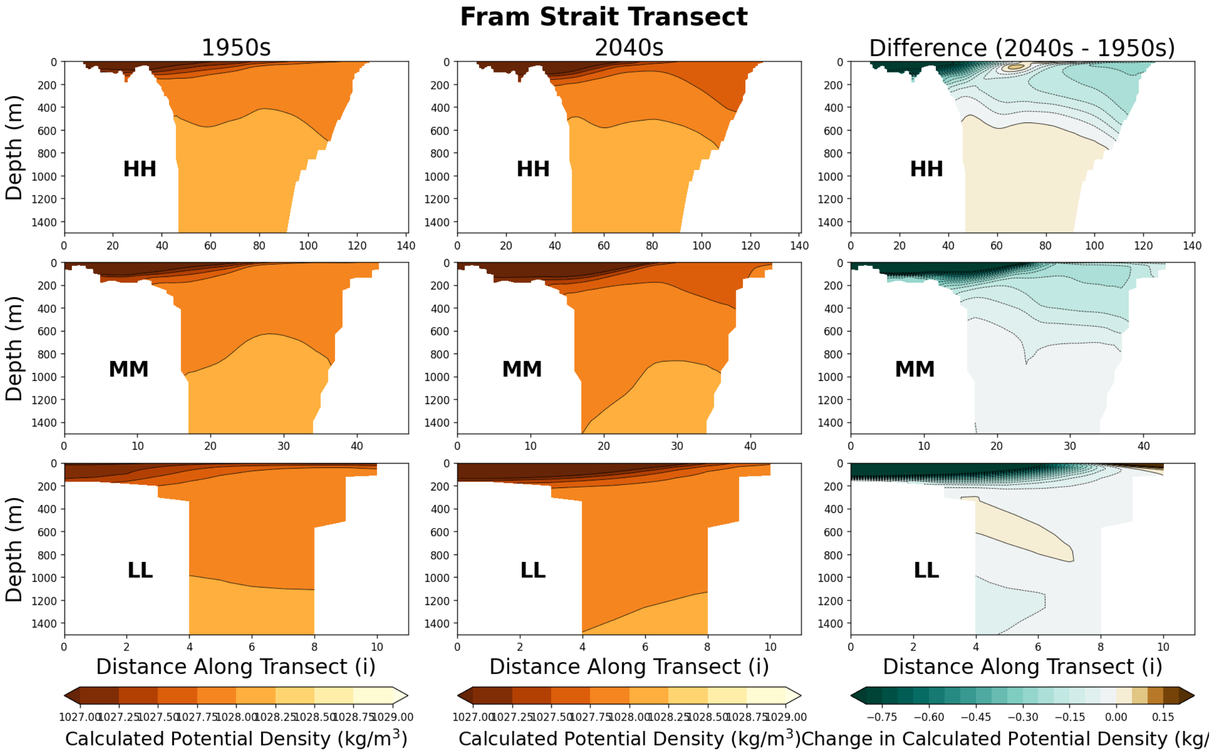

Figure 4.13: Cross-sections showing the upper 1500 m of mean calculated potential density at Fram Strait for the 1950s, the 2040s and the difference between these decadal means (2040s minus 1950s), for each model grid resolution.

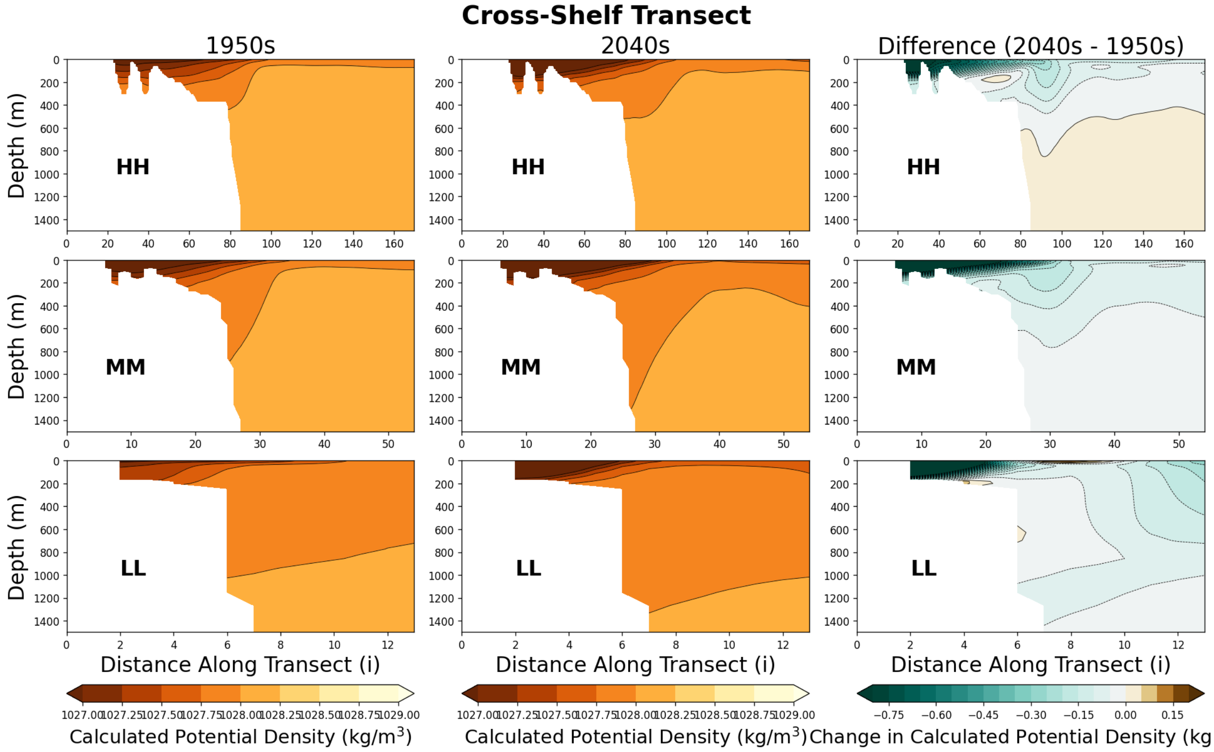

Figure 4.14: Cross-sections showing the upper 1500 m of mean calculated potential density at the Cross-Shelf Transect for the 1950s, the 2040s and the difference between these decadal means (2040s minus 1950s), for each model grid resolution.

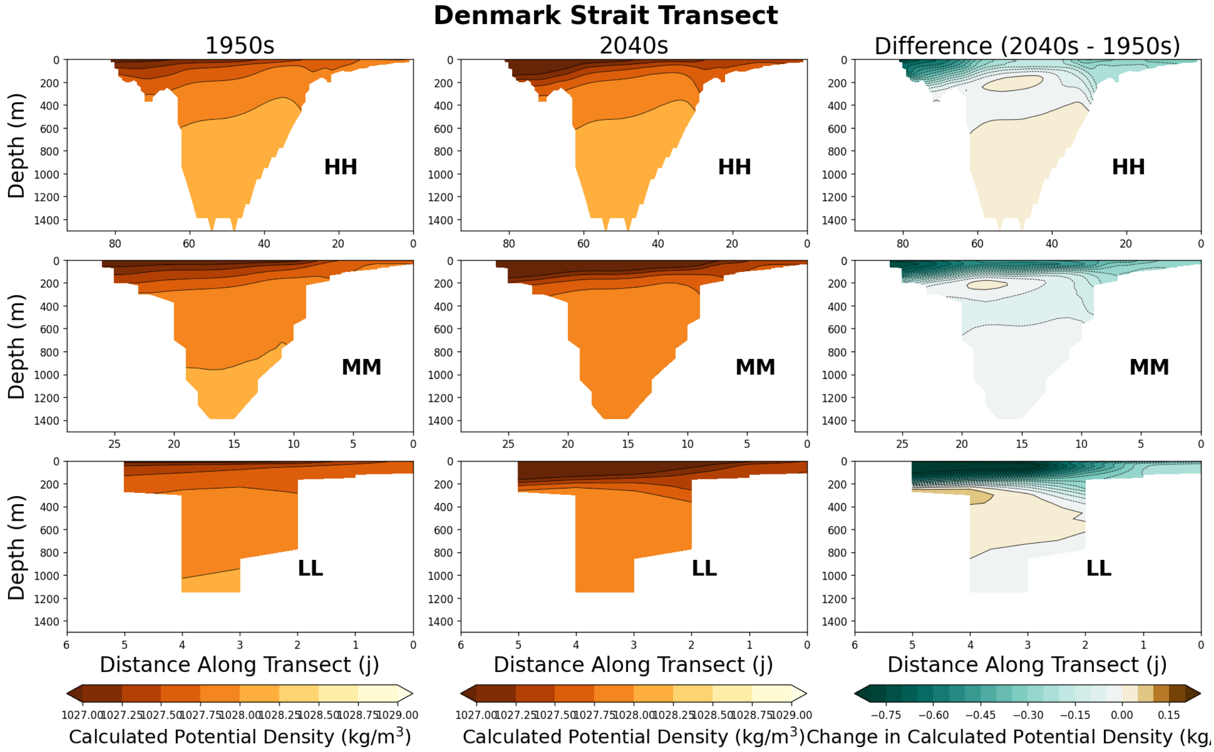

Figure 4.15: Cross-sections showing the mean calculated potential density at Denmark Strait for the 1950s, the 2040s and the difference between these decadal means (2040s minus 1950s), for each model grid resolution.

4.4 Conclusions

In this chapter we have used the HadGEM3 simulations to investigate the response of the Nordic Seas to a high-emissions climate change scenario, with a particular focus on the properties and dynamics of the East Greenland Current. By comparing historical and future projections we have shown there is high spatial variability in the rate of change of upper ocean diagnostics and near-surface coupled interactions, and that this differs with model grid resolution.

Our analysis indicates that the boundary currents in the Nordic Seas play a crucial role in distributing excess heat and salt from the North Atlantic and regulating the climatic response. The future increased inflow of Atlantic-Origin Water along the Norwegian Atlantic Current and West Spitsbergen Current drives rising temperatures and salinification in the Barents Sea, the area around north-east Svalbard and the exterior boundaries of the Greenland Sea Gyre. This decreases the upper-ocean potential density in these regions, reducing stratification and increasing the mixed layer depth which promotes water mass transformation via enhanced open-ocean convection. This response encourages dense water formation which is a vital process for the AMOC. This result aligns with findings from Årthun et al. (2023a) who suggest that the overturning circulation in some regions of the high-latitude sub-Arctic is strengthening with climate forcing, and this will be explored in more detail in the next chapter (Chapter 5).

We have also shown that the increased inflow of Atlantic-Origin Water dominates the salinity response in the EGC, despite significant increases in freshwater flux from sea-ice melt. While regions of continued sea-ice cover (e.g. north of Greenland and towards the high Arctic) see smaller increases in surface potential temperature and a strong upper-ocean freshening trend, the EGC in fact gets more saline overall. The opposing regional salinity trends drive opposing trends in potential density. This results in a stronger horizontal density gradient at the continental shelf-break in the locality of the EGC which could, at least in part, geostrophically contribute to the dynamical changes exhibited in the model.

The simulations predict an increase in the velocity of the boundary currents in the Nordic Seas, including the EGC, particularly in the higher resolution simulations. This could trigger responses in other regions such as the Arctic Ocean, Labrador Sea and North Atlantic, thus highlighting the importance of the Nordic Seas for the global climate system.

As sea-ice declines, there tends to be a northwards shift in other closely linked mechanisms (such as sites of strong ocean–to–atmosphere heat flux) which could result in a general migration of sub-Arctic mechanisms (such as ocean densification) towards higher latitudes.

Overall, we have shown that there are significant future changes projected for the Nordic Seas in the HadGEM3 climate model. With climate forcing, regional changes in the properties and structure of the water column can drive larger-scale dynamical responses, many of which play a critical role in the water mass transformation that feeds the northern branch of the AMOC with dense water. We have also demonstrated that some of these responses vary with horizontal grid resolution and that overall the higher-resolution simulation is best for capturing this complex highly-coupled climate system in the Nordic Seas. In the next chapter, we further our investigations into Nordic Seas changes, focussing on those in the high-resolution simulation.

Future Projections of Dense Water Formation and Overturning Circulation in the Nordic Seas

5.1 Introduction

Dense water formation in the high-latitudes is a crucial element of the global ocean circulation system (Zhang et al., 2019; Buckley and Marshall, 2016). In the Nordic Seas, freshwater and heat exchanges play key roles in driving water mass transformation along the northern-most branch of the Atlantic Meridional Overturning Circulation (AMOC) (Buckley and Marshall, 2016; Dickson and Brown, 1994; Chafik and Rossby, 2019; Tsubouchi et al., 2021) but with the changing climate, the future stability of this important coupled process is becoming less certain (Liu and Liu, 2014; Weijer et al., 2019; Jackson et al., 2022).

In the current scientific literature, there is an active and ongoing debate around the future response of the AMOC to climate change at high-latitudes. Some studies suggest there will be a significant reduction in dense water formation with substantial weakening of the AMOC (e.g. Weijer et al., 2019; Asbjørnsen and Årthun, 2023; Heuzé et al., 2015). A decade ago, Rahmstorf et al. (2015) synthesised results from observational data to argue that the slowdown in the AMOC seen in the 20th-century is substantial and they raised concerns about future decline. Since then, observational data has shown a weakening in the AMOC of around 3 Sv since the mid-20th century (Caesar et al., 2018) while analysis of numerous CMIP6 models indicates that a decline of around 7 Sv (∼40%) by 2100 is possible (Weijer et al., 2020).

In some more extreme cases, a complete "shutdown" is predicted, usually due to vast freshwater input which inhibits vertical convection (e.g. Drijfhout, 2015; Drijfhout et al., 2025). In Jackson (2013) a coupled General Circulation Model is used to investigate how large freshwater advection into the Atlantic Ocean leads to a collapse of the AMOC, although they show that recovery over longer time scales is also likely.

Furthermore, while some models predict a collapse of deep convection in a future Arctic (e.g. Heuzé and Liu, 2024), at the other end of the scale, some actually predict a future strengthening in the AMOC attributed to the onset of deep convection in the Arctic Ocean under strong warming and ice-free summers (e.g. Lique and Thomas, 2018; Bretones et al., 2022). Increased ocean densification at higher latitudes might sustain overflow production and could partly offset a large-scale AMOC reduction. A growing number of studies are being published that point towards this compensating mechanism.

For example, a recent study by Årthun et al. (2025), shows that, as the sea-ice retreats northwards, the increased exposure of Atlantic-Origin water to the atmosphere allows for enhanced water mass transformation along the poleward-flowing boundary currents of the Nordic Seas. This process, defined as the poleward expansion of Atlantic water and sea-ice loss, is often referred to as "Arctic Atlantification" (Polyakov et al., 2002, 2023) and is evident from reanalysis and observational data that show a poleward shift in the dense water source regions, away from the Nordic Seas and into the Arctic Ocean. Årthun et al. (2025) suggest that this increasing surface transformation in the Arctic acts as an additional source of dense water which can help to sustain overflow to the AMOC.

Modelling analysis has also been shown to support this theory of potential compensation in northern source regions, with reduced transformation in the Nordic Seas being linked to a strengthening or shift in overturning at higher latitudes (Årthun et al., 2023a; Wu et al., 2025). This is corroborated by Bretones et al. (2022) who analyse model results to show a strengthening in the AMOC as deep mixing moves north following sea-ice retreat. Additionally, Dey et al. (2024) use Lagrangian analysis and high-resolution modelling to emphasise the role of Atlantic-Arctic mixing and Arctic contributions to the lower limb of the AMOC, pointing towards compensation pathways between the Arctic Ocean and the Nordic Seas. Furthermore, a recent publication by Wei et al. (2024) uses modelling experiments to show that densification in the Labrador Sea is strengthening while the AMOC weakens. This demonstrates that local increases in densification (e.g. in the Labrador Sea) can accompany an overall weakening of the AMOC, providing an example of compensatory regional responses in the sub-polar northern latitudes, at least in model experiments.

In a perhaps more balanced perspective, Baker et al. (2025) recently published a multi-model study showing that, in their ensemble, the AMOC is resilient to extreme forcings because of compensating processes, such as Southern Ocean upwelling and alternate sites of downwelling. They argue that a complete collapse this century is unlikely, while still showing large weakening is possible.

Altogether, the current body of scientific literature covers a range of possible future scenarios for the AMOC and ocean densification at high latitudes. The study of changes in dense water formation and overturning circulation in the Nordic Seas is of great significance and as greenhouse gas emissions and global temperatures continue to increase, so does the need for improved understanding of future variability in this highly-coupled domain. The requirement for further research on the processes driving the projected response in water mass transformation in the Nordic Seas with the changing climate, in addition to the wider-scale impacts, is undoubtedly of great value and provides motivation for this work.

In this chapter we evaluate the response of dense water formation in the Nordic Seas and investigate the processes that might drive changes in the overturning strength. We use the high-resolution HadGEM3-HH global coupled climate model (25 km and 1/12°) to consider the climatic response and investigate future projections. We compare the transient and control simulations to understand which processes are driven by anthropogenic climate forcing and account for artifacts of model drift.

It should be noted that previous work using the HadGEM3 model has shown that, with climate forcing, the AMOC is projected to weaken over the 21st century in these simulations (Jackson et al., 2020; Baker et al., 2023; Roberts et al., 2020). However, most work has made use of the medium and low-resolution simulations and it remains unclear if the response is the same in the high-resolution simulation. Roberts et al. (2020) is one of the few studies to include the high-resolution HadGEM3 simulation in their multi-model analysis of the AMOC. They find that the HadGEM3-HH simulation is one of the best-performing models in their sample set as it captures the AMOC depth profiles well, has relatively small zonal mean temperature and salinity biases and has a northward heat transport consistent with observations.

Given this information, along with the model validation we have done in Chapter 3 and previous evaluation studies (Wu et al., 2021; Roberts et al., 2019), we have confidence in the fidelity of the HadGEM3-HH model. We use the model to consider the changes in the density structure of the Nordic Seas over a 100-year period, which has not been done previously. We also investigate possible processes driving the ocean density response, including atmosphere-ice-ocean coupled mechanisms. Additionally, we assess the response in the overturning circulation under a future climate change scenario, building on work from Årthun et al. (2025) which only uses historical data. Altogether, this work provides a novel analysis of simulated projections from a high-resolution global coupled climate model, which demonstrates valuable insights on the future of dense water formation and interesting results regarding the climate forcing of the AMOC in the Nordic Seas.

5.2 Model Simulations Under Climate Change

5.2.1 Water Mass Volume Changes in the Nordic Seas

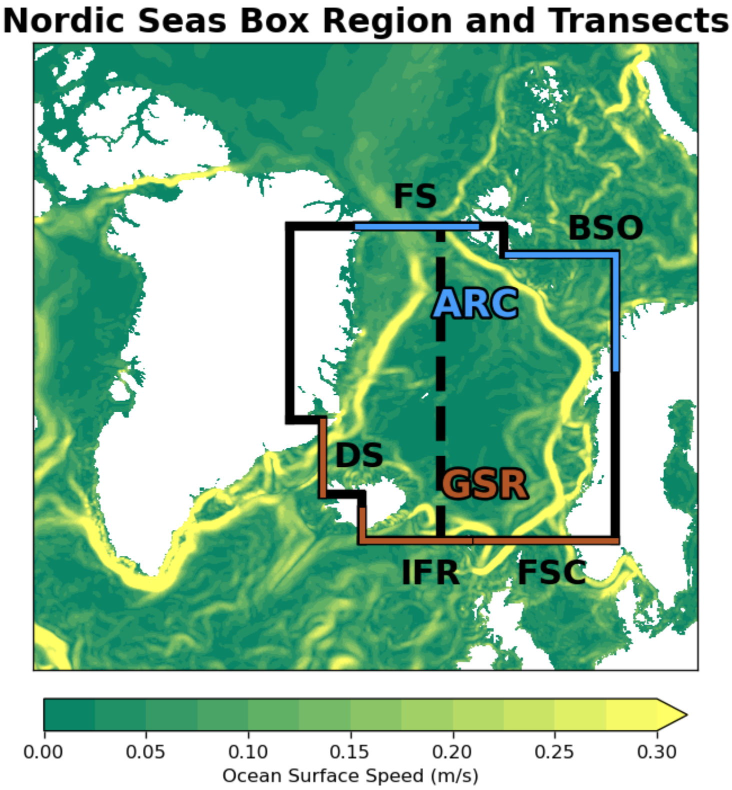

Figure 5.1: Model time-mean ocean surface speed map of the Nordic Seas region from the transient HadGEM3-HH simulation, presented on the model ocean grid. The area inside the box is used for spatial analysis and the highlighted transects are used for ocean transport calculations. The Fram Strait (FS) and Barents Sea Opening (BSO) are combined to represent the Arctic transect (ARC) used in calculations of the overturning stream function, while the Denmark Strait (DS), Iceland-Faroe Ridge (IFR) and Faroe-Scotland Channel (FSC) comprise the Greenland-Scotland Ridge transect (GSR), following the approach of Årthun et al. (2025).

Observational studies show that ocean properties in the Nordic Seas have been changing in recent years (e.g. Polyakov et al., 2017, 2023; Smedsrud et al., 2022; Årthun et al., 2019; Wekerle et al., 2017; Park et al., 2022; Wang et al., 2020; Bretones et al., 2022; Shi et al., 2024) and published modelling work suggests increased variability under future climate change scenarios (e.g. Årthun et al., 2023a; Gu et al., 2024; Langehaug et al., 2023). To ascertain the response in the HadGEM3-HH model, we use the box region shown in Figure 5.1 and compare results from the transient simulation with those from the control run to determine which trends may be attributed to anthropogenic forcing. We also evaluate the climatic response when the model drift is removed. Detailed descriptions of the HadGEM3 model and experimental setup are in Chapter 3.

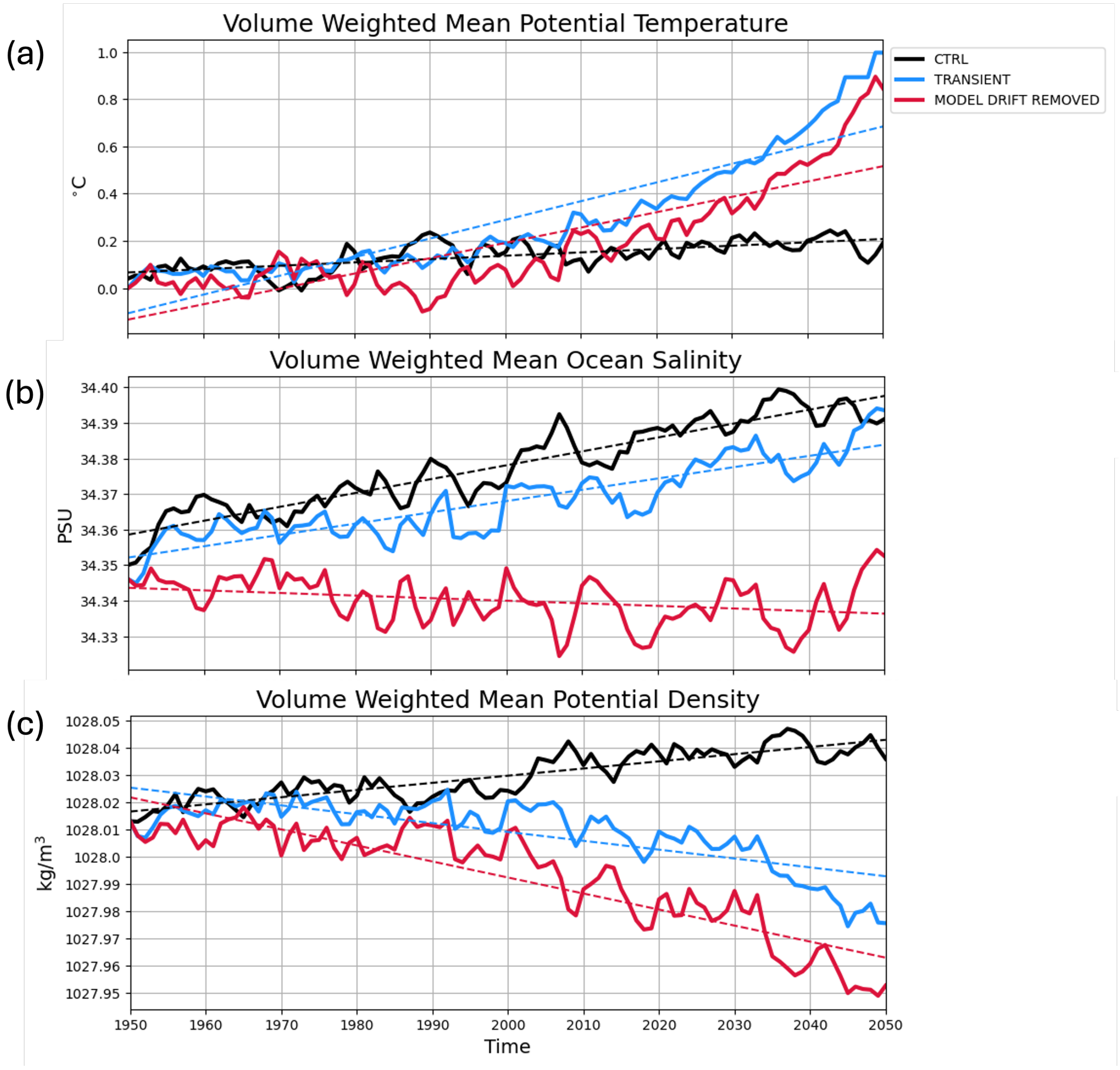

Figure 5.2: Time series of the annual mean volume-weighted (a) potential temperature, (b) ocean salinity and (c) calculated potential density for the box region representing the Nordic Seas (shown in Figure 5.1 for the transient and control simulations (in blue and black respectively) and for the transient run with the model drift removed (in red). The linear regression trends are shown by the dashed lines of corresponding colour.

As one might expect, the transient simulation shows significant ocean warming in the Nordic Seas. In Figure 5.2 (a), the time series of the annual volume weighted mean potential temperature shows an increase of approximately 1°C between 1950 and 2050, with most of this warming occurring from the mid-2000s onwards. The control simulation also shows a small positive trend but with only approximately 0.1°C of warming over the model run period. Although small in comparison to the transient simulation, this trend in the control run indicates that model drift skews the representation of ocean properties in the Nordic Seas. In fact, if we remove the model drift from the transient data we see a reduction in the mean potential temperature values and a small decrease in the warming trend, although this is still significant at 0.007 °C/year compared to 0.008 °C/year for the raw transient output (Figure 5.2).

Perhaps more surprisingly, the ocean salinity in this region increases at a steady rate from the start of the model run in both the transient and control simulations (Figure 5.2 (b)). The trends are similar here with the control increasing at a slightly faster rate of 0.0004 PSU/year compared to 0.0003 PSU/year for the transient run, indicating that the salinity drift in the HadGEM3-HH model dominates and masks the transient variability. Indeed, when we remove the model drift from the transient data we see a small negative trend of -0.00008 PSU/year and lower mean salinity values of approximately 34.34 PSU. This fits with results from other observational-based studies that show an upper-ocean freshening trend in this region (e.g. Shi et al., 2024).

A drift in ocean salinity, particularly in the North Atlantic region, is a common feature of global climate models and systematic biases of a few tenths of a practical salinity unit (PSU) are common (e.g. Langehaug et al., 2019, 2023). Flato et al. (2014) show that multi-model means from CMIP5 and CMIP6 simulations show a characteristic fresh bias in the upper 300 m of the North Atlantic Ocean of around 0.2 to 0.4 PSU, with intermediate-depth biases that can locally reach up to 0.6 PSU depending on the basin and circulation regime. These biases persist across model generations and are often linked to errors in surface freshwater fluxes, vertical mixing and large-scale circulation. By comparison, Kuhlbrodt et al. (2018) show that the low-resolution HadGEM3 control simulations have relatively modest global mean salinity biases when compared with observational climatologies (approximately 0.1 to 0.2 PSU), although regional biases in the Atlantic can be larger (approaching 0.3 to 0.4 PSU in some depth ranges). An analysis of HadGEM3 control simulations is also presented in Roberts et al. (2019), where it is shown that the magnitude of the model ocean salinity drift varies with resolution. At all resolutions, HadGEM3 shows a global drift in the upper 300 m, with an increasing fresh bias over time, but a salinity increase at mid-depths ($\sim$ 1000 - 2000 m) due to deep circulation evolution. The lower-resolution ocean models exhibit larger drifts in both global and Atlantic Ocean salinity structures, whereas the higher-resolution configurations substantially reduce the Atlantic salinity drift.

Overall, the ocean salinity drift in the high-resolution HadGEM3 simulations is relatively minimal compared to many other global coupled climate models and it exhibits substantially reduced basin-scale salinity drift compared to lower-resolution simulations. Given that the HadGEM3-HH model has a realistic representation of Atlantic inflow currents, overflow pathways and the mesoscale processes that dominate Nordic Seas hydrography (Roberts et al., 2019), its use in our research is advantageous despite this salinity drift and on balance, the benefits of using the model outweigh these limitations.

The differing thermal and haline responses of the transient and control simulations result in differing trends in the ocean potential density (Figure 5.2 (c)). The mean calculated potential density decreases in the transient simulation, particularly from the mid-2000s, highlighting the impact of the ocean warming seen in response to the changing climate. For the control run, the mean potential density increases, driven by the increasing mean salinity in the region. The rate of increasing potential density in the control run is 0.00025 kg m^{-3}/year, only about two-thirds of the rate of decrease of potential density in the transient run (-0.0003 kg m^{-3}/year). This indicates that, although enhanced mean ocean salinity promotes dense water formation in the Nordic Seas, the significant ocean warming in response to the changing climate inhibits dense water formation by a greater magnitude, resulting in a reduced ocean potential density overall. By removing the model drift here, the reduction in potential density seen in the transient simulation is exaggerated and the trend increases to -0.0005 kg m^{-3}/year. These results indicate that the HadGEM3-HH model has a notable ocean salinity drift in the Nordic Seas which causes a drift towards elevated potential density. However, with climate change, the density of the ocean water in the Nordic Seas is projected to reduce, largely driven by significant ocean warming, although salinity changes also make a small contribution. This aligns with results from Shi et al. (2024), where analysis of observational data between 1980 and 2022 suggests that a decrease in overflow water storage volume in the Nordic Seas is mostly due to the rise in ocean temperature (specifically in the upper 600 meters), rather than an ocean salinity response.

To consider in detail the changes in ocean density in these simulations, we define five density classes and calculate the annual mean volume of ocean water within each density class for the Nordic Seas box region over time. Note that the model drift has *not* been removed from the transient data. The density classes are defined as follows;

- σ_A - all water lighter than 1027.80 kg m^{-3},
- σ_B - water denser than 1027.80 kg m^{-3} but lighter than 1028.05 kg m^{-3},
- σ_C - denser than 1028.05 kg m^{-3} but lighter than 1028.08 kg m^{-3},
- σ_D - denser than 1028.08 kg m^{-3} but lighter than 1028.10 kg m^{-3}, and
- σ_E - all water denser than 1028.10 kg m^{-3}.

These density classes have been chosen based on values used in literature (e.g. Brakstad, 2023; Almeida et al., 2025) and to highlight changes in the densest waters.

The annual mean volume within each density class for the Nordic Seas box region over time is visualized in Figure 5.3 such that the thickness of each coloured section represents the total volume of water in the corresponding density class for any given year. The decadal mean values are also shown in Table 5.1. Over the century-long simulation there is notable variability in the density structure of the water column in the Nordic Seas.

	Density Class	1950s	1960s	1970s	1980s	1990s	2000s	2010s	2020s	2030s	2040s
Transient	σ_A	0.34	0.31	0.35	0.35	0.38	0.38	0.43	0.44	0.49	0.56
	σ_B	0.78	0.55	0.51	0.57	0.49	0.46	0.48	0.52	0.50	0.65
	σ_C	1.96	1.80	1.00	0.87	1.12	0.64	0.59	0.61	0.55	0.62
	σ_D	1.25	1.67	2.39	2.52	2.28	2.85	2.83	2.76	2.80	2.50
	σ_E	0	0	0.08	0.02	0.07	0	0	0	0	0
Control	σ_A	0.33	0.33	0.32	0.34	0.36	0.32	0.32	0.32	0.31	0.33
	σ_B	0.68	0.53	0.45	0.46	0.47	0.44	0.43	0.41	0.41	0.39
	σ_C	1.89	1.56	0.89	0.46	0.43	0.35	0.28	0.23	0.23	0.18
	σ_D	1.43	1.91	2.68	3.08	3.08	3.04	2.65	2.27	2.13	0.98
	σ_E	0	0	0	0	0	0.17	0.65	1.11	1.26	2.45

Table 5.1: Decadal means values for the volume of water in each density class in the Nordic Seas region from the transient and control HadGEM3-HH simulations ($\times 10^{15}$ m^3).

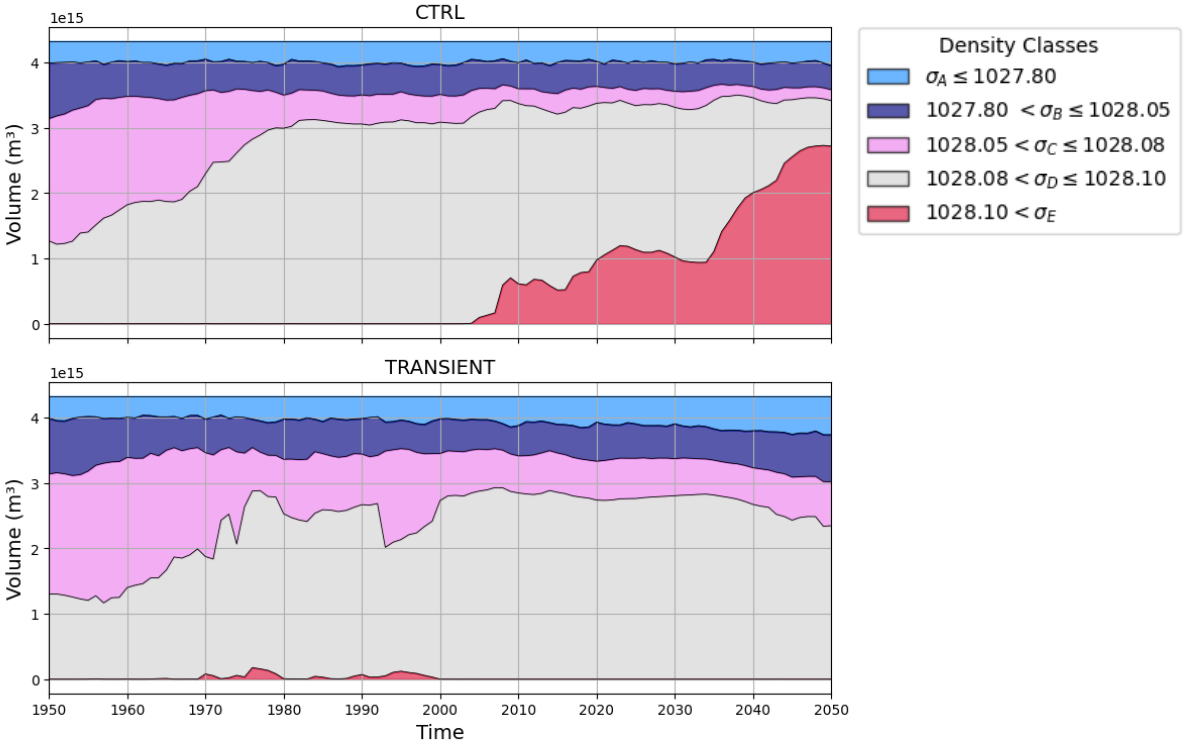

Figure 5.3: The annual volume of ocean water in each density class (see legend) in the Nordic Seas for the control and transient simulations between 1950 and 2050. At any point, the thickness of each coloured section represents the total volume of water in the corresponding density class for the box region shown in Figure 5.1 for that year.

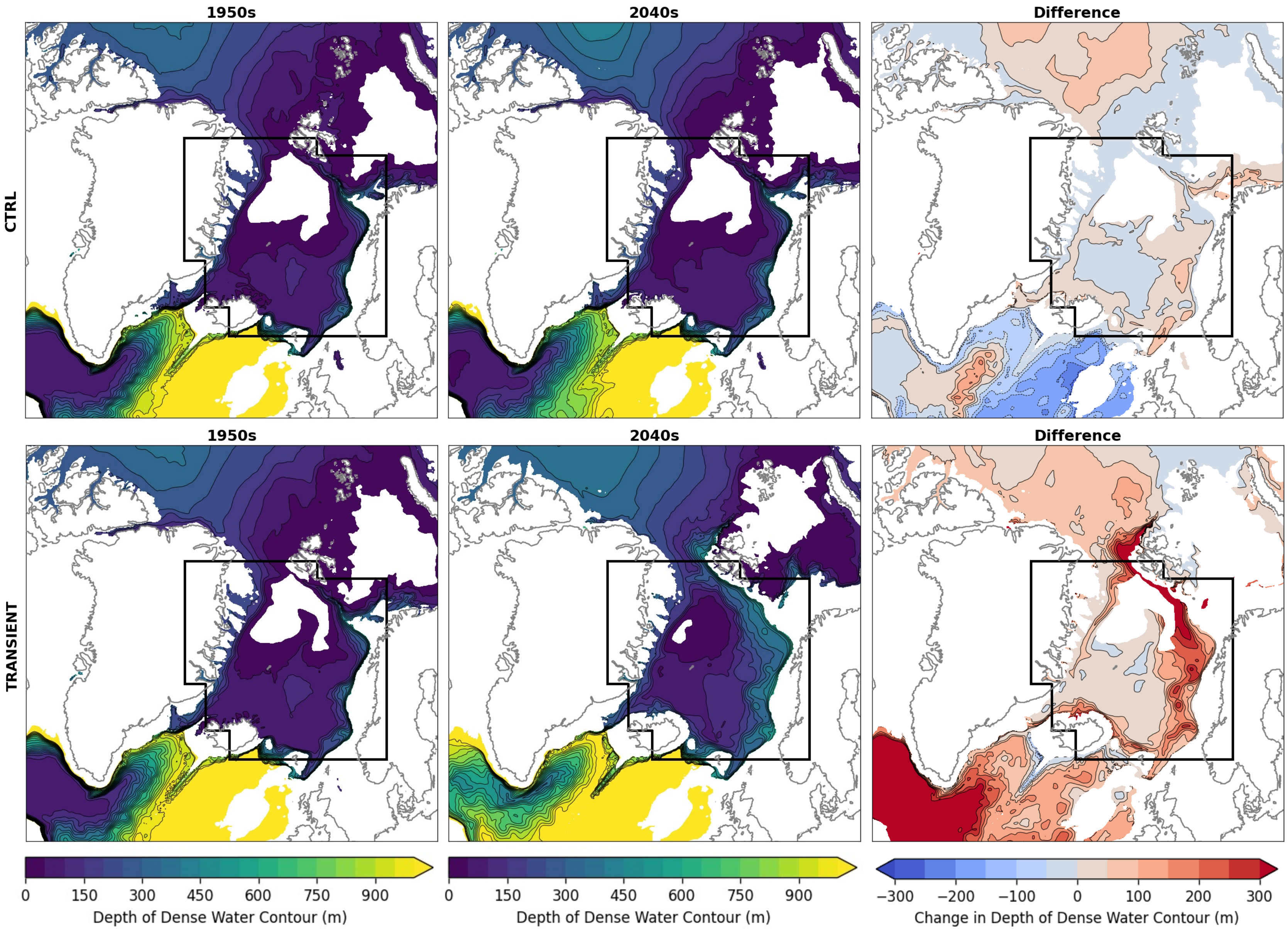

Figure 5.4: Spatial maps show the mean depth of the 1027.80 kg m^{-3} isopycnal for the 1950s and 2040s, as well as the difference between these decadal means (2040s minus 1950s). This isopycnal marks the boundary between light σ_A and intermediate σ_B water. The results for both the transient and control simulations are presented.

In the transient simulation, the lightest waters (σ_A) increase in volume from approximately 0.34×10^{15} m^3 (8% of the total Nordic Seas volume) in the 1950s to approximately 0.56×10^{15} m^3 (14%) in the 2040s. This is not the case for the control simulation where the volume of σ_A water remains steady at around 0.33×10^{15} m^3 (8%). Therefore, the HadGEM3-HH model projects that there will be a larger volume of lighter water in the Nordic Seas in the future in response to climate change.

Given that there is a larger volume of lighter water in the transient future projections, it follows that there is a smaller volume of denser water. The volume of water denser than 1027.80 kg m^{-3} (this includes σ_B, σ_C, σ_D and σ_E) reduces from 3.99×10^{15} m^3 (92%) in the 1950s to 3.77×10^{15} m^3 (87%) in the 2040s.

Continuing to focus on the lighter waters, Figure 5.4 shows the time-mean depth of the 1027.80 kg m^{-3} isopycnal for the 1950s and 2040s and also the difference between these (2040s minus 1950s). For the transient simulation we see a strong increase in the depth of this density contour within the Nordic Seas region, particularly along the boundary currents and especially along the northwards flowing Atlantic Water pathway to the east of the domain (along the Norwegian Atlantic Current and West Spitsbergen Current). Water mass transformation by heat and freshwater exchange along these boundary current pathways plays an important role in the high-latitude AMOC but these results show a clear deepening of the 1027.80 kg m^{-3} isopycnal over time. This suggests that there is projected to be less dense water formation along this pathway with climate change and a thicker layer of lighter σ_A water in the upper ocean.

The volume of water denser than 1027.80 kg m^{-3} in the control run remains steady at around 4.00 $\times10^{15}$ m^3 and little overall change is seen in the spatial maps shown in Figure 5.4, although further analysis shows that there is some variability within these denser water classes.

For the other, more dense water classes, both the transient and control simulations show gradual changes in the first three decades (1950 - 1980) when the volume of σ_B, σ_C and σ_D all decrease steadily. (There is almost no σ_E water in the region during this period.) This initial response could be due to model drift following the relatively short spin-up of these model simulations.

From around 1970 onwards there are some differences in the model responses. For example, there is higher variability in the transient run between 1970 and the early 2000s. This is also the only period for which we see a notable proportion of σ_E water in the transient simulation (mean of 0.075×10^{15} m^3 for the 1970s and 1990s, which is around 2% of the total Nordic Seas volume). The volume of σ_B water is relatively consistent here but there appears to be an active exchange occurring between the σ_C and σ_D density classes with an initial decrease in σ_C of approximately 3% from the 1970s to the 1980s followed by an increase of 6% from the 1980s to the 1990s. This is mirrored by an opposing response in the volume of σ_D water. This variability is not seen in the control simulation where the density class volumes remain largely constant over these decades. However, things change in the mid-2000s in the control run, and from then onwards there is an increasing volume of the densest σ_E water, and a decreasing volume of σ_C and especially σ_D water. Whereas in the transient simulation there is a steady decrease in the volume of σ_D water in the latter half of the model run, accompanied by an increase in the volume of σ_B water.

Spatial maps showing the depth of the 1028.05 kg m^{-3} isopycnal (upper limit of σ_C) for the first and last decade of the simulation, and the difference between these, are shown in Figure 5.5, for both the transient and control simulations. The distribution of this density class of water in the Nordic Seas is very different to that of σ_A, as shown in Figure 5.4. In fact, apart from the shallower continental shelf regions around Greenland, Iceland, Svalbard and Norway, most of the domain within the box contains some σ_C water in the water column. Ocean water at densities of more than 1028.05 kg m^{-3} tend to be most present in the Greenland Sea Basin, where the 1028.05 kg m^{-3} isopycnal is shallow, at depths of less 50 m. This water is also seen in the other basins of the Nordic Seas but at greater depths of around 400 m.

Ocean water of this density class is also seen outside our box domain, in the Northern Barents Sea (shallow 1028.05 kg m^{-3} isopycnal) and Arctic Ocean (deeper 1028.05 kg m^{-3} isopycnal). The spatial patterns shown in Figure 5.5 indicate that water of this density class is mainly formed in the Greenland Sea and Northern Barents Sea. It then appears to travel to greater depths as it spreads towards the Arctic and other basins of the Nordic Seas, along boundary currents and pathways influenced by topographic steering. This figure also points towards notable densification of ocean waters at higher-latitudes, even within the Arctic Ocean, corroborating results from Årthun et al. (2025).

If we consider the changes in the control simulation (upper panels of Figure 5.5) we see that the depth of the 1028.05 kg m^{-3} isopycnal decreases throughout the region, often quite significantly. In some areas, such as in the Arctic Ocean, a deepening by more than 350 m is seen, whereas in the Greenland Sea basin the response is comparatively smaller with a deepening of a less than 50 m between the 1950s and 2040s. This aligns with the results shown in Figures 5.2 and 5.3, which indicate that the rate of dense water formation is overestimated in the control run, with model drift causing an accumulation in the volume of denser waters in the Nordic Seas.

In the transient simulation (lower panels of Figure 5.5) there is a similar decrease in the depth of the 1028.05 kg m^{-3} isopycnal in the Arctic Ocean, suggesting a robustness to this response of an increased volume of dense water at high-latitudes. However, in the Greenland Sea basin we see the opposite. There is an increase in the depth of the σ_C isopycnal, illustrating a decrease in the volume of water denser than 1028.05 kg m^{-3} here. This supports our previous findings of a reduced volume of σ_C water in the Nordic Seas between the 1950s and 2040s under a climate change scenario, but shows that this change is mostly concentrated in the Greenland Sea. This response differs to that of the lighter σ_A water (see lower panels of Figure 5.4) where the deepening of the 1027.80

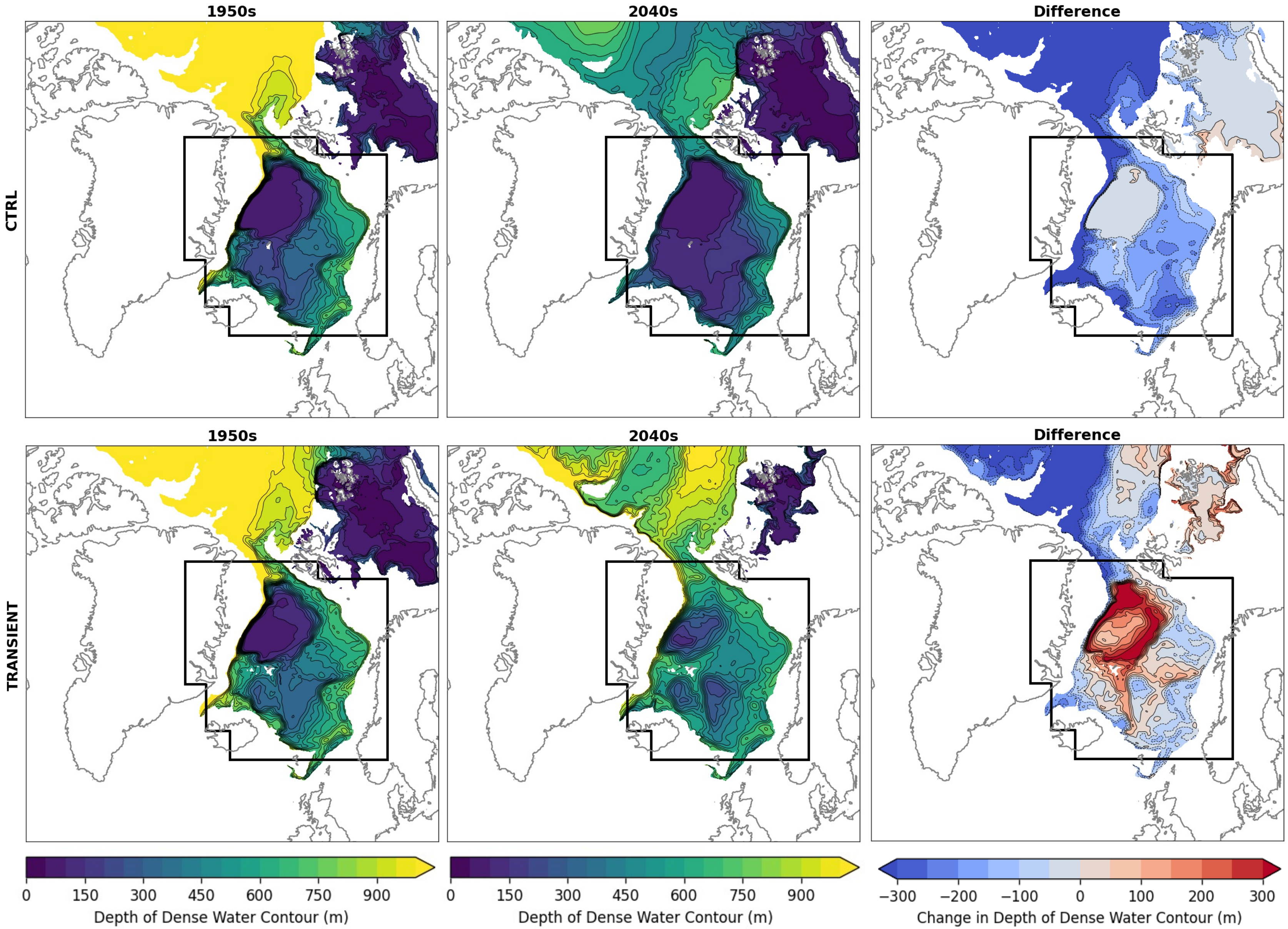

Figure 5.5: Spatial maps show the mean depth of the 1028.05 kg m^{-3} isopycnal for the 1950s and 2040s, as well as the difference between these decadal means (2040s minus 1950s). This isopycnal marks the boundary between intermediate σ_B and dense σ_C water. The results for both the transient and control simulations are presented.

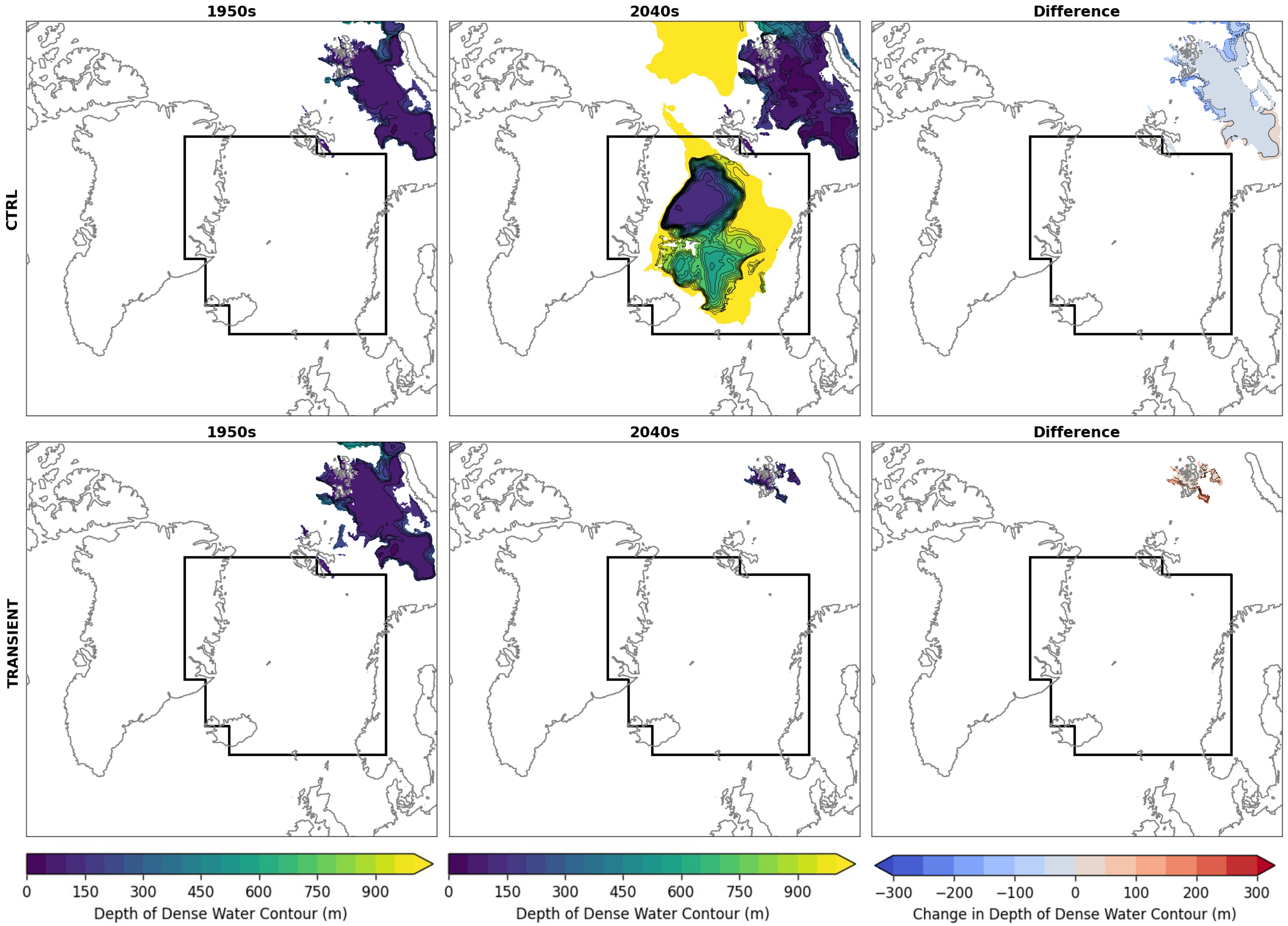

Figure 5.6: Spatial maps show the mean depth of the 1028.10 kg m^{-3} isopycnal for the 1950s and 2040s, as well as the difference between these decadal means (2040s minus 1950s). This isopycnal marks the boundary between very dense σ_D water and the densest σ_E water. The results for both the transient and control simulations are presented.

kg m^{-3} isopycnal is concentrated along the boundary current pathways (particularly of Atlantic Water inflow) indicating that different processes are at play in each case. The deepening of the 1028.05 kg m^{-3} isopycnal in the Greenland Sea is indicative of changes in open-ocean convection in the gyre interior, perhaps during wintertime when the mixed layers are deeper (Moore et al., 2015; Wu et al., 2021). The 1028.05 kg m^{-3} isopycnal lies within the density range commonly used in studies of open-ocean convection in the Nordic Seas and adjacent sub-polar basins (e.g. Marshall and Schott, 1999; Pickart et al., 2003; Jackson and Petit, 2023; Jensen et al., 2018), although the precise density levels associated with active convection vary between basins and circulation regimes (e.g. Rossby et al., 2009).

These results also suggest that, although the volume of denser waters in the Nordic Seas is projected to decrease with climate forcing, this appears not to be the case at higher-latitudes because the presence of denser waters in the Arctic Ocean increases in both the control and transient simulations. This is supportive of results from other studies which find that ***reduced*** dense water formation in the Nordic Seas maybe be compensated for by ***enhanced*** densification further north in the future (e.g. Årthun et al. (2023a, 2025); Bretones et al. (2022)). This is further demonstrated by the emergence of the 1028.10 kg m^{-3} isopycnal at a depth of more than 1000 m in the Arctic Ocean between the 1950s and 2040s in the control simulations, showing the wider-scale accumulation of σ_E water further north due to model drift.

Figure 5.6 shows the depth of the 1028.10 kg m^{-3} isopycnal (upper limit of the densest σ_E water) for the region. As demonstrated by the panels on the left, there is almost no water denser than 1028.10 kg m^{-3} within the Nordic Seas domain in the 1950s in either the control or transient simulation. However, in both simulations, this σ_E water is seen in the north-eastern Barents Sea, near the Novaya Zemlya archipelago. In the transient simulation the presence of this water in the north-eastern Barents Sea is reduced over the course of the model run, such that there is very little σ_E water at all by the 2040s, with only a few small concentrated areas around the islands of Franz Josef Land. By comparison, in the control simulation, the area in which σ_E water is present here has increased, although the 1028.10 kg m^{-3} isopycnal in this north-eastern Barents Sea region has deepened, illustrating an overall decrease in the volume of this densest water.

In contrast to the transient simulation, the control run shows a significant increase in this densest σ_E ocean water within the Nordic Seas. This is particularly true for the Greenland Sea where most of the water column consists of water denser than 1028.10 kg m^{-3} in the 2040s, showing that the enhanced ocean densification in the HadGEM3-HH simulations occurs primarily in the Greenland Sea, and spreads towards the other regions along pathways steered by the topography, for example, towards the Arctic through Fram Strait. This further confirms the importance of the densification process in the Greenland Sea, as it impacts the ocean properties in the rest of the Nordic Seas, the Arctic Ocean and elsewhere. In fact, the formation of the denser waters (σ_C, σ_D and σ_E) occurring mostly in the vicinity of the Greenland Sea Gyre points towards open-ocean convection being an extremely important mechanism for water mass transformation in the Nordic Seas and thus for the northernmost branch of the AMOC.

Our analysis of HadGEM3-HH shows enhanced dense water formation in the Greenland Sea Gyre in control simulations. This is most likely linked to the overestimation of transport of Atlantic Water along inflow current pathways in the HadGEM3-HH simulations and thus overly saline ocean water in this region. However, the transient run shows significant reductions in dense water under a climate change scenario. This difference appears to be driven by the significant ocean warming seen in the climate-forced transient simulation (e.g. Figure 5.2). For lighter/intermediate waters (e.g. σ_A and σ_B), the decrease in densification occurs along the boundary current pathways of the Norwegian Atlantic Current and West Spitsbergen Current, but is concentrated within the Greenland Sea Gyre for denser waters (e.g. σ_C, σ_D and σ_E). This distinction indicates a climate change response in numerous mechanisms of water mass transformation.

Water mass transformation along the boundary currents in the Nordic Seas, and its variability in response to the changing climate, can be driven by several physical processes. For example, dense water formation along the boundary currents could be reduced by:

- Surface freshening which suppresses vertical convection
- Surface warming which inhibits sinking and may lead to reduced atmospheric buoyancy forcing
- Increasing stratification which limits deep convection and impedes wind-driven vertical mixing, which can confine Atlantic-Origin water to shallower depths
- Sea-ice retreat in summer which can enhance atmospheric and upper ocean warming
- Sea-ice advance in winter which reduces the ocean-to-atmosphere heat flux
- Changes in circulation pathways which could alter the depths and velocities at which boundary currents transport water of various densities
- Weaker atmosphere–ocean forcing from winter cold-air outbreaks and fewer deep-reaching convective events.

So, densification of the boundary currents weakens under climate change when fresher, warmer and more stratified surface conditions suppress vertical convection and transformation processes, while circulation shifts and reduced atmospheric forcing limit the cooling and densification of inflowing Atlantic Water. We have already seen some of these changes in the Nordic Seas over the course of the transient simulation in the results shown in the previous chapter. These responses could partly explain the changes we see in the σ_A and σ_B density classes in the HadGEM3-HH simulations.

In contrast, the densification of ocean waters within the Greenland Sea Gyre is mainly driven by open-ocean convection in the gyre interior, particularly during wintertime when the mixed layers are deep. With the changing climate, the interior convection can be altered through a number of often interacting physical mechanisms. For example, dense water formation in the Greenland Sea Gyre could be inhibited by:

- Upper-ocean freshening which might lead to a shallow, stable fresh lens that resists deep convective overturning
- Surface and subsurface warming that can reduce the potential for winter cooling and impede the intrusion of Atlantic-Origin water beneath the surface layer thus reducing the density contrast available for convective overturning
- Increased stratification and a stronger pycnocline which blocks mixing and hinders wind-driven deep convection
- Fewer/weaker cold-air outbreaks and reduced winter surface heat loss which results in less frequent/shallower convective events
- Less brine rejection from decreased/shifting sea-ice formation which undermines the winter densification pathway that feeds interior convection
- Changes in wind forcing and mixed-layer dynamics which can alter Ekman pumping, preconditioning of the water column and the supply/removal of freshwater, while additionally, reduced cyclonic forcing can weaken the gyre circulation
- Enhanced entrainment of warmer/lighter waters into the gyre which can maintain a stable upper layer, while conversely, a weakened import of dense water which preconditions it against convection
- Reductions in eddy activity and lateral mixing that can enhance the stability of the water column

In short, if the surface water is not dense enough in winter the mechanism of deep convection that forms deep water in the Greenland Sea is weakened. The changes in some of these processes seen in the HadGEM3-HH simulations could explain the response in the σ_C, σ_D and σ_E density classes in the Nordic Seas.

A flattening and shallowing of the 1028.08 kg m^{-3} isopycnal in the Greenland Sea Gyre is seen in both the transient and control high-resolution simulations (Figure 5.7). This implies reduced lateral density gradients and weaker geostrophic shear, consistent with a weakening in the gyre cyclonic circulation strength while pointing towards increased stratification, reduced deep convection and decreased ventilation. If we consider the 1028.05 kg m^{-3} isopycnal, we see the same response in the control simulation but not in the transient simulation. As visualised in Figure 5.7, between the 1950s and the 2040s, the high-resolution transient simulation in fact shows a deepening of the 1028.05 kg m^{-3} isopycnal in the Greenland Sea Basin, along with a flattening. This specific response of the downward displacement of of the 1028.05 kg m^{-3} density surface ***without*** increased curvature indicates a ***large-scale buoyancy gain***. This would push isopycnals deeper rather than dynamically doming them within the gyre and could be driven by a basin-wide warming and/or freshening. This response also suppresses deep convection because even though the density surface gets deeper, the increased stratification inhibits vertical mixing, leading to shallower mixed layers and reduced renewal of the deep waters. Overall, the change in the density structure in the Greenland Sea seen in the HadGEM3-HH model is indicative of a slowdown in the Greenland Sea Gyre and a shift towards a less dynamically active, more stratified future state.

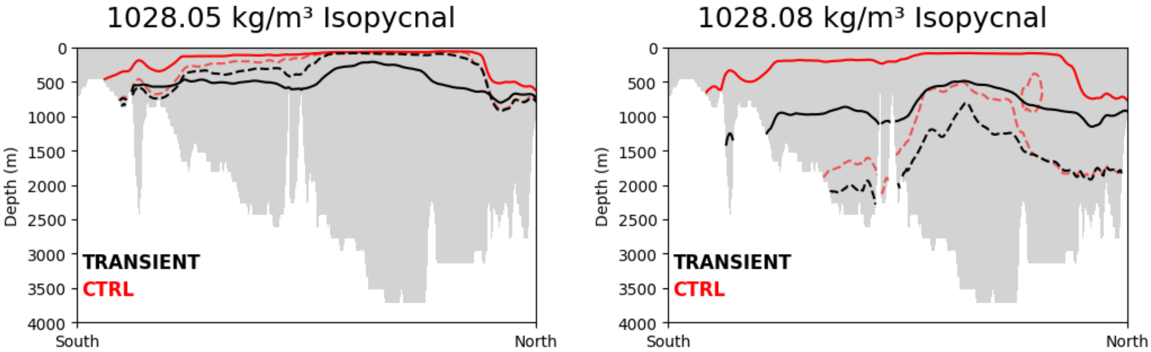

Figure 5.7: The flattening and shallowing of the domed isopycnals from a transect running through the Greenland Sea Gyre indicate a weakening in the cyclonic circulation strength while pointing towards increased stratification, reduced deep convection and declining ventilation. This transect is shown by the dashed line in Figure 5.1. The dashed contours are the 1950s mean and the solid lines are the 2040s mean, with results form the transient simulation in black and the control simulation in red. The large basin in the northern half of the transect is the Greenland Sea Basin, where the domed isopycnals indicate the location of the Greenland Sea Gyre.

5.2.2 A Reorganisation of Dense Water Transport in the Nordic Seas

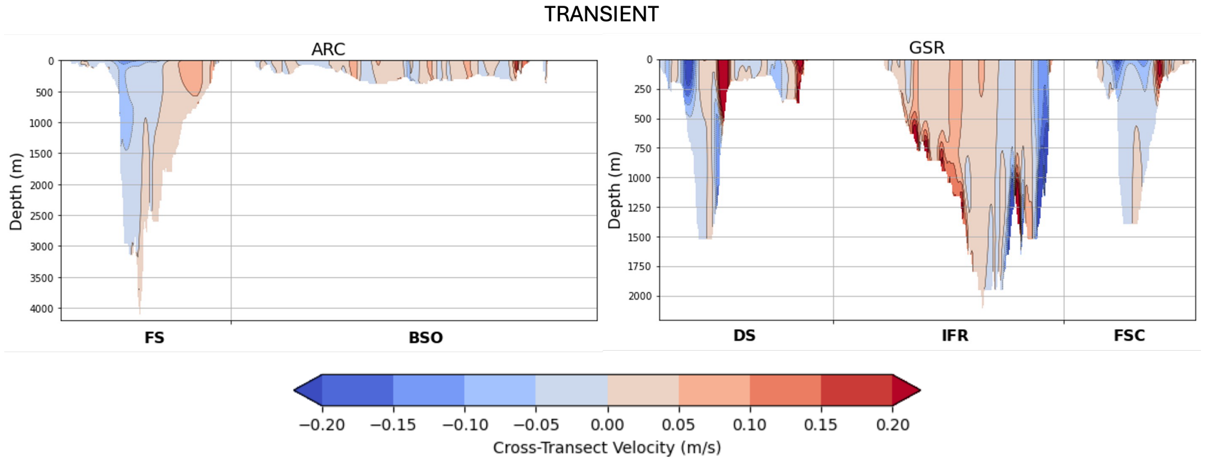

Figure 5.8: The transient model time-mean velocity profile for the Greenland-Scotland Ridge (GSR) and Arctic (ARC) transects (shown in Figure 5.1). These transects are comprised of the Denmark Strait (DS), Iceland-Faroe Ridge (IFR) and Faroe-Scotland Ridge sections (FSC) and the Fram Strait (FS) and Barents Sea Opening (BSO) sections respectively. The velocity shown is perpendicular to the transect line so positive values indicate a northwards or eastwards flow direction (red shading represents approximately poleward flow, and the blue shading represents approximately equatorward flow).

Once the model drift is removed, ocean properties in the Nordic Seas in the transient HadGEM3-HH simulations show projected trends of ***decreasing*** salinity and ***increasing*** potential temperature. Together, these responses lead to an overall reduction in the potential density under a climate change scenario. To investigate the physical mechanisms driving this reduction in dense water in the model, we consider several possible processes. In this section, we investigate the transport of ocean water into the Nordic Seas, using the transects shown in Figure 5.1.

The transient model time-mean velocity profiles for these transects are shown in Figure 5.8. Here the velocity perpendicular to the transect line is presented, with positive values indicating a northwards or eastwards flow direction (so the red shading represents approximately poleward flow and the blue shading represents approximately equatorward flow). The visualisation of this complex interaction of boundary currents, recirculation systems and overflows aids us in understanding the intricacies of ocean dynamics in this region and the extent to which they are captured by the high-resolution model. As discussed in previous studies (e.g. Wu et al., 2021; Roberts et al., 2019) and our work in Chapter 3, we have confidence in the fidelity of the HadGEM3-HH simulation and its ability to represent detailed ocean processes in the Nordic Seas.

The mean potential density profiles for the 1950s and 2040s at the ARC and GSR transects are shown for the transient and control simulations in Figures 5.9 and 5.10

respectively. In these figures, we use the same colour shading as for the five density classes used in our earlier analysis.

For the ARC transect, there is a deepening of the 1027.80 kg m^{-3} isopycnal between the 1950s and 2040s in the transient simulation, with a reduction in the volume of ocean water denser than this value. There is also a thinning in the layer of σ_B water (between 1027.80 kg m^{-3} and 1028.05 kg m^{-3}). This is particularly true at the Barents Sea Opening, where most of the water column consists of σ_B water in the 1950s, but by the 2040s it is almost all lighter σ_A water. Conversely, we see a thickening of the σ_C layer (water between 1028.05 kg m^{-3} and 1028.08 kg m^{-3}) at Fram Strait. This suggests a change in the water mass transformation process at depth, such that water of a different density class is being transformed into σ_C water, or less σ_C water is being transformed into a different density class. Importantly, the σ_D layer (between 1028.08 kg m^{-3} and 1028.10 kg m^{-3}) also decreases in thickness at Fram Strait indicating a reduced volume of dense water overflow. Note that we also see a steepening in the isopycnals here, particularly the 1028.05 kg m^{-3} and 1028.08 kg m^{-3} contours, which become more domed at Fram Strait. This could be the result of increased circulation due to stronger boundary current velocities at either side of the transect (northwards flow in the east and southwards flow in the west). As demonstrated in Chapter 4 (Figure 4.4) the boundary current velocities in the West Spitsbergen Current and East Greenland Current are projected to increase with climate forcing in the HadGEM3-HH transient simulation which would spin up the recirculation at Fram Strait.

In the case of the GSR transect, with climate forcing we see the loss of σ_D water from the deeper levels of the Denmark Strait and Faroe-Scotland Channel transects. This could be important for the density of overflow water that feeds into the Labrador Sea and North Atlantic, impacting the lower-latitude branches of the AMOC. This change is largely compensated for by σ_C water.

There is very little change in the water column between the 1950s and 2040s at the Iceland-Faroe Ridge transect, where there is mainly a northerly flow regime at depth, suggesting potential density changes are contained within the Nordic Seas box at this locality and not reflected by a response at the transect.

Also, there is no σ_E water in any of these decadal mean potential density profiles in the transient simulation.

For the control simulation we see the impacts of model drift, as mentioned in Section 5.2.1 (Figure 5.10). Here there is no significant change in the quantities of lighter σ_A water at either the ARC or GSR transects. However, we see a shallowing of the 1028.05 kg m^{-3} and 1028.08 kg m^{-3} isopycnals in Fram Strait, Denmark Strait and the Faroe-Scotland Ridge and larger quantities of denser water accumulate at depth. Unlike in the transient simulation, in the control simulation we see the emergence of denser waters at both the ARC and GSR transects between the 1950s and 2040s.

At Fram Strait the layer of σ_D water gets thicker, and denser σ_E water (more than

1028.10 kg m^{-3}) appears at the bottom of the water column in the 2040s. At Denmark Strait and the Faroe-Scotland Channel, the deepest waters change from σ_C in the 1950s to σ_D in the 2040s. Again, there is little response in the Iceland-Faroe Ridge.

These findings support those of Section 5.2.1 regarding the volume trends for each density class and the changes in the depth of the various density isopycnals over time. In general, the volume of denser waters is decreasing in the Nordic Seas with climate forcing and this change is seen at the transects along its boundaries too, particularly in the northern ARC sections.

In combination with the velocity profiles at these transects (e.g. Figure 5.8), this suggests changes in the ocean transports of the various density classes. In fact, a reorganisation of the density structure of the water column in the Nordic Seas impacts, and is impacted by, the density structure of the water column in the surrounding regions (e.g. the Arctic Ocean, Barents Sea and North Atlantic) due to the strong interactions between them via exchanges through these transects.

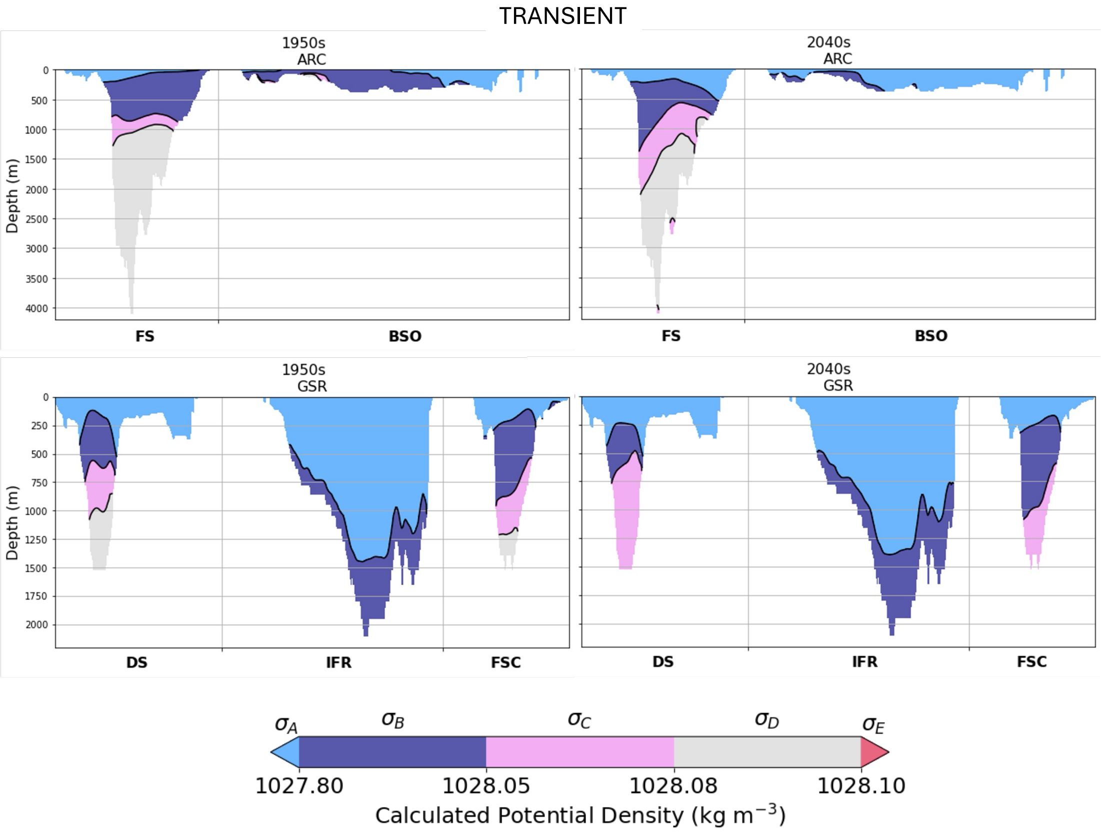

Figure 5.9: Cross-section profiles of the decadal mean calculated potential density for the ARC transect (upper panels) and GSR transect (lower panels) from the transient HadGEM3-HH simulation. The mean for the 1950s (left panels) and 2040s (right panels) are presented, using colour shading that represents the five density classes used in Figure 5.3.

To investigate this, for each of the five density classes we calculate the annual mean net ocean volume transport into the Nordic Seas box region (sum of all transects). The time series for these quantities are shown in Figure 5.11. Note that positive values represent a

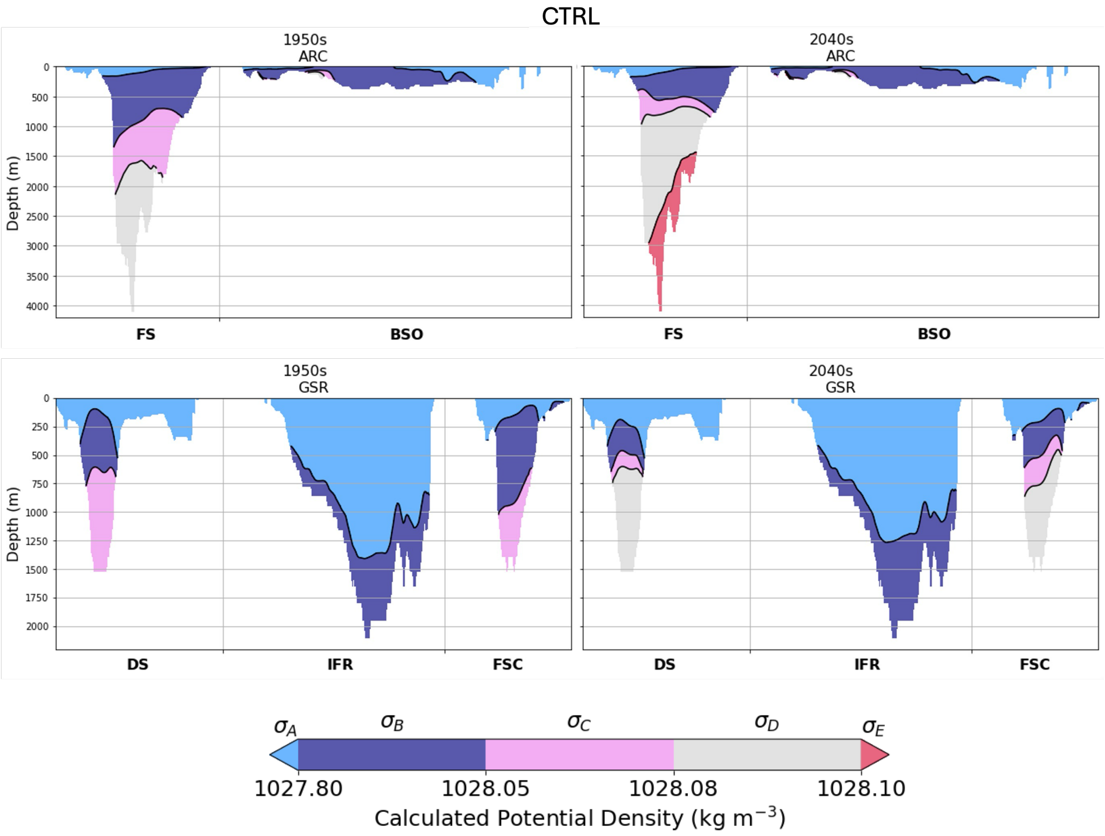

Figure 5.10: Cross-section profiles of the decadal mean calculated potential density for the ARC transect (upper panels) and GSR transect (lower panels) from the control HadGEM3-HH simulation. The mean for the 1950s (left panels) and 2040s (right panels) are presented, using colour shading that represents the five density classes used in Figure 5.3.

flux of water into the box, negative values represent an outflow from the box.

The largest transports are in the upper ocean, with a influx of σ_A (lighter water) of approximately 6 Sv between 1950 and 2050. This is approximately balanced by a net outflow of σ_B water. Over the course of the model run, there is a decreasing trend in the volume transport of σ_A water at a rate of approximately -0.0028 Sv/year in the transient and -0.0063 Sv/year in the control simulation, indicating a small climate-driven response and some model drift here. Similarly, the net export of σ_B water from the Nordic Seas increases in strength over time, more so in the transient than in the control simulation (trends of -0.013 Sv/year and -0.003 respectively), indicating a slight strengthening due to climate forcing. Further investigation shows that most of these changes in the ocean transports of σ_A and σ_B water occur due to changes at Fram Strait and the Barents Sea Opening, with a less significant response seen at the other transects. This suggests a larger response at the northern boundaries of the Nordic Seas compared to the southern boundaries, i.e. it indicates a faster rate of change in Arctic Ocean exchange than with the North Atlantic in the upper ocean.

The transports of the denser waters are much smaller in comparison but still reach up to around 2 Sv. We see a clear positive trend in the transport of σ_C water, with a change in sign from net outflow to net inflow in both the control and transient simulations, which occurs around the year 1980. The trend of increasing inflow of σ_C water is stronger in the transient simulation than in the control simulation. This is largely due to significant increases of transport of σ_C water into the Nordic Seas through Fram Strait but there is also an increase in inflow through the Faroe-Scotland Ridge.

This step-change feature is also partially seen in the time series of σ_D transport, where there is increased interannual variability after the early-1980s. This is also the point at which the transient and control simulations begin to deviate. Until around 1980, the transport of σ_D water fluctuates around zero, but then in the transient simulation it tends to become more negative showing an increased export from the Nordic Seas of this density class, while in the control simulation the transport becomes more positive representing increased inflow of σ_D water. The large differences between the simulations here indicate a strong response to climate forcing despite opposing model drift. The control simulation trend is largely dominated by an increasing flux of σ_D water from the Arctic through Fram Strait. Whereas, in the transient simulation there is little change at Fram Strait and the trend is largely due to increasing export/decreasing import of σ_D water through the Faroe-Scotland Ridge transect.

For σ_E there is little change in transient simulation with the transport hovering close to zero Sv, but there is a trend of increasing outflow in the control simulation due to larger volume transports of this water out of the Nordic Seas from the mid-2020s onwards. This signal is almost entirely due to changes seen at Fram Strait as there is very little response seen at the other transects.

There is high interannual variability in the volume transport of almost all the density classes, in the transient and control simulations.

A schematic illustrating some of the discussed changes seen in the high-resolution HadGEM3 transient simulation is shown in Figure 5.12.

Altogether, Figure 5.11 indicates that the inflow of lighter σ_A water remains mostly steady with climate change, with only a very small weakening trend, while the net export of intermediate σ_B water is projected to increase. There is also projected to be a notable strengthening in the inflow of dense σ_C water and a significant reduction in the inflow of the denser σ_D water, suggesting changes in the balance of Atlantic-Origin vs Arctic dense waters with climate change. There is no significant change in the transport of the densest waters in the transient simulation as this remains close to zero throughout the model run.

A shifting in the composition of the dense water inflows suggests a redistribution within the densest classes of the Nordic Seas and the high rates of exchange with the surrounding regions emphasises strong linkages with the Arctic Ocean, Barents Sea and North Atlantic.

The response in the ocean transports shown here is consistent with the previous results discussed in Section 5.2.1. Our findings point towards reduced deep convection in the Nordic Seas with climate change and a reorganisation in the density structure as a result. While the total ocean volume transports are important for understanding the dynamics of different density classes, it is crucial to also consider the transport of fresh water as this plays a vital role in regulating stratification and rates of dense water formation in the Nordic Seas.

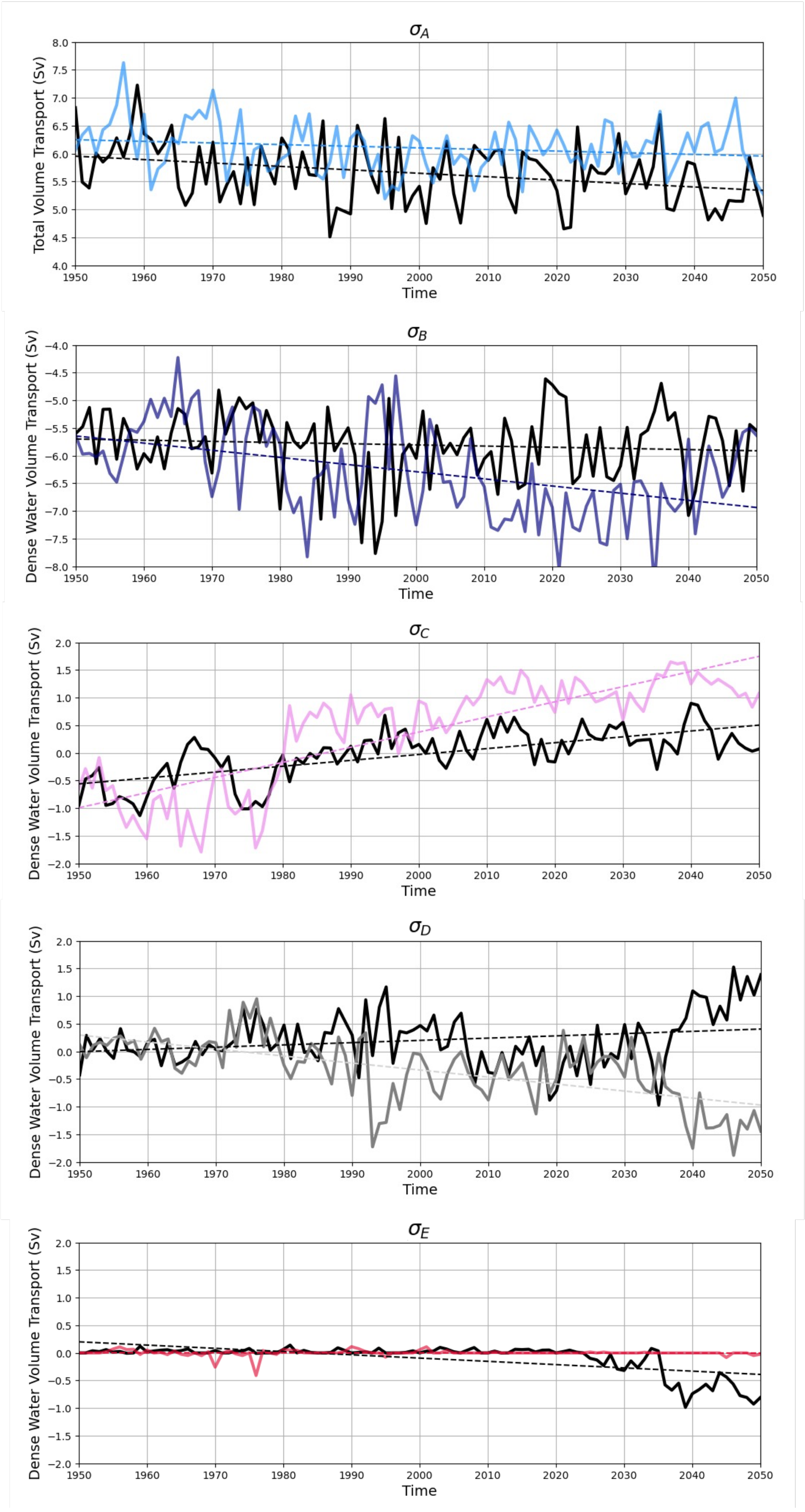

Figure 5.11: Total ocean volume transport (sum of all transects) into the Nordic Seas box region (see Figure 5.1) for each of the five density classes used in our analysis ($\sigma_A \leq$ 1027.80 kg m^{-3}, 1027.80 kg m^{-3} $\leq \sigma_B <$ 1028.05 kg m^{-3}, 1028.05 kg m^{-3} $\leq \sigma_C <$ 1028.08 kg m^{-3}, 1028.08 kg m^{-3} $\leq \sigma_D <$ 1028.10 kg m^{-3}, and 1028.10 kg m^{-3} $\leq \sigma_E$). Note the scale of the y-axes is consistent but the range varies for each subplot. Positive values indicate transport into the Nordic Seas box region, while negative values indicate transport out of the box region. For each density class, the results from the transient simulation are coloured accordingly, with the results from the control simulation in black.

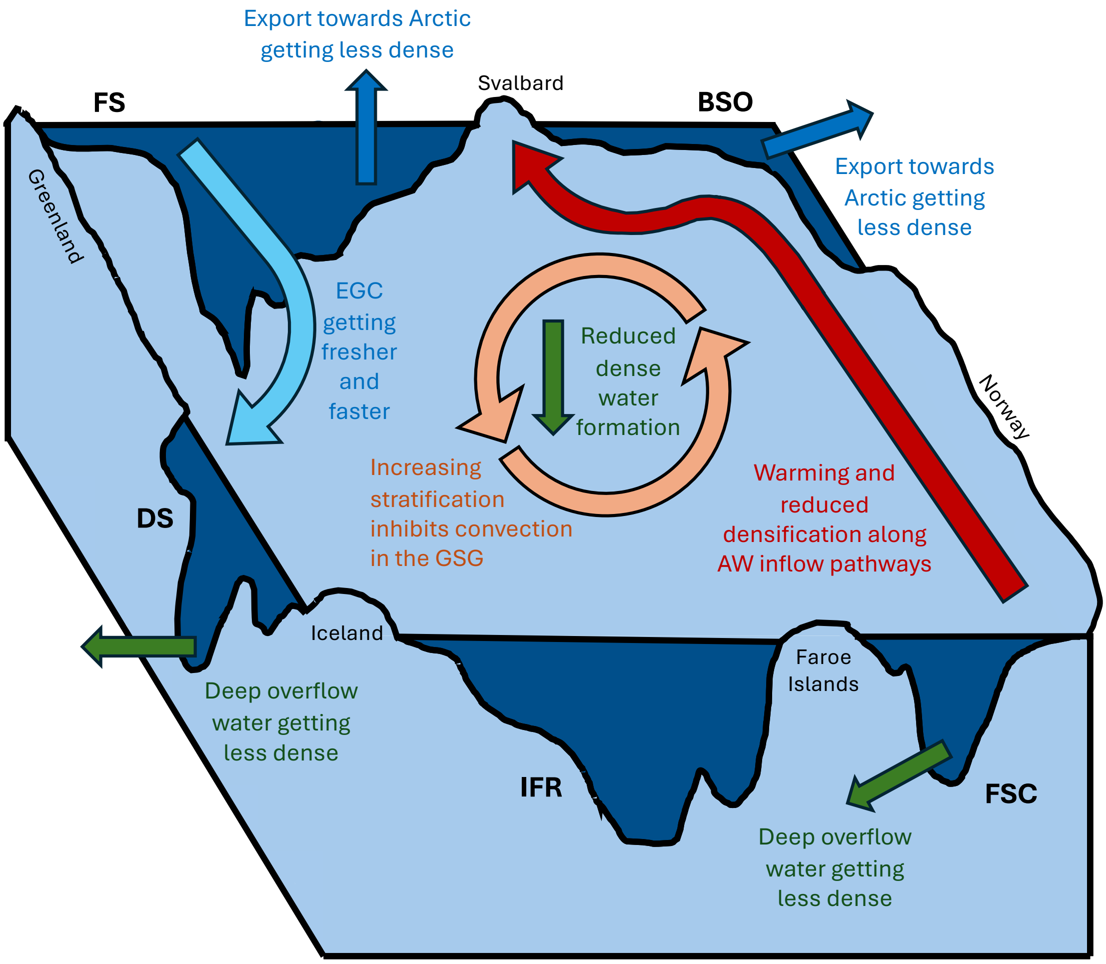

Figure 5.12: Schematic illustrating some of the changes in ocean dynamics seen in the Nordic Seas in the high-resolution HadGEM3 transient simulation. With climate forcing, the model projects warming and reduced water mass transformation along Atlantic Water (AW) inflow pathways, in addition to increasing stratification in the Greenland Sea Gyre (GSG) which inhibits convection, such that we see a reduction in dense water formation. This leads to the export of lighter water from the Nordic Seas to the Arctic and North Atlantic, both in the upper-ocean and at depth.

5.2.3 A Limited Response in the Freshwater Fluxes in the Nordic Seas

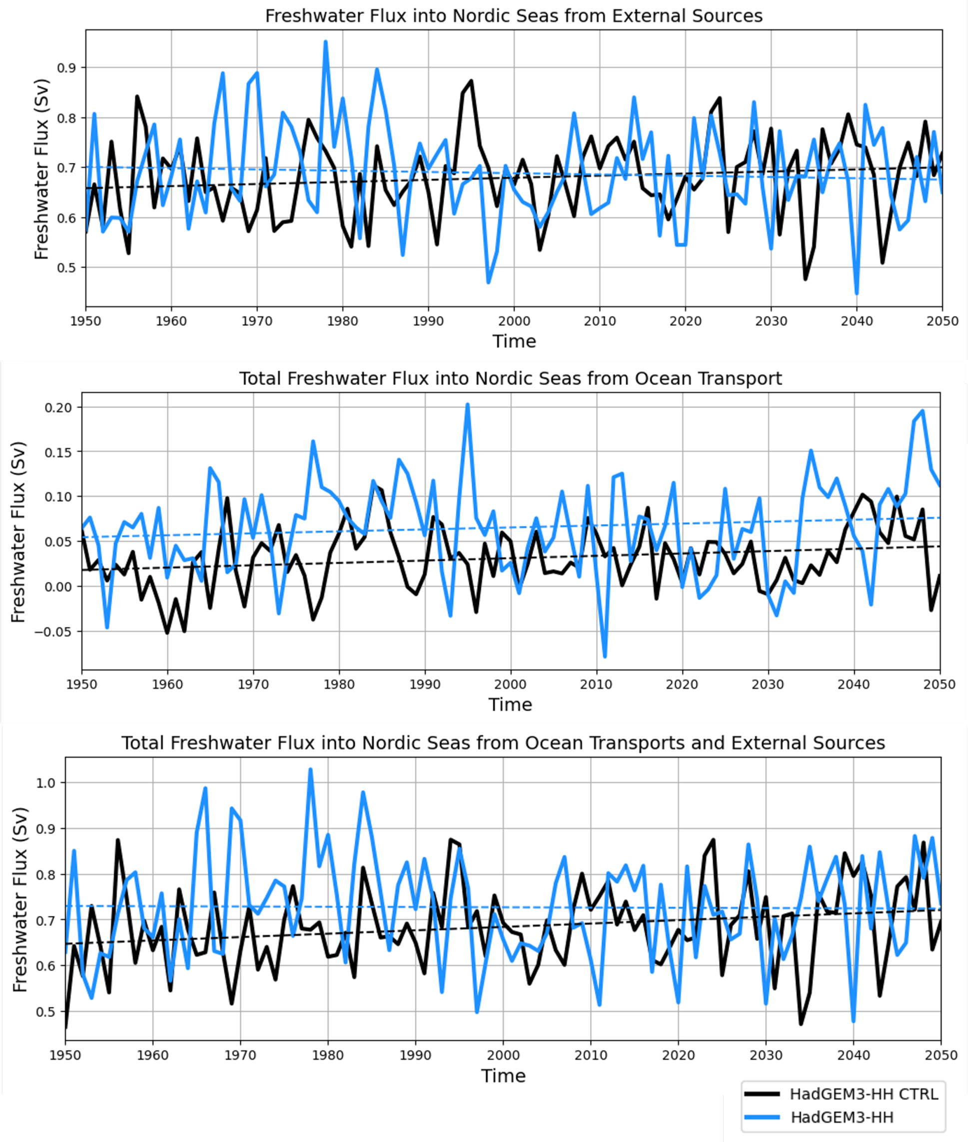

Figure 5.13: Time series of the total annual mean freshwater flux into the Nordic Seas from external sources (upper panel), ocean transport (middle panel) and the net sum of these (lower panel) between 1950 and 2050. The results for the transient (blue) and control (black) simulations are presented and the dashed line of corresponding colour represents the linear regression trend for each case. Positive values indicate a flux into the box region shown in Figure 5.1.

Freshwater fluxes are crucial for understanding changes in dense water formation in the Nordic Seas because they strongly influence surface salinity and stratification. Inputs of freshwater from precipitation, ice melt and Arctic outflow can cap the water column and suppress convection, while processes like evaporation or brine rejection during sea-ice growth increase salinity and promote sinking. Changes in the ocean transports of freshwater also impact the density gradient and stratification, thus leading to conditions that either promote or inhibit vertical mixing, depending on the response. Since dense water formation in this region feeds the Atlantic overturning circulation, shifts in freshwater fluxes can have far-reaching impacts on ocean circulation and the wider climate system.

To ascertain the projected response of freshwater fluxes, and the role they play in the trend of decreasing dense water in the transient HadGEM3-HH simulation, we consider freshwater fluxes from both ocean transport and external sources, including atmospheric exchanges, sea-ice and land run-off.

Firstly, the time series of the total freshwater flux from external sources (sum of all sources) from 1950 to 2050 is shown in the upper panel of Figure 5.13. Note that positive values represent a flux into the Nordic Seas box region. Both the transient and control simulations show annual mean values of approximately 0.7 Sv. Although there is some interannual variability, there is little change over the course of the model run. There is a small increasing trend in the control simulation of approximately 0.0004 Sv/year and a small decreasing trend of approximately -0.0002 Sv/year in the transient simulations. Overall, there is a constant but steady flux of freshwater into the Nordic Seas from external sources. This is not projected to change much in the model simulations, neither with nor without climate forcing.

However, if we look at the external sources of freshwater in more detail, we see that there are in fact responses to climate forcing in some cases, but that these balance out to show virtually no overall change. The time series for the individual external sources of freshwater are shown in Figure 5.14. We show annual means of the freshwater flux into the Nordic Seas from (a) evaporation, (b) precipitation, (c) sea-ice melt and drainage, and (d) land run-off and icebergs. Negative values for the flux due to evaporation show that there is an evaporate loss to the atmosphere at a rate of around 0.55 Sv. For the other external sources, the flux values are positive, so there is always freshwater being added to the Nordic Seas from precipitation, sea-ice and land run-off and rates of approximately 0.9 Sv, 0.25 Sv and 0.12 Sv respectively. These values are perhaps higher than expected and it should be noted that a margin of error is introduced when using diagnostics from the atmosphere component of the simulations. In our analysis, atmospheric model output has been re-grid to the ocean model projection before performing calculations, but it is likely that our method was not exactly consistent with the method employed by the MetOffice.

For the control simulations, there are no large trends between 1950 and 2050, with only a small decrease in precipitation and small increases in the other sources. This is not the case for the transient run which indicates a significant response to climate forcing in each case. The freshwater being lost to the atmosphere by evaporation is projected to increase (overall trend of -0.0008 Sv/year) but the influx from precipitation also increases (overall trend of 0.002 Sv/year). As the presence of sea-ice in the Nordic Seas is predicted to decline with climate change, as is the freshwater flux from sea-ice melt and drainage (overall trend of -0.003 Sv/year), while rising air temperatures and increased melt of the Greenland Ice Sheet mean there is a trend of increasing freshwater from land run-off and icebergs (overall trend of -0.0005 Sv/year). These trends are all hallmarks of an accelerated hydrological cycle under climate change (Thorne et al., 2021; Rawlins et al., 2010; Sato et al., 2022).

Note that sea-ice export from the Arctic into the Nordic Seas is projected to decrease in the transient simulation but this process is already accounted for when considering these external sources of freshwater along with the ocean volume transports. Although there are projected responses in the fluxes of freshwater into the Nordic Seas from external sources, on balance, these result in no net trend due to climate change.

The story is similar for the ocean volume transport of freshwater. The time series of the total freshwater flux into the Nordic Seas from ocean transport is shown in the middle panel of Figure 5.13. The positive values here show that there is always a net influx of freshwater into the region through ocean transport. Overall there are slightly higher values seen in the transient simulation (mean of approximately 0.07 Sv) compared to the control simulation (mean of approximately 0.04 Sv). The trends are similarly small at around 0.0002 Sv/year for both cases, indicating that the slight increase in the ocean transport of freshwater over time is likely due to model drift not climate forcing.

When investigating the changes in the ocean transport of freshwater in more detail we find that there is little overall change at the Barents Sea Opening, Iceland-Faroe Ridge and Faroe-Scotland Channel transects. However, there is a clear response to climate forcing at Fram Strait and Denmark Strait (see Figure 5.15). Much like for the external freshwater sources, considering only the net change hides the true intricacies of the response in different regions of the Nordic Seas. Overall, we see just a small increase in the freshwater flux into the region from ocean transports, but in fact there is a significant increase in the freshwater flux from the Arctic through Fram Strait in the transient simulation, from approximately 0.18 Sv in the 1950s to 0.35 Sv in the 2040s (trend of 0.0018 Sv/year). This is mostly balanced by a large increase in the outflow of freshwater through Denmark Strait, from approximately -0.15 Sv in the 1950s to -0.26 Sv in the 2040s (trend of -0.0013 Sv/year). The trends are small in the control simulation at Fram Strait (0.0004 Sv/year) and Denmark Strait (-0.00001 Sv/year), highlighting that these changes are driven by climate-forced processes and not due to model drift.

These values are slightly elevated compared to those calculated based on observations, likely due to relatively higher simulated ocean velocities in the boundary currents. Karpouzoglou et al. (2022) estimate the annual mean southward liquid freshwater transport through Fram Strait to be around 0.06 Sv using data available between 2015 and 2019, although they only include the Polar Water component in their calculations. Marnela et al. (2013) obtain a result of approximately 0.08 Sv for the southward liquid freshwater transport from hydrographic sections located in the western half of Fram Strait. Generally, long-term mooring and hydrographic analyses indicate Fram Strait freshwater export is approximately 0.08 Sv, though values vary with temporal period considered and reference salinity definition (e.g. de Steur et al., 2017; Håvik et al., 2017a; Rabe et al., 2013; Zhang et al., 2025). At Denmark Strait, observations of liquid freshwater transport are typically a little higher at around 0.1 Sv. Gjelstrup (2024) calculate the annual mean liquid freshwater transport just north of Denmark Strait to be approximately 0.094 Sv, while Le Bras et al. (2018b) calculate it to be around 0.089 Sv.

Altogether, in the HadGEM3 simulations, the flux of freshwater going into the Nordic Seas is positive (largely dominated by the net positive inflow from external sources, particularity precipitation) but steady at a value of approximately 0.73 Sv (see lower panel of Figure 5.13). There is no significant trend in the climate-forced transient simulation and only a small increasing trend in the control simulation (0.0006 Sv / year), indicating some model drift.

This result implies that the flux of freshwater into the Nordic Seas does not play a crucial role in the response of dense water formation under a climate change scenario in the HadGEM3-HH model, suggesting that other processes within the box region have a larger impact in driving water mass transformation.

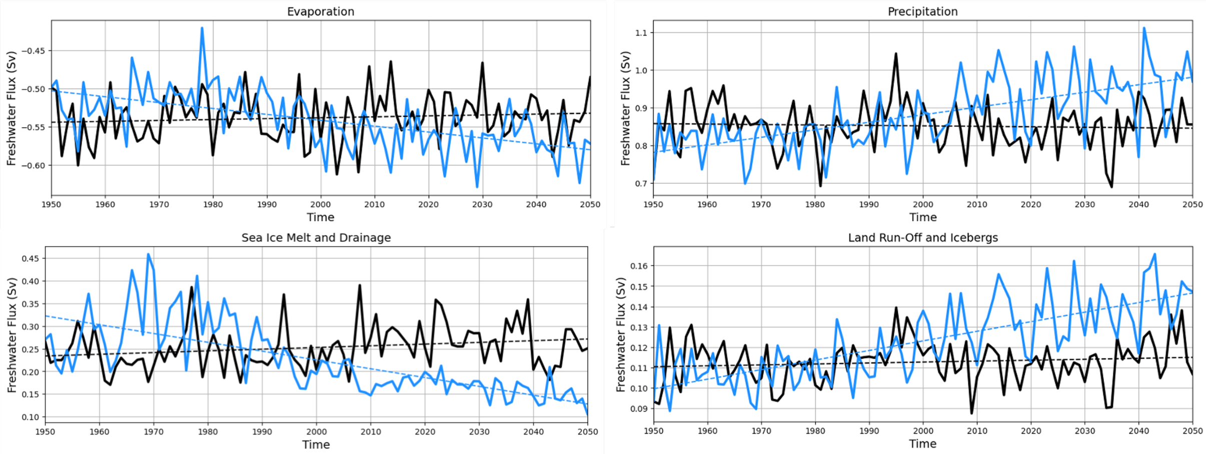

Figure 5.14: Time series of the annual mean freshwater flux into the Nordic Seas from various external sources, namely evaporation (upper left), precipitation (upper right), sea-ice melt and drainage (lower left) and land run-off and icebergs (lower right). The results from 1950 to 2050 are shown for the transient (blue) and control (black) simulations with the dashed line of corresponding colour represents the linear regression trend for each case. Positive values indicate a flux of freshwater into the box region shown in Figure 5.1.

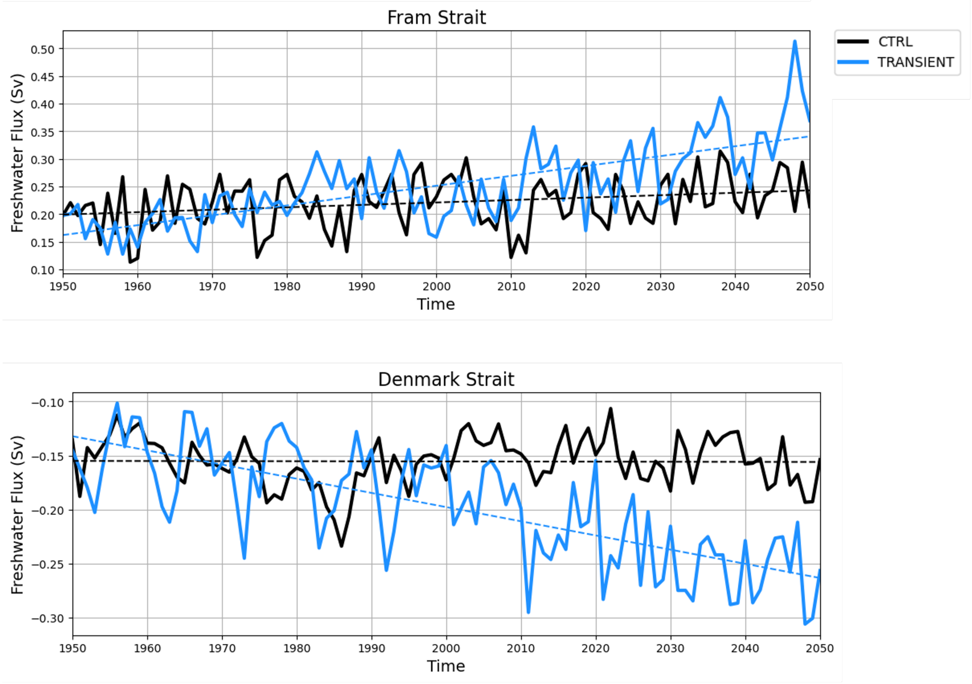

Figure 5.15: Time series of the annual mean freshwater flux into the Nordic Seas from ocean transport through the Fram Strait section (upper panel) and Denmark Strait section (lower panel). The results from 1950 to 2050 are shown for the transient (blue) and control (black) simulations with the dashed line of corresponding colour represents the linear regression trend for each case. Positive values indicate a flux of freshwater into the box region shown in Figure 5.1, whereas negative values indicate an export from this region.

5.2.4 Multiple Interacting Mechanisms Drive the Reduction in Dense Water in the Nordic Seas

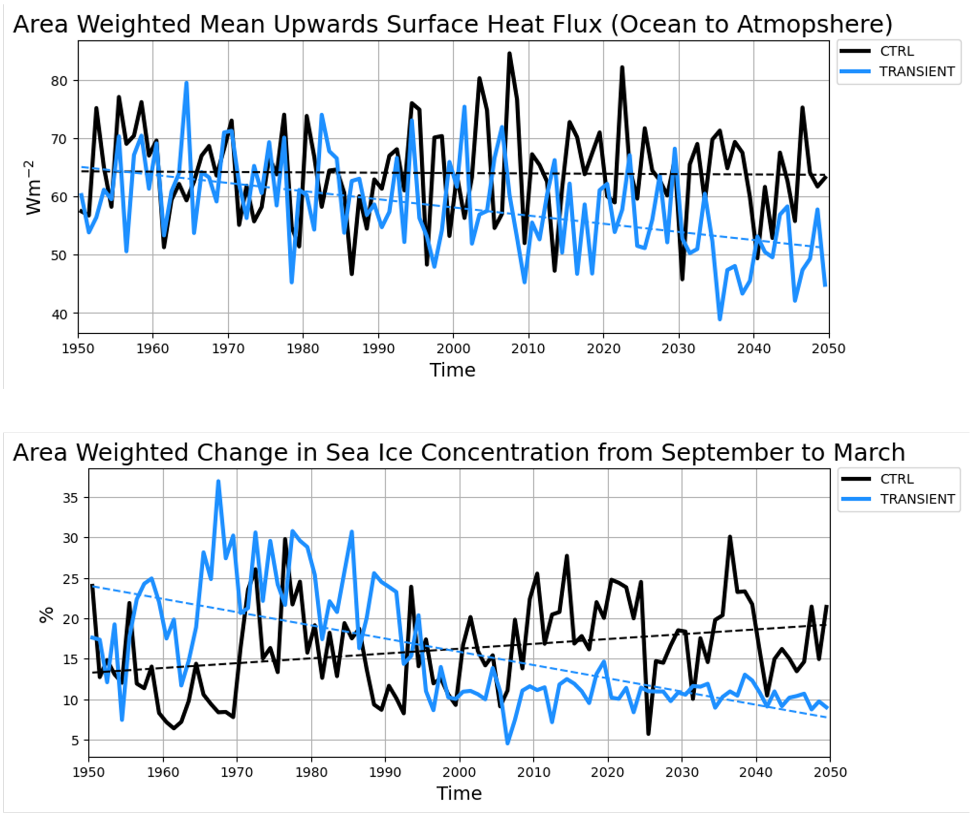

Figure 5.16: The upper panel shows the 1950 to 2050 time series of the area-weighted annual mean upwards surface heat flux, where positive values represent a flux from the ocean to the atmosphere. The lower panel shows the time series for the area-weighted annual mean change in sea-ice concentration from September to March. This diagnostic is used as a proxy for annual sea-ice formation during the freezing period and thus is indicative of rates of brine rejection. The transient and control data are shown in blue and black respectively with the linear regression trend shown with corresponding dashed lines.

With no significant overall response in the freshwater fluxes into the Nordic Seas with climate change, we consider other, more localised physical mechanisms that could be driving the reduced dense water formation seen in the transient HadGEM3-HH simulation.

The release of heat from the ocean to the atmosphere is perhaps one of the most important processes triggering water mass transformation in the sub-polar North Atlantic region. When warmer ocean waters reach the colder high-latitudes, the transfer of heat to the atmosphere allows for the cooling, densification and sinking of ocean waters. This has been shown to be particularly vital for dense water formation in the Barents Sea, which is often referred to as the “Arctic Cooling Machine” (Smedsrud et al., 2013; Skagseth et al., 2020; Shu et al., 2021; Wu, 2022).

To consider this process in the Nordic Seas in the HadGEM3-HH model we look at the surface heat flux. The upper panel of Figure 5.16 shows a time series of the area-weighted annual mean upwards surface heat flux between 1950 and 2050. For the control simulation, there is no long-term trend and the average value remains consistent at approximately 64 W/m^2, although there is high interannual variability. In the case of the transient run, we see a decrease in the ocean-to-atmosphere heat flux from approximately 64 W/m^2 in the 1950s to around 51 W/m^2 in the 2040s (trend of -0.13 W/m^2/year). This clear reduction in the transfer of heat from the ocean to the atmosphere with the changing climate is closely linked to sea-ice retreat. Maps showing the spatial distribution of this change in the HadGEM3-HH model indicate that the decrease in upwards surface heat flux within the Nordic Seas is compensated for by an increase further north as the area of highest heat flux, corresponding to the strongest off-ice-edge low-level winds, shifts poleward with sea-ice decline (Figure 5.17). Note that the region of increased surface heat flux lies *outside* of the box region used in the area weighted averages for the time series shown in Figure 5.16, while the region of decreased surface heat flux is included, thus contributing to the negative trend.

Additionally, the upper ocean is warming at a faster rate than the near-surface air temperature in this region, resulting in a reduced temperature difference at the ocean surface (not shown). With climate-forced future projections, the near-surface atmosphere and upper ocean approach similar temperatures and therefore the rate of heat exchange between the two components is reduced. The declining heat flux emphasises that changes in the atmosphere-ocean interactions impact water mass transformation in the Nordic Seas which is an important process for densification along the high-latitude branch of the AMOC.

The transient future projections of decreased surface heat fluxes suggest that upper-ocean warming plays a role in the lower density in the Nordic Seas. However, reduced brine rejection during sea-ice formation could also be a factor influencing the rate of densification.

When sea-ice forms during the freezing season, brine rejection occurs as part of the process. This leads to higher salinity water at the surface which increases the density and promotes sinking, thus encouraging dense water formation. To consider this more local process we look at the change in sea-ice concentration from September to March, as this "freezing" period covers when there is most sea-ice formation, so we can use this as a proxy for annual sea-ice formation. The time series for the area-weighted mean sea-ice concentration in the Nordic Seas for the transient and control simulations are shown in the lower panel of Figure 5.16. We also show the spatial distribution for the 1950s and 2040s in maps in Figure 5.18. Note that this diagnostic is not a true representation of sea-ice formation as it is affected by the advection of sea-ice into and out of the box region, and we only use it as a proxy for examining the estimated long-term change in sea-ice formation and thus brine rejection. Specific sea-ice formation diagnostics are not available as model output for the HadGEM3-HH simulations.

As we can see from the time series, there is a significant decrease in the *"annual sea-ice formation"* diagnostic in the transient simulation, from an area of approximately 24

% in the 1950s to approximately 9 % in the 2040s. The gradient of the trend line is -0.17 %/year. This points to ***reduced*** brine rejection with climate change and decreased rates of sinking and densification, as seen in the previous results sections. The time series for the control run shows an increasing trend of 0.11 %/year with *more* annual sea-ice formation over time. This suggests there is some model drift in the sea-ice concentration in the HadGEM3-HH model.

The maps in Figure 5.18 show a significant response in the spatial distribution of this *"annual sea-ice formation"* diagnostic, with a clear change in the transient simulation between the 1950s and 2040s, unlike in the control case where the spatial pattern remains largely consistent. Most of the sea-ice formation in the 1950s occurs around the south-east of Greenland, where strong northerly winds promote sea-ice export and formation over the freezing period. (Note that sea-ice export does not contribute to brine rejection). There are also relatively high rates of sea-ice formation in the Greenland and Iceland Seas. This is the picture for both the control and transient simulations. However, by the 2040s, the transient simulation shows a clear divide between regions of high annual sea-ice formation (more than 80%) and regions of low annual sea-ice formation (less than 10%). Most of the sea-ice formation is concentrated along the continental shelf of east Greenland, with very little sea-ice formation elsewhere and very little year-to-year variability in the time series. The Arctic Ocean and Baffin Bay also show high values of annual sea-ice formation during the freezing period.

This response suggests a drastic shift in the mechanisms driving sea-ice formation in the Nordic Seas and the associated processes, such as brine rejection. Significant reductions in rates of annual sea-ice formation throughout the region, particularly in the Greenland Sea basin, are correlated to the reductions in dense water formation seen in the transient simulation, suggesting that changes in brine rejection notably influence water mass transformation here.

In Chapter 4, changes between the first and last decade of the HadGEM3 model were presented. The results show significant ocean surface warming in the high-resolution transient simulation, with the largest increases seen in the boundaries of the Greenland Sea Gyre (change of approximately 5°C) and the northernmost branch of the West Spitsbergen Current leading to the northern Barents Sea, where large increases in upwards surface heat flux are shown in Figure 5.17.

We also see increasing ocean surface salinity in the central Nordic Seas region, although areas of sea-ice cover in the north-west of the domain show a freshening trend which appears to remain largely confined to the continental shelf of East Greenland. These results are consolidated by the time series shown in Figure 5.2.

In Chapter 4, we also considered the change in the mixed layer depth and found that the response was dominated by a large decrease in the Greenland Sea of more than 300 m between the 1950s and 2050s in the transient simulation. This suggests reduced upper ocean vertical mixing and points towards increased stratification in this region, which inhibits convection and reduces dense water formation. The downward stress acting on the ocean is also projected to decrease in this region suggesting reduced wind-driven mixing in the upper ocean.

Furthermore, the ocean surface velocities in the Nordic Seas are generally projected to increase, particularly along the boundary current pathways, which results in enhanced Atlantic-Origin water inflow and Arctic-Origin water outflow.

Along with our findings in this chapter, all of this work points towards significant changes in the complex interactions of numerous physical mechanisms in response to climate change, which ultimately leads to reduced dense water in the Nordic Seas.

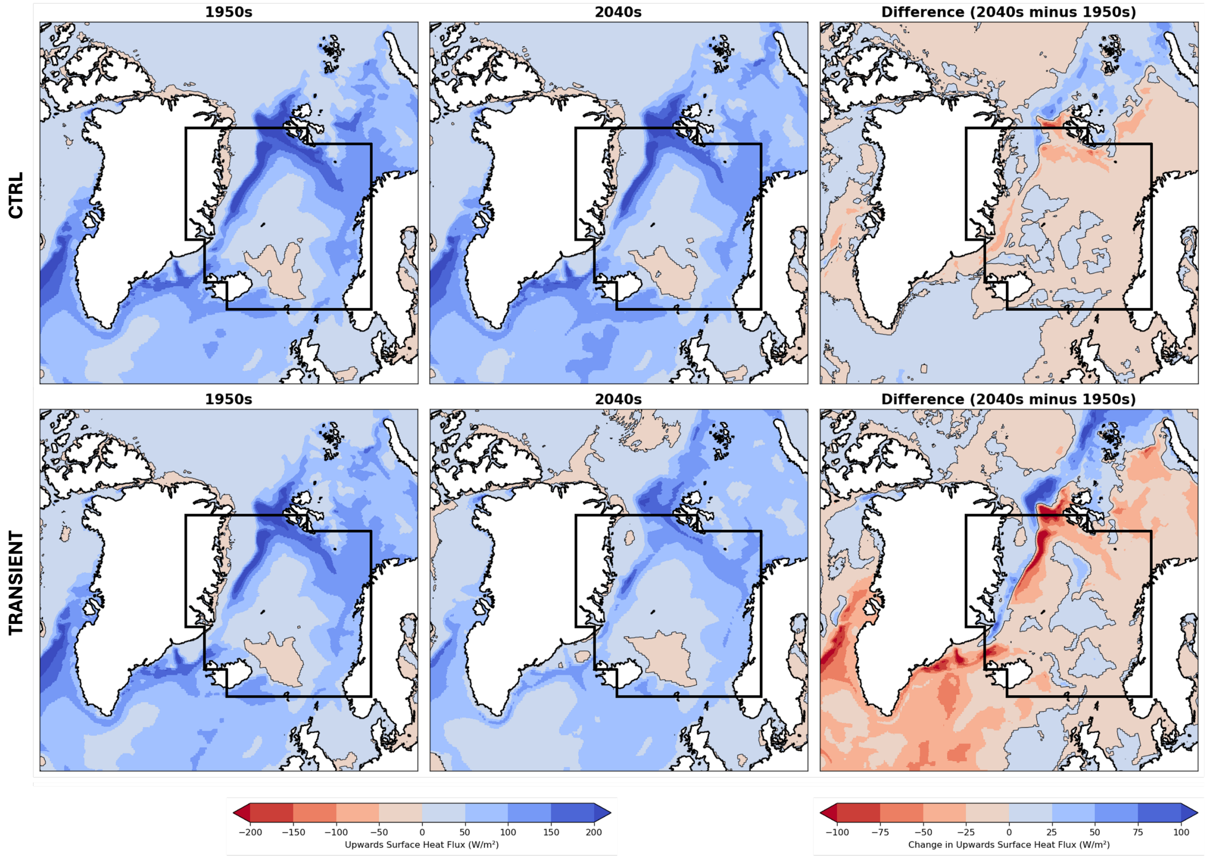

Figure 5.17: Spatial maps show the decadal mean upwards surface heat flux for the 1950s and 2040s, as well as the difference between these decadal means (2040s minus 1950s) from the transient and control simulations (upper and lower panels respectively). For the decadal means, positive values (blue shading) indicate a flux from ocean-to-atmosphere. In the difference plots, the positive values (blue shading) represent an increase in the upwards surface heat flux and negative values (red shading) represent a decrease.

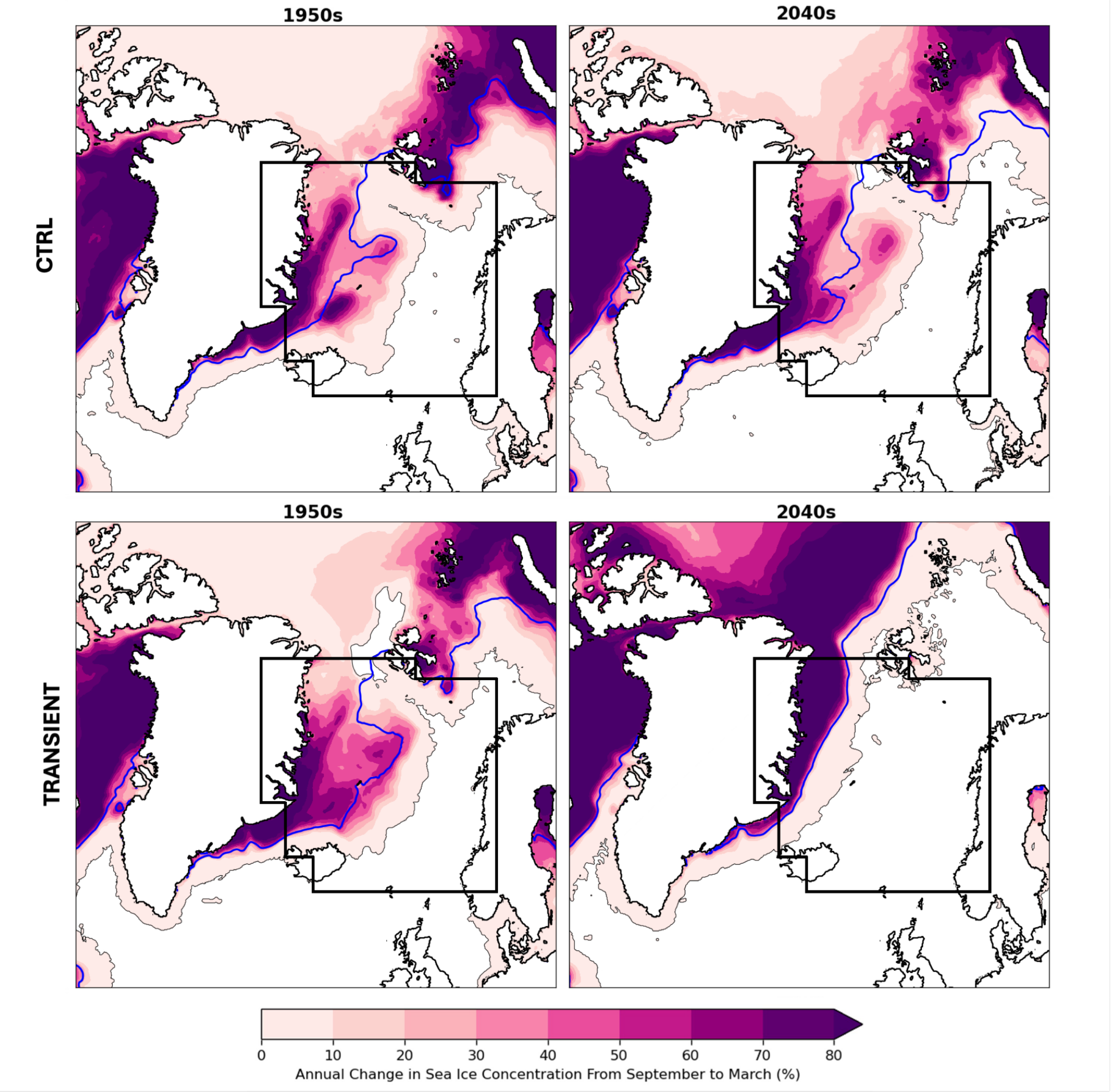

Figure 5.18: Spatial maps show the decadal mean annual change in sea-ice concentration from September to March as a proxy for annual sea-ice formation. Results for the transient and control simulations (upper and lower panels respectively) are presented for the 1950s (left panels) and 2040s (right panels). The decadal mean 15% sea-ice concentration contour line is shown in blue in each subplot.

5.2.5 Stronger but Lighter Overturning Circulation in the Future Nordic Seas

Thus far, our results have shown that the HadGEM3-HH model projects a reduction in dense water in the Nordic Seas under a future climate change scenario. This appears to be largely driven by rising ocean potential temperatures and the poleward retreat of sea-ice leading to decreasing ocean-to-atmosphere surface heat fluxes and reduced brine rejection over the freezing season. All play roles in changing the rate of water mass transformation that drives dense water formation.

The densification of lighter waters along the boundary current pathways of Atlantic Water inflow, such as the Norwegian Atlantic Current and West Spitsbergen Current, decreases due to weaker atmospheric forcing and higher ocean temperatures. There may also be some shoaling of inflow water along the boundary currents (Wu, 2022), confining the Atlantic-Origin water to shallower depths and lighter density classes, as indicated by the increase in volume of lighter σ_A water and a deepening of the 1027.80 kg m^{-3} isopycnal shown in Figures 5.3 and 5.4 respectively.

Meanwhile, the formation of the densest waters in the Greenland Sea basin is reduced due to increased stratification which inhibits vertical mixing and deep convection (as demonstrated by the increased mixed layer depth shown in Chapter 4, Figure 4.7). These changes are seen in the high-resolution transient simulation due to climate forcing (e.g. Figure 5.5) despite some model drift that in fact promotes dense water formation in the Nordic Seas, as is seen in the control simulation (Figure 5.2).

The climate-forced changes in dense water formation have implications for the local overturning circulation which forms the high latitude branch of the AMOC and thus, in turn, has a wide-reaching influence on the global climate system.

To investigate the response of the overturning circulation in the HadGEM3-HH model we use the Greenland-Scotland Ridge (GSR) and Arctic (ARC) transects shown in Figure 5.1. These are similar to transects used by Årthun et al. (2025), although it should be noted that the transects are not exactly the same and we perform our calculations using the model grid. That said, the overturning estimates are comparable. The time mean overturning stream function at both the GSR and ARC transects show similar results to those presented in Årthun et al. (2025), which are based on the reanalysis product GLORYS12 and observational mooring data (see Figure 5.19).

The density-space overturning streamfunction is calculated by binning the volume transport at each model grid point along the transect into discrete potential density classes, which are derived from temperature and salinity fields, and then cumulatively integrating from the densest to the lightest waters. This allows the overturning circulation to be interpreted in terms of water mass transformation and changes in density structure.

Overall, the density-space overturning stream functions compare well and the modelled density values are similar (within approximately 0.1 kg m^{-3}). Both the HadGEM3-HH model and observation-based results show a two-cell structure in the overturning

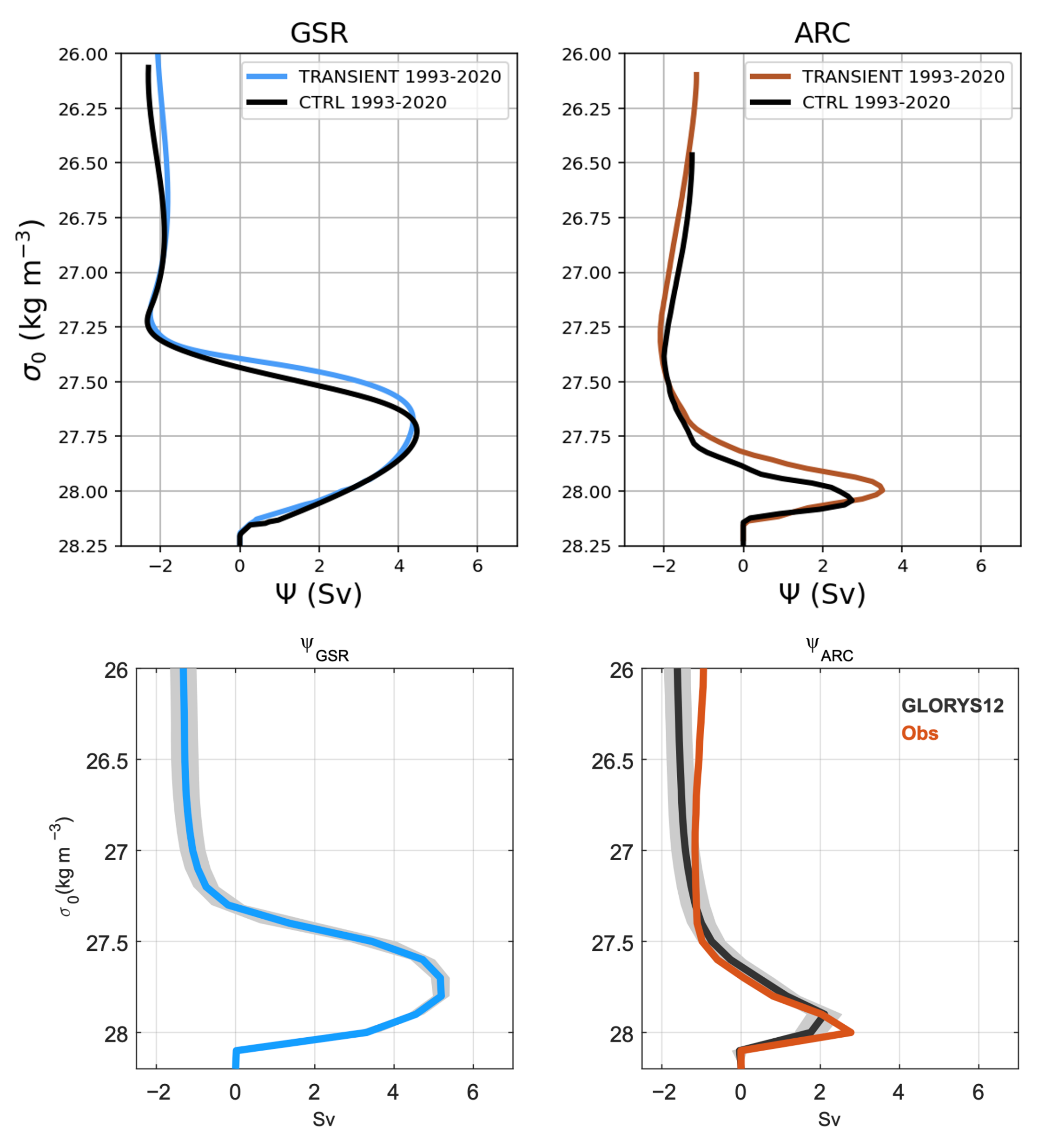

Figure 5.19: The HadGEM3-HH model 1993 to 2020 mean density-space overturning stream functions for the GSR and ARC transects are shown in the upper panels for both the control (black) and transient simulations (blue and orange respectively). The lower panels show figures taken from (Årthun et al., 2025). They present the same 1993 to 2020 mean density-space overturning stream functions calculated from GLORYS12 reanalysis data for the GSR and ARC transects. The 2005 to 2009 mean stream function calculated using observational mooring data is also shown for the ARC transect (lower right panel).

circulation, with a shallow inflow cell of lighter water ($\sim$ 27.3 kg m^{-3}) and a deeper return cell of denser water ($\sim$ 27.8 - 28.1 kg m^{-3}). The maximum overturning in the model is approximately consistent in magnitude with that calculated by Årthun et al. (2025), suggesting the model captures the overall strength of the Nordic Seas overturning accurately and has a realistic representation of the formation of dense overflow waters feeding the GSR overflows. Note, the magnitude of the overturning circulation at the ARC transect is smaller than at GSR, with a narrower, more defined maximum peak.

At the GSR transect, the HadGEM3-HH simulations show a slightly lighter density in the upper cell and a slightly weaker overturning strength in the lower cell, suggesting some underestimation of dense water export or lighter deep water production. The time-mean maximum density-space overturning for both the transient and control is 4.42 Sv, while Årthun et al. (2025) calculate it to be 5.2 Sv on average between 1993 and 2020. The density associated with this maximum from Årthun et al. (2025), is 27.80 kg m^{-3}. We calculate the density at the maximum overturning to be 27.71 kg m^{-3} for the control simulation and 27.69 kg m^{-3} for the transient simulation.

At the ARC transect, the model reproduces the profile of the overturning stream function but with a more distinct deep return flow and a lighter upper inflow, consistent with stronger Arctic-Atlantic exchange in the model. The maximum overturning here is 3.51 Sv in the transient simulation and 3.04 Sv in the control. These are seen at density values of 27.99 kg m^{-3} and 28.03 kg m^{-3} respectively. By comparison, Årthun et al. (2025) find a lower value of 2.1 Sv at a density of 27.9 kg m^{-3}.

Although focussing on the North Atlantic region, while comparing mean depth profiles of the AMOC stream function at 26.5°N for the period between 2004 and 2014, Roberts et al. (2020) show that many HighResMIP models underestimate the depth of the return flow such that the overturning cell is too shallow, but the notable exception is the high-resolution HadGEM3 model, which has an overturning stream function that is very close to the observed profile calculated from RAPID-MOCHA data over the 2004 to 2017 period. The values of maximum overturning at this latitude are higher than those for the Nordic Seas region and have been measured to be in the range of approximately 16 Sv to 18 Sv (e.g. Lee et al., 2024; McCarthy et al., 2015; Kanzow et al., 2010).

To consider the response in the overturning circulation with climate change we show the decadal mean overturning stream functions between 1950 and 2050 from the HadGEM3-HH model. These results are presented for both the transient and control runs in Figure 5.20. The two cell structure is consistently well represented in both the transient and control simulations with the stronger positive overturning cell associated with dense water formation and outflow, and the weaker negative upper cell representing the inflow of lighter Arctic water (at the ARC transect) or lighter Atlantic water (at the GSR transect). In the transient run, at both transects, the overturning strengthens in magnitude but shifts towards lighter densities. In contrast, the control run shows minimal change through the decades, implying that the transient evolution reflects a forced climate response rather

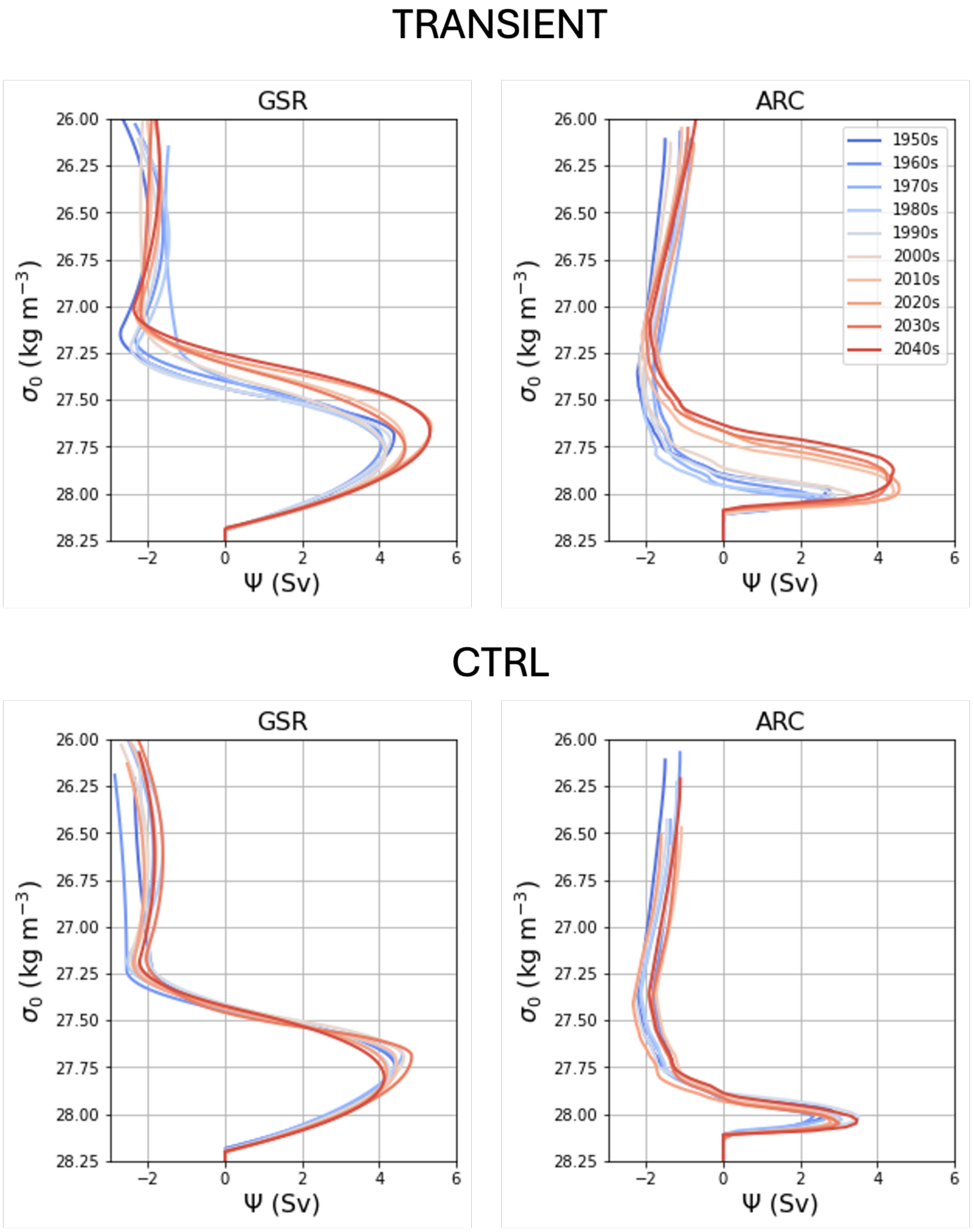

Figure 5.20: The decadal mean density-space overturning stream functions for the GSR (left) and ARC (right) transects between 1950 and 2050 are shown for both the HadGEM3-HH transient (upper panels) and control simulations (lower panels).

than model drift.

The GSR section shows stronger overturning than the ARC section, consistent with GSR being the main exchange gateway between the Nordic Seas and the North Atlantic. However the transient projections show significant strengthening in the ARC overturning, indicating that it is projected to be a more important exchange gateway with increased deep water outflow through Fram Strait and (perhaps to a lesser extent) the Barents Sea Opening in the future. The shift towards lighter densities in the transient run is indicative of a freshening/warming of source waters which suppresses deep convection and weakens the formation of dense overflow waters. This is consistent with the time series shown in Figure 5.2 in Section 5.2.1 which show a reducing ocean potential density in the Nordic Seas under a future climate change scenario.

The weakening of the dense water cell in the transient simulation relative to the control (at ~ 27.8 kg m^{-3}) aligns with the fact that there is reduced deep water formation under a climate change scenario. This reduction at both GSR and ARC suggests a basin-wide slowdown of the overturning circulation driven by lighter surface waters and reduced convection.

The changing strength of the maximum overturning for the GSR and ARC transects in the high-resolution HadGEM3 transient and control simulations is also demonstrated by the decadal mean values shown in Table 5.2.

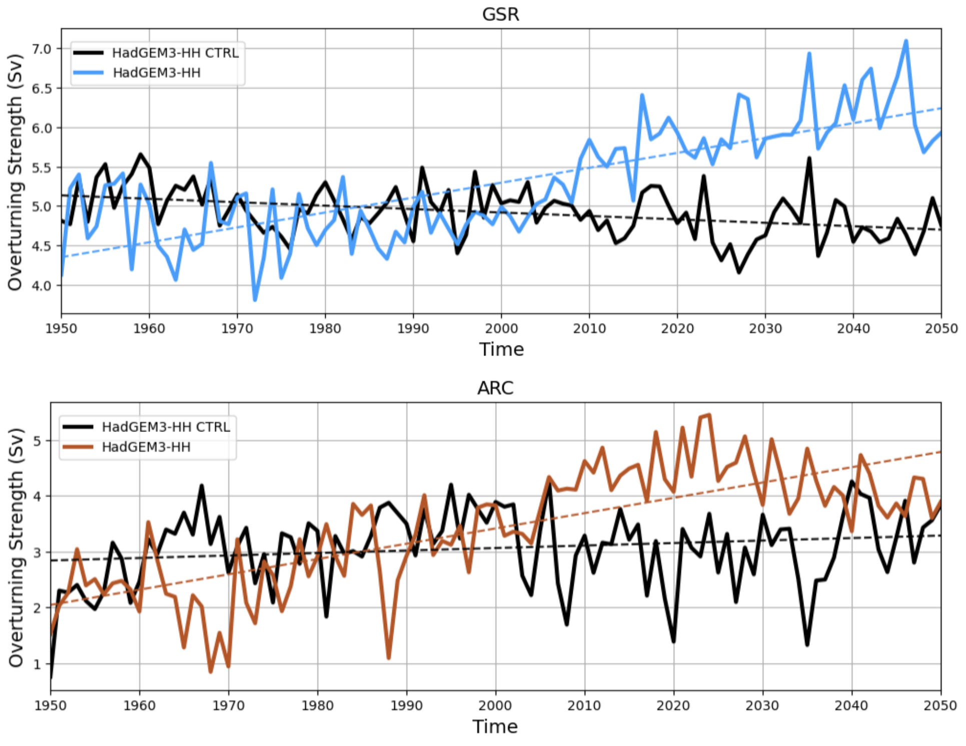

Figure 5.21: Time series of the overturning circulation strength at a density of 1027.80 kg m^{-3} for GSR (upper panel) and 1028.00 kg m^{-3} for ARC (lower panel) between 1950 and 2050. Note that these density values where chosen as they represent the mean density of maximum overturning circulation strength in the model at each transect.

As dense water formation in the Nordic Seas is projected to decrease, the density of the maximum overturning circulation is also projected to decrease. However, the strength of the overturning circulation is projected to increase, especially at higher latitudes (closer to the Arctic). This is clearly demonstrated in Figure 5.21 which shows the time series of the maximum overturning circulation at the GSR and ARC transects between 1950 and 2050 for both the control and transient simulations. The positive trends in the transient time series (0.019 Sv/year for GSR and 0.029 Sv/year for ARC) illustrate the significant increase in overturning circulation in the Nordic Seas between 1950 and 2050, while the reduced rate of change in the control run (trends of around -0.004 Sv/year for GSR and 0.005 Sv/year for ARC) confirms this response is climate-forced. Note that the transient simulated time series of maximum overturning circulation for the GSR transect shows a steady increase from around the year 1990, whereas for the ARC transect the time series has an initial increasing trend until the mid-2020s, after which there is a small decline.

Årthun et al. (2025) also calculate positive linear trends (of approximately 0.004 Sv/year and 0.08 Sv/year for the GSR and ARC transects respectively) from GLORYS12 reanalysis data between 1993 and 2020, indicating a significant increase in the Arctic overturning circulation. The calculated trends for the same period (1993 to 2020) for the transient HadGEM3-HH simulation are slightly elevated by comparison at 0.07 Sv/year and 0.11 Sv/year for the GSR and ARC transects respectively. Given the high climate sensitivity of the model, it is understandable that it exhibits a more extreme portrait of the future, resulting in larger trends in response to increasing greenhouse gas emissions than those measured by present-day observations.

The shift towards less dense overturning in the transient simulation is further demonstrated by the decadal mean values of the density of the maximum overturning circulation for the GSR and ARC transects shown in Table 5.3. At GSR there is a clear response, with a change in the density of maximum overturning from 27.70 kg m^{-3} in the 1950s to 27.67 kg m^{-3} in the 2040s. Meanwhile, at the ARC transect, the density of maximum overturning is 27.97 kg m^{-3} and 27.87 kg m^{-3} for the 1950s and 2040s respectively. The values for the control simulation are also presented. They show little variability over the course of the model run, with a mean value of 27.74 kg m^{-3} for GSR and 28.02 kg m^{-3} for ARC.

The combination of stronger overturning but at lighter densities suggests that, while deep convection in the densest classes weakens, shallower convection and intermediate overturning intensify in some areas. That is, the overturning depth shoals (becomes shallower) but the overturning circulation itself strengthens in the upper layers. This is most likely due to surface buoyancy forcing which must still drive vigorous overturning, despite the fact that the ocean has warmed, preventing very dense water formation. Hence, overturning becomes more active but less deep, centred in lighter density classes. This complex response points to an intricate reorganisation of the Nordic Seas overturning circulation with climate change, rather than a straightforward shift towards weakened convection.

The density of the Nordic Seas overturning circulation largely controls the depth and strength of the overflow waters that feed into the deep limb of the AMOC before it flows southward towards the North Atlantic. If the overturning circulation becomes stronger locally, but the waters formed by this mechanism are less dense, we might expect a reduced contribution to the deep, dense overflow feeding the AMOC here, although this is dependent on whether the lighter water crossing the GSR transect can contribute to the deep AMOC water. In work by Dickson and Brown (1994) and Huang et al. (2020), ***overflow water*** is defined as having a density of more than 27.8 kg m^{-3}, which approximately coincides with our calculated model streamfuntion maximum for the lower cells, suggesting it is possible. If so, this could eventually contribute to a weakening of the AMOC, or a change in the AMOC water properties, even as local overturning intensifies in the upper layers. That being said, a partial compensation is possible, with some of our findings suggesting there may be an enhanced contribution of dense waters from higher latitude source regions (e.g. the Arctic Ocean) as suggested by other studies in literature (Thomas and Fedorov, 2019; van den Berk et al., 2021; Årthun et al., 2023a, 2025; Moore et al., 2022; Bretones et al., 2022). Further research is required to fully explore this possibility.

	Transect	1950s	1960s	1970s	1980s	1990s	2000s	2010s	2020s	2030s	2040s
Transient	GSR	4.40	4.08	4.16	4.17	4.30	4.17	4.67	5.36	4.68	**5.33**
	ARC	2.81	2.35	2.66	2.89	2.91	3.36	4.44	**4.57**	4.29	4.42
Control	GSR	4.42	4.44	4.61	4.43	4.28	4.65	4.46	4.20	**4.85**	4.14
	ARC	2.81	2.35	2.63	3.08	**3.51**	2.95	2.92	2.79	3.01	3.47

Table 5.2: Decadal mean values for the strength of the maximum overturning at the GSR and ARC transects in both the transient and control simulations. Units are Sv. For each case, the strongest maximum overturning decadal mean value is highlighted with bold text.

	Transect	1950s	1960s	1970s	1980s	1990s	2000s	2010s	2020s	2030s	2040s
Transient	GSR	27.70	27.72	27.79	27.76	27.72	27.78	27.73	**27.65**	27.76	27.67
	ARC	27.97	28.01	28.03	28.03	28.01	28.01	27.99	27.97	27.95	**27.87**
Control	GSR	27.75	27.73	**27.68**	27.71	27.78	27.70	27.74	27.77	27.69	27.81
	ARC	**27.97**	28.01	28.03	28.03	28.01	28.03	28.03	28.05	28.05	28.03

Table 5.3: Decadal mean values for the density of maximum overturning strength at the GSR and ARC transects in both the transient and control HadGEM3-HH simulations. Units are kg m^{-3}. For each case, the least dense decadal mean value is highlighted with bold text.

5.3 Conclusions

Our analysis of the HadGEM3-HH global coupled climate model has allowed us to explore the possible future projections in dense water formation and overturning circulation in the Nordic Seas. In our research, we find that the transient simulations show a decreasing volume of dense water in the Nordic Seas, driven by rising ocean potential temperatures under a climate change scenario. We also see that reduced densification is concentrated at the surface, along boundary current pathways of Atlantic Water inflow and at depth in the Greenland Sea basin, likely, at least in part, due to significant trends in increasing upper-ocean potential temperature and increasing stratification in the water column respectively.

Ocean volume transports show small responses in the upper ocean of decreasing inflow of light water and increasing export of intermediate density water. The ocean volume transports also show a notable reorganisation in the exchange of the denser water classes with the Arctic Ocean and North Atlantic. Although freshwater fluxes show a response to climate change, the net effect remains steady so there is no overall trend in freshwater flux into the Nordic Seas (including ocean freshwater transport and fluxes from external sources). In addition, the poleward retreat of the sea-ice edge drives a northwards shift in regions of strong ocean-to-atmosphere heat flux, resulting in sites of surface-forced water mass transformation driven by this cooling process being relocated to higher-latitudes and away from the Nordic Seas. Reduced brine rejection during the sea-ice formation process over the freezing season also plays a part by decreasing rates of near-surface salinity-driven densification.

Analysis of the overturning circulation in the Nordic Seas shows that, although dense water formation is projected to decrease, the maximum strength of the overturning circulation is in fact projected to increase (particularly closer to the Arctic). However, the density of this maximum overturning is projected to decline which may result in shoaling of the overturning circulation system. This points towards some compensation of the wider-scale weakening of the AMOC by an increasing overturning circulation strength at higher latitudes, although the extent of this compensation remains unclear and the deep overflow water feeding into the AMOC here is projected to get less dense with climate forcing. Finally, we illustrate that the HadGEM3-HH simulations show some model drift towards enhanced dense water formation in the Nordic Seas, such that trends are magnified when removing this trend from the transient results.

Concluding Remarks

The work presented in this thesis comprises the results of extensive scientific research on the Nordic Seas region. We explore the climatological variability and atmospheric forcing of sea-ice features, the changing processes associated with complex ocean dynamics and the important interactive feedback mechanisms within the coupled ocean-ice-atmosphere system. Using both observational data and climate model output, we analyse historical records and investigate future projections to better understand the response of the Nordic Seas to climate change. We place our novel findings in context of the current scientific literature and discuss the limitations of our present-day knowledge. We hope this work contributes to the current understanding in both the scientific and the broader community. The following section provides a brief synopsis of the thesis.

6.1 Thesis Overview

Introductory material is provided in Chapter 1. This introduces the concepts covered in the research and explains what is already known from published studies. We also highlight what currently remains unknown and provide some open questions which we then aim to answer in our work.

In Chapter 2 we present our published study on the Northeast Water Polynya. This body of work uses more than 40 years of reanalysis data to provide a novel and detailed climatology of the polynya and surrounding area. Our results highlight the high spatiotemporal variability of sea-ice in the region and indicates that atmospheric processes mainly determine the location, size and structure of the polynya, all of which vary significantly interannually. The upper-ocean also exhibits a large seasonal cycle of variability in response to surface forcing. The extent of the Northeast Water Polynya, along with the annual timing of its opening and closing, is tightly coupled to the near-surface atmospheric flow regime. The direction of the low-level winds is controlled by the relative locations of high and low sea-level pressure centres over the region and this dynamic wind forcing largely controls the opening of the polynya, while thermodynamic forcing dominates its closure. With the changing climate, the polynya is opening earlier and closing later in the year, approaching a state of reduced annual variability and moving towards more closely resembling a broad marginal ice zone. As ocean and atmospheric warming continues and the sea-ice edge retreats northwards, the future of the NEW Polynya becomes more uncertain and it is possible that this important feature of the high-latitude Nordic Seas will no longer form as it has in the past. Analysis of other observational-based data validates our results.

In Chapter 3 we expand our research of the Nordic Seas, implementing climate model output from the CMIP6 HadGEM3 simulations. In this chapter, the global coupled model is evaluated against observational sea-ice and oceanographic data and differences between the low, medium and high-resolution simulations are highlighted. Overall the model captures sea-ice distribution and variability in the Nordic Seas accurately, although the response to climate change tends to be enhanced compared to current in-situ measurements. Smaller features such as the NEW Polynya are poorly resolved, particularly at lower resolutions. In a similar manner, the ocean properties and dynamics in the Nordic Seas are generally well represented in the higher-resolution HadGME3 simulations but the velocities of the boundary currents tend to be elevated compared to observational records. It should be noted that the low-resolution model run does not fully resolve the ocean circulations in the Nordic Seas, suggesting a horizontal grid of at least 1/4° is necessary for accurate oceanographic research in this region.

We go on to explore the response of the Nordic Seas to a high-emissions climate change scenario in Chapter 4. By considering the changes over the period of the HadGEM3 simulations (1950 - 2050) we show the dramatic evolution of upper-ocean diagnostics and near-surface coupled interactions from pre-industrial conditions to a projected anthropogenically-forced future regime. We find strong warming trends throughout the domain and show that increasing Atlantic Water inflow dominates the spatial distribution of changes in ocean temperature, as well as the salinity response in the EGC, despite significant increases in freshwater flux from ice melt. Opposing salinity trends in different locations leads to large horizontal density gradients and a generally more energetic Nordic Seas, with stronger boundary current velocities and enhanced atmosphere-ocean coupling that drives a dynamical ocean response with important implications for regional water mass transformation processes. Additionally, the analysis of low, medium and high horizontal grid resolutions demonstrates that, overall, the higher-resolution simulation is best for precise analysis of this complex highly-coupled sub-polar environment.

Finally, in Chapter 5 we use the high-resolution HadGEM3 model to conduct a detailed study of water mass volume changes in the Nordic Seas. Projections of reduced dense water are driven by multiple interacting mechanisms (such as rising ocean potential temperatures and increasing stratification) and result in a reorganisation of dense water transport. We see a limited response overall in freshwater fluxes. Our calculations point towards a stronger but lighter overturning circulation in the future, along with a northward shift of key sites of surface-forced water mass transformation towards higher latitudes and the Arctic Ocean. These anthropogenically driven changes in the Nordic Seas have important implications for the AMOC and global climate system.

6.2 Ideas for Future Work

Although the research presented in this thesis has improved our understanding of the Nordic Seas coupled system, there remain many unanswered questions and there is always the possibility to learn more. As human activity in the region expands and intensifies, and as the climate continues to change, the need for detailed and accurate knowledge regarding this important environment will only increase with time.

One major finding of this thesis is that, in the Nordic Seas, near-surface responses to anthropogenic forcing, such as sea-ice decline and rising temperatures, have significant impacts on dynamic ocean processes, such as water mass transformation and overturning circulation. As discussed, these mechanisms play an important role in the AMOC and thus the global climate system, but the extent and details of these impacts could be further investigated. How might the projected reductions in dense water formation in the Nordic Seas influence the overflow waters feeding into the AMOC? In the future, will lighter waters exit the domain through Denmark Strait at depth? Could this trigger a response further downstream in the Labrador Seas (another important site of dense water formation in the global thermohaline circulation)? Could these localised responses be traced to larger-scale reductions in the overall strength of the AMOC?

Furthermore, how could the increasing strength of the overturning circulation in the Nordic Seas influence the AMOC? Might the northwards shift of densification sites compensate somewhat for the predicted future weakening trend? How might the structure of the Arctic Ocean evolve in the future if sea-ice decline and “Atlantification” continues?

Although we show that the change in freshwater fluxes in the Nordic Seas remains limited overall, there is a response in this diagnostic. A closer look at how freshwater anomalies propagate through the region and explicitly influence ocean stratification, convection or overflow properties, would be valuable. It would also be interesting to assess the predictability of associated mechanisms, for example, are there early-warning signals for suppressed convection or regime shifts? What components of the coupled system dominate predictability?

Future work considering the decoupling of the Nordic Seas overturning strength from ventilation effectiveness could also be impactful. How relevant are the changes in the overturning circulation for deep ocean ventilation rates and tracer uptake? Crucially, the efficacy of deep water renewal has implications for ocean heat uptake and carbon storage, both currently important processes in regions such as the Greenland Sea Gyre.

These questions are currently the topic of much scientific research. In further work, it would be interesting to analyse modelled future projections from various climate simulations to consider changes in the AMOC and the Arctic Ocean and ideally, comparisons to in-situ observations could provide validation of modelling results where possible. While we provide some evaluation of the HadGEM3 model in the Nordic Seas against observation-based products, further comparison would be necessary for reliable comprehensive studies of the AMOC, particularly at higher latitudes and in the Arctic Ocean (although this is difficult as in-situ measurements of the atmosphere and ocean are sparse).

Overall, the HadGEM3 simulations comprise a very valuable source of data for climate research and the model is of high quality. However, as with any model, we acknowledge that there are some limitations. The relatively short spin-up time of the simulations, for example, leads to some model drift over the initial period. Additionally, the model output is only available to the year 2050, which is not particularly far into the future when it comes to timescales of climate change. Furthermore, the HadGEM3 simulations are of relatively high climate sensitivity and are forced by a high greenhouse gas emissions scenario. Comparing our results from the analysis of the HadGEM3 simulations to those from other climate models would provide a more balanced perceptive and give us insight into the robustness and uncertainty of our results. Further analysis of different emissions scenarios and longer future timescales could also help to determine more precisely the extent to which anthropogenic forcing drives the responses seen in the Nordic Seas.

While we have looked at atmospheric forcing of the surface, research focussed more specifically on coupled feedback mechanisms (especially radiative ones) could prove useful. For example, how are local cloud regimes and evaporation-precipitation processes changing as sea-ice declines in the Nordic Seas? How might the response of Arctic polynyas influence cloud formation and persistence in future scenarios? Does this affect long-wave radiation at the surface and, in turn, ocean heat loss/gain? This could be linked to our study on the Northeast Water Polynya (Chapter 2) and, having analysed the historical record, it would be interesting to consider the future of the polynya in climate model projections.

One highlight of our research on the Nordic Seas is that human-driven climate change is linked to a wide range of atmospheric, oceanic and cryospheric physical processes and that many of these mechanisms are tightly interconnected. For future work, it should be noted that a holistic research approach is important in such a highly coupled environment.

These are some brief ideas for possible future study in this field. When it comes to the Nordic Seas there is still a vast amount of scientific work to be done and many aspects the climate system in this region remain to be fully understood.

Bibliography

Aagaard, K. and Coachman, L. (1968). The East Greenland Current north of Denmark Strait: Part I. *Arctic*, pages 181–200.

Aagaard, K., Meincke, J., and Rudels, B. (2004). Water-mass formation and distribution in the Nordic Seas during the 1990s. *ICES Journal of Marine Science*, 61(5):846–868.

Abot, L. et al. (2023). Recent convection decline in the Greenland Sea: Insights from observational hydrography. *Journal of Geophysical Research: Oceans*, 128.

Almeida, L., Kolodziejczyk, N., and Lique, C. (2023). Large scale salinity anomaly has triggered the recent decline of winter convection in the Greenland Sea. *Geophysical Research Letters*, 50(21):e2023GL104766.

Almeida, L., Lique, C., Kolodziejczyk, N., and Desbruyères, D. (2025). Drivers of water mass volume changes in the Nordic Seas (2005–2020). *Journal of Geophysical Research: Oceans*, 130(7):e2024JC022209.

Andrews, M. B., Ridley, J. K., Wood, R. A., Andrews, T., Blockley, E. W., Booth, B., Burke, E., Dittus, A. J., Florek, P., Gray, L. J., et al. (2020). Historical simulations with HadGEM3-GC3.1 for CMIP6. *Journal of Advances in Modeling Earth Systems*, 12(6):e2019MS001995.

Årthun, M., Asbjörnsen, H., Chafik, L., Johnson, H. L., and Våge, K. (2023a). Future strengthening of the Nordic Seas overturning circulation. *Nature Communications*, 14:2065.

Årthun, M., Brakstad, A., Dörr, J., Johnson, H. L., Mans, C., Semper, S., and Våge, K. (2025). Atlantification drives recent strengthening of the Arctic overturning circulation. *Science Advances*, 11(28):eadu1794.

Årthun, M., Eldevik, T., Chafik, L., Langehaug, H. R., Lien, V., and Fer, I. (2023b). Surface-forced variability in the Nordic Seas overturning circulation and overflows. *Nature Communications*, 14(1):1234.

Årthun, M., Eldevik, T., and Smedsrud, L. H. (2019). The role of Atlantic heat transport in future Arctic winter sea ice loss. *Journal of Climate*, 32(11):3327–3341.

Årthun, M., Eldevik, T., Smedsrud, L. H., Skagseth, Ø., and Ingvaldsen, R. (2012). Quantifying the influence of Atlantic heat on Barents Sea ice variability and retreat. *Journal of Climate*, 25(13):4736–4743.

Asbjørnsen, H. and Årthun, M. (2023). Deconstructing future AMOC decline at 26.5° N. *Geophysical Research Letters*, 50(14):e2023GL103515.

Asbjørnsen, H., Eldevik, T., Skrefsrud, J., Johnson, H. L., and Sanchez-Franks, A. (2024). Observed change and the extent of coherence in the Gulf Stream system. *Ocean Science*, 20(3):799–816.

Asbjørnsen, H. et al. (2021). Variable Nordic Seas inflow linked to shifts in North Atlantic circulation. *Journal of Climate*, 34:1–20.

Babb, D. G., Kirillov, S., Howell, S. E., Landy, J. C., Glissenaar, I., Stroeve, J., Brady, M., and Ehn, J. K. (2023). The complete annual record of sea ice volume export through Fram Strait as observed by satellite from 2010-2022. *Authorea Preprints*.

Bagnardi, M., Kurtz, N. T., Petty, A. A., and Kwok, R. (2021). Sea surface height anomalies of the Arctic Ocean from ICESat-2: A first examination and comparisons with CryoSat-2. *Geophysical Research Letters*, 48(14):e2021GL093155.

Baker, J., A., Bell, M., J., Jackson, L., C., Renshaw, R., Vallis, G., K., Watson, A., J., and Wood, R. A. (2023). Overturning pathways control AMOC weakening in CMIP6 models. *Geophysical Research Letters*, 50:e2023GL103381.

Baker, J. A., Weijer, W., et al. (2025). Continued Atlantic overturning circulation even under extreme greenhouse forcing. *Nature*, 625:123–129.

Barber, D. and Massom, R. (2007). The role of sea ice in Arctic and Antarctic polynyas. *Elsevier oceanography series*, 74:1–54.

Barrell, C., Renfrew, I. A., King, J. C., Abel, S. J., and Elvidge, A. D. (2023). Projected changes to wintertime air-sea turbulent heat fluxes over the subpolar North Atlantic Ocean. *Earth's Future*, 11(4):e2022EF003337.

Barton, B. I., Lenn, Y.-D., and Lique, C. (2018). Observed Atlantification of the Barents Sea causes the Polar Front to limit the expansion of winter sea ice. *Journal of Physical Oceanography*, 48(8):1849–1866.

Bashmachnikov, I. L. et al. (2023). Heat transport by mesoscale eddies in the Norwegian and Barents Seas. *Journal of Geophysical Research: Oceans*.

Bashmachnikov, I. L., Fedorov, A. M., Vesman, A. V., et al. (2021). Mechanisms of interannual variability of deep convection in the Greenland Sea. *Deep Sea Research Part I*, 174:103557.

Bashmachnikov, I. L., Kozlov, I. E., Petrenko, L. A., Glok, N. I., and Wekerle, C. (2020). Eddies in the North Greenland Sea and Fram Strait from satellite altimetry, SAR and high-resolution model data. *Journal of Geophysical Research: Oceans*, 125(7):e2019JC015832.

Bennett, M. G., Renfrew, I. A., Stevens, D. P., and Moore, G. (2024). The Northeast Water Polynya, Greenland: climatology, atmospheric forcing and ocean response. *Journal of Geophysical Research: Oceans*, 129(5):e2023JC020513.

Beszczynska-Möller, A., Fahrbach, E., Schauer, U., and Hansen, E. (2012). Variability in Atlantic water temperature and transport at the entrance to the Arctic Ocean, 1997–2010. *ICES Journal of Marine Science*, 69(5):852–863.

Beszczynska-Möller, A., Woodgate, R. A., Lee, C., Melling, H., and Karcher, M. (2011). A synthesis of exchanges through the main oceanic gateways to the Arctic Ocean. *Oceanography*, 24(3):82–99.

Blindheim, J. and Østerhus, S. (2005). The Nordic Seas, main Oceanographic features. *Geophysical Monograph Series*, 158:11–35.

Böhm, E., Hopkins, T., and Minnett, P. (1997). Passive microwave observations of the Northeast Water Polynya interannual variability: 1978–1994. *Journal of marine systems*, 10(1-4):87–98.

Bracegirdle, T. J. and Gray, S. L. (2008). An objective climatology of the dynamical forcing of polar lows in the Nordic Seas. *International Journal of Climatology*, 28(14):1903–1919.

Brakstad, A. (2023). Formation and pathways of dense water in the Nordic Seas.

Bretones, A., Nisancioglu, K. H., Jensen, M. F., Brakstad, A., and Yang, S. (2022). Transient increase in Arctic deep-water formation and ocean circulation under sea ice retreat. *Journal of Climate*, 35(1):109–124.

Broomé, S., Chafik, L., and Nilsson, J. (2020). Mechanisms of decadal changes in sea surface height and heat content in the eastern Nordic Seas. *Ocean Science*, 16(3):715–737.

Buckley, M. W. and Marshall, J. (2016). Observations, inferences, and mechanisms of the Atlantic Meridional Overturning Circulation: A review. *Reviews of Geophysics*, 54(1):5–63.

Budéus, G. and Schneider, W. (1995). On the hydrography of the Northeast Water Polynya. *Journal of Geophysical Research: Oceans*, 100(C3):4287–4299.

Caesar, L., Rahmstorf, S., Robinson, A., Feulner, G., and Saba, V. (2018). Observed fingerprint of a weakening Atlantic Ocean overturning circulation. *Nature*, 556:191–196.

Casanova-Masjoan, M., Pérez-Hernández, M. D., Pickart, R. S., Valdimarsson, H., Ólafsdóttir, S., Macrander, A., Grisolía-Santos, D., Torres, D. J., Jónsson, S., Våge, K., et al. (2020). Along-stream, seasonal, and interannual variability of the North Icelandic Irminger Current and East Icelandic Current around Iceland. *Journal of Geophysical Research: Oceans*, 125(9):e2020JC016283.

Cavalieri, D. J., Gloersen, P., and Campbell, W. J. (1984). Determination of sea ice parameters with the Nimbus 7 SMMR. *Journal of Geophysical Research: Atmospheres*, 89(D4):5355–5369.

Chafik, L., Hátún, H., Kjellsson, J., Larsen, K. M. H., Rossby, T., and Berx, B. (2020). Discovery of an unrecognized pathway carrying overflow waters toward the Faroe Bank Channel. *Nature communications*, 11(1):3721.

Chafik, L. and Rossby, T. (2019). Volume, heat, and freshwater divergences in the subpolar North Atlantic suggest the Nordic Seas as key to the state of the meridional overturning circulation. *Geophysical Research Letters*, 46(9):4799–4808.

Chapman, R. and Wood, R. (2025). Quantifying tipping behavior: Geometric early warnings and quasipotentials for a box model of amoc. *Chaos: An Interdisciplinary Journal of Nonlinear Science*, 35.

Chatterjee, S., Raj, R. P., Bertino, L., Skagseth, Ø., Ravichandran, M., and Johannessen, O. M. (2018). Role of Greenland Sea gyre circulation on Atlantic water temperature variability in the Fram Strait. *Geophysical Research Letters*, 45(16):8399–8406.

Comiso, J. C. (1986). Characteristics of Arctic winter sea ice from satellite multispectral microwave observations. *Journal of Geophysical Research: Oceans*, 91(C1):975–994.

Condron, A. and Renfrew, I. A. (2013). The impact of polar mesoscale storms on northeast Atlantic Ocean circulation. *Nature Geoscience*, 6(1):34–37.

Dare, R. and Atkinson, B. (2000). Atmospheric response to spatial variations in concentration and size of polynyas in the Southern Ocean sea-ice zone. *Boundary-layer meteorology*, 94(1):65–88.

de Boer, A. M., Jeansson, E., Jakobsson, M., Rudels, B., Woodgate, R. A., and Bengtsson, L. (2018). Interconnectivity between volume transports through Arctic straits. *Journal of Geophysical Research: Oceans*, 123(10):6995–7016.

de Steur, L., Beszczynska-Möller, A., Hávik, L., Nordgaard, J., von Appen, W.-J., Darelius, E., et al. (2017). Liquid freshwater transport estimates from the East Greenland Current north of Denmark Strait. *Journal of Geophysical Research: Oceans*, 122:1974–1994.

de Steur, L., Sumata, H., Divine, D. V., Granskog, M. A., and Pavlova, O. (2023). Upper ocean warming and sea ice reduction in the East Greenland Current from 2003 to 2019. *Communications Earth & Environment*, 4(1):261.

Deming, J. (1993). Northeast Water Polynya: Polar sea cruise results. *Eos, Transactions American Geophysical Union*, 74(16):185–196.

Dey, D., Falina, A., et al. (2024). Formation of the Atlantic Meridional Overturning Circulation in the Arctic Mediterranean. *Nature Communications*, 15:2400.

Dickson, R. R. and Brown, J. (1994). The production of North Atlantic Deep Water: sources, rates, and pathways. *Journal of Geophysical Research: Oceans*, 99(C6):12319–12341.

Dickson, R. R. et al. (2002). Rapid freshening of the deep North Atlantic Ocean over the past four decades. *Nature*, 416:832–837.

Ding, Y., Cheng, X., Li, X., Shokr, M., Yuan, J., Yang, Q., and Hui, F. (2020). Specific relationship between the surface air temperature and the area of the Terra Nova Bay Polynya, Antarctica. *Advances in Atmospheric Sciences*, 37:532–544.

Docquier, D. et al. (2024). Evaluation of Arctic sea ice in high-resolution coupled climate models. *The Cryosphere*, 18:2739–2761.

Docquier, D., Grist, J. P., Roberts, M. J., Roberts, C. D., Semmler, T., Ponsoni, L., Massonnet, F., Sidorenko, D., Sein, D. V., Iovino, D., Bellucci, A., and Fichefet, T. (2019). Impact of model resolution on Arctic sea ice and North Atlantic Ocean heat transport. *Climate Dynamics*, 53:4989–5017.

Doglioni, F., Ricker, R., Rabe, B., Barth, A., Troupin, C., and Kanzow, T. (2023). Sea surface height anomaly and geostrophic current velocity from altimetry measurements over the Arctic Ocean (2011–2020). *Earth System Science Data*, 15(1):225–263.

Donlon, C. J., Martin, M., Stark, J., Roberts-Jones, J., Fiedler, E., and Wimmer, W. (2012). The operational sea surface temperature and sea ice analysis (OSTIA) system. *Remote sensing of Environment*, 116:140–158.

Döscher, R., Vihma, T., and Maksimovich, E. (2014). Recent advances in understanding the Arctic climate system state and change from a sea ice perspective: a review. *Atmospheric Chemistry and Physics*, 14(24):13571–13600.

Drange, H. et al. (2006). The Nordic Seas: an integrated perspective on oceanography, climatology, biogeochemistry and modeling. *Progress in Oceanography*, 71:1–20.

Drijfhout, S. (2015). Competition between global warming and an abrupt collapse of the AMOC in Earths energy imbalance. *Scientific reports*, 5(1):14877.

Drijfhout, S., Angevaare, J. R., Mecking, J., van Westen, R. M., and Rahmstorf, S. (2025). Shutdown of northern Atlantic overturning after 2100 following deep mixing collapse in CMIP6 projections. *Environmental Research Letters*, 20(9):094062.

Du, Y., Zhang, Y., and Shi, J. (2019). Relationship between sea surface salinity and ocean circulation and climate change. *Science China Earth Sciences*, 62(5):771–782.

DuVivier, A. K., Cassano, J. J., Greco, S., and Emmitt, G. D. (2017). A case study of observed and modeled barrier flow in the Denmark Strait in May 2015. *Monthly Weather Review*, 145(6):2385–2404.

Eastwood, S., Lavergne, T., and Tonboe, R. (2014). Algorithm theoretical basis document for the OSI SAF global reprocessed sea ice concentration product. *EUMETSAT Network Satellite Application Facilities*, 28.

Eldevik, T., Årthun, M., Smedsrud, L. H., Skagseth, Ø., and Ingvaldsen, R. B. (2012). Quantifying the influence of Atlantic heat on Barents Sea ice variability and retreat. *Journal of Climate*, 25(9):4736–4743.

Eldevik, T. and Nilsen, J. E. Ø. (2013). The Arctic–Atlantic thermohaline circulation. *Journal of Climate*, 26(22):8698–8709.

Eldevik, T., Risebrobakken, B., Bjune, A. E., Andersson, C., Birks, H. J. B., Dokken, T. M., Drange, H., Glessmer, M. S., Li, C., Nilsen, J. E. Ø., et al. (2014). A brief history of climate–the northern seas from the Last Glacial Maximum to global warming. *Quaternary Science Reviews*, 106:225–246.

Fichefet, T. and Maqueda, M. M. (1997). Sensitivity of a global sea ice model to the treatment of ice thermodynamics and dynamics. *Journal of Geophysical Research: Oceans*, 102(C6):12609–12646.

Flato, G., Marotzke, J., Abiodun, B., Braconnot, P., Chou, S. C., Collins, W., Cox, P., Driouech, F., Emori, S., Eyring, V., et al. (2014). Evaluation of climate models. In *Climate change 2013: the physical science basis. Contribution of Working Group I to the Fifth Assessment Report of the Intergovernmental Panel on Climate Change*, pages 741–866. Cambridge University Press.

Foldvik, A., Aagaard, K., and Tørresen, T. (1988). On the velocity field of the East Greenland Current. *Deep Sea Research Part A. Oceanographic Research Papers*, 35(8):1335–1354.

Fox, A. D., Handmann, P., Schmidt, C., Fraser, N., Rühs, S., Sanchez-Franks, A., Martin, T., Oltmanns, M., Johnson, C., Rath, W., et al. (2022). Exceptional freshening and cooling in the eastern subpolar North Atlantic caused by reduced Labrador Sea surface heat loss. *Ocean Science*, 18(5):1507–1533.

Frigstad, H., Gundersen, H., Andersen, G. S., Borgersen, G., Kvile, K. Ø., Krause-Jensen, D., Boström, C., Bekkby, T., Anglès d'Auriac, M., Ruus, A., et al. (2021). *Blue Carbon–climate adaptation, CO2 uptake and sequestration of carbon in Nordic blue forests: Results from the Nordic Blue Carbon Project.* Nordic Council of Ministers.

Fu, Y., Lozier, M. S., Bower, A., Burmeister, K., Carrilho Biló, T., Cyr, F., Cunningham, S. A., deYoung, B., Fehmi Dilmahamod, A., de Jong, M. F., et al. (2025). Meridional Overturning Circulation Observed by the Overturning in the Subpolar North Atlantic Program (OSNAP) Array from August 2014 to July 2022.

Gascard, J.-C., Watson, A., Messias, M.-J., Olsson, K. A., Johannessen, T., and Simonsen, K. (2002). Long-lived vortices as a mode of deep ventilation in the Greenland Sea. *Nature*, 416(6880):525–527.

Gascard, J.-C., Zhang, J., and Rafizadeh, M. (2019). Rapid decline of Arctic sea ice volume: Causes and consequences. *The Cryosphere Discussions*, 2019:1–29.

Gebbie, G. and Huybers, P. (2011). How is the ocean filled? *Geophysical Research Letters*, 38(6).

Geyer, F., Fer, I., and Smedsrud, L. H. (2010). Structure and forcing of the overflow at the storfjorden sill and its connection to the Arctic coastal polynya in Storfjorden. *Ocean Science*, 6:401–411.

Gillie, E. R., Bryndum-Buchholz, A., Willis, S. G., and Eddy, T. D. (2024). Exploring novel North Water Polynya ecosystems under climate change. *PLOS Climate*, 3(10):e0000490.

Gjelstrup, C. V. B. (2024). Changing oceanographic conditions in East Greenland.

Glessmer, M. S., Eldevik, T., Våge, K., Øie Nilsen, J. E., and Behrens, E. (2014). Atlantic origin of observed and modelled freshwater anomalies in the Nordic Seas. *Nature Geoscience*, 7(11):801–805.

González-Pola, C., Fratantoni, P., Larsen, K. M., Holliday, N. P., Dye, S., Mork, K. A., Beszczynska-Möller, A., Valdimarsson, H., Trofimov, A., Parner, H., et al. (2019). The ICES working group on oceanic hydrography: a bridge from in-situ sampling to the remote autonomous observation era. *Frontiers in Marine Science*, 6:103.

Good, S., Fiedler, E., Mao, C., Martin, M. J., Maycock, A., Reid, R., Roberts-Jones, J., Searle, T., Waters, J., While, J., et al. (2020). The current configuration of the OSTIA system for operational production of foundation sea surface temperature and ice concentration analyses. *Remote Sensing*, 12(4):720.

Gu, Q., Gervais, M., Danabasoglu, G., Kim, W.-M., Castruccio, F., Maroon, E., and Xie, S.-P. (2024). Wide range of possible trajectories of North Atlantic climate states in a warming world. *Nature Communications*, 15:4221.

Haarpaintner, J., Gascard, J., and Haugan, P. M. (2001). Ice production and brine formation in Storfjorden, Svalbard. *Journal of Geophysical Research: Oceans*, 106(C7):14001–14013.

Hand, R., Keenlyside, N. S., Omrani, N.-E., Bader, J., and Greatbatch, R. J. (2019). The role of local sea surface temperature pattern changes in shaping climate change in the North Atlantic sector. *Climate Dynamics*, 52(1):417–438.

Hansen, B. and Østerhus, S. (2000). North AtlanticNordic Seas exchanges. *Progress in Oceanography*, 45(2):109–208.

Hansen, B. and Østerhus, S. (2004). Variability of the Nordic Seas overflow. *Progress in Oceanography*, 61:1–29.

Harden, B., Renfrew, I., and Petersen, G. (2011). A climatology of wintertime barrier winds off Southeast Greenland. *Journal of Climate*, 24(17):4701–4717.

Harden, B. E., Pickart, R. S., Valdimarsson, H., Våge, K., de Steur, L., Richards, C., Bahr, F., Torres, D., Børve, E., Jónsson, S., et al. (2016). Upstream sources of the Denmark Strait overflow: Observations from a high-resolution mooring array. *Deep Sea Research Part I: Oceanographic Research Papers*, 112:94–112.

Hátún, H., Chafik, L., and Larsen, K. M. H. (2021). The Norwegian Sea gyre–a regulator of Iceland-Scotland ridge exchanges. *Frontiers in Marine Science*, 8:694614.

Håvik, L., Pickart, R. S., Våge, K., Harden, B., von Appen, W.-J., Jónsson, S., and Österhus, S. (2017a). Evolution of the East Greenland Current from Fram Strait to Denmark Strait: Synoptic measurements from summer 2012. *Journal of Geophysical Research: Oceans*, 122:1974–1994.

Håvik, L., Våge, K., Pickart, R., Harden, B., Appen, W.-J. v., Jónsson, S., and Østerhus, S. (2017b). Structure and variability of the shelfbreak East Greenland Current north of Denmark Strait. *Journal of Physical Oceanography*, 47(10):2631–2646.

Hersbach, H., Bell, B., Berrisford, P., Hirahara, S., Horányi, A., Muñoz-Sabater, J., Nicolas, J., Peubey, C., Radu, R., Schepers, D., et al. (2020). The ERA5 global reanalysis. *Quarterly journal of the royal meteorological society*, 146(730):1999–2049.

Heuzé, C. and Liu, H. (2024). No emergence of deep convection in the Arctic Ocean across CMIP6 models. *Geophysical Research Letters*, 51(4):e2023GL106499.

Heuzé, C. et al. (2019). The Atlantic inflow across the GreenlandScotland Ridge: observations and model representations. *Elementa: Science of the Anthropocene*, 7:1–28.

Heuzé, C., Heywood, K. J., Stevens, D. P., and Ridley, J. K. (2015). Changes in global ocean bottom properties and volume transports in CMIP5 models under climate change scenarios. *Journal of Climate*, 28(8):2917–2944.

Hirano, D., Fukamachi, Y., Watanabe, E., Iwamoto, K., Mahoney, A. R., Eicken, H., Shimizu, D., Ohshima, K. I., and Tamura, T. (2014). A wind-driven, hybrid latent and sensible heat coastal polynya at Barrow, Alaska. In *AGU Fall Meeting Abstracts*, volume 2014, pages C11B–0371.

Holland, D. M. et al. (2007). A QuikSCAT climatology of ocean surface winds in the Nordic Seas. *Journal of Geophysical Research*, 112.

Holliday, N. P. et al. (2020). Ocean circulation causes the largest freshening event for 120 years in the eastern subpolar North Atlantic. *Nature Communications*, 11:585.

Holliday, N. P., Meyer, A., Bacon, S., Alderson, S. G., and de Cuevas, B. (2007). Retroflection of part of the East Greenland Current at Cape Farewell. *Geophysical Research Letters*, 34(7).

Holt, J., Polton, J., Huthnance, J., Wakelin, S., O'dea, E., Harle, J., Yool, A., Artioli, Y., Blackford, J., Siddorn, J., et al. (2018). Climate-driven change in the North Atlantic and arctic oceans can greatly reduce the circulation of the North Sea. *Geophysical Research Letters*, 45(21):11–827.

Hoppmann, M., Granskog, M. A., Barber, D. G., Else, B. G. T., Rysgaard, S., Gould, W. J., Tremblay, B., and Mwangi, H. N. (2015). Multidecadal variability of polynya characteristics and ice production in the North Water Polynya, Baffin Bay, from passive microwave and visible satellite imagery. *Remote Sensing*, 7(12):15807–15837.

Høyer, J. L. and Karagali, I. (2016). Sea surface temperature climate data record for the North Sea and Baltic Sea. *Journal of Climate*, 29(7):2529–2541.

Høyer, J. L., Karagali, I., Dybkjær, G., and Tonboe, R. (2012). Multi sensor validation and error characteristics of Arctic satellite sea surface temperature observations. *Remote Sensing of Environment*, 121:335–346.

Huang, J., Pickart, R. S., Chen, Z., et al. (2023). Role of air–sea heat flux on the transformation of Atlantic Water encircling the Nordic Seas. *Nature Communications*, 14:141.

Huang, J., Pickart, R. S., Huang, R. X., Lin, P., Brakstad, A., and Xu, F. (2020). Sources and upstream pathways of the densest overflow water in the Nordic Seas. *Nature Communications*, 11(1):5389.

Hurrell, J. W. (1995). Decadal trends in the North Atlantic Oscillation. *Science*, 269:676–679.

Hwang, B., Landy, J., et al. (2020). Impacts of climate change on Arctic sea ice. *MCCIP Science Review 2020*, pages 208–227.

Isachsen, P. E. et al. (2007). Dense water formation in the Nordic Seas diagnosed from sea surface buoyancy fluxes. *Journal of Geophysical Research*, 112:C04005.

Isachsen, P. E., Koszalka, I., and LaCasce, J. H. (2012). Observational evidence of the Sverdrup circulation in the Nordic Seas. *Geophysical Research Letters*, 39:L23601.

Isachsen, P. E., Sørlie, S. R., Mauritzen, C., Lydersen, C., Dodd, P., and Kovacs, K. M. (2014). Upper-ocean hydrography of the Nordic Seas during the International Polar Year (2007–2008) as observed by instrumented seals and Argo floats. *Deep Sea Research Part I: Oceanographic Research Papers*, 93:41–59.

Isaksen, K., Nordli, Ø., Ivanov, B., Køltzow, M. A., Aaboe, S., Gjelten, H. M., Mezghani, A., Eastwood, S., Førland, E., Benestad, R. E., Hanssen-Bauer, I., Brækkan, R., Sviashchennikov, P., Demin, V., Revina, A., and Karandasheva, T. (2022). Exceptional warming over the Barents area. *Scientific Reports*, 12(1):9371.

Ivanov, V. (2023). Arctic sea ice loss enhances the oceanic contribution to climate change. *Atmosphere*, 14(2):409.

Ivanova, N., Johannessen, O. M., Pedersen, L. T., and Tonboe, R. T. (2014). Retrieval of Arctic sea ice parameters by satellite passive microwave sensors: A comparison of eleven sea ice concentration algorithms. *IEEE Transactions on Geoscience and Remote Sensing*, 52(11):7233–7246.

Iwamoto, K., Ohshima, K. I., and Tamura, T. (2014). Improved mapping of sea ice production in the Arctic Ocean using AMSR-E thin ice thickness algorithm. *Journal of Geophysical Research: Oceans*, 119(6):3574–3594.

Jackson, L. C., Roberts, M. J., Hewitt, H. T., Iovino, D., Koenigk, T., Meccia, V. L., Roberts, C. D., Ruprich-Robert, Y., and Wood, R. A. (2020). Impact of ocean resolution and mean state on the rate of AMOC weakening. *Climate Dynamics*, 55:17111732.

Jackson, L. (2013). Shutdown and recovery of the AMOC in a coupled global climate model: The role of the advective feedback. *Geophysical Research Letters*, 40(6):1182–1188.

Jackson, L. C., Alastrué de Asenjo, E., Bellomo, K., Danabasoglu, G., Haak, H., Hu, A., Jungclaus, J., Lee, W., Meccia, V. L., Saenko, O., et al. (2022). Understanding AMOC stability: The North Atlantic hosing model intercomparison project. *Geoscientific Model Development Discussions*, 2022:1–32.

Jackson, L. C. and Petit, T. (2023). North Atlantic overturning and water mass transformation in CMIP6 models. *Climate Dynamics*, 60(9):2871–2891.

Jakobson, E., Vihma, T., and Palo, T. (2012). Atmospheric forcing of the Nordic Seas. *Tellus A*, 64:18402.

Jeansson, E., Jutterström, S., Rudels, B., Anderson, L. G., Olsson, K. A., Jones, E. P., Smethie Jr, W. M., and Swift, J. H. (2008). Sources to the East Greenland Current and its contribution to the Denmark Strait Overflow. *Progress in Oceanography*, 78(1):12–28.

Jeansson, E., Olsen, A., Eldevik, T., Skjelvan, I., Omar, A. M., Lauvset, S. K., Nilsen, J. E. Ø., Bellerby, R. G., Johannessen, T., and Falck, E. (2011). The Nordic Seas carbon budget: Sources, sinks, and uncertainties. *Global Biogeochemical Cycles*, 25(4).

Jensen, M. F., Nilsson, J., and Nisancioglu, K. H. (2016). The interaction between sea ice and salinity-dominated ocean circulation: implications for halocline stability and rapid changes of sea ice cover. *Climate Dynamics*, 47(9):3301–3317.

Jensen, M. F., Nisancioglu, K. H., and Spall, M. A. (2018). Large changes in sea ice triggered by small changes in Atlantic water temperature. *Journal of Climate*, 31(12):4847–4863.

Jian, D., Zhai, X., Stevens, D. P., and Renfrew, I. A. (2026). Oceanic heat transport along the Norwegian Atlantic Slope Current and the role of eddies. *Journal of Geophysical Research: Oceans*, 131(1):e2025JC022960.

Jung, T. and Hilmer, M. (2001). The link between the North Atlantic oscillation and Arctic sea ice export through Fram Strait. *Journal of Climate*, 14(19):3932–3941.

Jung, T., Miller, M., Palmer, T., Towers, P., Wedi, N., Achuthavarier, D., Adams, J., Altshuler, E., Cash, B., Kinter Iii, J., et al. (2012). High-resolution global climate simulations with the ECMWF model in Project Athena: Experimental design, model climate, and seasonal forecast skill. *Journal of Climate*, 25(9):3155–3172.

Jung, T., Serrar, S., and Wang, Q. (2014). The oceanic response to mesoscale atmospheric forcing. *Geophysical Research Letters*, 41(4):1255–1260.

Kageyama, M., Sime, L. C., Sicard, M., Guarino, M.-V., de Vernal, A., Stein, R., Schroeder, D., Malmierca-Vallet, I., Abe-Ouchi, A., Bitz, C., et al. (2021). A multi-model CMIP6-PMIP4 study of Arctic sea ice at 127 ka: sea ice data compilation and model differences. *Climate of the Past*, 17(1):37–62.

Kanzow, T., Cunningham, S., Johns, W., Hirschi, J. J., Marotzke, J., Baringer, M., Meinen, C., Chidichimo, M., Atkinson, C., Beal, L., et al. (2010). Seasonal variability of the Atlantic meridional overturning circulation at 26.5 N. *Journal of Climate*, 23(21):5678–5698.

Karpouzoglou, T., de Steur, L., and Dodd, P. (2023). Freshwater transport over the Northeast Greenland shelf in Fram Strait. *Geophysical Research Letters*, 50(2):e2022GL101775.

Karpouzoglou, T., de Steur, L., Smedsrud, L. H., and Sumata, H. (2022). Observed changes in the Arctic freshwater outflow in Fram Strait. *Journal of Geophysical Research: Oceans*, 127(3):e2021JC018122.

Käse, R. H., Girton, J. B., and Sanford, T. B. (2003). Structure and variability of the Denmark Strait Overflow: Model and observations. *Journal of Geophysical Research: Oceans*, 108(C6).

Kenigson, J. S. and Timmermans, M. (2021). Nordic Seas hydrography in the context of Arctic and North Atlantic ocean dynamics. *Journal of Physical Oceanography*, 51(1):101114.

Kern, S., Kaleschke, L., and Spreen, G. (2010). Climatology of the Nordic (Irminger, Greenland, Barents, Kara and White/Pechora) Seas ice cover based on 85 GHz satellite microwave radiometry: 19922008. *Tellus A: Dynamic Meteorology and Oceanography*, 62:1–20.

Kern, S., Lavergne, T., Notz, D., Pedersen, L. T., Tonboe, R. T., Saldo, R., and Sørensen, A. M. (2019). Satellite passive microwave sea-ice concentration data set intercomparison: closed ice and ship-based observations. *The Cryosphere*, 13(12):3261–3307.

Klenke, M. and Schenke, H. W. (2002). A new bathymetric model for the central Fram Strait. *Marine Geophysical Researches*, 23(4):367–378.

Koch, L. (1935). A day in North Greenland. *Geografiska Annaler*, 17:609–620.

Koenigk, T., Berg, P., Döscher, R., Gjermundsen, A., Johannessen, O. H., Nikulin, G., Schimanke, S., Suo, L., Välimaa, J., and Willén, U. (2015). Arctic climate change in an ensemble of regional CORDEX simulations. *Polar Research*, 34(1):24603.

Kolstad, E. (2008). A QuikSCAT climatology of ocean surface winds in the Nordic Seas: Identification of features and comparison with the ncep/ncar reanalysis. *Journal of Geophysical Research: Atmospheres*, 113(D11).

Kottmeier, C. and Engelbart, D. (1992). Generation and atmospheric heat exchange of coastal polynyas in the Weddell Sea. *Boundary-layer meteorology*, 60(3):207–234.

Kuhlbrodt, T., Jones, C. G., Sellar, A., Storkey, D., Blockley, E., Stringer, M., Hill, R., Graham, T., Ridley, J., Blaker, A., et al. (2018). The low-resolution version of HadGEM3 GC3.1: Development and evaluation for global climate. *Journal of advances in modeling earth systems*, 10(11):2865–2888.

Kwok, R., Cunningham, G. F., Wensnahan, M., Rigor, I., Zwally, H. J., and Yi, D. (2009). Thinning and volume loss of the Arctic Ocean sea ice cover: 2003–2008. *Journal of Geophysical Research: Oceans*, 114(C7).

Kwok, R. and Morison, J. (2016). Sea surface height and dynamic topography of the ice-covered oceans from CryoSat-2: 2011–2014. *Journal of Geophysical Research: Oceans*, 121(1):674–692.

Lai, W., Robson, J., Wilcox, L., and Dunstone, N. (2022). Mechanisms of internal Atlantic multidecadal variability in HadGEM3-GC3. 1 at two different resolutions. *Journal of Climate*, 35(4):1365–1383.

Langehaug, H. R. and Falck, E. (2012). Changes in the properties and distribution of the intermediate and deep waters in the Fram Strait. *Progress in Oceanography*, 96(1):57–76.

Langehaug, H. R., Sagen, H., Stallemo, A., Uotila, P., Rautiainen, L., Olsen, S. M., Devilliers, M., Yang, S., and Storheim, E. (2023). Constraining CMIP6 estimates of Arctic Ocean temperature and salinity in 2025-2055. *Frontiers in Marine Science*, 10:1211562.

Langehaug, H. R., Sandø, A. B., Årthun, M., and Ilıcak, M. (2019). Variability along the Atlantic water pathway in the forced Norwegian Earth System Model. *Climate dynamics*, 52(1):1211–1230.

Latarius, K. and Quadfasel, D. (2016). Water mass transformation in the deep basins of the Nordic Seas: Analyses of heat and freshwater budgets. *Deep Sea Research Part I: Oceanographic Research Papers*, 114:23–42.

Le Bras, I., Yashayaev, I., van Aken, H. M., Holliday, N. P., Fischer, J., and Pickart, R. S. (2018a). The East Greenland Current system south of Denmark Strait. *Journal of Geophysical Research: Oceans*, 123(12):9340–9360.

Le Bras, I. A.-A., Straneo, F., Holte, J., and Holliday, N. P. (2018b). Seasonality of freshwater in the East Greenland Current system from 2014 to 2016. *Journal of Geophysical Research: Oceans*, 123(12):8828–8848.

Lee, S.-K., Kim, D., Gomez, F. A., Lopez, H., Volkov, D. L., Dong, S., Lumpkin, R., and Yeager, S. (2024). A pause in the weakening of the Atlantic meridional overturning circulation since the early 2010s. *Nature Communications*, 15(1):10642.

Lee, Y.-C., Liu, W., Deser, C., and Holland, M. (2025). Distinct impacts of diverse forcing agents on Arctic sea ice since the mid-twentieth century. *npj Climate and Atmospheric Science*, 8(1):362.

Lherminier, P., Gascard, J.-C., and Quadfasel, D. (1999). The Greenland Sea in water 1993 and 1994: Preconditioning for deep convection. *Deep Sea Research Part II: Topical Studies in Oceanography*, 46(6-7):1199–1235.

Li, F., Lozier, M., Bacon, S., Bower, A., Cunningham, S., de Jong, M., DeYoung, B., Fraser, N., Fried, N., Han, G., et al. (2020). Meridional overturning circulation observed by the OSNAP (overturning in the subpolar north Atlantic program) Array from August 2014 to May 2018.

Lien, V. S., Schlichtholz, P., Skagseth, Ø., and Vikebø, F. B. (2017). Wind-driven Atlantic water flow as a direct mode for reduced Barents Sea ice cover. *Journal of Climate*, 30(2):803–812.

Lique, C., Lenn, Y.-D., Rabe, B., and Cottier, F. (2025). Sea ice and Arctic Ocean oceanography. *Sea Ice: Its Physics, Chemistry, Biology, Geology and Societal Importance*, pages 283–308.

Lique, C. and Thomas, M. D. (2018). Latitudinal shift of the Atlantic Meridional Overturning Circulation source regions under a warming climate. *Nature Climate Change*, 8(11):1013–1020.

Liu, W. and Liu, Z. (2014). Assessing the stability of the Atlantic meridional overturning circulation of the past, present, and future. *Journal of Meteorological Research*, 28(5):803–819.

Loeng, H., Ozhigin, V., and Ådlandsvik, B. (1997). Water fluxes through the Barents Sea. *ICES Journal of Marine Science*, 54(3):310–317.

Lozier, M. S. (2019). A sea change in our view of overturning in the subpolar North Atlantic. *Science*, 363:516–521.

Lozier, M. S. (2023). Overturning in the subpolar North Atlantic: A review. *Philosophical Transactions of the Royal Society A*, 381(2249):20220191.

Ludwig, V., Spreen, G., and Pedersen, L. T. (2020). Evaluation of a new merged sea-ice concentration dataset at 1 km resolution from thermal infrared and passive microwave satellite data in the Arctic. *Remote Sensing*, 12(19):3183.

Lundesgaard, O., Sundfjord, A., Lind, S., Nilsen, F., and Renner, A. H. H. (2022). Import of Atlantic Water and sea ice controls the ocean environment in the northern Barents Sea. *Ocean Science*, 18:1389–1418.

Luo, J. et al. (2021). Sea-ice retreat suggests reorganization of water mass transformation in the Nordic and Barents Seas. *Nature Communications*, 12:27641.

Macrander, A., Valdimarsson, H., and Jõnsson, S. (2014). Improved transport estimate of the East Icelandic Current 2002–2012. *Journal of Geophysical Research: Oceans*, 119(6):3407–3424.

Madec, G. and Imbard, M. (1996). A global ocean mesh to overcome the North Pole singularity. *Climate Dynamics*, 12:381–388.

Marnela, M. et al. (2013). Fram Strait and Greenland Sea transports, water masses and water mass transformations. *Journal of Geophysical Research: Oceans*, 118:XX–YY.

Marshall, J. and Schott, F. (1999). Open–ocean convection: Observations, theory, and models. *Reviews of Geophysics*, 37:1–64.

Martin, S. and Cavalieri, D. J. (1989). Contributions of the Siberian shelf polynyas to the Arctic Ocean intermediate and deep water. *Journal of Geophysical Research: Oceans*, 94(C9):12725–12738.

Marzocchi, A., Nurser, A. G., Clément, L., and McDonagh, E. L. (2021). Surface atmospheric forcing as the driver of long-term pathways and timescales of ocean ventilation. *Ocean Science Discussions*, 2021:1–27.

Mattingly, K. S., Turton, J. V., Wille, J. D., Noël, B., Fettweis, X., Rennermalm, Å. K., and Mote, T. L. (2023). Increasing extreme melt in Northeast Greenland linked to föhn winds and atmospheric rivers. *Nature Communications*, 14(1):1743.

Mauritzen, C. (1996). Production of dense overflow waters feeding the North Atlantic across the Greenland-Scotland Ridge. Part 1: Evidence for a revised circulation scheme. *Deep Sea Research Part I: Oceanographic Research Papers*, 43(6):769–806.

Mauritzen, C. and Häkkinen, S. (1997). Influence of sea ice on the thermohaline circulation in the ArcticNorth Atlantic Ocean. *Geophysical Research Letters*, 24(24):3257–3260.

Mayer, M., Tietsche, S., Haimberger, L., et al. (2020). Arctic Ocean boundary exchanges: A review. *Oceanography*, 33(2):76–89.

Maykut, G. A. (1982). Large-scale heat exchange and ice production in the central Arctic. *Journal of Geophysical Research: Oceans*, 87(C10):7971–7984.

Maykut, G. A. and McPhee, M. G. (1982). Air-sea interaction at an Arctic coastal polynya. *Journal of Geophysical Research*, 87(C2):10499–10515.

McCarthy, G. D., Smeed, D. A., Johns, W. E., Frajka-Williams, E., Moat, B. I., Rayner, D., Baringer, M. O., Meinen, C. S., Collins, J., and Bryden, H. L. (2015). Measuring the Atlantic meridional overturning circulation at 26 N. *Progress in Oceanography*, 130:91–111.

Meier, W. N., Hovelsrud, G. K., van Oort, B. E., Key, J. R., Kovacs, K. M., Michel, C., Haas, C., Granskog, M. A., Gerland, S., Perovich, D. K., Makshtas, A., and Reist, J. D. (2014). Arctic sea ice in transformation: A review of recent observed changes and impacts on biology and human activity. *Reviews of Geophysics*, 52(3):185–217.

Menary, M. B., Roberts, M. J., Blockley, E. W., Andrews, M. B., Booth, B. B. B., Burke, E., Broccoli, A. J., Calvert, D., Dittus, A. J., Florek, P., Hogan, E., Jones,

G. S., Kuhlbrodt, T., Mizielinski, M. S., and Robson, J. I. (2018). Preindustrial control simulations with HadGEM3-GC3.1 for CMIP6. *Journal of Advances in Modeling Earth Systems*, 10:3049–3075.

Min, C., Mu, L., Yang, Q., Ricker, R., Shi, Q., Han, B., Wu, R., and Liu, J. (2019). Sea ice export through the Fram Strait derived from a combined model and satellite data set. *The Cryosphere*, 13(12):3209–3224.

Mohamed, B., Nilsen, F., and Skogseth, R. (2022). Interannual and decadal variability of sea surface temperature and sea ice concentration in the Barents Sea. *Remote Sensing*, 14(17):4413.

Monroe, E. E., Taylor, P. C., and Boisvert, L. N. (2021). Arctic cloud response to a perturbation in sea ice concentration: The North Water Polynya. *Journal of Geophysical Research: Atmospheres*, 126(16):e2020JD034409.

Moore, G. (2012). A new look at Greenland flow distortion and its impact on barrier flow, tip jets and coastal oceanography. *Geophysical research letters*, 39(22).

Moore, G., Pickart, R., and Renfrew, I. (2008). Buoy observations from the windiest location in the world ocean, Cape Farewell, Greenland. *Geophysical research letters*, 35(18).

Moore, G. and Renfrew, I. (2005). Tip jets and barrier winds: A QuikSCAT climatology of high wind speed events around Greenland. *Journal of Climate*, 18(18):3713–3725.

Moore, G., Våge, K., Renfrew, I., and Pickart, R. (2022). Sea-ice retreat suggests re-organization of water mass transformation in the Nordic and Barents Seas. *Nature communications*, 13(1):67.

Moore, G. W. K., Våge, K., Pickart, R. S., and Renfrew, I. A. (2015). Decreasing intensity of open-ocean convection in the Greenland and Iceland Seas. *Nature Climate Change*, 5(9):877–882.

Morales Maqueda, M., Willmott, A., and Biggs, N. (2004). Polynya dynamics: A review of observations and modeling. *Reviews of Geophysics*, 42(1).

Mork, K. A. and Skagseth, Ø. (2010). A quantitative description of the Norwegian Atlantic Current by combining altimetry and hydrography. *Ocean Science*, 6(4):901–911.

Mork, K. A., Skagseth, Ø., and Søiland, H. (2019). Recent warming and freshening of the Norwegian Sea observed by Argo data. *Journal of Climate*, 32(12):3695–3705.

Mueller, B. L., Gillett, N. P., Monahan, A. H., and Zwiers, F. W. (2018). Attribution of Arctic sea ice decline from 1953 to 2012 to influences from natural, greenhouse gas, and anthropogenic aerosol forcing. *Journal of Climate*, 31(19):7771–7787.

Müller, F. L., Wekerle, C., Dettmering, D., Passaro, M., Bosch, W., and Seitz, F. (2019). Dynamic ocean topography of the northern Nordic Seas: a comparison between satellite altimetry and ocean modeling. *The Cryosphere*, 13(2):611–626.

Münchow, A. (2006). An observational estimate of volume and freshwater flux leaving the Arctic Ocean through Nares Strait. *Journal of Physical Oceanography*, 36(11):2025–2041.

National Centers for Environmental Information, N. (2021). State of the climate in 2019.

Nilsen, J. E. Ø., Falck, E., and Gjevik, B. (2008). Large-scale patterns in the hydrography of the Nordic Seas. *Journal of Geophysical Research*, 113:C08010.

Noer, G., Saetra, Ø., Lien, T., and Gusdal, Y. (2011). A climatological study of polar lows in the Nordic Seas. *Quarterly Journal of the Royal Meteorological Society*, 137:1549–1558.

Ohshima, K. I., Nihashi, S., and Iwamoto, K. (2016). Global view of sea-ice production in polynyas and its linkage to dense/bottom water formation. *Geoscience Letters*, 3(1):1–14.

Onarheim, I. H., Årthun, M., Teigen, S. H., Eik, K. J., and Steele, M. (2024). Recent thickening of the Barents Sea ice cover. *Geophysical Research Letters*, 51(10):e2024GL108225.

Onarheim, I. H., Eldevik, T., Smedsrud, L. H., and Stroeve, J. C. (2018). Seasonal and regional manifestation of Arctic sea ice loss. *Journal of Climate*, 31(12):4917–4932.

Onarheim, I. H., Smedsrud, L. H., Ingvaldsen, R. B., and Nilsen, F. (2014). Loss of sea ice during winter North of Svalbard. *Tellus A: Dynamic Meteorology and Oceanography*, 66:23933.

Onarheim, I. H. and Årthun, M. (2017). Toward an ice-free Barents Sea. *Geophysical Research Letters*, 44(16):8387–8395.

Orvik, K. A. (2022). Longterm moored current and temperature measurements of the Atlantic Inflow into the Nordic Seas in the Norwegian Atlantic Current; 19952020. *Geophysical Research Letters*, 49(3):e2021GL096427.

Orvik, K. A. and Niiler, P. (2002). Major pathways of Atlantic water in the northern North Atlantic and Nordic Seas. *Geophysical Research Letters*, 29(19):1896.

Østerhus, S. et al. (2019). Arctic Mediterranean exchanges: A consistent volume budget and trends in transports from two decades of observations. *Ocean Science*, 15:379–399.

Østerhus, S. and Turrell, W. R. (2001). The inflow of Atlantic water to the Nordic Seas. *Ocean Dynamics*, 52:1–15.

Otterå, O. H., Drange, H., Bentsen, M., KvamstÅ, N. G., and Jiang, D. (2004). Transient response of the Atlantic meridional overturning circulation to enhanced freshwater input to the Nordic Seas Arctic ocean in the Bergen climate model. *Tellus A: Dynamic Meteorology and Oceanography*, 56(4):342–361.

Overland, J. E. and Wang, M. (2012). Large-scale atmospheric circulation changes associated with the recent loss of Arctic sea ice. *Tellus A*, 64:18501.

Overland, J. E., Wang, M., and Walsh, J. E. (2011). Effects of Arctic sea ice decline on weather and climate. *Surveys in Geophysics*, 32:495–511.

Ozhigin, V., Ingvaldsen, R., Loeng, H., Boitsov, V., and Karsakov, A. (2011). Introduction to the Barents Sea. In *The Barents Sea: ecosystem, resources, management. Half a century of Russian-Norwegian cooperation*, pages 39–76.

Oziel, L., Baudena, A., Ardyna, M., Massicotte, P., Randelhoff, A., Sallée, J.-B., Ingvaldsen, R. B., Devred, E., and Babin, M. (2020). Faster Atlantic currents drive poleward expansion of temperate phytoplankton in the Arctic Ocean. *Nature Communications*, 11:1–8.

Park, J.-E., Kim, H.-C., and Cho, K.-H. (2022). Variability of near-surface salinity in the Nordic Seas over the past three decades (1991-2019). *Frontiers in Marine Science*, 9:969159.

Pawlowicz, R. (1995). A note on seasonal cycles of temperature and salinity in the upper waters of the Greenland Sea Gyre from historical data. *Journal of Geophysical Research: Oceans*, 100(C3):4715–4726.

Pedersen, A., Löscher, C. R., and Olsen, S. M. (2025). Northern North Atlantic climate variability controls on ocean carbon sinks in EC-Earth3-CC. *Biogeosciences*, 22(18):5009–5029.

Pemberton, P., Nilsson, J., Hieronymus, M., and Meier, H. M. (2015). Arctic Ocean water mass transformation in S–T coordinates. *Journal of Physical Oceanography*, 45(4):1025–1050.

Perkins, H., Hopkins, T. S., Malmberg, S.-A., Poulain, P.-M., and Warn-Varnas, A. (1998). Oceanographic conditions east of Iceland. *Journal of Geophysical Research: Oceans*, 103(C10):21531–21542.

Petersen, G. N., Renfrew, I., and Moore, G. (2009). An overview of barrier winds off southeastern Greenland during the Greenland Flow Distortion Experiment. *Quarterly Journal of the Royal Meteorological Society: A journal of the atmospheric sciences, applied meteorology and physical oceanography*, 135(645):1950–1967.

Petit, T. et al. (2023). Understanding the sensitivity of the North Atlantic Subpolar Overturning in different resolution versions of HadGEM3-GC3.1. *Journal of Geophysical Research: Oceans*, 128(11):e2023JC019672.

Pickart, R. S., Spall, M. A., and Lazier, J. R. N. (2003). Mid-depth ventilation in the western boundary current system of the sub-polar gyre. *Deep-Sea Research Part I*, 50(9):1025–1053.

Pickart, R. S., Spall, M. A., Torres, D. J., Våge, K., Valdimarsson, H., Nobre, C., Moore, G. W. K., Jonsson, S., and Mastropole, D. (2017). The North Icelandic Jet and its relationship to the North Icelandic Irminger Current. *Journal of Marine Research*, 75(5):605–639.

Polyakov, I. V., Alekseev, G. V., Bekryaev, R. V., Bhatt, U., Colony, R. L., Johnson, M. A., Karklin, V. P., Makshtas, A. P., Walsh, D., and Yulin, A. V. (2002). Observationally based assessment of polar amplification of global warming. *Geophysical research letters*, 29(18):25–1.

Polyakov, I. V., Alkire, M. B., Bluhm, B. A., Brown, K. A., Carmack, E. C., Chierici, M., Danielson, S. L., Ellingsen, I., Ershova, E. A., Gårdfeldt, K., et al. (2020). Weakening of cold halocline layer exposes sea ice to oceanic heat in the eastern Arctic Ocean. *Journal of Climate*, 33(18):8107–8123.

Polyakov, I. V., Ingvaldsen, R. B., Pnyushkov, A. V., Bhatt, U. S., Francis, J. A., Janout, M., Kwok, R., and Skagseth, Ø. (2023). Fluctuating Atlantic inflows modulate Arctic atlantification. *Science*, 381(6661):972–979.

Polyakov, I. V., Pnyushkov, A. V., Alkire, M. B., Ashik, I. M., Baumann, T. M., Carmack, E. C., Goszczko, I., Guthrie, J., Ivanov, V. V., Kanzow, T., et al. (2017). Greater role for Atlantic inflows on sea-ice loss in the Eurasian Basin of the Arctic Ocean. *Science*, 356(6335):285–291.

Post, E., Bhatt, U. S., Bitz, C. M., Brodie, J. F., Fulton, T. L., Hebblewhite, M., Kerby, J., Kutz, S. J., Stirling, I., and Walker, D. A. (2013). Ecological consequences of sea-ice decline. *Science*, 341(6145):519–524.

Preußer, A., Heinemann, G., Willmes, S., and Paul, S. (2016). Circumpolar polynya regions and ice production in the Arctic: Results from MODIS thermal infrared imagery from 2002/2003 to 2014/2015 with a regional focus on the Laptev Sea. *The Cryosphere*, 10(6):3021–3042.

Rabe, B., Dodd, P., Hansen, E., Falck, E., Schauer, U., Mackensen, A., Beszczynska-Möller, A., Kattner, G., Rohling, E., and Cox, K. (2013). Liquid export of Arctic freshwater components through the Fram Strait 19982011. *Ocean Science*, 9:91–109.

Rabe, B., Münchow, A., Johnson, H. L., and Melling, H. (2010). Nares strait hydrography and salinity field from a 3-year moored array. *Journal of Geophysical Research: Oceans*, 115:C07010.

Rae, J., Hewitt, H., Keen, A., Ridley, J., West, A., Harris, C., Hunke, E. C., and Walters, D. (2015). Development of the global sea ice 6.0 CICE configuration for the Met Office global coupled model. *Geoscientific Model Development*, 8(7):2221–2230.

Rahmstorf, S. et al. (2015). Exceptional twentieth-century slowdown in Atlantic Ocean overturning circulation. *Nature Climate Change*, 5:475–480.

Raj, R., Halo, I., Chatterjee, S., Belonenko, T., Bakhoday-Paskyabi, M., Bashmachnikov, I., Fedorov, A., and Xie, J. (2020). Interaction between mesoscale eddies and the gyre circulation in the Lofoten Basin. *Journal of Geophysical Research: Oceans*, 125(7):e2020JC016102.

Raj, R. P., Chafik, L., Nilsen, J. E. Ø., Eldevik, T., and Halo, I. (2015). The Lofoten vortex of the Nordic Seas. *Deep Sea Research Part I: Oceanographic Research Papers*, 96:1–14.

Raj, R. P., Chatterjee, S., Bertino, L., Turiel, A., and Portabella, M. (2019). The Arctic Front and its variability in the Norwegian Sea. *Ocean Science*, 15(6):1729–1744.

Rawlins, M. A. et al. (2010). Analysis of the Arctic System for freshwater cycle intensification: Observations and expectations. *Journal of Climate*, 23(21):5715–5737.

Reistad, M., Breivik, Ø., Haakenstad, H., Aarnes, O. J., Furevik, B. R., and Bidlot, J. R. (2014). A highresolution hindcast of wind and waves for the North Sea, the Norwegian Sea and the Barents Sea. *Journal of Atmospheric and Oceanic Technology*, 31:934–952.

Ren, H., Shokr, M., Zhang, T., Zhang, Z., Hui, F., and Cheng, X. (2024). Turbulent heat fluxes in the North Water Polynya and ice estimated based on ASRv2 data. *Advances in Climate Change Research*.

Renfrew, I. A., Barrell, C., Elvidge, A., Brooke, J., Duscha, C., King, J., Kristiansen, J., Cope, T. L., Moore, G. W. K., Pickart, R. S., et al. (2021). An evaluation of surface meteorology and fluxes over the Iceland and Greenland Seas in ERA5 reanalysis: The impact of sea ice distribution. *Quarterly Journal of the Royal Meteorological Society*, 147(734):691–712.

Rhein, M. et al. (2011). Deep water formation, ventilation and renewal. *Ocean Science*, 7:229–286.

Richter, K., von Appen, W.-J., and Thomsen, S. (2018). Meandering of the East Greenland Current north of Denmark Strait. *Ocean Science*, 14(1):141–157.

Ridley, J. K., Blockley, E. W., Keen, A. B., Rae, J. G., West, A. E., and Schroeder, D. (2018). The sea ice model component of HadGEM3-GC3.1. *Geoscientific Model Development*, 11(2):713–723.

Roberts, C. D. et al. (2019). Description of the HadGEM3-GC3.1 model configuration and spin-up for CMIP6. *Geoscientific Model Development*, 12(11):4999–5028.

Roberts, M. J., Jackson, L. C., Roberts, C. D., Meccia, V., Docquier, D., Koenigk, T., Ortega, P., Moreno-Chamarro, E., Bellucci, A., Coward, A., Drijfhout, S., Exarchou, E., Gutjahr, O., Hewitt, H., Iovino, D., Lohmann, K., Putrasahan, D., Schiemann, R., Seddon, J., Terray, L., Xu, X., and Zhang, Q. (2020). Sensitivity of the Atlantic Meridional Overturning Circulation to model resolution in CMIP6 HighResMIP simulations and implications for future changes. *Journal of Advances in Modeling Earth Systems*, 12(8):e2019MS002014.

Rojo, M., Claud, C., Mallet, P., Noer, G., Carleton, A. M., and Vicomte, M. (2015). Polar low tracks over the Nordic Seas: a 14winter climatic analysis. *Tellus, Series A: Dynamic Meteorology and Oceanography*, 67(1):24660.

Rose, S. K., Andersen, O. B., Passaro, M., Ludwigsen, C. A., and Schwatke, C. (2019). Arctic Ocean sea level record from the complete radar altimetry era: 1991–2018. *Remote Sensing*, 11(14):1672.

Rossby, T., Ozhigin, V., Ivshin, V., and Bacon, S. (2009). An isopycnal view of the Nordic Seas hydrography with focus on properties of the Lofoten Basin. *Deep-Sea Research Part I*, 56:1955–1971.

Rudels, B., Björk, G., Nilsson, J., Winsor, P., Lake, I., and Nohr, C. (2005). The interaction between waters from the Arctic Ocean and the Nordic Seas north of Fram Strait. *Polar Research*, 24(1-2):1–17.

Rudels, B. et al. (2002). Structure and variability of the Nordic Seas. *Deep-Sea Research Part I*, 49:1151–1184.

Rudels, B. and Friedrich, H. J. (2000). The transformations of Atlantic water in the Arctic Ocean and their significance for the freshwater budget. *The freshwater budget of the Arctic Ocean*, pages 503–532.

Sadatzki, H., Maffezzoli, N., Dokken, T. M., Simon, M. H., Berben, S. M. P., Fahl, K., Kjer, H. A., Spolaor, A., Stein, R., Vallelonga, P., Vinther, B. M., and Jansen, E. (2020). Rapid reductions and millennial-scale variability in Nordic Seas sea ice cover during abrupt glacial climate changes. *Proceedings of the National Academy of Sciences of the United States of America*, 117(47):29478–29486.

Sandø, A. B. et al. (2010). Importance of heat transport and local air-sea heat fluxes for the Barents Sea climate. *Journal of Geophysical Research*, 115:C06020.

Sato, T. et al. (2022). Enhanced Arctic moisture transport toward Siberia in response to sea ice retreat. *npj Climate and Atmospheric Science*, 5:1–11.

Schaffer, J. et al. (2019). Dynamic ocean topography of the northern Nordic Seas: a comparison between satellite altimetry and ocean modeling. *The Cryosphere*, 13:611–628.

Schauer, U. and Beszczynska-Möller, A. (2004). Problems with estimation and interpretation of oceanic heat transport. *Journal of Geophysical Research*, 109:C02009.

Schauer, U. and Beszczynska-Möller, A. (2008). Volume and heat transport across Fram Strait. *Journal of Geophysical Research*, 113:C01005.

Schauer, U., Fahrbach, E., Osterhus, S., and Rohardt, G. (2004). Arctic warming through the Fram Strait: Oceanic heat transport from 3 years of measurements. *Journal of Geophysical Research: Oceans*, 109(C6).

Schauer, U., Loeng, H., Rudels, B., Ozhigin, V. K., and Dieck, W. (2002). Atlantic water flow through the Barents and Kara Seas. *Deep Sea Research Part I: Oceanographic Research Papers*, 49(12):2281–2298.

Schlichtholz, P. and Goszczko, I. (2006). Interannual variability of the Atlantic water layer in the West Spitsbergen Current at 76.5°N in summer 19912003. *DeepSea Research Part I: Oceanographic Research Papers*, 53(4):608–626.

Schmitt, A. U. and Lüpkes, C. (2023). Attributing near-surface atmospheric trends in the Fram Strait region to regional sea ice conditions. *The Cryosphere*, 17(8):3115–3136.

Screen, J. A., Blackport, R., Deser, C., Cohen, J. L., Sun, L., McCusker, K. E., and Tomas, R. (2022). Sea iceair interactions amplify multidecadal variability in the North Atlantic and Arctic region. *Nature Communications*, 13:1576.

Screen, J. A. et al. (2018). Arctic amplification and mid-latitude weather. *Nature Climate Change*, 8:627–637.

Screen, J. A. and Simmonds, I. (2010). The central role of diminishing sea ice in recent Arctic temperature amplification. *Nature*, 464(7293):1334–1337.

Screen, J. A. and Simmonds, I. (2012). Declining summer snowfall in the Arctic: Causes, impacts and feedbacks. *Climate Dynamics*, 38:2243–2256.

Screen, J. A. and Simmonds, I. (2013). Influence of Arctic sea ice loss on atmospheric circulation: review of observational and modeling evidence. *Quarterly Journal of the Royal Meteorological Society*, 139:1756–1770.

Sejr, M. K., Stedmon, C. A., Bendtsen, J., Abermann, J., Juul-Pedersen, T., Mortensen, J., and Rysgaard, S. (2017). Evidence of local and regional freshening of Northeast Greenland coastal waters. *Scientific Reports*, 7(1):1–6.

Selivanova, J., Iovino, D., and Cocetta, F. (2024). Past and future of the Arctic sea ice in High-Resolution Model Intercomparison Project (HighResMIP) climate models. *The Cryosphere*, 18(6):2739–2763.

Selyuzhenok, V., Bashmachnikov, I., Ricker, R., Vesman, A., and Bobylev, L. (2020). Sea ice volume variability and water temperature in the Greenland Sea. *The Cryosphere*, 14(2):477–495.

Semedo, A., Vettor, R., Breivik, O. y., Sterl, A., Reistad, M., and Soares, C. (2015). The wind sea and swell waves climate in the Nordic Seas. *Ocean Dynamics*, 65:221–237.

Semper, S., Våge, K., Pickart, R. S., Jónsson, S., and Valdimarsson, H. (2022). Evolution and transformation of the North Icelandic Irminger Current along the North Iceland shelf. *Journal of Geophysical Research: Oceans*, 127(3):e2021JC017700.

Serreze, M. C. and Barry, R. G. (2011). Processes and impacts of Arctic amplification: A research synthesis. *Global and Planetary Change*, 77:85–96.

Serreze, M. C., Cassano, E., Crawford, A., Cassano, J. J., and Zhang, C. (2026). The observed evolution of Arctic amplification over the past 45 years. *The Cryosphere*, 20:411–425.

Serreze, M. C. and Meier, W. N. (2019). The Arctics sea ice cover: trends, variability, predictability, and comparisons to the Antarctic. *Annals of the New York Academy of Sciences*, 1436:36–53.

Shi, W., Li, N., and Lv, X. (2021). Study of the overflow transport of the Nordic Sea. *Water*, 13(19):2675.

Shi, W., Xu, M., and Lv, X. (2024). Research on the change of the storage volume of the Nordic Seas Overflows over the last 40 years. *Frontiers in Marine Science*, 11:1302978.

Shu, Q. and et al. (2022). Arctic Ocean amplification in a warming climate in CMIP6 models. *Science Advances*, 8:eabn9755.

Shu, Q., Wang, Q., Song, Z., and Qiao, F. (2021). The poleward enhanced Arctic Ocean cooling machine in a warming climate. *Nature Communications*, 12(1):2966.

Sicard, M., de Boer, A., and Sime, L. (2022). Last Interglacial Arctic sea ice as simulated by the latest generation of climate models. *Past Global Changes Magazine*, 30(2):92–93.

Simonsen, K. and Haugan, P. M. (1996). Heat budgets of the Arctic Mediterranean and sea surface heat flux parameterizations for the Nordic Seas. *Journal of Geophysical Research: Oceans*, 101(C3):6553–6576.

Skagseth, Ø., Eldevik, T., Årthun, M., Asbjørnsen, H., Lien, V. S., and Smedsrud, L. H. (2020). Reduced efficiency of the Barents Sea cooling machine. *Nature Climate Change*, 10(7):661–666.

Smedsrud, L. H. et al. (2013). The role of the Barents Sea in the Arctic climate system. *Reviews of Geophysics*, 51:415–449.

Smedsrud, L. H., Halvorsen, M. H., Stroeve, J. C., Zhang, R., and Kloster, K. (2017). Fram Strait sea ice export variability and September Arctic sea ice extent over the last 80 years. *The Cryosphere*, 11(1):65–79.

Smedsrud, L. H., Muilwijk, M., Brakstad, A., Madonna, E., Lauvset, S. K., Spensberger, C., Born, A., Eldevik, T., Drange, H., Jeansson, E., et al. (2022). Nordic Seas heat loss, Atlantic inflow, and Arctic sea ice cover over the last century. *Reviews of Geophysics*, 60(1):e2020RG000725.

Smedsrud, L. H., Sirevaag, A., Kloster, K., Sorteberg, A., and Sandven, S. (2011). Recent wind driven high sea ice area export in the Fram Strait contributes to Arctic sea ice decline. *The Cryosphere*, 5(4):821–829.

Smith, D. M. et al. (2017). An interannual link between Arctic seaice cover and the North Atlantic Oscillation. *Climate Dynamics*, 49:33133323.

Smith, S. D., Muench, R. D., and Pease, C. H. (1990). Polynyas and leads: An overview of physical processes and environment. *Journal of Geophysical Research: Oceans*, 95(C6):9461–9479.

Smith Jr, W. and Barber, D. (2007). Polynyas and climate change: a view to the future. *Elsevier Oceanography Series*, 74:411–419.

Somavilla, R. (2019). Draining and upwelling of Greenland Sea deep waters. *Journal of Geophysical Research: Oceans*, 124(4):2842–2860.

Spall, M. A. (2011). On the role of eddies and surface forcing in the heat transport and overturning circulation in marginal seas. *Journal of Physical Oceanography*, 41(5):912–930.

Spall, M. A., Almansi, M., Huang, J., Haine, T. W., and Pickart, R. S. (2021). Lateral redistribution of heat and salt in the Nordic Seas. *Progress in Oceanography*, 196:102609.

Speer, L., Nelson, R., Casier, R., Gavrilo, M., von Quillfeldt, C. H., Cleary, J., Halpin, P. N., and Hooper, P. (2017). *Natural marine world heritage in the Arctic Ocean: Report of an expert workshop and review process.*

Spreen, G., De Steur, L., Divine, D., Gerland, S., Hansen, E., and Kwok, R. (2020). Arctic sea ice volume export through Fram Strait from 1992 to 2014. *Journal of Geophysical Research: Oceans*, 125(6):e2019JC016039.

Spreen, G., Kaleschke, L., and Heygster, G. (2008). Sea ice remote sensing using AMSR-E 89-GHz channels. *Journal of Geophysical Research: Oceans*, 113(C2).

Stoll, P. J., Graversen, R. G., Noer, G., and Hodges, K. I. (2018). An objective global climatology of polar lows based on reanalysis data. *Quarterly Journal of the Royal Meteorological Society*, 144:2099–2117.

Strehl, A. M. et al. (2024). A 70-year perspective on water-mass transformation in the Greenland Sea: From thermobaric to thermal convection. *Progress in Oceanography*, 227:103304.

Stroeve, J. C. et al. (2012). The Arctic's rapidly shrinking sea ice cover: A research synthesis. *Climatic Change*, 110:1005–1027.

Su, J., Hao, G., Ye, X., and Wang, W. (2013). The experiment and validation of sea ice concentration AMSR-E retrieval algorithm in polar region. *Journal of Remote Sensing*, 17(3):495–513.

Sutherland, D. A. and Pickart, R. S. (2008). The East Greenland Coastal Current: Structure, variability, and forcing. *Progress in Oceanography*, 78(1):58–77.

Swift, J. H., Aagaard, K., and Malmberg, S.-A. (1980). The contribution of the Denmark Strait overflow to the deep North Atlantic. *Deep Sea Research Part A. Oceanographic Research Papers*, 27(1):29–42.

Tamura, T. and Ohshima, K. I. (2011). Mapping of sea ice production in the Arctic coastal polynyas. *Journal of Geophysical Research: Oceans*, 116(C7).

Thiede, J., Pfirman, S., Schenke, H. W., and Reil, W. (1990). Bathymetry of Molloy Deep: Fram Strait between Svalbard and Greenland. *Marine Geophysical Researches*, 12(3):197–214.

Thomas, M. D. S. and Fedorov, A. V. (2019). Mechanisms and impacts of a partial AMOC recovery under enhanced freshwater forcing. *Geophysical Research Letters*, 46:3308–3316.

Thorne, P. W. et al. (2021). New climate models reveal faster and larger increases in Arctic precipitation than previously projected. *Nature Communications*, 12:1–13.

Thornes, T. and Longva, O. (2007). Norwegian Sea: bathymetric and morphological features. *Continental Shelf Research*, 27:35–58.

Titchner, H. A. and Rayner, N. A. (2014). The Met Office Hadley Centre sea ice and sea surface temperature data set, version 2: 1. Sea ice concentrations. *Journal of Geophysical Research: Atmospheres*, 119(6):2864–2889.

Tollefson, J. (2018). Sensor array provides new look at global ocean current. *Nature*, 554(7693).

Tooth, O. J., Johnson, H. L., and Wilson, C. (2023). Lagrangian overturning pathways in the eastern Subpolar North Atlantic. *Journal of Climate*, 36(3):823–844.

Treguier, A. M., Mathiot, P., Graham, T., Copsey, D., Lique, C., and Sterlin, J. (2021). Heat balance in the nordic seas in a global 1/12 coupled model. *Journal of Climate*, 34(1):89–106.

Tsubouchi, T., Bacon, S., Aksenov, Y., Garabato, A. C. N., Beszczynska-Möller, A., Hansen, E., de Steur, L., Curry, B., Lee, C. M., and et al. (2018). The Arctic Ocean seasonal cycle of heat and freshwater fluxes: Observation-based inverse estimates of volume, heat and freshwater budgets. *Progress in Oceanography*, 160:1–26.

Tsubouchi, T., Våge, K., Hansen, B., Larsen, K. M. H., Østerhus, S., Johnson, C., Jónsson, S., and Valdimarsson, H. (2021). Increased ocean heat transport into the Nordic Seas and Arctic Ocean over the period 1993–2016. *Nature Climate Change*, 11(1):21–26.

Tsukernik, M., Deser, C., Alexander, M., and Tomas, R. (2010). Atmospheric forcing of Fram Strait sea ice export: A closer look. *Climate Dynamics*, 35(7–8):1349–1360.

Våge, K., Pickart, R. S., Spall, M. A., Moore, G., Valdimarsson, H., Torres, D. J., Erofeeva, S. Y., and Nilsen, J. E. Ø. (2013). Revised circulation scheme north of the Denmark Strait. *Deep Sea Research Part I: Oceanographic Research Papers*, 79:20–39.

Våge, K., Pickart, R. S., Spall, M. A., and Moore, G. W. K. (2011). Deep convection in the Irminger Sea: Role of the Greenland tip jet. *Journal of Physical Oceanography*, 41(12):2418–2435.

Van Angelen, J., Van den Broeke, M., and Kwok, R. (2011). The Greenland Sea Jet: A mechanism for wind-driven sea ice export through Fram Strait. *Geophysical Research Letters*, 38(12).

van den Berk, J., Drijfhout, S. S., and Hazeleger, W. (2021). Circulation adjustment in the Arctic and Atlantic in response to Greenland and Antarctic mass loss. *Climate Dynamics*, 57:1689–1707.

van der Wiel, K., Bloomfield, H. C., Lee, R. W., Stoop, L. P., Blackport, R., Screen, J. A., and Selten, F. M. (2019). The influence of weather regimes on European renewable energy production and demand. *Environmental Research Letters*, 14(9):094010.

Vihma, T., Screen, J. A., Tjernström, M., Newton, B., Zhang, X., Popova, V., Deser, C., Holland, M., and Prowse, T. (2014). Atmospheric circulation and climate variability in the Arctic. *Reviews of Geophysics*, 52(3):589–626.

Vikhamar-Schuler, D., Isaksen, K., Haugen, J. E., Tømmervik, H., Luks, B., Schuler, T. V., and Bjerke, J. W. (2016). Changes in winter warming events in the Nordic Arctic region. *Journal of climate*, 29(17):6223–6244.

Vinje, T. et al. (2004). Historical variability of sea ice edge position in the Nordic Seas. *Journal of Geophysical Research: Oceans*, 109(C02015).

von Schuckmann, K., Moreira, L., Cancet, M., Gues, F., Autret, E., Baker, J., Bricaud, C., Bourdalle-Badie, R., Castrillo, L., Cheng, L., et al. (2024). The state of the global ocean. *State of the Planet*, 4:1–30.

Våge, K., Papritz, L., Håvik, L., Spall, M. A., and Moore, G. W. (2015). Ocean convection linked to the recent ice edge retreat along east Greenland. *Nature Communications*, 6:1–8.

Walczowski, W. and Piechura, J. (2011). Influence of the West Spitsbergen Current on the local climate. *International Journal of Climatology*, 31(7):1088–1093.

Walter, K. and Graf, H.-F. (2005). The North Atlantic variability structure, storm tracks, and precipitation depending on the polar vortex strength. *Atmospheric Chemistry and Physics*, 5:239–248.

Wang, Q., Wekerle, C., Wang, X., Danilov, S., Koldunov, N., Sein, D., Sidorenko, D., von Appen, W.-J., and Jung, T. (2020). Intensification of the Atlantic Water supply to the Arctic Ocean through Fram Strait induced by Arctic sea ice decline. *Geophysical Research Letters*, 47(3):e2019GL086682.

Wang, Q., Wekerle, C., Wang, X., Danilov, S., Koldunov, N. V., Sein, D., Sidorenko, D., von Appen, W.-J., and Jung, T. (2022). Intensification of the Atlantic Water supply to the Arctic Ocean through Fram Strait induced by Arctic sea ice decline. *Authorea Preprints*.

Wei, J., Zhang, X., and Wang, Z. (2019). Reexamination of Fram Strait sea ice export and its role in recently accelerated Arctic sea ice retreat. *Climate Dynamics*, 53(3):1823–1841.

Wei, X. et al. (2024). Contrasting Labrador Sea convection and AMOC trends in warming climate simulations. *Geophysical Research Letters*, 51:e2024GLXXXXXX.

Weijer, W., Cheng, W., Drijfhout, S. S., Fedorov, A. V., Hu, A., Jackson, L. C., Liu, W., McDonagh, E. L., Mecking, J. V., and Zhang, J. (2019). Stability of the Atlantic Meridional Overturning Circulation: A review and synthesis. *Journal of Geophysical Research: Oceans*, 124(8):5336–5375.

Weijer, W., Cheng, W., Garuba, O. A., Hu, A., and Nadiga, B. T. (2020). CMIP6 models predict significant 21st century decline of the Atlantic meridional overturning circulation. *Geophysical Research Letters*, 47(12):e2019GL086075.

Wekerle, C., Wang, Q., Danilov, S., Schourup-Kristensen, V., von Appen, W.-J., and Jung, T. (2017). Atlantic Water in the Nordic Seas: Locally eddy-permitting ocean simulation in a global setup. *Journal of Geophysical Research: Oceans*, 122(2):914–940.

Weer, W., Haine, T. W., Siddiqui, A. H., Cheng, W., Veneziani, M., and Kurtakoti, P. (2022). Interactions between the Arctic Mediterranean and the Atlantic Meridional Overturning Circulation: A Review. *Oceanography*, 35(LA-UR-22-27688):118–127.

Wilkinson, D. and Bacon, S. (2005). The spatial and temporal variability of the East Greenland Coastal Current from historic data. *Geophysical Research Letters*, 32(24).

Wilkinson, J. P. et al. (2022). Separating annual, interannual and regional change in sea surface temperature in the northeastern North Atlantic and Nordic Seas. *Journal of Geophysical Research: Oceans*, 127.

Williams, K. D., Copsey, D., Blockley, E. W., Bodas-Salcedo, A., Calvert, D., Comer, R., Davis, P., Graham, T., Hewitt, H. T., Hill, R., Hyder, P., Ineson, S., Johns, T. C., Keen, A. B., Lee, R. W., et al. (2018). The Met Office Global Coupled Model 3.0 and 3.1 (GC3.0 and GC3.1) configurations. *Journal of Advances in Modeling Earth Systems*, 10:doi:10.1002/2017MS001115.

Wong, C. H. M., Heuzé, C., Ickes, L., and Zhou, L. (2025). The spatio-temporal variability, trends, and drivers of winter Arctic polynyas.

Woodgate, R. A., Fahrbach, E., and Rohardt, G. (1999). Structure and transports of the East Greenland Current at 75 N from moored current meters. *Journal of Geophysical Research: Oceans*, 104(C8):18059–18072.

Woollings, T. et al. (2010). Variability of the North Atlantic jet stream. *Quarterly Journal of the Royal Meteorological Society*, 136:856–868.

Wu, B., Wang, J., and Walsh, J. (2006). Dipole anomaly in the winter Arctic atmosphere and its association with sea ice motion. *Journal of Climate*, 19(2):240–253.

Wu, Y. (2022). *Searching for the sub-Arctic Ocean response to wintertime sea ice retreat.* PhD thesis, University of East Anglia.

Wu, Y., Stevens, D. P., Renfrew, I. A., and Zhai, X. (2021). The response of the Nordic Seas to wintertime sea ice retreat. *Journal of Climate*, 34(15):6041–6056.

Wu, Y., Zheng, Z., Chen, X., Zhong, W., Yuan, X., Zhong, W., Lei, R., Li, C., Zhuang, Y., Gao, X., et al. (2025). Amplified warming accelerates deoxygenation in the Arctic Ocean. *Nature Climate Change*, 15(8):859–865.

Yager, P. L., Wallace, D. W., Johnson, K. M., Smith, W. O., Minnett, P. J., and Deming, J. W. (1995). The Northeast Water Polynya as an atmospheric CO2 sink: A seasonal rectification hypothesis. *Journal of Geophysical Research: Oceans*, 100(C3):4389–4398.

Yamagami, Y., Watanabe, M., Mori, M., and Ono, J. (2022). Barents-Kara sea-ice decline attributed to surface warming in the Gulf Stream. *Nature communications*, 13(1):3767.

Yool, A., Palmiéri, J., Jones, C. G., Sellar, A. A., Stringer, S. M., Walton, J., de Mora, L., Kuhlbrodt, T., and Popova, E. E. (2021). Evaluating the physical and biogeochemical state of the ocean component of UKESM1 in CMIP6 historical simulations. *Geoscientific Model Development*, 14(6):3437–3472.

Zhang, J. et al. (2025). Freshwater transport variation through Fram and Davis Strait influenced by atmospheric circulation. *Frontiers in Marine Science*.

Zhang, J., Steele, M., and Schweiger, A. (2010). Arctic sea ice response to atmospheric forcings with varying levels of anthropogenic warming and climate variability. *Geophysical Research Letters*, 37(20).

Zhang, R., Sutton, R., Danabasoglu, G., Kwon, Y.-O., Marsh, R., Yeager, S. G., Amrhein, D. E., and Little, C. M. (2019). A review of the role of the Atlantic meridional overturning circulation in Atlantic multidecadal variability and associated climate impacts. *Reviews of Geophysics*, 57(2):316–375.

Zhang, S., Shi, J., Wang, Z., Zhang, J., Xu, C., and Bi, H. (2023). Assessment of CMIP6 simulations of Arctic sea-ice drift and Fram Strait ice area flux. *Advances in Polar Science*, 34(1):30–42.

Zhao, J., Drinkwater, K., and Wang, X. (2019). Positive and negative feedbacks related to the Arctic Oscillation revealed by air-sea heat fluxes. *Tellus A: Dynamic Meteorology and Oceanography*, 71(1):1596519.

Zuo, H., Balmaseda, M. A., Tietsche, S., Mogensen, K., and Mayer, M. (2019). The ECMWF operational ensemble reanalysis–analysis system for ocean and sea ice: a description of the system and assessment. *Ocean science*, 15(3):779–808.